

# **Mechanisms of Enhanced SIRT6 Catalysis**

By

Mark Alexander Klein

A dissertation submitted in partial fulfillment of

The requirements for the degree of

Doctor of Philosophy

(Biochemistry)

At the

UNIVERSITY OF WISCONSIN – MADISON

2020

Date of final oral examination: 10/29/2020

The dissertation is approved by the following members of the Final Oral Committee:

John M. Denu, Professor, Department of Biomolecular Chemistry

Rozalyn M. Anderson, Associate Professor, Department of Medicine

Brian G. Fox, Professor, Department of Biochemistry

James L. Keck, Professor, Department of Biomolecular Chemistry

James M. Ntambi, Professor, Department of Biochemistry

## **Mechanisms of Enhanced SIRT6 Catalysis**

Mark Alexander Klein

Under the supervision of Professor John M. Denu

At the University of Wisconsin – Madison

Protein acetylation is recognized as a widespread post-translational modification that serves as a key regulatory mechanism for protein function across diverse cellular processes. The best studied and most appreciated function of lysine acetylation is the dynamic regulation of the histone proteins which serve as the building blocks of chromatin. Acetylation of the unstructured N-terminal tails of histones is enriched at sites of active gene transcription and their deacetylation results in the local silencing of genes and chromatin compaction. Sirtuin-6 (SIRT6) has emerged as an important chromatin regulator through its role as a nuclear histone deacetylase. SIRT6 couples the hydrolysis of nicotinamide adenine dinucleotide ( $\text{NAD}^+$ ) to the removal of an acetyl-moiety from a histone lysine, placing it at the intersection between metabolism and epigenetic regulation. Through its function as a histone deacetylase, SIRT6 has widespread cellular roles including regulation of metabolic genes, DNA repair, telomere maintenance, and tumor suppression. Furthermore, SIRT6 has been positively correlated with longevity and protection against a host of age-related diseases. Despite these widely accepted cellular functions, SIRT6 is an extremely inefficient deacetylase *in vitro*, catalyzing deacetylation at a rate  $\sim 1,000$  times slower than other highly active sirtuins. Just prior to the start of my thesis research, our group discovered that SIRT6 deacetylation could be modestly

activated by several long-chain free fatty acids, providing a foundation for the long-sought therapeutic targeting of SIRT6.

Through rigorous biochemical and biophysical studies, I have discovered and optimized potent synthetic small molecule activators of SIRT6 deacetylation and used them to interrogate and determine the mechanism by which they enhance SIRT6 catalysis. Throughout these studies, I discovered a non-activatable SIRT6 mutant (R65A) and leveraged it to isolate a previously unreported slow conformational step in SIRT6 catalysis which is enhanced by small molecule activators. Studies performed outside our lab demonstrated that SIRT6 R65A lacked cellular activity, leading to our hypothesis that SIRT6 requires endogenous activation to perform its role as a histone deacetylase. To this end, I have discovered that nucleosome binding strongly enhances the deacetylase activity of SIRT6 in an R65-dependent fashion similar to that of our small molecule activator. Additionally, I have shown that a distinct class of recently reported cellularly active small molecule activators of SIRT6 are capable of further stimulate histone deacetylation. This finding underscores the multifaceted nature of SIRT6 activation and provides a framework for the future development of therapeutic small molecule activators. My research has proceeded through the stepwise mechanistic understanding of factors that enhance SIRT6 catalysis, from small molecules to protein-protein interactions. This work culminates in providing a mechanistic rationale for a ~5,000-fold increase in catalytic efficiency observed against nucleosomes compared to peptide substrate and justifies the ability of SIRT6 to perform widespread cellular histone deacetylation despite its seemingly poor *in vitro* kinetics. Given the impact of nucleosome binding on SIRT6 catalysis, I developed a split-luciferase assay allowing for rapid *in vitro* equilibrium and dissociation binding studies of SIRT6 with nucleosomes that can be applied to live-cell studies of chromatin occupation by SIRT6.

Chapter 1 provides a thorough introduction of the biological and catalytic functions of SIRT6 and discusses the implications of targeting SIRT6 by small molecule activators. Chapter 2 covers the screening and development of the novel small molecule activator, CL5D. This study includes exhaustive mechanistic work resulting in the identification of the non-activatable SIRT6 mutant R65A and the isolation of a novel conformational step enhanced by CL5D to facilitate activated catalysis. Chapter 3 identifies nucleosome binding as the most potent, robust, and cellularly relevant means of activating SIRT6 deacetylation to date. Additionally, this chapter demonstrates the ability of small molecule activators to further enhance nucleosome deacetylation, providing optimism for the therapeutic targeting of SIRT6. Chapter 4 outlines the early development of a split-luciferase NanoBiT based assay for the *in vitro* characterization of SIRT6-nucleosome binding kinetics with implications for live-cell use. Overarching conclusions and future directions will be presented in Chapter 5.

## Acknowledgements

I don't think anything or anyone can prepare you for graduate school. It is an arduous journey which compared to previous formal education lacks a predetermined and structured track. It is this nebulous training ground, however, that forces us to learn how to make our own path. I can say with complete confidence that any success I have had navigating graduate school is due to the guidance, encouragement, and support I received from numerous colleagues, friends, and family. First and foremost, I would like to acknowledge my Ph.D. advisor and mentor, Dr. John Denu. John's unrelenting excitement and genuine curiosity towards science is inspiring and contagious. Whether we were discussing this thesis work, the epigenetics of queen bees, or starting a fecal transplant clinic, I never left a conversation bored. John was invaluable in the firsthand training he provided me towards becoming a mechanistic biochemist and I have a great appreciation for his ability to think critically and skeptically. Perhaps what I've cherished most is his openness to all things, be it science or life. I look up to John as a scientist, but also as a nature lover, woodworker, car enthusiast, and tinkerer. John, thank you for all the scientific and life lessons you have taught me.

I would like to thank my thesis committee: Dr. Roz Anderson, Dr. Brian Fox, Dr. Jim Keck, Dr. James Ntambi, and Dr. Ron Raines (former) for their guidance and insight throughout my training. Your advice has not only directed my thesis work, but my career path as well. I have had the pleasure of participating in a number of collaborative studies throughout my time as a graduate student and am grateful to the following people for their interactions and shared excitement: Dr. Raul Mostoslavsky (Harvard Medical School), Dr. Weiping Tang (University of Wisconsin), Dr. Manish Patankar (University of Wisconsin), Dr. Clemens Steegborn (University of Bayreuth), and Dr. Scott Wildman (University of Wisconsin).

I had the honor of participating in the Chemistry-Biology Interface Training Program which provided me with valuable exposure to multidisciplinary graduate research. I would like to thank Dr. Helen Blackwell, Dr. Cara Jenkins, and Dr. Laura Kiessling for the massive effort and passion they put into running the training program. This training program afforded me the ability to participate in an internship at Promega where I gained my first exposure to industrial biotechnology research. The value of this experience cannot be overstated, and I would like to thank my mentor, Dr. Chris Hosfield, for the guidance and friendship he provided.

I would like to thank all of the Denu lab members I had the opportunity to share my daily life with over the years; Jess Feldman, Josh Baeza, Zhangli Su, Jin-Hee Lee, Jing Fan, Michael Smallegan, Rush Dhillon, James Dowell, Eric Armstrong, Kim Krautkramer, Ana Lindahl, Slava Kuznetsov, Sherry Bakhtiar, Wallace Liu, Spencer Haws, Sydney Thomas, Alexis Lawton, Yiming Qin, Lily Miller, José Moran, Cassie Leech, Bianca Chavez, and Jessica Han. I have truly enjoyed coming to lab and sharing in science and life with all of you. At least until the pandemic. I would like to especially thank Ann Denu for her ability to make lab feel like a home and everything she does behind the scenes to keep it running. Jess Feldman mentored me during my first months of grad school and provided seminal work and guidance to get me on my feet. I would not be where I am if it were not for her, thank you Jess! José Moran has joined our lab this past year and I could not be more honored and excited to be passing the SIRT6 torch on to him. To Spencer, I do not think sharing a cube with anyone else would have been the same. Cheers to the friendship we have shared, the laughs we have had, and the beers we have drank.

To my partner Christina, your support and steadfastness while we have navigated graduate school together has been immeasurable. Thank you for being there with love, hugs, and stodgy foods at the end of a long day. You are my best friend and I love you dearly. Cheers to all

our adventures ahead and fun along the way. I would also like to thank our dog Zeke for his fluffy ears, emotional support, and demands for me to take a break.

Finally, I would like to thank my parents, Larry and Kate, and my brother, Peter, for their unconditional love and support. To my Dad, for taking me in to your lab when I was a kid to run TLC plates and teaching me attention to detail. To my Mom, for instilling in me your creativity and warmth. To my brother, for pursuing what interests you most and having a fun time doing it. I love you all.

## TABLE OF CONTENTS

<b>CHAPTER 1: Introduction - Biological and Catalytic Functions of SIRT6 as Targets for Small Molecule Modulators.....</b>	<b>1</b>
<b>1.1 Abstract.....</b>	<b>2</b>
<b>1.2 Introduction: Sirtuin family history and introduction to SIRT6.....</b>	<b>3</b>
<b>1.3 SIRT6 cellular and physiological functions.....</b>	<b>7</b>
1.3.1 Overview of SIRT6 molecular functions.....	7
1.3.2 DNA repair and chromatin maintenance.....	10
1.3.3 Metabolic regulation.....	14
1.3.4 Aging and lifespan.....	17
1.3.5 Cancer.....	19
<b>1.4 Molecular architecture of SIRT6.....</b>	<b>22</b>
1.4.1 Domain overview.....	22
1.4.2 Rossmann fold domain and NAD <sup>+</sup> binding.....	24
1.4.3 Zinc-binding domain.....	27
1.4.4 Hydrophobic pocket.....	29
1.4.5 N- and C-terminal extensions.....	32
<b>1.5 Catalytic activities.....</b>	<b>34</b>
1.5.1 Catalytic mechanism.....	34
1.5.2 Activation.....	39
1.5.2.1 Natural compounds as activators.....	43
1.5.2.2 Synthetic activators.....	46



1.5.2.3 Kinetic implications of SIRT6 activation.....	50
1.5.3 Inhibition.....	53
<b>1.6 Perspective.....</b>	<b>57</b>
<b>1.7 Acknowledgements.....</b>	<b>59</b>
<b>1.8 References.....</b>	<b>60</b>
<b>CHAPTER 2: Mechanism of activation for the sirtuin 6 protein deacylase.....</b>	<b>88</b>
<b>2.1 Abstract.....</b>	<b>89</b>
<b>2.2 Introduction.....</b>	<b>90</b>
<b>2.3 Results.....</b>	<b>93</b>
2.3.1 Targeted screen for SIRT6 activators.....	93
2.3.2 Biochemical characterization of small molecule activators.....	99
2.3.3 Development and analysis of CL5D as a SIRT6 activator.....	104
2.3.4 Role of CL5D in mediating SIRT6-substrate interaction.....	109
2.3.5 Identification of non-activatable SIRT6 R65A mutant.....	113
2.3.6 Characterization of SIRT6 R65A catalysis and binding parameters.....	118
2.3.7 Single turnover kinetic analysis of SIRT6 R65A demyristoylation.....	123
2.3.8 Evidence for slow conformational change after substrate binding.....	125
2.3.9 Involvement of R65 in SIRT6 conformation.....	133
<b>2.4 Discussion.....</b>	<b>134</b>
<b>2.5 Experimental procedures.....</b>	<b>138</b>
2.5.1 Expression and purification of recombinant SIRT1-3 and SIRT5-6.....	138
2.5.2 Synthesis and analysis of H3K9 peptides.....	138
2.5.3 Small molecule SIRT6 activator screen.....	139

2.5.4 Steady-state sirtuin deacylation assay and HPLC analysis.....	140
2.5.5 Synthesis of CL5D and derivatives.....	140
2.5.6 Histone extraction and immunoblot.....	141
2.5.7 Partial proteolysis.....	142
2.5.8 Fluorescence polarization.....	143
2.5.9 Global bisubstrate kinetic analysis.....	143
2.5.10 Thermal denaturation assay.....	144
2.5.11 Isothermal titration calorimetry.....	144
2.5.12 Rapid quench flow kinetics.....	145
2.5.13 Burst kinetic analysis of SIRT6 deacetylation.....	146
<b>2.6 References.....</b>	<b>147</b>
<b>CHAPTER 3: Nucleosome binding enhances SIRT6 deacetylation.....</b>	<b>154</b>
<b>3.1 Introduction.....</b>	<b>155</b>
<b>3.2 Results and discussion.....</b>	<b>158</b>
3.2.1 Nucleosome binding stimulates SIRT6 deacetylation of peptide substrate.....	158
3.2.2 Validating acetylated H3K9ac nucleosomes as a SIRT6 substrate.....	162
3.2.3 SIRT6 performs efficient deacetylation against acetylated nucleosomes.....	166
3.2.4. Small molecules can stimulate deacetylation of nucleosomes.....	171
<b>3.3 Conclusion.....</b>	<b>176</b>
<b>3.4 Experimental procedures.....</b>	<b>178</b>
3.4.1 Expression and purification of SIRT6.....	178
3.4.2 Expression and purification of 147 bp DNA.....	178
3.4.3 Expression and purification of canonical histones.....	179

3.4.4 Expression and purification of Histone H3K9ac.....	180
3.4.5 Assembly of nucleosome core particles.....	182
3.4.6 Nucleosome deacetylation assays.....	183
3.4.7 Dot blot analysis of H3K9ac.....	183
3.4.8 SIRT6 activity assays against peptide substrate.....	184
3.4.9 Culture and small-molecule treatment of mouse embryonic fibroblasts.....	185
3.4.10 Histone Isolation from mouse embryonic fibroblasts.....	186
3.4.11 Immunoblot of H3K9ac and total H3 from histone isolate.....	186
<b>3.5 References.....</b>	<b>188</b>
<b>CHAPTER 4: Development of a NanoBiT assay for monitoring binding kinetics of a SIRT6-nucleosome complex.....</b>	<b>195</b>
<b>4.1 Introduction.....</b>	<b>196</b>
<b>4.2 Results and discussion.....</b>	<b>198</b>
4.2.1 Cellular optimization of NanoBiT reconstitution by SIRT6 and histones.....	198
4.2.2 ADPr stimulates tighter binding of SIRT6 to H3K9ac nucleosomes.....	203
4.2.3 SIRT6 catalysis facilitates dissociation from nucleosomes.....	208
<b>4.3 Conclusion.....</b>	<b>212</b>
<b>4.4 Experimental procedures.....</b>	<b>214</b>
4.4.1 Cloning of NanoBiT constructs for cellular transfection.....	214
4.4.2 Transient transfection of NanoBiT constructs and luciferase detection.....	214
4.4.3 Cloning and expression of recombinant wild-type and SIRT6-LgBiT.....	215
4.4.4 Cloning and expression of recombinant SmBiT-H2B.....	216
4.4.5 Expression and purification of canonical histones.....	218

4.4.6 Expression and purification of 147 bp DNA.....	219
4.4.7 Assembly of nucleosome core particles.....	220
4.4.8 SIRT6 activity assays against peptide substrate.....	221
4.4.9 NanoBiT assay for the detection of binding equilibriums.....	221
4.4.10 Dissociation kinetic analysis by NanoBiT.....	222
<b>4.5 References.....</b>	<b>224</b>
<b>5.1 Overall conclusions from research.....</b>	<b>231</b>
<b>5.2 Future directions.....</b>	<b>235</b>
5.2.1 Evaluation of potential SIRT6 intermolecular deacetylation of nucleosomes.....	235
5.2.2 Characterization of SIRT6 deacetylation of nucleosome H3K56ac.....	238
5.2.3 Cellular application of NanoBiT system to assess SIRT6-chromatin association throughout cell-cycle progression and during DNA damage repair.....	240
<b>5.3 Impact statement.....</b>	<b>241</b>
<b>5.4 References.....</b>	<b>242</b>

## LIST OF FIGURES

Figure 1-1: SIRT6 is an NAD <sup>+</sup> -dependent protein deacylase.....	6
Figure 1-2: Cellular and molecular functions of SIRT6.....	8
Figure 1-3: Overall domain architecture of SIRT1-7.....	23
Figure 1-4: SIRT6 structural features of ligand binding and overall architecture.....	25
Figure 1-5: Mechanism of SIRT6 catalysis.....	37
Figure 1-6: SIRT6 activators bind to the terminus of the hydrophobic pocket.....	45
Figure 2-1: Identification of novel SIRT6 activators.....	95
Figure 2-2: Targeted selection of 178 additional compounds for SIRT6 screening.....	97
Figure 2-3: Characterization of SIRT6 activators identified from screen.....	101
Figure 2-4: Methylation of the CL5D carboxylate abolishes potency.....	107
Figure 2-5: Characterization of SIRT6 activator CL5D.....	108
Figure 2-6: SIRT6 displays ordered binding and CL5D does not improve H3K9ac binding....	111
Figure 2-7: Identification of the non-activatable R65A SIRT6 mutant.....	115
Figure 2-8: Kinetic analysis of SIRT6 WT and R65A demyristoylation.....	120
Figure 2-9: H3K9myr binding to SIRT6 WT and R65A.....	122
Figure 2-10: R65 facilitates conformational change during enhanced catalysis.....	127
Figure 2-11: SIRT6 burst kinetics suggest rate limiting step occurs prior to catalysis.....	129
Figure 2-12: Kinetic modeling of SIRT6 demyristoylation and activation of deacetylation....	130
Figure 3-1: Nucleosomes stimulate SIRT6 deacetylation of peptide substrate in.....	160
Figure 3-2: Recombinant nucleosomes are an <i>in vitro</i> substrate for SIRT6.....	164
Figure 3-3: SIRT6 performs efficient deacetylation of nucleosomes.....	169
Figure 3-4: CL5D fails to stimulate cellular deacetylase activity of SIRT6.....	173

Figure 3-5: MDL-800 stimulates SIRT6 deacetylation of nucleosomes.....	174
Figure 4-1: NanoBiT assay to monitor nucleosome binding by SIRT6.....	200
Figure 4-2: Determination of SmBiT and LgBiT orientation for productive luciferin.....	201
Figure 4-3: ADPr increases affinity of H3K9ac-dependent nucleosome binding by SIRT6.....	206
Figure 4-4: Catalysis facilitates nucleosome dissociation by SIRT6.....	211
Figure 5-1: Model for SIRT6 inter/intramolecular deacetylation of nucleosomes.....	237
Figure 5-2: Molecular location of H3K9 and H3K56.....	239

## LIST OF TABLES & SCHEMES

Table 1-1: Identified activators of SIRT6 deacetylation.....	42
Table 2-1: Structures of top 10 identified SIRT6 activators from small molecule screening.....	98
Table 2-2: Dose-response and Michaelis-Menten parameters of activation by novel SIRT6 activators.....	102
Scheme 2-1: Mechanism of SIRT6 catalyzed deacetylation.....	103
Table 2-3: Structure-activity relationship of CL 5D and derivatives.....	106
Table 2-4: Steady-state rates of deacetylation for SIRT6 point mutants.....	117
Table 2-5: Sequential bi-substrate reaction parameters and single-turnover rates for SIRT6 WT and R65A demyristoylation.....	121

## **CHAPTER 1: Introduction - Biological and Catalytic Functions of SIRT6 as Targets for Small Molecule Modulators\***

**Mark A. Klein<sup>1,2</sup> & John M. Denu<sup>1,2, Ψ</sup>.**

From the <sup>1</sup>Wisconsin Institute for Discovery, University of Wisconsin-Madison; <sup>2</sup>Department of Biomolecular Chemistry, School of Medicine and Public Health, University of Wisconsin-Madison.

\*This chapter was published in the Journal of Biological Chemistry. 2020 Aug 7; 295: 11021-11041

## ***1.1 Abstract***

SIRT6 is an NAD<sup>+</sup>-dependent deacetylase of histone H3 that regulates genome stability and gene expression. However non-histone substrates and additional catalytic activities including long-chain deacylation and mono-ADP-ribosylation of proteins are reported. At the physiological level, SIRT6 activity promotes increased longevity by regulating metabolism and DNA repair. Recent work has identified natural products and synthetic small molecules capable of activating the inefficient in vitro deacetylase activity of SIRT6. Here, we discuss the cellular functions of SIRT6 with a focus on attributing catalytic activity with proposed biological functions. We cover the molecular architecture and catalytic mechanisms that distinguish SIRT6 from other NAD<sup>+</sup>-dependent deacylases. We emphasize the development of small molecule modulators that provide biological insight into SIRT6 functions and a therapeutic pathway to treat metabolic and age-associated diseases.



## ***1.2 Introduction: Sirtuin family history and introduction to SIRT6***

Sirtuin 6 (SIRT6) is a histone deacetylase with critical homeostatic roles in many cellular pathways. SIRT6-deficient mice display spontaneous genomic instability, dysregulated glycolysis, increased tumorigenesis, and early onset aging-like degeneration ultimately dying at around 4 weeks (1, 2). Loss-of-function homozygous mutation of SIRT6 led to brain and muscle developmental defects and ultimately in late fetal loss, marking the first instance of a mutated chromatin factor causing perinatal lethality in humans (3). Similar phenotypes were observed in a SIRT6-knockout study using CRISPR-Cas9 generated cynomolgus monkeys, indicating a conserved and obligatory role for SIRT6 function in primate development (4). Loss-of-function mutations were identified in naturally arising human cancers and later shown to be sufficient to drive tumor formation in mice (5). These genetic insights illustrate critical cellular functions of SIRT6 and establish the need to understand which catalytic functions and molecular pathways are driving SIRT6 associated phenotypes.

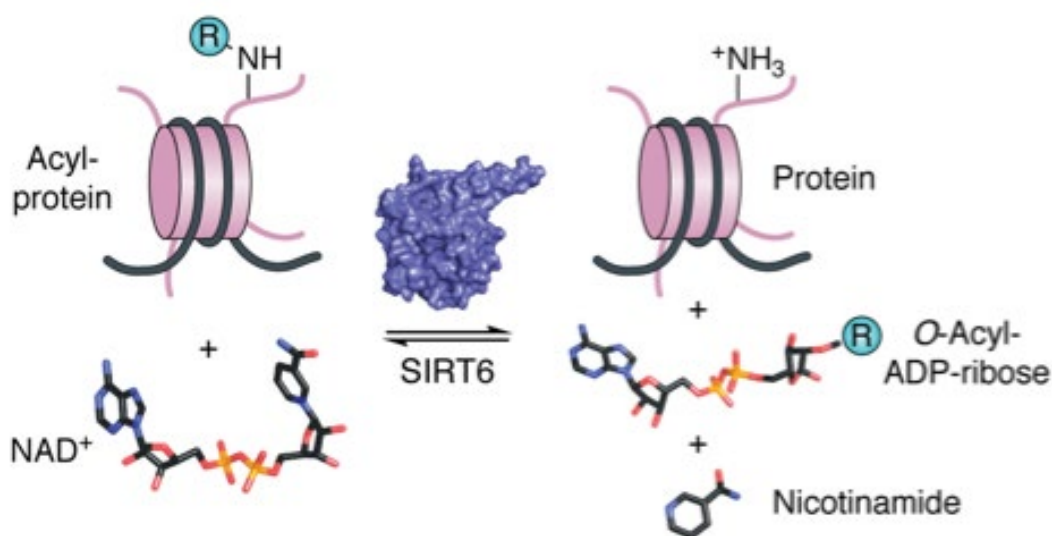
SIRT6 is a member of a highly conserved family of enzymes that couple nicotinamide adenine dinucleotide (NAD<sup>+</sup>) cleavage to the removal of an acyl-group from the lysine of protein substrates, producing deacylated protein, nicotinamide, and *O*-acyl-ADP-ribose (Fig. 1-1). Prior to the discovery of enzymatic activity, the founding member of this family, Sir2 (silent information regulator 2), was identified in *Saccharomyces cerevisiae* from a screen for genome silencing factors (6–8) and was later shown to promote longevity by suppressing the formation of extrachromosomal rDNA circles (9–11). Compelling evidence indicates that Sir2 represses transcription at silent mating type loci and subtelomeric sequences via its histone deacetylase activity (8, 12–14).

Sirtuin homologs exist in all phyla of life (15–17) and comprise class III histone deacetylases (HDACs) which uniquely utilize  $\text{NAD}^+$  as a cofactor of catalysis rather than a catalytic zinc as observed in class I, II, and IV HDACs (18). The catalytic requirement for  $\text{NAD}^+$  has led the field to regard sirtuins as critical factors linking energy metabolism to cellular homeostasis (19). Although initially defined as histone deacetylases, sirtuins have many non-histone substrates and can catalyze the removal of acetyl, long-chain acyl, and acid acyl moieties from lysine substrates. The seven mammalian sirtuins (SIRT1-7) show varying cellular localization and regulate diverse functions. All sirtuins can catalyze the removing of an acyl-group of the  $\epsilon$ -amino of lysine, though the specificities for distinct acyl groups and catalytic efficiencies vary greatly.

Mechanistic studies of SIRT6 activity lagged behind those of other sirtuins owing in part to the difficulty in detecting *in vitro* deacetylase activity. As with the early reports on Sir2 and other Sirtuins, the possibility that SIRT6 acts as a protein ADP-ribosyltransferase was reported (20–22). The development of more sensitive assays revealed that SIRT6 is a deacetylase with catalytic efficiencies nearly  $\sim 100$ -1000 times lower than the most active sirtuins (23). Strong support for enzymatic deacylation activity was provided when it was revealed that SIRT6 is a more efficient long-chain deacylase and can be catalytically activated towards deacetylation by small molecules, many of which are long-chain fatty acids (24, 25). SIRT6 is implicated in many diverse biological functions, although the specific biochemical activity essential for each phenotype remains rather murky. Identifying which activity mediates which biological phenotype is therefore critical to understand the molecular functions of SIRT6 and to accurately develop small-molecule effectors that target appropriate activities. Here we highlight cellular functions ascribed to SIRT6 where evidence allows the inherent biochemical activities of SIRT6 to be matched with the

observed phenotype. The first section of this review covers the physiological and cellular phenotypes noted when SIRT6 is removed, mutated, or overexpressed. We comment on the strength of the evidence linking biological functions with biochemical activity and provide substrate identities when possible. SIRT6 has emerged as a potential therapeutic target given its biological roles and ability to be modulated by small molecules. The prospect of targeting SIRT6 necessitates a detailed understanding of its structure and biochemical activities. Accordingly, we devote much of this review to describe the unique structural and catalytic features of SIRT6, with particular attention paid to small-molecule modulators that have the potential to resolve SIRT6 functions and provide a pathway for SIRT6-targeted therapeutics.

**Figure 1-1: SIRT6 is an NAD<sup>+</sup>-dependent protein deacylase.** SIRT6 couples the cleavage of NAD<sup>+</sup> to the removal of an acyl-group from substrate protein. Catalysis produces deacylated protein, *O*-acyl-ADP-ribose, and nicotinamide. Acyl modifications (-R) of lysine can be but are not limited to acetyl, propionyl, hexanoyl, octanoyl, decanoyl, dodecanoyl, myristoyl, or palmitoyl moieties.



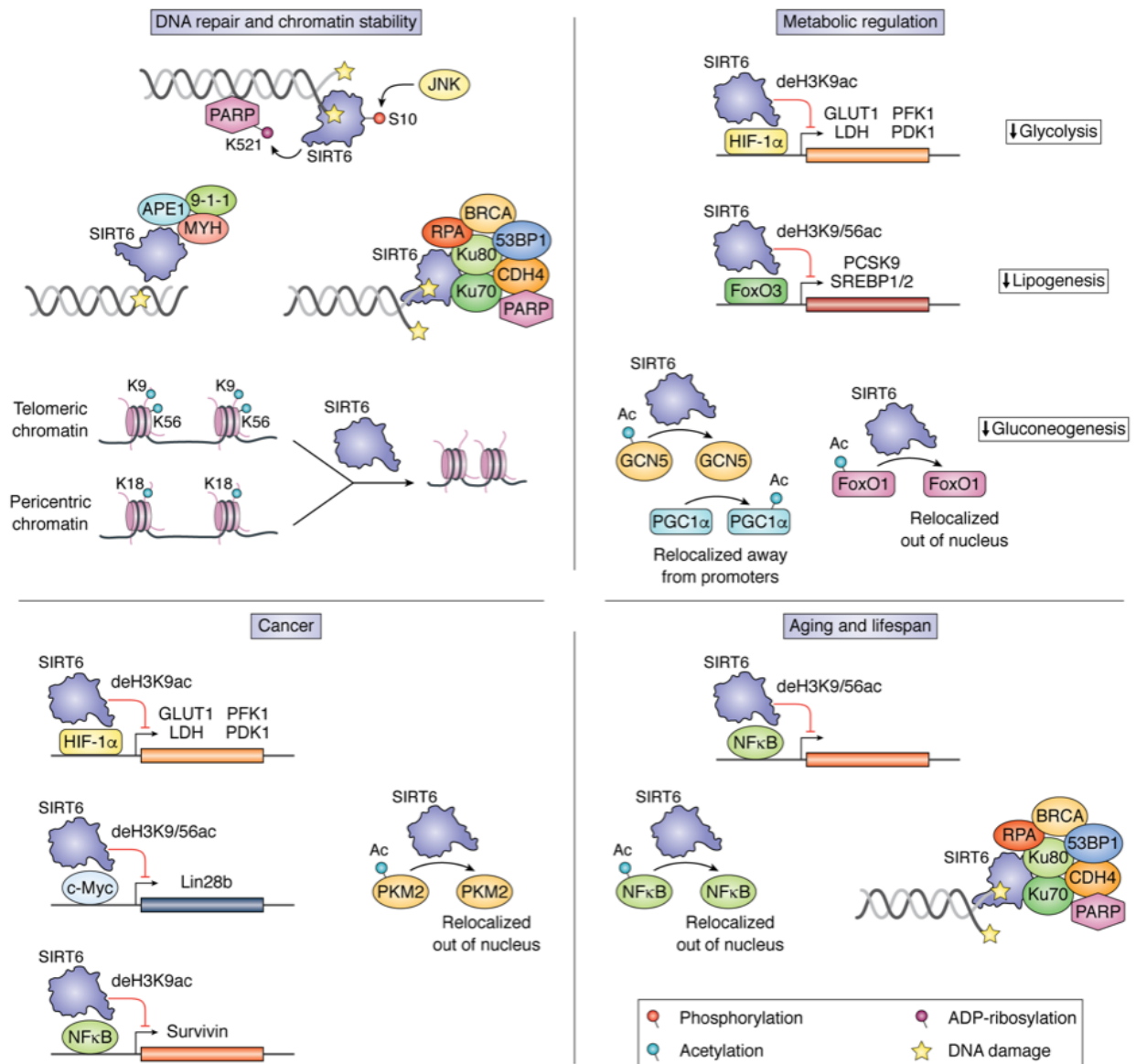
### ***1.3 SIRT6 cellular and physiological functions***

#### ***1.3.1 Overview of SIRT6 molecular functions***

SIRT6 is localized to the nucleus where it mediates DNA repair, regulates the expression of metabolic genes, and maintains genomic stability (Fig. 1-2). Through these functions, SIRT6 has been described as a tumor suppressor and positive regulator of longevity. Evidence indicates that SIRT6 regulates these processes primarily via deacetylation of histone and non-histone proteins, though long-chain deacylation, ADP-ribosylation and recruitment of proteins to chromatin are other biochemical functions ascribed to some SIRT6-dependent phenotypes. This review will focus on processes in which direct SIRT6 substrates or protein binding partners have been identified.

**Figure 1-2: Cellular and molecular functions of SIRT6.** SIRT6 is a critical regulator of cellular homeostasis with roles in mediating DNA repair, regulating expression of genes, and maintaining genomic stability. This figure outlines mechanistically understood functions of SIRT6 that contribute to DNA repair and chromatin stability, metabolic regulation, cancer, and aging and lifespan. These functions can be broadly separated into three classes: (1) recruitment of factors to chromatin, (2) corepression of transcription factors through histone deacetylation, and (3) deacetylation of non-histone proteins resulting in a change of localization or activity. In addition to these functions, SIRT6 also acts as a pioneer factor through direct binding of DNA damage and performs global deacetylation of pericentric and telomeric DNA to prevent aberrant transcription and telomeric damage.

**Figure 1-2: Cellular and molecular functions of SIRT6**



### *1.3.2 DNA repair and chromatin maintenance*

Some of the earliest phenotypic studies on SIRT6 knockout cells demonstrated increased susceptibility to DNA damaging agents and higher levels of chromosomal aberrations, suggesting a critical role for SIRT6 in maintaining genomic stability (1). Later reports demonstrated that SIRT6 is recruited to double-strand breaks (DSB) within seconds and further recruits DNA repair factors to initiate DNA damage response (DDR) (26, 27). This fast response is attributed to the ability of SIRT6 to directly bind to open-ended DSBs, where Onn et al. postulate that each monomer of a SIRT6 dimer binds one loose ssDNA end of a DSB (28). Onn et al. suggested a potential DNA binding tunnel along the core of SIRT6 that mediates ssDNA binding independent of the N- and C-termini. Another study demonstrated that JNK phosphorylates SIRT6 on Ser-10 in response to oxidative stress, leading to binding of SIRT6 to DSBs and subsequent recruitment and mono-ADP-ribosylation of poly(ADP-ribose) polymerase 1 (PARP1) (29). The mechanism by which PARP1 is recruited to DSB following SIRT6 phosphorylation and whether this is mediated by direct SIRT6 interactions is unknown. Serine 10 is located on the N-terminus of SIRT6 that was previously shown to be dispensable for DNA binding, suggesting multiple pathways of passive and active recruitment to DSBs (30).

Following recruitment of SIRT6 to sites of DNA damage, multiple studies have indicated contexts in which SIRT6 either deacetylates nucleosomes or actively recruits repair factors to mediate DDR. SIRT6 knockout mouse embryonic fibroblasts and knockdown human fibroblasts show impaired non-homologous end joining (NHEJ) and homologous recombination (HR) efficiencies, respectively, whereas SIRT6 overexpression improves both processes (21). Mao et al. demonstrated that this effect was facilitated by SIRT6-mediated recruitment of repair factors 53BP1 and NBS1 to sites of DNA-damage, and loss-of-function mutants suggested that both



deacetylase and ADP-ribosyltransferase activities of SIRT6 were required to facilitate NHEJ (21). The requirement of SIRT6 ADP-ribosyltransferase activity was attributed to the modification of the DNA repair factor PARP1 on Lys-521, resulting in its activation, however the target of the requisite deacetylase activity in this study was not identified. Separately, SIRT6 has been shown to globally deacetylate H3K9 in response to DNA damage and co-localize with DNA-dependent protein kinase, Ku70, and Ku80 at DSBs (27), although it remains unknown which factor pioneers DSB binding. Hou et al. showed that SIRT6 can recruit chromodomain helicase DNA-binding protein 4 (CDH4) to sites of DNA damage to facilitate chromatin relaxation and efficient homologous recombination (31). This effect was lost with the SIRT6 catalytic mutant H133Y, implicating a role for SIRT6 catalysis in this DDR pathway. Toiber et al. reported that SIRT6 deacetylates H3K56 in response to DNA damage and recruits the SNF2H chromatin remodeler, making chromatin more accessible and allowing for efficient recruitment of DNA repair factors RPA, 53BP1, BRCA1 (26). In this study, sites of DNA damage were identified by the presence of  $\gamma$ H2AX (26), a phosphorylated form of the histone subtype H2AX present at sites of DSBs (32, 33). A complex containing SIRT6 and SNF2H was later reported to stabilize  $\gamma$ H2AX at DSB sites (34). In contrast to the well-studied roles of SIRT6 in DSB repair, limited data also suggests that SIRT6 mediates base excision repair (BER). Overexpression of SIRT6 exhibited improved BER efficiency in mouse fibroblasts while deletion increased sensitivity to BER associated DNA-damaging agents (1, 35). Separate studies demonstrated that SIRT6 interacts with and stimulates BER factors including APE1, MYH, and Rad9-Rad1-Hus1 following oxidative damage (36). A recent study compared SIRT6 proteins from rodents with varying lifespan and found a correlation between SIRT6-mediated DSB repair efficiency and the lifespan of the host organism (37). The difference between repair efficiencies of orthologous SIRT6 enzymes was largely isolated to 5

amino acids that were predicted to be surface exposed based on homology modeling with human SIRT6. Substitution of these five amino acids from a short-lived mouse SIRT6 sequence to those of long-lived beaver SIRT6 sequence were sufficient to increase NHEJ and decrease global acetylation in culture and improve the survivability of human fibroblasts exposed to  $\gamma$ -irradiation (37).

Several studies implicated roles for SIRT6 in maintaining genome stability through the repression of telomeric and pericentric regions of chromatin. SIRT6 was shown to deacetylate telomeric chromatin in mammalian cells at H3K9 and H3K56 (38, 39). Michishita et al. reported that SIRT6 deacetylation of H3K9 was required for stable association of WRN protein and depletion of SIRT6 resulted in telomeric defects that resembles those observed in Werner syndrome, an aging disorder characterized by mutated WRN (38). Furthermore, SIRT6 deficient HeLa cells displayed telomeric sequence loss, genomic instability, and chromosomal end-to-end fusions (40). Following oxidative damage, Gao et al. observed that SIRT6 was required for directional telomere movement, a process that facilitates efficient DNA damage repair at telomeric chromatin (41). Additionally, SIRT6 overexpression in mice was reported to upregulate telomerase reverse transcriptase and telomere repeat binding factor, although this study did not explore the mechanism of upregulation or potential downstream effects on telomere length (42). Proper mitosis requires condensed pericentric heterochromatin at centromeres to protect against genomic instability and cellular senescence during cell division. Tasselli et al. showed that SIRT6 repressed these regions through the deacetylation of H3K18 and also noted that knockdown of SIRT6 resulted in hyperacetylation and aberrant transcription of these pericentric chromatin domains (43). Collectively, SIRT6's ability to deacetylate proteins, ADP-ribosylate PARP1, or to mediate protein-protein interactions with repair proteins have been implicated in controlling DNA stability

and repair. Clearly, better genetic and biochemical tools are needed to provide a deeper molecular understanding of which biochemical functions of SIRT6 control various aspects of these processes and dictate histone substrate specificity. The development of better tools will require a robust understanding of catalytic mechanism, regulated activity, and structure-function relationships. Therefore, our current knowledge in these areas is presented later in the review. Despite these outstanding questions, the extensive research summarized here depicts a clear role for SIRT6 in facilitating DNA repair and stabilizing heterochromatic regions.

### 1.3.3 Metabolic regulation

A number of studies have demonstrated the ability of SIRT6 to maintain cellular homeostasis through the regulation of glucose and lipid metabolism. Early studies characterizing SIRT6 knockout mice showed a lethal phenotype at 2-3 weeks of age likely resulting from hypoglycemia (1, 44). This hypoglycemic phenotype was later attributed to misregulation of glycolytic genes in the absence of SIRT6. Specifically, SIRT6 was found to co-repress the transcription factor hypoxia-inducible factor 1- $\alpha$  (HIF-1 $\alpha$ ), in effect downregulating glycolytic genes including glucose transporter-1 (GLUT1), lactate dehydrogenase (LDH), phosphofructokinase-1 (PFK1), and pyruvate dehydrogenase kinase-1 (PDK1) (45). In the same study, SIRT6 was reported to directly inhibit expression of these genes by deacetylating H3K9 at promoters of targeted genes. SIRT6 knockout resulted in the derepression of these glycolytic genes and increased glucose uptake, reminiscent of the “Warburg effect”, a metabolic hallmark often observed in cancer cells (46). Accordingly, SIRT6 loss-of-function mutation and downregulation is observed in several naturally arising human cancers. Mouse model studies by Sebastián et al. and Kugel et al. demonstrated that loss-of-function mutation in SIRT6 was sufficient to form tumors and was independent of known oncogene activation (2, 5). A detailed summary of the roles of SIRT6 in cancer are discussed in a following section. Separately, Gertman et al. generated two SIRT6 mutants with enhanced *in vitro* rates of  $k_{cat}$  against long-chain myristoyl-substrate. Stable transfection of these mutants in mouse embryonic fibroblasts demonstrated an increased ability to inhibit the expression of GLUT1, PDK1, and PFK1 relative to wild-type SIRT6. Interestingly, a global increase in acetylation of H3K9 and H3K56 (47) was noted, suggesting that the demyristoylase activity of SIRT6 may regulate glycolysis and may be distinct from H3 deacetylase activity. However, these mutants also bound HIF-1 $\alpha$  more tightly *in vitro* making it difficult to

definitively conclude whether more efficient recruitment to HIF-1 $\alpha$  genes or higher demyristoylase activity was responsible for the downregulation of these glycolytic genes (47).

SIRT6 also regulates glucose metabolism by inhibiting gluconeogenesis, a metabolic process that generates glucose from non-carbohydrate sources. Mostoslavsky et al. found that SIRT6 knockout mice are hypoglycemic and display elevated expression of gluconeogenic genes (1). Although this observation alone could simply be dismissed as a proper liver response to hypoglycemia, work by Dominy et al. demonstrated active regulation of gluconeogenesis in the liver by SIRT6. Mechanistically, SIRT6 was described to deacetylate general control non-repressed protein 5 (GCN5) which enhanced its acetyltransferase activity towards peroxisome proliferator-activated receptor- $\gamma$  coactivator 1- $\alpha$  (PGC-1 $\alpha$ ) (48). PGC-1 $\alpha$  is the primary regulator of hepatic gluconeogenesis and induces the expression of gluconeogenic genes (49). Following acetylation by GCN5, PGC-1 $\alpha$  was found to relocate away from the promoters of gluconeogenic genes resulting in decreased expression (48). Another study demonstrated that SIRT6 overexpression reduced gluconeogenic gene expression in wild type, but not Forkhead box O1 (FoxO1) knockout mice (50). FoxO1 is a transcription factor required for activation of gluconeogenic genes in hepatic cells (49). Subsequent work by Zhang et al. mechanistically described the FoxO1/SIRT6 regulatory axis by demonstrating that SIRT6 directly deacetylates FoxO1 leading to its nuclear export, thus resulting in decreased gluconeogenic gene expression (51).

SIRT6 has also been implicated in the regulation of lipid metabolism with studies reporting roles in both lipolysis and lipogenesis. Early work in mice demonstrated that liver specific knockout of SIRT6 resulted in fatty liver formation owing to increased triglyceride synthesis and reduced  $\beta$ -oxidation, whereas mice overexpressing SIRT6 were protected from the accumulation

of visceral fat, LDL-cholesterol, and triglycerides when fed high-fat diets (52, 53). Fat-specific SIRT6 knockout increased obesity-related phenotypes in mice (54, 55). Mechanistically, SIRT6 was found to represses the expression of proprotein convertase subtilisin/kexin type 9 (PCSK9) and sterol-regulatory element binding protein 1 and 2 (SREBP1 and SREBP2). This was demonstrated to occur through SIRT6 recruitment to the promoter of *Pcsk9*, a critical regulator of LDL-cholesterol, via interactions with the transcription factor FoxO3 where SIRT6 deacetylates H3K9 and H3K56 to reduce expression of *Pcsk9*, resulting in lowered LDL-cholesterol levels (56). FoxO3 was also shown to recruit SIRT6 to promoters of SREBP genes, positive regulators of lipogenic genes, resulting in inhibition of expression by promoter-specific SIRT6 deacetylation of H3K9 and H3K56 (57–59). Interestingly, miRNAs expressed from the introns of SREBP, miR-33a and miR-33b, as well as the most common hepatic miRNA, miR-122, were shown by Elhanati et al. to downregulate SIRT6 expression, indicating intricate regulation of SIRT6 towards lipid metabolism (58, 60). Separately, SIRT6 was noted to promote  $\beta$ -oxidation of fatty acids during fasting through regulation of the PPAR $\alpha$  coactivator, NCOA2. In this distinct mechanism, SIRT6 was found to decrease NCOA2 acetylation at Lys-780 resulting in the activation of PPAR $\alpha$  and increased expression of hepatic  $\beta$ -oxidation genes (61). It remains to be determined whether NCOA2 Lys-780 is a direct substrate of SIRT6 deacetylation.

### 1.3.4 Aging and lifespan

The yeast homolog and founding member of the sirtuin family, Sir2, is implicated in lifespan extension through repression of tandem ribosomal RNA gene arrays (rDNA) (62, 63). Subsequent studies have solidified links between aging and the mammalian homolog, SIRT6. SIRT6 overexpression in mice was found to extend the lifespan of male mice by 15% in a mechanism thought to be driven through reduced insulin-like growth factor 1 (IGF1) signaling. Zhang et al. demonstrated that caloric restriction prevented aging-related renal insufficiency and suggested that this effect was mediated via the upregulation of SIRT6 in response to caloric restriction, which resulted in the repression of nuclear factor- $\kappa$ B (NF- $\kappa$ B) (64). NF- $\kappa$ B is a nuclear transcription factor associated with inflammatory responses, aging, and apoptosis (65). SIRT6 was found to represses NF- $\kappa$ B activity both by deacetylating H3K9 at NF- $\kappa$ B promoters and by deacetylating Lys-310 of the NF- $\kappa$ B p65 subunit (RelA) resulting in its nuclear export (64). Xu et al. observed a decrease in SIRT6 levels with age in human fibroblasts (35). In separate studies, aging-related decreases in SIRT6 levels impaired the reprogramming potential of iPSCs from old mice and decrease DNA repair efficiency (66, 67). Another study demonstrated that increased copy number of *Sirt6* was sufficient to restore lifespan in *Atm*, a DNA repair factor, deficient *C. elegans* (68). Studies on human populations have discovered various single nucleotide polymorphisms that correlate both positively and negatively with longevity (69–71). The mechanistic outcomes of these polymorphisms are yet unknown; however, they present a potentially powerful tool for further probing the link between SIRT6 and aging. Work by Tian et al., discussed previously, compared long and short-lived rodents and demonstrated a SIRT6-mediated increase in DNA-repair efficiency among long-lived species corresponding to increased *in vitro* deacetylase and self mono ADP-ribosyltransferase activities (37). Transgenic *Drosophila*

expressing beaver (long-lived) SIRT6 showed increased lifespan relative to those expressing mouse (short-lived) SIRT6, directly linking SIRT6 activity to increased lifespan.



### *1.3.5 Cancer*

With dysregulated DNA damage repair and metabolic homeostasis as hallmarks of cancer, SIRT6 has been implicated in oncogenesis, proliferation, and poor prognosis. Downregulation of SIRT6 in human cancers has been reported in hepatocellular carcinomas, ovarian cancers, and colon cancers (72–75). Furthermore, the cancer cell line encyclopedia reports that the SIRT6 gene is deleted in 35% of all cancer cell lines in their database (76, 77). SIRT6 knockout in mouse embryonic fibroblasts led to tumor formation in mouse xenograft studies independent of known oncogene activation (2). This tumorigenesis was attributed to derepression of glycolytic genes resulting in a Warburg-like phenotype characterized by increased glucose uptake and anaerobic glycolysis. Similarly, SIRT6 point mutations identified in human cancers were shown to be loss-of-function and xenograft studies by Kugel et al. demonstrated that these loss-of-function mutations were sufficient to drive tumor formation in mice (5). Copy loss number of SIRT6 has been observed in 60% of pancreatic cancer cell lines and studies on low SIRT6-expressing cell lines demonstrated accelerated tumorigenesis in a mechanism independent of enhanced glycolysis (78). Rather, SIRT6 was shown to deacetylate H3K9 and H3K56 at the promoter of Lin28b, an RNA-binding fetal oncogene that promotes transformation and tumor progression (78, 79). It was therefore concluded by Kugel et al. that loss of SIRT6 leads to c-Myc transcription factor driven overexpression of Lin28b and subsequent tumor growth. Additionally, SIRT6 was shown to deacetylate H3K9 at the promoter of survivin, an oncoprotein upregulated in most cancers that impairs tumorigenesis (72, 80). Positive outcomes for breast cancer patients correlated with SIRT6 levels and inversely correlated with SIRT6 phosphorylation at Ser-338 (81). This was mechanistically supported through the demonstration that Ser-338 phosphorylation of SIRT6 by the kinase AKT1 induced SIRT6 ubiquitination by MDM2, targeting SIRT6 for protease

degradation. In colon cancer cells, USP10 was found to be critical for deubiquitinating SIRT6 and stabilizing protein levels in order to negatively regulate the transcriptional activity of the c-Myc oncogene (82). In separate studies, SIRT6 SUMOylation was shown to promote interaction with c-Myc, resulting in the deacetylation of H3K56, but not H3K9, and transcriptional repression at the promoters of c-Myc genes (83). The site of SIRT6 SUMOylation was localized to the C-terminus and isolated to either Lys-296, Lys-300, Lys-316, or Lys-332. Furthermore, Bhardwaj et al. demonstrated that SIRT6 interacts with and deacetylates nuclear pyruvate kinase M2 (PKM2), an oncogenic transcriptional coactivator, on Lys-433 which resulted in its nuclear export and a downstream reduction in cell proliferation, migration potential, and invasiveness (84).

Despite the vast majority of data supporting the roles of SIRT6 as a tumor suppressor, some evidence suggests that SIRT6 may promote tumor survival in a context dependent manner. It has been observed that SIRT6 is upregulated in cases of squamous cell carcinoma, chronic lymphocytic leukemia, multiple myeloma, and acute myeloid leukemia (85–88). Three of the aforementioned diseases are hematopoietic cancer lines which curiously are the only tumor type exhibiting gain of SIRT6 gene copies according to the cancer line encyclopedia (2, 77). In the case of multiple myeloma, a disease characterized by a highly unstable genome, Cea et al. noted increased SIRT6 expression as an adaptive response to combat genomic instability (85). In acute myeloid leukemia, SIRT6 overexpression was demonstrated to protect tumors from DNA damage through the deacetylation and activation of DNA-dependent protein kinase (DNA-PKcs), a DDR element that facilitates DSB repair (85, 89). In the same study, SIRT6 depletion in multiple myeloma cells was found to potentiate genotoxic treatment and increase proliferation rate. Mechanistically, SIRT6 was shown to interact with the transcription factor ELK1 to deacetylate H3K9 and suppress the expression of ERK signaling-related genes and reduce proliferation (85).

Bauer et al. reported that SIRT6 promotes metastasis through the upregulation of pro-inflammatory cytokines including IL8 and TNF- $\alpha$  (90). This effect was noted to occur through SIRT6 catalytic activity, resulting in increased intracellular ADP-ribose levels, an activator of the Ca<sup>2+</sup> channel TRPM2 required for LPS-induced production of IL8 and TNF-  $\alpha$  (90, 91). In hepatocellular carcinoma (HCC), Lee et al. identified SIRT6 as a tumor promoter that prevented DNA damage and cellular senescence (92). Separate studies of HCC by Ran et al. identified a separate oncogenic role for SIRT6. Namely, SIRT6 was found to deacetylate H3K9 at the promoter of Bcl-2-associated X protein (Bax), an apoptotic activator, resulting in HCC protection from apoptosis (93). Contrasting research by Zhang et al. suggested a tumor suppressing role of SIRT6 towards HCC cells by blocking the ERK1/2 signaling pathway, although the mechanism of SIRT6/ERK crosstalk is unknown (94).

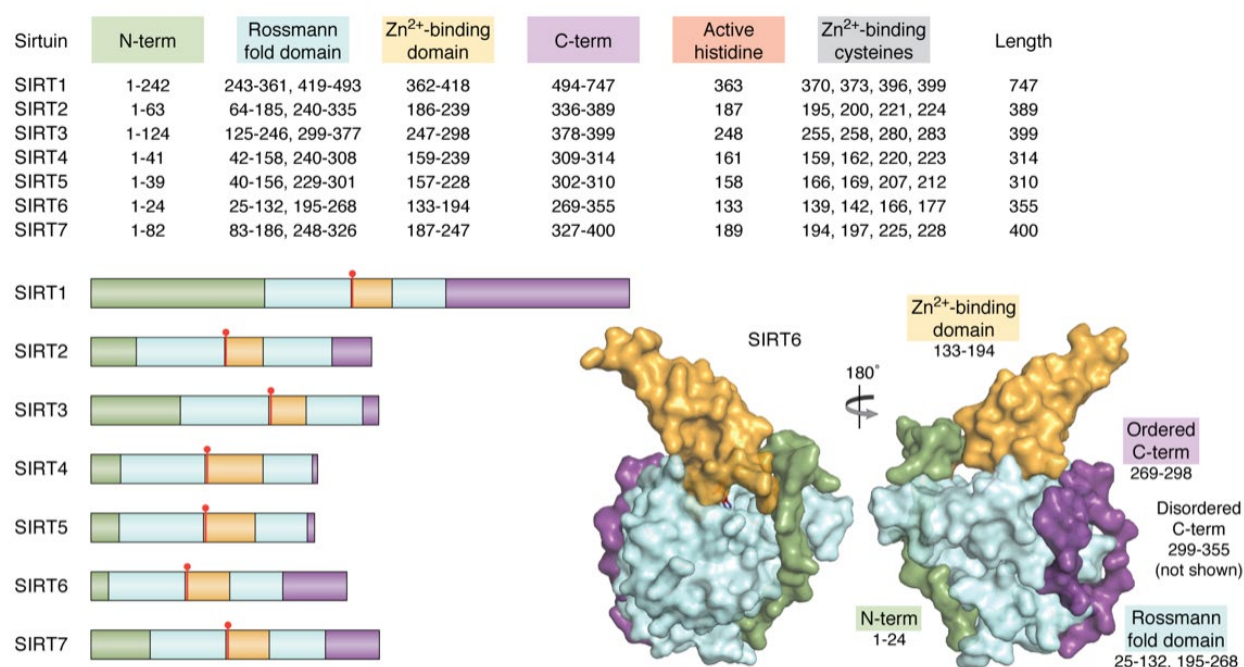
Clearly, SIRT6 is an important regulator of metabolism and genome maintenance, and the ability to suppress tumor formation is well documented. Nevertheless, cell and context dependent examples of SIRT6-driven tumor survival have also been reported. These contrasting studies suggest a complex role for SIRT6 in tumor development and survival that is still being evaluated. One interpretation of current data is that within the context of a healthy cell, DNA repair and genomic stability prevents oncogenesis, however following specific types of transformation, these same functions can protect the aberrant cells from genotoxic therapies or the accumulation of excess deleterious mutations. The context-dependent role of SIRT6 as either a tumor suppressor or tumor driver opens the door to informed disease specific pharmacological activation or inhibition. Likewise, the development of small molecule SIRT6 modulators will aid the study of SIRT6 activity in varying disease contexts.

## ***1.4 Molecular architecture of SIRT6***

### ***1.4.1 Domain overview***

Sirtuin 1-7 are an evolutionarily conserved family of enzymes that share a core catalytic domain spanning approximately 250 amino acids (Fig. 1-3). The catalytic core comprises an NAD<sup>+</sup>-binding Rossmann fold domain and a structural zinc-binding domain containing four conserved cysteine residues which coordinate a zinc ion (95). Catalysis occurs in a hydrophobic cleft situated between these two domains that varies in size and composition between sirtuin family members to confer specificity towards acyl-substrates (24, 96, 97). Additionally, sirtuins contain diverse N- and C-termini that can direct cellular localization and protein-protein interactions.

**Figure 1-3: Overall domain architecture of SIRT1-7.** Sirtuins share a conserved catalytic core consisting of a Rossmann fold domain (light blue), Zn<sup>2+</sup>-binding domain (orange), and catalytic histidine (red). Human sirtuins have unique N- (green) and C-terminal (purple) domains that vary in length and sequence. The overall architecture of SIRT6 shows that the Rossmann fold domain, although separated by primary sequence, forms a single globular domain that the N-terminus and part of the C-terminus (269-294) are structured around. The majority of the C-terminus (295-355) is disordered and has not been structurally solved. This structure was produced using 3ZG6 from the RCSB protein data bank.

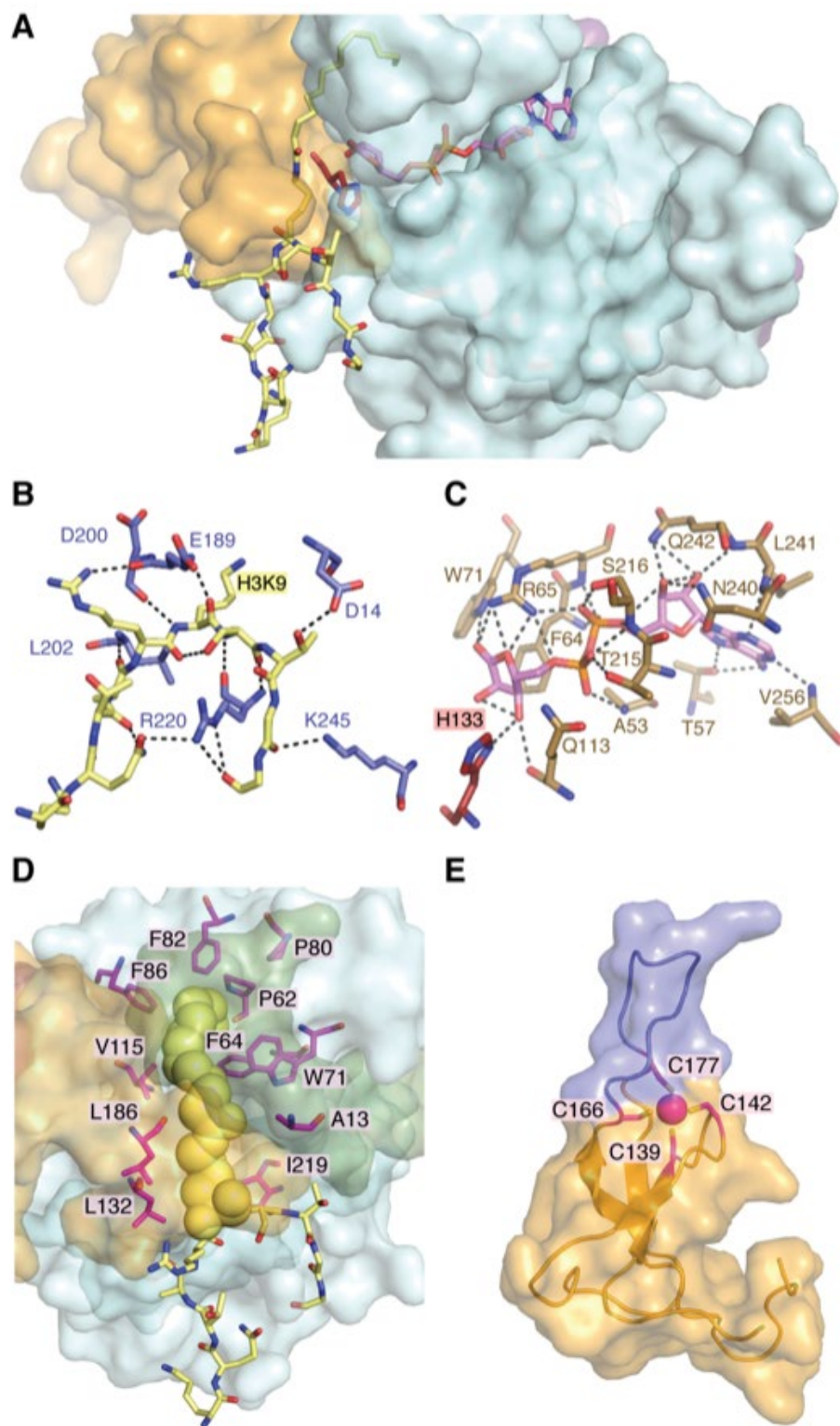


### 1.4.2 Rossmann fold domain and NAD<sup>+</sup> binding

SIRT6 contains a Rossmann fold structural motif responsible for NAD<sup>+</sup>-binding that is common among nucleotide-binding proteins (Fig. 1-3) (98). This domain spans residues 27-132 and 195-268 and is structurally represented by a six-stranded parallel  $\beta$ -sheet in between two helices on one side and four helices on the other (23). The Rossmann fold domain forms a platform for the NAD<sup>+</sup>-binding site while the flanking cofactor binding loop forms additional contacts with NAD<sup>+</sup> to stabilize the bound form (99). Structural analysis of bound adenosine diphosphate ribose (ADPr) revealed 18 possible polar contacts between primarily the Rossmann fold domain and ADPr (Fig. 1-4C). ADPr is an NAD<sup>+</sup> metabolite lacking the nicotinamide moiety that inhibits SIRT6 catalysis, suggesting it similarly occupies the NAD<sup>+</sup>-binding pocket (23, 100). Substrate binding by SIRT1-3 has been reported to follow an ordered binding mechanism in which acetyl-peptide precedes that of NAD<sup>+</sup> (101, 102). SIRT6 is the only known sirtuin to bind NAD<sup>+</sup> in the absence of acyl-substrate (23, 103). The ability to bind NAD<sup>+</sup> in the absence of acyl-peptide substrate is structurally explained by the NAD<sup>+</sup> binding loop of SIRT6 maintaining an ordered helix in the absence of peptide substrate (23), whereas this loop is disordered in the absence of substrate for SIRT2,3,5 (101, 104, 105). Interestingly, a naturally occurring point mutation (D63Y) in human cancer exists in the NAD<sup>+</sup>-binding loop and has been shown to abolish deacetylase activity (5). Additionally, a study by Mao et al. reported that S56Y and R65A variants lacked cellular deacetylase activity (21). Subsequent studies further demonstrated that Arg-65 is critical for *in vitro* activation of deacetylation (103). These studies suggest that the NAD<sup>+</sup>-binding domain of SIRT6 is a hotspot for loss-of-function mutation.

**Figure 1-4: SIRT6 structural features of ligand binding and overall architecture.** SIRT6 sequentially binds  $\text{NAD}^+$  followed by acyl-substrate prior to initiating chemical catalysis. The non-catalytic  $\text{NAD}^+$  surrogate lacking nicotinamide, ADP-ribose, is often used in structural studies to prevent catalytic turnover. *A)* ADP-ribose (pink) binds to the interior of the Rossmann fold domain with the nicotinamide-ribose proximal to the catalytic His-133 (red). H3K9 myristoyl peptide (yellow) binds to the solvent exposed exterior of both the Rossmann fold and  $\text{Zn}^{2+}$ -binding domain with the substrate lysine inserted in to the catalytic site proximal to the opposing side of His-133. The N-terminus has been excluded to more clearly demonstrate the relative positioning of ligands. *B)* Polar contacts between the H3K9 peptide substrate (yellow) and residues SIRT6 (light blue). *C)* Extensive polar contacts between residues of SIRT6 (tan) and ADP-ribose (pink). *D)* SIRT6 contains an extended hydrophobic tunnel, relative to the latent tunnels observed in other structurally solved sirtuins, that accommodates the myristoyl-chain (yellow spheres) of an H3K9myr peptide (yellow sticks). This hydrophobic tunnel is formed between the Rossmann fold domain (light blue surface) and  $\text{Zn}^{2+}$ -binding domain (orange surface), is composed of numerous nonpolar residues (magenta sticks) and is sealed by the N-terminus (green surface). *E)* The  $\text{Zn}^{2+}$ -binding domain of SIRT6 utilizes four conserved cysteines (magenta sticks) to coordinate a zinc-ion (magenta sphere). This domain contains a 10 amino acid extension between the third and fourth cysteines resulting in an unordered loop (blue) unique to SIRT6. These structures were produced using 3ZG6 from the RCSB protein data bank.

Figure 1-4: SIRT6 structural features of ligand binding and overall architecture.





### 1.4.3 Zinc-binding domain

The  $\text{Zn}^{2+}$ -binding domain of the sirtuins (class III HDACs) is thought to be strictly structural and does not participate in catalysis, in contrast to the active-site zinc ion in the zinc-dependent class I, II, and IV HDACs (99). The sirtuin zinc domain utilizes four conserved cysteine residues to coordinate  $\text{Zn}^{2+}$  (SIRT6: Cys-141, Cys-144, Cys-167, and Cys-178). Most sirtuins contain the conserved sequence motif Cys-*X-X*-Cys-*X*<sub>15-20</sub>-Cys-*X-X*-Cys, however, SIRT6 incorporates a 10 amino acid insert between the third and fourth cysteine resulting in a unique extended flexible loop (Fig. 1-4E) (23). Interestingly, carboxyl terminus of Hsp70-interacting protein (CHIP) has been shown to noncanonically ubiquitinate SIRT6 on Lys-170, a residue which resides in the extended flexible loop on the  $\text{Zn}^{2+}$ -binding domain (106). This ubiquitination prevented proteasome-mediated degradation of SIRT6 and led to increased protein half-life. Studies involving SIRT1 and the yeast homolog, Sir2, demonstrated that cysteine *S*-nitrosation or mutation of these zinc-coordinating cysteines to alanine results in loss of deacetylase function (107–109). Molecular dynamics simulations suggested that loss of activity was due to repositioning of the  $\text{Zn}^{2+}$ -binding domain away from the catalytic domain following zinc release resulting in allosteric changes that disrupt  $\text{NAD}^+$  and acyl-substrate binding (110). Trichostatin A (TSA) is well documented as a Class I and II HDAC inhibitor that functions by chelating the active-site zinc of these enzymes (111). Curiously, it was demonstrated that TSA specifically inhibits SIRT6 ( $K_i = 2 \mu\text{M}$ ) over SIRT1-3 and SIRT5 ( $K_i = >50 \mu\text{M}$ ) against H3K9ac peptide substrate (107). Subsequent kinetic analyses suggested that TSA competitively inhibited SIRT6 with respect to H3K9ac substrate (110). A structure of SIRT6 bound to TSA was solved in a separate study revealing binding to a SIRT6 specific region at the distal end of the hydrophobic cleft, explaining its isoform selectivity (112). TSA is often used in an effort to specifically inhibit

class I and II HDACs in cellular experiments at concentrations ranging from 0.1-2  $\mu\text{M}$ . Given this expanded role of TSA as a zinc-chelating-independent inhibitor of SIRT6 with a  $K_i$  of 2  $\mu\text{M}$ , methodological caution should be taken to rule out “non-specific” inhibition of SIRT6.

#### *1.4.4 Hydrophobic pocket*

A conserved salt bridge between the Rossmann fold and zinc-binding domains of SIRT5 and many Sir2 homologs is thought to contribute to the stabilized positioning of these domains (105, 109). SIRT6 lacks this salt bridge (predicted by homology modeling to occur between Arg-182 and Asp-190), resulting in a structure that is splayed open relative to other sirtuins (23). This expanded cleft between domains contains an elongated hydrophobic pocket that accommodates long-chain acyl substrates. A structure of SIRT6 bound to H3K9myr revealed non-polar contacts of the myristoyl-chain with Ala-13, Pro-62, Phe-64, Trp-71, Pro-80, Phe-82, Phe-86, Val-115, Leu-132, Met-157, Leu-186, and Ile-219 (Fig. 1-4D) (24). Furthermore, structures containing bound myristoyl-peptide are the only to date in which the SIRT6 N-terminus became structured, revealing that it covers part of this hydrophobic pocket at the interface of the Rossmann fold and Zinc-binding domains (24, 113). Together this suggests that acyl-substrate occupation of the hydrophobic pocket can lead to an ordered structure and provides one possible explanation for why long-chain deacylation is more efficient than short-chain deacetylation. This hydrophobic pocket has also been implicated as an activator binding site through both kinetic and structural studies. Kinetically, the activators CL5D and myristic acid displayed competitive inhibition towards myristoyl-substrate (25, 103). Crystal structures of SIRT6 in the presence of the activators UBCS039 and MDL-801 demonstrated that they both occupied the distal hydrophobic pocket away from the active site (114). Structural alignment of SIRT6/UBCS039 with SIRT6/myristoyl-peptide shows overlap between the terminal 7 carbons of the myristoyl-group and UBCS039. Competitive inhibition of demyristoylation by UBCS039 was not observed during kinetic analysis, however the presence of myristoyl-peptide reduced the binding affinity of UBCS039, suggesting that although these molecules occupy an overlapping pocket, myristoyl-peptide efficiently

outcompetes UBCS039 for binding. An additional small molecule activator of SIRT6, cyanidin, was also crystallized and located in the same distal hydrophobic pocket, however no kinetic data of long-chain deacylation was presented (115). Structural analysis of H3K9 peptide binding reveals primarily hydrogen bonds between the main chain of the peptide and the surface of SIRT6 with just Thr-11 and Gln-6 of the peptide substrate participating in side chain interactions (Fig. 1-4B). Microarray analysis using ~6,800 acetyllysine substrates demonstrated a SIRT6 preference for uncharged residues around acetyllysine except for negatively charged residues at -4 and +2 (116), however, none of the three identified *in vivo* histone substrates (H3K9/18/56ac) satisfy these reported *in vitro* preferences. This suggests that selectivity for histone substrate may be dependent on other factors such as protein-protein binding and optimized orientation between SIRT6 and target sites on nucleosomes. The nature of the acyl-group modification on lysine might also facilitate SIRT6-substrate interactions. Consistent with this notion, SIRT6 performs more efficient deacylation *in vitro* against substrates containing acyl groups ranging 8-14 carbons in length (25), however identification and validation of long-chain acyl substrates *in vivo* remains limited (117, 118). Directed evolution of SIRT6 conducted using SIRT6 ancestral libraries identified multiple point mutations which resulted in enhanced demyristoylation of peptide substrate (47). The mutation M157H, located in the hydrophobic pocket, was identified in two separately evolved SIRT6 variants and resulted in improved  $k_{\text{cat}}$  of demyristoylation. *In silico* modeling led the authors to propose improved catalysis through better positioning of  $\text{NAD}^+$  and peptide substrate, however, the precise contributions of this mutation are unknown. Despite the structural and biochemical evidence that SIRT6 preferentially hydrolyses long-chain acyl groups, compelling cellular evidence suggests that SIRT6 exerts biological regulation primarily through the direct

deacetylation of specific sites on histone and non-histone proteins (38, 39, 43). These observations will be discussed in greater detail in subsequent sections of this review.

#### 1.4.5 N- and C-terminal extensions

In addition to the conserved catalytic core consisting of a Rossmann fold and zinc-binding domain, individual sirtuins harbor unique N- and C-terminal extensions (Fig. 1-3). Structurally, the 24 amino acid N-terminus of SIRT6 is surface exposed and lacks secondary structural elements. The second half of the N-terminus (Asp-14 through Phe-24) is ordered in crystal structures and is adjacent to the Rossmann fold domain. The first half of the N-terminus (Met-1 through Ala-13) has only been observed to be ordered upon H3K9myr peptide binding which makes contacts with both the Rossmann fold domain and zinc-binding domain to seal the hydrophobic pocket. Given that SIRT6 performs more efficient long-chain deacylation *in vitro*, it follows that the ordering of this domain may facilitate catalysis. The N-terminus of SIRT6 has been shown to be critical for H3K9 and H3K56 deacetylase activity and for chromatin association in cells, however, this region is dispensable for nuclear localization (30). No SIRT6 structures to date have been solved in the presence of acetylated substrates so it remains to be seen whether canonical acetyl-substrates can induce ordering of the N-terminus. The N-terminal domain of SIRT6 is highly conserved among mammalian homologs and can be phosphorylated at Ser-10 to facilitate DNA-repair (29, 119). The contributions of SIRT6 towards DNA repair will be discussed in subsequent sections of this review.

The C-terminus of SIRT6 (Leu-269 through Ser-355) is significantly larger than the N-terminus and is reported to contain a nuclear localization signal (30). This C-terminus is predicted to be an intrinsically disordered region (IDR) and is composed of 24.7% prolines with an isoelectric point of 10.1 (119). To date, only a short region (Leu-269 through Glu-298) of this C-terminus has been solved by crystallography with the rest remaining unstructured (Fig. 1-3). Given the difficulty in crystallizing this inherently disordered domain, some researchers have opted to

remove this region to facilitate crystal formation (23, 24). Interestingly, it has recently been suggested that heterochromatin can form through phase separation into liquid-droplets and many of the proteins that form these condensates contain IDRs (120, 121). Given the role of SIRT6 in maintaining heterochromatin and telomeres (38, 40, 122) it is an emerging and exciting question as to whether the C-terminal IDR participates in heterochromatic condensates. *In vivo* phosphorylation of the C-terminus at Thr-294, Ser-303, Ser-330, and Ser-338 has been reported (119, 123, 124). The SIRT6 variant S338A disrupted interactions with nuclear pore complexes as determined by IP-MS suggesting that phosphorylation of the C-terminus may modulate protein-protein interactions (119). However, there is no additional data suggesting the cellular function for this potentially regulated interaction.

## 1.5 Catalytic activities

### 1.5.1 Catalytic mechanism

Sirtuins remove acyl-moieties from  $\epsilon$ -amino group of lysines, and in the process, consume one molecule of  $\text{NAD}^+$  for every one molecule of acyl-chain removed (125). Three products are generated: nicotinamide, deacylated peptide/protein and acylated-ADP-ribose. After both substrates are bound, the glycosidic bond between nicotinamide and ribose is cleaved and the acyl oxygen attacks the C1 of ribose, resulting in an adduct between the two substrates (Fig. 1-5). Kinetic isotope effect experiments suggest that the glycoside bond is largely broken before addition of the acyl-oxygen (126), though the net rate-constant for this first chemical step is greatly influenced by the nucleophilicity of the attacking oxygen (127). The lifetime of the resulting alkylimidate intermediate can be extended by replacing a catalytic histidine (His-133 in SIRT6), which would normally facilitate (via general base action) the attack of the ribose 2'-OH on the imidate intermediate (Fig. 1-5), forming a bicyclic adduct (128, 129). During catalysis, the histidine to alanine mutant protein is partially stalled at the imidate intermediate, allowing water or other solvent nucleophiles (methanol/ethanol) to react, essentially turning the enzyme into an acetyl-substrate dependent  $\text{NAD}^+$  hydrolase, with no net deacetylation (128). These results have implication for the weak ability of sirtuins to mediate protein ADP-ribosylation under some circumstances (discussed further below). During the normal catalytic cycle for deacylation, formation of the bicyclic intermediate (Fig. 1-5, species iii.) is followed by attack of a water molecule to form intermediate iv, followed by cleavage of the C-N bond to liberate the final two products, *O*-acyl-ADP-ribose and deacetylated lysine. Evidence for these catalytic steps and intermediates has come from biochemical, structural and theoretical experiments (128, 130–133).



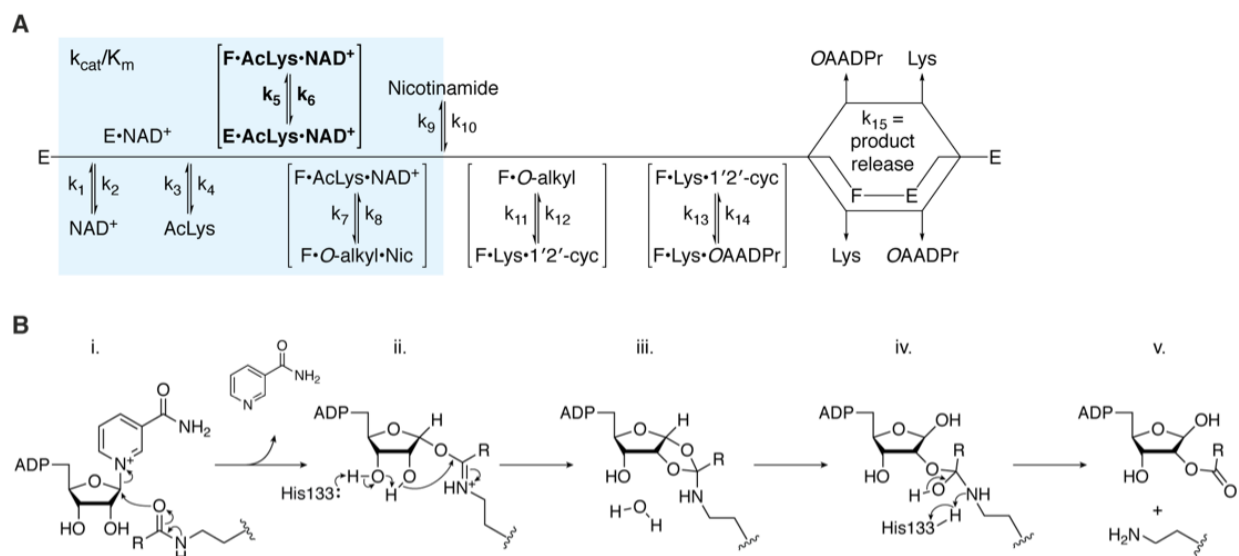
Early reports on the possible reactions catalyzed by sirtuins included both deacetylation and ADP-ribosylation (13–15, 125, 130, 134). To date, a preponderance of data supports the main catalytic activity as NAD<sup>+</sup>-dependent deacylation, with unique specificities between sirtuins for various acyl groups on the lysine  $\epsilon$ -amine. Current evidence indicates that Sirtuins do not act as  $\alpha$ -amino deacylases. While most studies have ascribed deacylation as the biological function of sirtuins, a few others have suggested that the protein ADP-ribosylation activity of some sirtuins is responsible for certain cellular functions. Such reports suggest that SIRT4 can ADP-ribosylate GDH (135), that SIRT2 can target BSA (134) and that SIRT6 can ADP-ribosylate PARP1 (21). The role of sirtuin-dependent ADP-ribosylation remains enigmatic. From a biochemical perspective, protein ADP-ribosylation can be explained through the intrinsic catalytic properties of sirtuins (22, 125, 136). However, parsing deacylation from ADP-ribosylation in cellular assays remains challenging, largely because both activities occur through the same active site. *In vitro*, ADP-ribosylation activity pales in comparison to deacylation, and the ability of SIRT6 to perform multiple rounds of catalytic turnover for ADP-ribosylation has not been reported. Nevertheless, in cellular contexts, it is possible that there are molecular circumstances that greatly promote ADP-ribosylation over deacylation. With SIRT6, the unique kinetic mechanism might allow SIRT6 to facilitate such a proposed switch toward more favorable ADP-ribosylation.

Detailed kinetic mechanisms for a few sirtuins are reported. Generally, sirtuins bind NAD<sup>+</sup> after acylated substrates are bound (101, 102, 137). Nicotinamide is the first product produced and released by the enzymes (Fig. 1-5). After completing the final chemical steps of catalysis, deacylated product and *O*-acyl-ADPr are released, with *O*-acyl-ADPr likely the last product to be released. Interestingly, SIRT6 displays a distinct kinetic mechanism that permits NAD<sup>+</sup> binding in the absence of acylated substrate (Fig. 1-5) (23, 103). Also, after both substrates bind SIRT6,

reports suggest a slow conformational step that enables formation of the first bi-substrate adduct, the alkylimidate intermediate (103). This conformational step was greatly enhanced when long-chain acylated substrates were used, or when SIRT6 was activated by FAs or other small molecule activators (103). Among sirtuins, the rate-limiting steps in turnover appear to vary depending on the intrinsic properties of each enzyme, choice of acylated substrate and whether the enzyme is activated. Accordingly, these factors affect the  $K_m$  for  $NAD^+$ , as well as the acylated substrate (138). These observations have important implications for the differential  $NAD^+$ -dependence for sirtuin-catalyzed deacylation. Current data suggests that low  $NAD^+$  levels will favor SIRT1, SIRT2, and SIRT6 long-chain deacylation over deacetylation, while higher  $NAD^+$  levels will preferentially enhance deacetylation (138). The idea of stimulating cellular sirtuin activity has long been a goal of many researchers and pharma industries. Two main strategies have been explored: *i.*) Use of vitamin B3 compounds to boost cellular  $NAD^+$  levels, and *ii.*) Use of allosteric activators that enhance catalytic efficiency. SIRT1 is the most studied human sirtuin and the first sirtuin targeted for therapeutic development with natural products and synthetic small molecules as allosteric activators (139–141). In mouse studies, promising evidence supports the therapeutic potential of targeting SIRT1 activation (142–144). These studies provided proof-of-concept for therapeutically targeting sirtuin activation.

**Figure 1-5: Mechanism of SIRT6 catalysis.** SIRT6 performs  $\text{NAD}^+$ -dependent deacylation of a substrate lysine (AcLys) resulting in the formation of nicotinamide (Nic), *O*-acyl-ADP-ribose (OAADPr) and deacylated lysine (Lys). *A*) The kinetic scheme of SIRT6 (E) begins with ordered sequential binding of  $\text{NAD}^+$  followed by acyl-lysine substrate. Next, the complex undergoes a conformational change (bold,  $\text{E} \rightarrow \text{F}$ ) that has been shown to be activated by some small molecule SIRT6 activators of deacetylation or directly by long-chain acyl substrates. Chemical catalysis is initiated by formation of the alkylimidate intermediate (*O*-alkyl) and release of nicotinamide. Subsequently, SIRT6 catalyzes the formation of the 1',2'-cyclic intermediate (1'2'-cyc) and then its subsequent water-mediated collapse to form the final products. After release of deacylated lysine and *O*-acyl-ADP-ribose, SIRT6 is ready for its next round of catalysis. *B*) Chemical catalysis; *i*, Substrate acyl-oxygen performs nucleophilic addition on the 1'-carbon of the nicotinamide ribose resulting in the C1'-*O*-alkylamidate intermediate and release of nicotinamide. *ii*, His-133 acts as a general base to facilitate the intramolecular nucleophilic attack of the nicotinamide ribose 2'-hydroxyl on the *O*-alkylamidate carbon affording the 1',2'-cyclic intermediate. *iii*, Water catalyzed hydrolysis of the 1',2'-cyclic intermediate yields the tetrahedral intermediate. *iv*, Positively charged His-133 donates a proton to the imino group of the tetrahedral intermediate resulting in cleavage of the C-N bond and yielding the final products. *v*, *O*-Acyl-ADPr and deacylated lysine products are released from SIRT6.

**Figure 1-5: Mechanism of SIRT6 catalysis.**



### 1.5.2 Activation

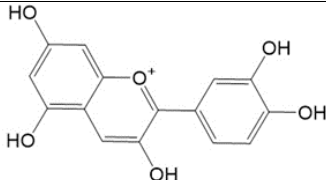
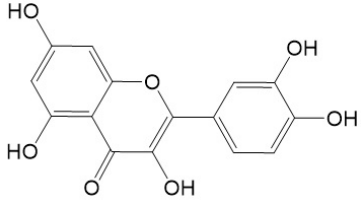
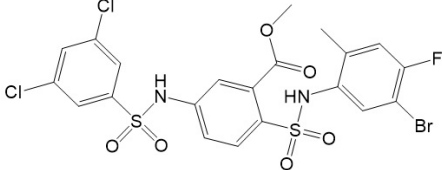
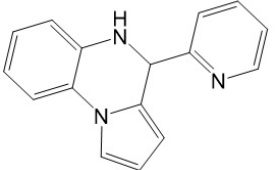
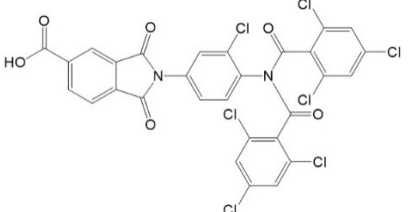
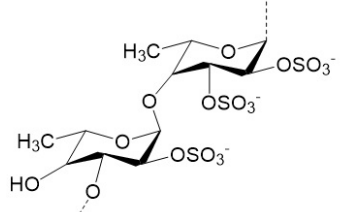
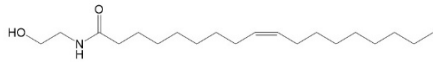
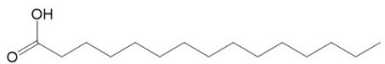
Sirtuins have been targets of drug discovery efforts since the discovery that their biological functions are implicated in age-related diseases (145). Investigations into the molecular function of SIRT6 had lagged that of SIRT1 in part because of SIRT6's poor *in vitro* deacetylase activity, which is nearly ~1000 times lower than other sirtuins (23). It was later demonstrated that SIRT6 is hundreds-fold more efficient at removing long-chain acyl modifications, such as myristoyl, compared to short-chain deacetylation, and structural studies revealed that the myristoyl group of this peptide is accommodated in a hydrophobic pocket extending past the catalytic site (24, 25). However there was a discrepancy between cellular data suggesting that SIRT6 acted as a H3K9 deacetylase and the poor *in vitro* activity of SIRT6 against acetylated substrates versus long-chain acylated peptides.

A major advance in our understanding of *in vitro* SIRT6 deacetylation came with the discovery that this activity could be greatly enhanced in the presence of certain long-chain free fatty acids. Studies by Feldman et al. demonstrated that free fatty acids ranging from 12-18 carbons were capable of improving the catalytic efficiency of SIRT6 deacetylation up to 35-fold (25). This evidence suggests that SIRT6 deacetylation can be regulated by small molecules and provides a possible mechanism for cellular SIRT6 to achieve efficient levels of deacetylase activity. While we predict SIRT6 can be activated by endogenous fatty acids (FAs), direct evidence of cellular SIRT6 activation by FAs has yet to be reported. A recent study provided compelling evidence that monounsaturated FAs activate SIRT1 specifically towards PGC-1 $\alpha$  and FOXO3, but not histone H3, both *in vitro* and *in vivo* (146). With SIRT6, Michaelis-Menten kinetic analysis revealed that FAs drive activation primarily through an improved  $k_{cat}/K_m$ , suggesting that one or more steps prior to and including the release of nicotinamide are enhanced during activation (Fig. 1-5) (25).

This same study showed that free myristic acid acts as a competitive inhibitor of long-chain demyristoylation. Together these biochemical studies suggest that the hydrophobic pocket of SIRT6 is an activation site that can be either accommodated directly by long-chain acyl substrates or by FA activators of deacetylation. These findings and others have led to the development of structurally diverse small molecule activators of SIRT6 (Table 1-1) that will be discussed in the following sections.

**Table 1-1: Identified activators of SIRT6 deacetylation.** A select set of SIRT6 activators are presented in which detailed studies have been conducted or that demonstrate the diversity of small molecule activators. Half-maximal effective concentration ( $EC_{50}$ ) values and kinetic parameters describing maximal observed activation were collected using the adjacent peptide substrate. Effects on SIRT6 demyristoylation of peptide substrate is also reported when available. N/A is reported when the referenced study did not provide pertinent data.

**Table 1-1: Identified activators of SIRT6 deacetylation**

	Compound	EC <sub>50</sub>	Max Activation	Substrate	DeMyr	Ref
	Cyanidin	460 $\mu$ M	55-fold rate increase at 40 $\mu$ M substrate	H3K9ac peptide (1-21)	N/A	44
	Quercetin	1.2 mM	2-fold rate increase at 200 $\mu$ M substrate	H3K9ac peptide (1-21)	N/A	84,83
	MDL-800	10 $\mu$ M	22-fold rate increase at 25 $\mu$ M substrate	H3K9ac peptide (4-13 + WW)	No inhibition	41
	UBCS039	38 $\mu$ M	3.5-fold rate increase at 200 $\mu$ M substrate	H3K9ac peptide (3-15)	No inhibition	43
	CL5D	15 $\mu$ M	50-fold increase in $k_{cat}/K_m$	H3K9ac peptide 4-17 + WW)	Competitive $K_i=13 \mu$ M	30
	Fucoidan	N/A	355-fold rate increase at 40 $\mu$ M substrate (100 $\mu$ g/mL fucoidan)	H3K9ac peptide (1-21)	N/A	87
	Oleoylethan olamide	3.1 $\mu$ M	2-fold rate increase at 40 $\mu$ M substrate	H3K9ac peptide (1-21)	N/A	83
	Myristic acid	246 $\mu$ M	35-fold increase in $k_{cat}/K_m$	H3K9ac peptide (4-17 + WW)	Competitive $K_i=15 \mu$ M	42



### 1.5.2.1 Natural compounds as activators

Utilizing magnetic beads coated with catalytically active SIRT6, the flavonoids quercetin and vitexin were initially identified from fenugreek seed extract as *in vitro* inhibitors of SIRT6 deacetylation (147). Later studies of quercetin as well as an additional flavonoid, luteolin, demonstrated IC<sub>50</sub> values of 24  $\mu$ M and 1.9  $\mu$ M respectively (148). Curiously, dose response assays of quercetin and luteolin showed 6- and 10-fold activation at higher concentrations with EC<sub>50</sub> values of 990  $\mu$ M and 270  $\mu$ M respectively. The concentration dependent dual function of these flavonoids opens the possibility of multiple modes of small molecule binding, although this has not been further explored. This same study demonstrated N-acyl ethanolamines, namely oleoyl ethanolamide and myristoyl ethanolamide (EC<sub>50</sub> of 3.1  $\mu$ M and 7.5  $\mu$ M), as more potent activators, albeit with lower maximum fold activation of SIRT6, than their fatty acid cousins, oleic and myristic acid (EC<sub>50</sub> of 90  $\mu$ M and 246  $\mu$ M) (25, 148).

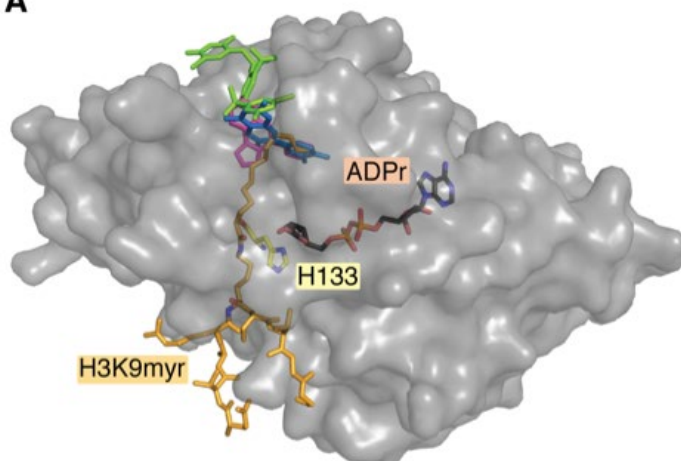
Additional flavonoids were subsequently investigated, resulting in the identification of multiple anthocyanidins which stimulated SIRT6 activity; the most effective of which, cyanidin, activated SIRT6 55-fold against acetyl-peptide with an EC<sub>50</sub> of 460  $\mu$ M as determined under proper steady-state dose response conditions (115). Delphinidin, which contains 3 rather than 2 hydroxyl groups on the B-benzene ring of the flavonoid scaffold, yielded a similar EC<sub>50</sub>, however showed a weaker maximum activation of 6.3-fold. *In silico* docking of these compounds suggested surface contacts with the  $\beta$ 6/ $\alpha$ 6 loop that capped the distal end of the hydrophobic pocket. This binding site is proximal to where UBCS039, a synthetic activator described by You et al. and discussed later, was observed binding in crystallographic studies (Fig. 1-6) (115). Interestingly, both the A- and B-benzene rings of cyanidin are predicted to rotate slightly compared with that of delphinidin resulting in a closer contact and conformational change of Trp-186 of SIRT6, providing a structural

rationale for its increased effectiveness. SIRT6 was subsequently crystallized in the presence of cyanidin confirming this binding orientation (Fig. 1-6) (149). Surprisingly, treatment of Caco-2 cells with cyanidin showed a dose-dependent 3.5-fold increase in SIRT6 protein levels (115). Anthocyanidins, including cyanidin, have been implicated in reducing the risk of aging-related diseases thought to be mediated by their protective effect against oxidative stress (150, 151). Given the protective effects of SIRT6 against aging-related diseases (discussed in detail later) it is compelling to consider whether these effects are mediated through SIRT6. Additionally, it raises the point that small molecules eliciting increased SIRT6 protein levels should be considered as a potential therapeutic strategy in addition to those which directly activate SIRT6.

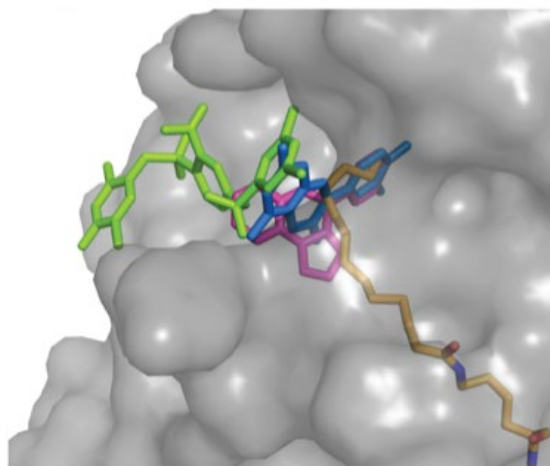
Screening of brown algae extracts led to the identification of fucoidan, a highly abundant sulfated polysaccharide as an activator of SIRT6 deacetylation (152). Fucoidan is a complex heterogeneous polysaccharide found in various brown algae and seaweeds making structural determination of this compound difficult. However fucoidan isolated from *F. vesiculosus* exhibited a ~355-fold activation of SIRT6 at 100 µg/mL under steady-state conditions. Dose-response assays of fucoidan did not reach saturation due to limitations of available fucoidan suggesting that maximum activation may be higher than reported. Fucoidan was additionally shown to activate SIRT6 *in vitro* against histone substrate and demonstrated strong specificity for SIRT6 over SIRT1-3. This finding marks the first identification of a high molecular weight polysaccharide activator of SIRT6, however, a lack of detailed kinetics of activation, in particular the effects on  $k_{cat}$  or  $k_{cat}/K_m$ , prevent the mechanism of activation to be compared with that of other small molecule activators.

**Figure 1-6: SIRT6 activators bind to the terminus of the hydrophobic pocket.** Crystallization of SIRT6 small molecule activators reveals a conserved site of activation located at the terminal end of the hydrophobic pocket. *A)* A structure of SIRT6 bound to myristoyl-peptide (yellow) and ADP-ribose (pink) overlaid with MDL-801 (green), UBCS039 (magenta), and cyanidin (blue) shows that these activators bind away from the active site His-133 (red). *B)* UBCS039 and cyanidin cap the hydrophobic pocket and directly overlap with the myristoyl chain of peptide substrate. MDL-801 also caps this hydrophobic pocket however is shifted back allowing for the accommodation of myristoyl-substrate. This structure was produced using 5Y2F, 5MF6, 6QCH, and 3ZG6 from the RCSB protein data bank.

**A**



**B**



### 1.5.2.2 Synthetic activators

The first validated set of synthetic SIRT6 deacetylase activators, pyrrolo[1,2- $\alpha$ ]quinoxaline derivatives, were characterized by You et al. (114). This work was motivated by a previous study in which virtual docking and subsequent *in vitro* studies suggested a weak stimulation of SIRT6 by the compound 4-(pyridin-3-yl)-5-((3-(trifluoromethyl)-phenyl)sulfonyl)-4,5-dihydropyrrolo[1,2- $\alpha$ ]quinoxaline (153). This lead compound was ultimately derivatized to 4-(pyridin-3-yl)-4,5-dihydropyrrolo[1,2- $\alpha$ ]quinoxaline (renamed UBCS039) which demonstrated a 3.5-fold increase in SIRT6 activity against an acetyl-peptide with an EC<sub>50</sub> of 38  $\mu$ M as determined under steady-state conditions utilizing a coupled assay that monitors the formation of nicotinamide (114, 154). UBCS039 was further validated as an activator of SIRT6 against endogenously sourced calf thymus histones and HeLa mononucleosomes, however no kinetic data were presented to clarify whether activation occurred via an improved  $k_{cat}$  or  $k_{cat}/K_m$ . The structure of UBCS039/SIRT6 was solved and showed the activator occupying the distal pocket of the hydrophobic channel, consistent with the previous notion of this pocket as an activation site (Fig. 1-6). When compared to the structure of SIRT6 bound to a myristoylated peptide (3ZG6), UBCS039 overlaps with the terminal 7 carbons of the myristoyl chain (114, 138). In line with this structural data, the presence of myristoylated peptide weakened the binding of UBCS039 by an order of magnitude. However, no inhibition of demyristoylation was observed in the presence of UBCS039, likely due to the weak binding of UBCS039 being unable to compete with the tight binding myristoyl-peptide. No structural rearrangement of SIRT6 was observed in the presence of UBCS039 compared to apo-SIRT6 perhaps due to preformed SIRT6 crystals soaked with UBCS039 being unable to adopt potential allosteric changes. In a subsequent study, UBCS039 was shown to elicit cellular activation of SIRT6 that resulted in decreased levels of H3K9ac and

H3K56ac and SIRT6-dependent autophagy-related cell death (155). This study was the first reported instance of a cellularly active small molecule SIRT6 activator, thus providing proof-of-principle for the potential therapeutic targeting of SIRT6.

An additional SIRT6 activator, MDL-800, with cellular activity was reported by Huang et al. (113). Researchers began by computationally predicting an allosteric site on SIRT6 and virtually docking five million compounds. *In vitro* testing of the top predicted binders validated lead compounds as SIRT6 activators with demonstrated EC<sub>50</sub> values in the 170-220  $\mu$ M range as determined under steady-state conditions. Chemical optimization of the substituents of the two terminal phenyl rings resulted in the compound MDL-800, which displayed a 22-fold increase in SIRT6 activity with an EC<sub>50</sub> value of 10.3  $\mu$ M. Activation was further validated against additional peptide substrates and HeLa extracted heterogeneously modified nucleosomes. Michaelis-Menten kinetic analysis against peptide substrate demonstrated an 18-fold increase in  $k_{\text{cat}}/k_m$  for H3K9ac, driven by a 7.4-fold increase in  $k_{\text{cat}}$  and a 2.2-fold decrease in  $K_m$ . Interestingly, these kinetics of activation vary from other synthetic activators in which detailed kinetic analyses have been performed. CL5D (discussed next) and myristic acid, for example, drive activation of SIRT6 primarily by reducing the  $K_m$  for H3K9ac and show minimal effects on  $k_{\text{cat}}$  (25, 103). These varied kinetics of activation are potentially explained by subsequent structural studies of MDL-801, a demethylated derivative of MDL-800, which revealed a unique activation pocket peripheral to that of UBCS039 (Fig. 1-6). A complex of SIRT6/MDL-801 could only be solved in the presence of myristoylated peptide and exhibited non-overlapping binding pockets of the two ligands. MDL-801 was located near the surface exposed distal region of the hydrophobic pocket and made contacts with the N-terminus and  $\pi$ -stacking interactions with Phe-82 and Phe-86 of SIRT6. Mutation of Phe-86 resulted in decreased potency of activation demonstrating the importance of

this  $\pi$ -stacking interaction. Despite the ability of myristoyl-peptide and MDL-801 to co-occupy SIRT6, no enhancement or inhibition of demyristoylation was observed. Importantly, MDL-801 and UBCS039 exhibited synergistic activation of SIRT6 deacetylation substantiating separate binding sites and suggesting multiple modes of allosteric activation. MDL-800 treatment of multiple human cancer cell lines showed a dose-dependent and SIRT6-dependent cell-cycle arrest and corresponding decrease in global H3K9ac and H3K56ac levels, confirming MDL-800 as a cellularly active SIRT6 activator. Together, studies of UBCS039 and MDL-800 demonstrate the viability of pharmacological activation of SIRT6 and suggest multiple modes of allosteric activation. The presence of distinct binding sites also opens the door to potential development of multivalent activators with improved affinity for SIRT6.

Recent work by Klein et al. identified the novel SIRT6 activator, CL5D, and used this compound to probe the mechanism of activation, resulting in the identification of a conformational step preceding chemical catalysis that is enhanced by small molecule activators of deacetylation or directly by long-chain myristoyl substrates (103). CL5D was derived through chemical optimization of a lead compound identified through targeted screening of lipid-like molecules. Kinetic analysis demonstrated an  $EC_{50}$  value of 15.5  $\mu$ M with a maximum 50-fold activation in  $k_{cat}/K_m$  under steady-state conditions. Although no structural data were presented, CL5D exhibited competitive inhibition of demyristoylation suggesting occupation of the hydrophobic pocket, as had previously been described for free myristic acid (25). Extensive kinetic analyses excluded the possibility of any previously identified catalytic steps being enhanced by CL5D. Kinetic modeling proposed that a slow conformational step following substrate binding but prior to the first chemical step –formation of the alkylimidate intermediate– could be activated by CL5D to account for the empirically determined 50-fold increase in  $k_{cat}/K_m$ . The SIRT6 variant, R65A, maintained base-

level deacetylase activity but was unable to be activated by CL5D towards deacetylation and demonstrated inefficient demyristoylation. Although SIRT6 R65A could bind  $\text{NAD}^+$ , this variant lacked the ability to mediate the conformational change observed for wild-type SIRT6 upon  $\text{NAD}^+$  binding. Together this suggested that CL5D activated SIRT6 deacetylation via an Arg-65-mediated conformational change prior to chemical catalysis and that this mechanism of enhanced catalysis is shared by long-chain demyristoylation.

### 1.5.2.3 Kinetic implications of SIRT6 activation

The therapeutic promise of pharmacological SIRT6 activation in combating aging-related diseases has motivated the identification of novel SIRT6 activators with diverse structures and varying levels of corresponding biochemical data. Studies which resolve the structural interaction of SIRT6 and activator have universally identified a region at the distal site of the hydrophobic pocket responsible for ligand interaction (113–115). Anthocyanidins, including cyanidin and delphinidin, as well as UBCS039 partially occupy the hydrophobic interior, in effect capping this pocket from the solvent exposed exterior (Fig. 1-6). MDL-801 similarly binds the distal region of this pocket, however, appears shifted back towards the solvent exposed exterior when compared to previously mentioned compounds (Fig. 1-6B). Curiously, MDL-801 is the only activator to date that catalytically activates SIRT6 primarily by driving an increased  $k_{\text{cat}}$ . Other activators including myristic acid and CL5D have been shown to primarily enhance  $k_{\text{cat}}/K_{\text{m}}$ . Therefore, it is of interest as to whether varying binding orientations within this distal hydrophobic pocket elicit varying allosteric mechanisms of SIRT6 activation.

The steady-state  $k_{\text{cat}}/K_{\text{m}}$  parameter describes the ability of the enzyme to capture substrate at low concentration and commit it to catalysis, therefore activation via an improved  $k_{\text{cat}}/K_{\text{m}}$  implicates the improvement of substrate binding or a catalytic step including or prior to the first irreversible step, the release of nicotinamide. These steps include  $\text{NAD}^+$  and acetyl-peptide binding, formation of an alkylimidate intermediate, and nicotinamide release, and are universal to sirtuin mediated catalysis (Fig. 1-5). As discussed previously, a recent study reported an additional conformational step in SIRT6 catalysis following substrate binding mediated by Arg-65 that was enhanced by CL5D (103). This conformational rate is slow in the absence of activator and occurs prior to nicotinamide release and is therefore also reflected in the  $k_{\text{cat}}/K_{\text{m}}$  term of SIRT6. It remains



to be determined whether other activators that improve  $k_{\text{cat}}/K_{\text{m}}$  similarly activate this conformational rate or whether this conformational step is present in other sirtuins. MDL-801 uniquely activates SIRT6 primarily through an improved  $k_{\text{cat}}$  which reflects an enhancement of a rate-limiting step. The terms reflected in  $k_{\text{cat}}$  can include any of the chemical steps or product release. The rate-limiting step of sirtuin catalysis varies depending on isoform as well as acyl-substrate and remains unknown in the case of SIRT6 deacetylation due to the inability to saturate SIRT6 with acetyl-substrate, a requisite condition for single-turnover kinetic analysis (138). Studies involving other sirtuins have suggested either the formation of the 1'2'-cyclic intermediate, water mediated collapse of the 1'2'-cyclic intermediate, or product release can be rate-limiting (128, 133, 138, 156). Further biochemical studies of MDL-801 are required to reach a full mechanistic understanding of its unique activation.

Kinetic studies used to characterize *in vitro* activation of SIRT6 thus far have been limited to the use of histone H3 tail-mimetic peptides and endogenously-sourced, heterogeneously modified nucleosomes. Multiple activators have been identified which improved  $k_{\text{cat}}/K_{\text{m}}$  for H3K9ac peptide substrates. In cells, SIRT6 has been reported to be almost exclusively bound to chromatin (1). Since  $k_{\text{cat}}/K_{\text{m}}$  describes the ability of SIRT6 to capture substrate for catalysis, it is important to understand how improving  $k_{\text{cat}}/K_{\text{m}}$  will affect an enzyme that is tightly bound to a nucleosome substrate. Perhaps SIRT6 is capable of undergoing activation during internucleosomal reaction where SIRT6 bound to one nucleosome can accept acetylated tail substrates from adjacent nucleosomes. Activators which improve  $k_{\text{cat}}$  could be imagined to affect both the activities of intra- and internucleosomal deacetylation of nucleosomes. How *in vitro* derived kinetic parameters influence SIRT6 towards physiologically complex polynucleosome substrates, and whether SIRT6 performs intra- or internucleosomal deacetylation is therefore of importance in evaluating small

molecule activators. Because endogenously sourced nucleosomes display as little as 2% acetylated H3K9 (157), additional studies will be needed to accurately ascertain the role of activation in SIRT6-dependent chromatin deacetylation.

### 1.5.3 Inhibition

Context dependent inhibition of SIRT6 is thought to have pharmacological value and has been successfully applied *in vitro* as a chemosensitizing and pro-differentiating strategy (158–160). Inhibitors of SIRT6 fall in to four classes: product inhibitors, thioacyl-lysine warheads, isoform specific small molecule inhibitors of deacetylation, and competitive inhibitors of long-chain deacylation.

The end products of SIRT6 catalysis are deacylated protein, *O*-acyl-ADP-ribose, and nicotinamide. Nicotinamide is a noncompetitive inhibitor of sirtuins, binding to the enzyme, and reacting with the substrate-ADP-ribose adduct to reform substrates (132, 161–164). Subsequent studies validated nicotinamide as an inhibitor of SIRT6 deacylation (138, 165). Studies in yeast demonstrated that nicotinamide depletion via overexpression of the nicotinamide metabolizing enzyme, PNC1, results in activation of Sir2 and lifespan extension (166). This suggests that inhibition of sirtuins by nicotinamide may serve as an endogenous regulator of activity, although this effect has not been studied in mammalian cells. Both ADP-ribose and the nonhydrolyzable analog of *O*-acetyl-ADP-ribose, *N*-acetyl-ADP-ribose, have also been shown to bind to SIRT6 at low to mid micromolar affinities (23). Kinetic studies demonstrated ADP-ribose as an inhibitor of SIRT6 deoctanoylation and demyristoylation with less potent IC<sub>50</sub> values compared with nicotinamide (100). The full potential for cellular regulation by end product inhibition has not been evaluated.

Thioacyl-lysine substrates of sirtuins demonstrate mechanism-based inhibition where following the first chemical step of catalysis, the corresponding 1'-*S*-alkylamidate intermediate displays impaired catalysis, in effect stalling the enzyme after the first chemical step (129, 167).

This mechanism-based inhibition has been exploited to create isoform specific thioacyl-peptides which specifically inhibit SIRT6 at micromolar levels (168, 169). Subsequent work created cyclic peptide thioacyl-lysine inhibitors with nanomolar  $IC_{50}$  values with specificity for SIRT6 (170). Although cyclic peptides tend to show improved stability against protease/peptidase activity, cellular targeting of SIRT6 with these compounds has not been realized.

Isoform specific inhibition of sirtuins is an attractive therapeutic strategy and has been utilized successfully in targeting SIRT1 in mouse models. Specifically, small molecule inhibitors of SIRT1 have been shown to sensitize cells to DNA-damaging agents, and inhibition of SIRT1 and SIRT2 appeared to slow tumor growth (171–174). The first identified small molecule inhibitors of SIRT6 were identified from an *in silico* screen, however, subsequent biochemical analysis suggested a lack of isoform specificity (153). Quercetin and vitexin were isolated from plant extracts and demonstrated SIRT6 inhibition, however these compounds were later shown to activate SIRT6 at higher concentrations and isoform specificity was never reported (147, 148). Research by Parenti et al. first identified a set of synthetic small molecule inhibitors with *in vitro* specificity for SIRT6 over SIRT1 and SIRT2 (175). These compounds elicited a time-dependent increase of H3K9ac levels in cultured cells, however SIRT6-dependence was not evaluated. One of the quinazolinone inhibitors identified by Parenti et al. was subsequently derivatized successfully to increase specificity over SIRT1 and SIRT2 (176). Kinetic analysis of these quinazolinone derivatives revealed competitive inhibition with respect to both  $NAD^+$  and acetyl-peptide substrate. Separate studies later determined that SIRT6 follows an ordered binding mechanism in which  $NAD^+$  binding precedes acetyl-peptide, suggesting that the inhibition noted by Sociali et al. is likely competitive with respect to  $NAD^+$  binding (103). Cell based assays further demonstrated that these quinazolinone compounds mimic the effect of SIRT6 knockdown in

potentiating the activity of PARP inhibitors and chemotherapeutics (21, 90, 177). A following study reported that this quinazolinone improved glucose tolerance in a type 2 diabetes mellitus (T2DM) mouse model, the first study implicating *in vivo* pharmacological SIRT6 inhibition (159). An additional salicylate-like compound, originally identified by Parenti et al., was further derivatized (renamed OSS\_128167), showed specificity for SIRT6 over SIRT1 and SIRT2, and elicited immunosuppressive and chemosensitizing effects in cell-based assays (158). Although OSS\_128167 was not tested in T2DM mouse models, pharmacokinetic studies in mice demonstrated a short half-life of ~10 minutes. A separate study demonstrated that SIRT6 overexpression in cell culture resulted in a decrease of H3K9ac levels that could be reversed by OSS\_128167 treatment, suggesting cellular inhibition of SIRT6 (178). Curiously, this same study reported that OSS\_128167 treatment resulted in inhibition of hepatitis B viral transcription and replication in mice despite the compound, with a half-life of ~10 minutes, only being administered every 4 days. Further studies are required to determine whether cellular half-life rates vary from previously reported serum half-life and whether this antiviral effect is due directly to intermittent SIRT6 inhibition.

As previously mentioned, various small molecule activators of SIRT6 deacetylation simultaneously inhibit long-chain deacylation. Both myristic acid and CL5D demonstrate competitive inhibition against demyristoylation, likely resulting from these compounds occupying the hydrophobic pocket and sterically occluding the myristoyl but not the acetyl group of substrate (Table 1) (25, 103). Other deacetylase activators including MDL-800 and UBC039 are unable to inhibit demyristoylation because the binding pocket is distinct from the hydrophobic pocket or such compounds have weak binding relative to myristoylated peptide, respectively (113,

114). To date, no inhibitor specific to long chain deacylation of SIRT6 has been evaluated in cellular models.

## 1.6 Perspective

Research progress over the past few years has described critical roles for SIRT6 in DNA repair, metabolic regulation, tumor suppression, and longevity (179, 180). Given these biological roles, SIRT6 has emerged as a candidate for small molecule activation to extend lifespan through the treatment or prevention of age-associated disease including non-alcoholic fatty liver disease, cancer, fibrosis, and cardiac hypertrophy (52, 181–183). Early work demonstrated the ability of SIRT6 to be activated *in vitro* by various small molecules including free fatty acids and natural products (25, 115, 147, 152). In recent years, new synthetic small molecule activators appear to exert cellular effects via SIRT6 stimulation (113, 155). The compound UBCS039 was reported to stimulate SIRT6 deacetylation of H3K9 and H3K56 and ultimately led to autophagy-dependent cell death in human cancer cells (155). However, autophagy has been shown to serve as a pro-survival response in some cancer cell contexts (184), suggesting that therapeutic targeting of SIRT6 in cancer to induce autophagy would need to be carefully considered. Huang et al. reported that MDL-800 reduced H3K9 and H3K56 acetylation in a SIRT6-dependent fashion and resulted in cell-cycle arrest of hepatocellular carcinoma cells (113). Administration of MDL-800 modestly decreased xenograft tumor growth in immunocompromised mice. These preliminary studies demonstrate proof of principle for the cellular targeting of SIRT6 and mark the beginning of a new phase of research in which small molecule probes aid in the biological evaluation of SIRT6 activities and therapeutic opportunities are assessed.

The therapeutic targeting of SIRT6 is still in its infancy and although several compounds have exhibited SIRT6-dependent cellular effects, questions regarding mechanisms of action and appropriate disease contexts remain. Our biochemical understanding of SIRT6 has lagged that of phenotypic studies in which loss of function mutants or manipulation of SIRT6 levels were

correlated with altered cellular or organismal physiology. As an understanding of *in vitro* activities of SIRT6 advances, our knowledge of the catalytic mechanisms and ability to modulate activity by small molecules has provided an important foundation for accelerated development of such molecules. Most cellular studies reporting the modulation of SIRT6 activity by small molecules utilize complementary *in vitro* data to support the activation or inhibition of SIRT6, however future studies will need to confirm direct engagement of SIRT6 with these small molecule modulators. Evidence of cellular engagement is critical to exclude the possibility of off-target effects that may otherwise be easily misattributed to SIRT6. Moreover, all catalytic activities ascribed to SIRT6 likely utilize a portion or all of the catalytic steps depicted in Figure 1-5 but employ distinct substrate binding regions just beyond the shared active site. Accordingly, loss of function mutations in SIRT6 could manifest phenotypes that represent the combination of all SIRT6 cellular functions. Similar thoughts would apply to increased expression of SIRT6. To target only one activity, small molecule modulators will need to preferential bind these unique structural regions. Highly specific and validated cellular SIRT6 activators/inhibitors have the potential to serve as powerful probes for elucidating the effects of modulating SIRT6 activity, including deacetylation, ADP-ribosylation, or long-chain deacylation. By combining select SIRT6 amino-acid substitutions, gleaned from enzymology studies, and activity-selective compounds could provide the needed selectivity to parse out SIRT6 functions in context specific settings, such as the potentially conflicting roles of SIRT6 in carcinogenesis and tumor development. SIRT6 is a complex enzyme with diverse functions implicated in human health and disease. With a detailed understanding of SIRT6 functions there exists an opportunity for precise selection of SIRT6 modulators to combat a host of common age-associated human diseases.



### ***1.7 Acknowledgements***

This work was supported by the NIH (GM065386 to J.M.D) and M.A.K. was supported by the Chemistry-Biology Interface Training Program (T32GM008505). We thank every scientist who has contributed to our collective understanding of sirtuins. J.M.D is a consultant for FORGE Life Science, and cofounder of Galilei BioSciences.

## 1.8 References

1. Mostoslavsky, R., Chua, K. F., Lombard, D. B., Pang, W. W., Fischer, M. R., Gellon, L., Liu, P., Mostoslavsky, G., Franco, S., Murphy, M. M., Mills, K. D., Patel, P., Hsu, J. T., Hong, A. L., Ford, E., Cheng, H.-L., Kennedy, C., Nunez, N., Bronson, R., Frendewey, D., Auerbach, W., Valenzuela, D., Karow, M., Hottiger, M. O., Hursting, S., Barrett, J. C., Guarente, L., Mulligan, R., Demple, B., Yancopoulos, G. D., and Alt, F. W. (2006) Genomic instability and aging-like phenotype in the absence of mammalian SIRT6. *Cell*. **124**, 315–329
2. Sebastián, C., Zwaans, B. M. M., Silberman, D. M., Gymrek, M., Goren, A., Zhong, L., Ram, O., Truelove, J., Guimaraes, A. R., Toiber, D., Cosentino, C., Greenson, J. K., MacDonald, A. I., McGlynn, L., Maxwell, F., Edwards, J., Giacosa, S., Guccione, E., Weissleder, R., Bernstein, B. E., Regev, A., Shiels, P. G., Lombard, D. B., and Mostoslavsky, R. (2012) The histone deacetylase SIRT6 is a tumor suppressor that controls cancer metabolism. *Cell*. **151**, 1185–1199
3. Ferrer, C. M., Alders, M., Postma, A. V., Park, S., Klein, M. A., Cetinbas, M., Pajkrt, E., Glas, A., van Koningsbruggen, S., Christoffels, V. M., Mannens, M. M. A. M., Knecht, L., Etcheberry, J.-P., Sadreyev, R. I., Denu, J. M., Mostoslavsky, G., van Maarle, M. C., and Mostoslavsky, R. (2018) An inactivating mutation in the histone deacetylase SIRT6 causes human perinatal lethality. *Genes Dev.* **32**, 373–388
4. Zhang, W., Wan, H., Feng, G., Qu, J., Wang, J., Jing, Y., Ren, R., Liu, Z., Zhang, L., Chen, Z., Wang, S., Zhao, Y., Wang, Z., Yuan, Y., Zhou, Q., Li, W., Liu, G.-H., and Hu, B. (2018) SIRT6 deficiency results in developmental retardation in cynomolgus monkeys. *Nature*. **560**, 661–665

5. Kugel, S., Feldman, J. L., Klein, M. A., Silberman, D. M., Sebastián, C., Mermel, C., Dobersch, S., Clark, A. R., Getz, G., Denu, J. M., and Mostoslavsky, R. (2015) Identification of and Molecular Basis for SIRT6 Loss-of-Function Point Mutations in Cancer. *Cell Rep.* **13**, 479–488
6. Rine, J., Strathern, J. N., Hicks, J. B., and Herskowitz, I. (1979) A suppressor of mating-type locus mutations in *Saccharomyces cerevisiae*: evidence for and identification of cryptic mating-type loci. *Genetics.* **93**, 877–901
7. Klar, A. J., Strathern, J. N., Broach, J. R., and Hicks, J. B. (1981) Regulation of transcription in expressed and unexpressed mating type cassettes of yeast. *Nature.* **289**, 239–244
8. Rine, J., and Herskowitz, I. (1987) Four genes responsible for a position effect on expression from HML and HMR in *Saccharomyces cerevisiae*. *Genetics.* **116**, 9–22
9. Gottlieb, S., and Esposito, R. E. (1989) A new role for a yeast transcriptional silencer gene, SIR2, in regulation of recombination in ribosomal DNA. *Cell.* **56**, 771–776
10. Smith, J. S., and Boeke, J. D. (1997) An unusual form of transcriptional silencing in yeast ribosomal DNA. *Genes Dev.* **11**, 241–254
11. Sinclair, D. A., and Guarente, L. (1997) Extrachromosomal rDNA circles--a cause of aging in yeast. *Cell.* **91**, 1033–1042
12. Aparicio, O. M., Billington, B. L., and Gottschling, D. E. (1991) Modifiers of position effect are shared between telomeric and silent mating-type loci in *S. cerevisiae*. *Cell.* **66**, 1279–1287
13. Imai, S., Armstrong, C. M., Kaerberlein, M., and Guarente, L. (2000) Transcriptional silencing and longevity protein Sir2 is an NAD-dependent histone deacetylase. *Nature.* **403**, 795–800

14. Landry, J., Sutton, A., Tafrov, S. T., Heller, R. C., Stebbins, J., Pillus, L., and Sternglanz, R. (2000) The silencing protein SIR2 and its homologs are NAD-dependent protein deacetylases. *Proc. Natl. Acad. Sci. U.S.A.* **97**, 5807–5811
15. Smith, J. S., Brachmann, C. B., Celic, I., Kenna, M. A., Muhammad, S., Starai, V. J., Avalos, J. L., Escalante-Semerena, J. C., Grubmeyer, C., Wolberger, C., and Boeke, J. D. (2000) A phylogenetically conserved NAD<sup>+</sup>-dependent protein deacetylase activity in the Sir2 protein family. *Proc. Natl. Acad. Sci. U.S.A.* **97**, 6658–6663
16. Frye, R. A. (2000) Phylogenetic classification of prokaryotic and eukaryotic Sir2-like proteins. *Biochem. Biophys. Res. Commun.* **273**, 793–798
17. Blander, G., and Guarente, L. (2004) The Sir2 family of protein deacetylases. *Annu. Rev. Biochem.* **73**, 417–435
18. Seto, E., and Yoshida, M. (2014) Erasers of histone acetylation: the histone deacetylase enzymes. *Cold Spring Harb Perspect Biol.* **6**, a018713
19. Imai, S.-I., and Guarente, L. (2016) It takes two to tango: NAD<sup>+</sup> and sirtuins in aging/longevity control. *NPJ Aging Mech Dis.* **2**, 16017
20. Liszt, G., Ford, E., Kurtev, M., and Guarente, L. (2005) Mouse Sir2 Homolog SIRT6 Is a Nuclear ADP-ribosyltransferase. *J. Biol. Chem.* **280**, 21313–21320
21. Mao, Z., Hine, C., Tian, X., Van Meter, M., Au, M., Vaidya, A., Seluanov, A., and Gorbunova, V. (2011) SIRT6 promotes DNA repair under stress by activating PARP1. *Science*. **332**, 1443–1446

22. Du, J., Jiang, H., and Lin, H. (2009) Investigating the ADP-ribosyltransferase activity of sirtuins with NAD analogues and 32P-NAD. *Biochemistry*. **48**, 2878–2890
23. Pan, P. W., Feldman, J. L., Devries, M. K., Dong, A., Edwards, A. M., and Denu, J. M. (2011) Structure and biochemical functions of SIRT6. *J. Biol. Chem.* **286**, 14575–14587
24. Jiang, H., Khan, S., Wang, Y., Charron, G., He, B., Sebastian, C., Du, J., Kim, R., Ge, E., Mostoslavsky, R., Hang, H. C., Hao, Q., and Lin, H. (2013) SIRT6 regulates TNF- $\alpha$  secretion through hydrolysis of long-chain fatty acyl lysine. *Nature*. **496**, 110–113
25. Feldman, J. L., Baeza, J., and Denu, J. M. (2013) Activation of the protein deacetylase SIRT6 by long-chain fatty acids and widespread deacylation by mammalian sirtuins. *J. Biol. Chem.* **288**, 31350–31356
26. Toiber, D., Erdel, F., Bouazoune, K., Silberman, D. M., Zhong, L., Mulligan, P., Sebastian, C., Cosentino, C., Martinez-Pastor, B., Giacosa, S., D’Urso, A., Näär, A. M., Kingston, R., Rippe, K., and Mostoslavsky, R. (2013) SIRT6 recruits SNF2H to DNA break sites, preventing genomic instability through chromatin remodeling. *Mol. Cell*. **51**, 454–468
27. McCord, R. A., Michishita, E., Hong, T., Berber, E., Boxer, L. D., Kusumoto, R., Guan, S., Shi, X., Gozani, O., Burlingame, A. L., Bohr, V. A., and Chua, K. F. (2009) SIRT6 stabilizes DNA-dependent protein kinase at chromatin for DNA double-strand break repair. *Aging (Albany NY)*. **1**, 109–121
28. Onn, L., Portillo, M., Ilic, S., Cleitman, G., Stein, D., Kaluski, S., Shirat, I., Slobodnik, Z., Einav, M., Erdel, F., Akabayov, B., and Toiber, D. (2020) SIRT6 is a DNA double-strand break sensor. *Elife*. 10.7554/eLife.51636

29. Van Meter, M., Simon, M., Tomblin, G., May, A., Morello, T. D., Hubbard, B. P., Bredbenner, K., Park, R., Sinclair, D. A., Bohr, V. A., Gorbunova, V., and Seluanov, A. (2016) JNK Phosphorylates SIRT6 to Stimulate DNA Double-Strand Break Repair in Response to Oxidative Stress by Recruiting PARP1 to DNA Breaks. *Cell Rep.* **16**, 2641–2650
30. Tennen, R. I., Berber, E., and Chua, K. F. (2010) Functional dissection of SIRT6: identification of domains that regulate histone deacetylase activity and chromatin localization. *Mech. Ageing Dev.* **131**, 185–192
31. Hou, T., Cao, Z., Zhang, J., Tang, M., Tian, Y., Li, Y., Lu, X., Chen, Y., Wang, H., Wei, F.-Z., Wang, L., Yang, Y., Zhao, Y., Wang, Z., Wang, H., and Zhu, W.-G. (2020) SIRT6 coordinates with CHD4 to promote chromatin relaxation and DNA repair. *Nucleic Acids Res.* 10.1093/nar/gkaa006
32. Rogakou, E. P., Pilch, D. R., Orr, A. H., Ivanova, V. S., and Bonner, W. M. (1998) DNA double-stranded breaks induce histone H2AX phosphorylation on serine 139. *J. Biol. Chem.* **273**, 5858–5868
33. Podhorecka, M., Skladanowski, A., and Bozko, P. (2010) H2AX Phosphorylation: Its Role in DNA Damage Response and Cancer Therapy. *J Nucleic Acids.* 10.4061/2010/920161
34. Atsumi, Y., Minakawa, Y., Ono, M., Dobashi, S., Shinohe, K., Shinohara, A., Takeda, S., Takagi, M., Takamatsu, N., Nakagama, H., Teraoka, H., and Yoshioka, K. (2015) ATM and SIRT6/SNF2H Mediate Transient H2AX Stabilization When DSBs Form by Blocking HUWE1 to Allow Efficient  $\gamma$ H2AX Foci Formation. *Cell Rep.* **13**, 2728–2740

35. Xu, Z., Zhang, L., Zhang, W., Meng, D., Zhang, H., Jiang, Y., Xu, X., Van Meter, M., Seluanov, A., Gorbunova, V., and Mao, Z. (2015) SIRT6 rescues the age related decline in base excision repair in a PARP1-dependent manner. *Cell Cycle*. **14**, 269–276
36. Hwang, B.-J., Jin, J., Gao, Y., Shi, G., Madabushi, A., Yan, A., Guan, X., Zalzman, M., Nakajima, S., Lan, L., and Lu, A.-L. (2015) SIRT6 protein deacetylase interacts with MYH DNA glycosylase, APE1 endonuclease, and Rad9-Rad1-Hus1 checkpoint clamp. *BMC Mol. Biol.* **16**, 12
37. Tian, X., Firsanov, D., Zhang, Z., Cheng, Y., Luo, L., Tomblin, G., Tan, R., Simon, M., Henderson, S., Steffan, J., Goldfarb, A., Tam, J., Zheng, K., Cornwell, A., Johnson, A., Yang, J.-N., Mao, Z., Manta, B., Dang, W., Zhang, Z., Vijg, J., Wolfe, A., Moody, K., Kennedy, B. K., Bohmann, D., Gladyshev, V. N., Seluanov, A., and Gorbunova, V. (2019) SIRT6 Is Responsible for More Efficient DNA Double-Strand Break Repair in Long-Lived Species. *Cell*. **177**, 622-638.e22
38. Michishita, E., McCord, R. A., Berber, E., Kioi, M., Padilla-Nash, H., Damian, M., Cheung, P., Kusumoto, R., Kawahara, T. L. A., Barrett, J. C., Chang, H. Y., Bohr, V. A., Ried, T., Gozani, O., and Chua, K. F. (2008) SIRT6 is a histone H3 lysine 9 deacetylase that modulates telomeric chromatin. *Nature*. **452**, 492–496
39. Michishita, E., McCord, R. A., Boxer, L. D., Barber, M. F., Hong, T., Gozani, O., and Chua, K. F. (2009) Cell cycle-dependent deacetylation of telomeric histone H3 lysine K56 by human SIRT6. *Cell Cycle*. **8**, 2664–2666
40. Tennen, R. I., Bua, D. J., Wright, W. E., and Chua, K. F. (2011) SIRT6 is required for maintenance of telomere position effect in human cells. *Nat Commun*. **2**, 433

41. Gao, Y., Tan, J., Jin, J., Ma, H., Chen, X., Leger, B., Xu, J., Spagnol, S. T., Dahl, K. N., Levine, A. S., Liu, Y., and Lan, L. (2018) SIRT6 facilitates directional telomere movement upon oxidative damage. *Sci Rep.* **8**, 5407
42. Li, Y., Meng, X., Wang, W., Liu, F., Hao, Z., Yang, Y., Zhao, J., Yin, W., Xu, L., Zhao, R., and Hu, J. (2017) Cardioprotective Effects of SIRT6 in a Mouse Model of Transverse Aortic Constriction-Induced Heart Failure. *Front Physiol.* **8**, 394
43. Tasselli, L., Xi, Y., Zheng, W., Tennen, R. I., Odrowaz, Z., Simeoni, F., Li, W., and Chua, K. F. (2016) SIRT6 deacetylates H3K18ac at pericentric chromatin to prevent mitotic errors and cellular senescence. *Nat. Struct. Mol. Biol.* **23**, 434–440
44. Xiao, C., Kim, H.-S., Lahusen, T., Wang, R.-H., Xu, X., Gavrilova, O., Jou, W., Gius, D., and Deng, C.-X. (2010) SIRT6 deficiency results in severe hypoglycemia by enhancing both basal and insulin-stimulated glucose uptake in mice. *J. Biol. Chem.* **285**, 36776–36784
45. Zhong, L., D’Urso, A., Toiber, D., Sebastian, C., Henry, R. E., Vadysirisack, D. D., Guimaraes, A., Marinelli, B., Wikstrom, J. D., Nir, T., Clish, C. B., Vaitheesvaran, B., Iliopoulos, O., Kurland, I., Dor, Y., Weissleder, R., Shirihai, O. S., Ellisen, L. W., Espinosa, J. M., and Mostoslavsky, R. (2010) The histone deacetylase Sirt6 regulates glucose homeostasis via Hif1alpha. *Cell.* **140**, 280–293
46. Warburg, O. (1956) On the origin of cancer cells. *Science.* **123**, 309–314
47. Gertman, O., Omer, D., Hendler, A., Stein, D., Onn, L., Khukhin, Y., Portillo, M., Zarivach, R., Cohen, H. Y., Toiber, D., and Aharoni, A. (2018) Directed evolution of SIRT6 for improved deacylation and glucose homeostasis maintenance. *Sci Rep.* **8**, 3538



48. Dominy, J. E., Lee, Y., Jedrychowski, M. P., Chim, H., Jurczak, M. J., Camporez, J. P., Ruan, H.-B., Feldman, J., Pierce, K., Mostoslavsky, R., Denu, J. M., Clish, C. B., Yang, X., Shulman, G. I., Gygi, S. P., and Puigserver, P. (2012) The deacetylase Sirt6 activates the acetyltransferase GCN5 and suppresses hepatic gluconeogenesis. *Mol. Cell.* **48**, 900–913
49. Puigserver, P., Rhee, J., Donovan, J., Walkey, C. J., Yoon, J. C., Oriente, F., Kitamura, Y., Altomonte, J., Dong, H., Accili, D., and Spiegelman, B. M. (2003) Insulin-regulated hepatic gluconeogenesis through FOXO1-PGC-1alpha interaction. *Nature.* **423**, 550–555
50. Xiong, X., Tao, R., DePinho, R. A., and Dong, X. C. (2013) Deletion of hepatic FoxO1/3/4 genes in mice significantly impacts on glucose metabolism through downregulation of gluconeogenesis and upregulation of glycolysis. *PLoS ONE.* **8**, e74340
51. Zhang, P., Tu, B., Wang, H., Cao, Z., Tang, M., Zhang, C., Gu, B., Li, Z., Wang, L., Yang, Y., Zhao, Y., Wang, H., Luo, J., Deng, C.-X., Gao, B., Roeder, R. G., and Zhu, W.-G. (2014) Tumor suppressor p53 cooperates with SIRT6 to regulate gluconeogenesis by promoting FoxO1 nuclear exclusion. *Proc. Natl. Acad. Sci. U.S.A.* **111**, 10684–10689
52. Kim, H.-S., Xiao, C., Wang, R.-H., Lahusen, T., Xu, X., Vassilopoulos, A., Vazquez-Ortiz, G., Jeong, W.-I., Park, O., Ki, S. H., Gao, B., and Deng, C.-X. (2010) Hepatic-specific disruption of SIRT6 in mice results in fatty liver formation due to enhanced glycolysis and triglyceride synthesis. *Cell Metab.* **12**, 224–236
53. Kanfi, Y., Peshti, V., Gil, R., Naiman, S., Nahum, L., Levin, E., Kronfeld-Schor, N., and Cohen, H. Y. (2010) SIRT6 protects against pathological damage caused by diet-induced obesity. *Aging Cell.* **9**, 162–173

54. Kuang, J., Zhang, Y., Liu, Q., Shen, J., Pu, S., Cheng, S., Chen, L., Li, H., Wu, T., Li, R., Li, Y., Zou, M., Zhang, Z., Jiang, W., Xu, G., Qu, A., Xie, W., and He, J. (2017) Fat-Specific Sirt6 Ablation Sensitizes Mice to High-Fat Diet-Induced Obesity and Insulin Resistance by Inhibiting Lipolysis. *Diabetes*. **66**, 1159–1171
55. He, J., Zhang, G., Pang, Q., Yu, C., Xiong, J., Zhu, J., and Chen, F. (2017) SIRT6 reduces macrophage foam cell formation by inducing autophagy and cholesterol efflux under ox-LDL condition. *FEBS J*. **284**, 1324–1337
56. Tao, R., Xiong, X., DePinho, R. A., Deng, C.-X., and Dong, X. C. (2013) FoxO3 transcription factor and Sirt6 deacetylase regulate low density lipoprotein (LDL)-cholesterol homeostasis via control of the proprotein convertase subtilisin/kexin type 9 (Pcsk9) gene expression. *J. Biol. Chem*. **288**, 29252–29259
57. Tao, R., Xiong, X., DePinho, R. A., Deng, C.-X., and Dong, X. C. (2013) Hepatic SREBP-2 and cholesterol biosynthesis are regulated by FoxO3 and Sirt6. *J. Lipid Res*. **54**, 2745–2753
58. Elhanati, S., Kanfi, Y., Varvak, A., Roichman, A., Carmel-Gross, I., Barth, S., Gibor, G., and Cohen, H. Y. (2013) Multiple regulatory layers of SREBP1/2 by SIRT6. *Cell Rep*. **4**, 905–912
59. Shimano, H., and Sato, R. (2017) SREBP-regulated lipid metabolism: convergent physiology - divergent pathophysiology. *Nat Rev Endocrinol*. **13**, 710–730
60. Elhanati, S., Ben-Hamo, R., Kanfi, Y., Varvak, A., Glazz, R., Lerrer, B., Efroni, S., and Cohen, H. Y. (2016) Reciprocal Regulation between SIRT6 and miR-122 Controls Liver Metabolism and Predicts Hepatocarcinoma Prognosis. *Cell Rep*. **14**, 234–242

61. Naiman, S., Huynh, F. K., Gil, R., Glick, Y., Shahar, Y., Touitou, N., Nahum, L., Avivi, M. Y., Roichman, A., Kanfi, Y., Gertler, A. A., Doniger, T., Ilkayeva, O. R., Abramovich, I., Yaron, O., Lerrer, B., Gottlieb, E., Harris, R. A., Gerber, D., Hirschey, M. D., and Cohen, H. Y. (2019) SIRT6 Promotes Hepatic Beta-Oxidation via Activation of PPAR $\alpha$ . *Cell Rep.* **29**, 4127–4143.e8
62. Kaeberlein, M., McVey, M., and Guarente, L. (1999) The SIR2/3/4 complex and SIR2 alone promote longevity in *Saccharomyces cerevisiae* by two different mechanisms. *Genes Dev.* **13**, 2570–2580
63. Fritze, C. E., Verschueren, K., Strich, R., and Easton Esposito, R. (1997) Direct evidence for SIR2 modulation of chromatin structure in yeast rDNA. *EMBO J.* **16**, 6495–6509
64. Zhang, N., Li, Z., Mu, W., Li, L., Liang, Y., Lu, M., Wang, Z., Qiu, Y., and Wang, Z. (2016) Calorie restriction-induced SIRT6 activation delays aging by suppressing NF- $\kappa$ B signaling. *Cell Cycle.* **15**, 1009–1018
65. Perkins, N. D. (2015) The importance of the p50 NF- $\kappa$ B subunit. *Cell Cycle.* **14**, 2877–2878
66. Sharma, A., Diecke, S., Zhang, W. Y., Lan, F., He, C., Mordwinkin, N. M., Chua, K. F., and Wu, J. C. (2013) The role of SIRT6 protein in aging and reprogramming of human induced pluripotent stem cells. *J. Biol. Chem.* **288**, 18439–18447
67. Chen, Q., Hao, W., Xiao, C., Wang, R., Xu, X., Lu, H., Chen, W., and Deng, C.-X. (2017) SIRT6 Is Essential for Adipocyte Differentiation by Regulating Mitotic Clonal Expansion. *Cell Rep.* **18**, 3155–3166

68. Qian, M., Liu, Z., Peng, L., Tang, X., Meng, F., Ao, Y., Zhou, M., Wang, M., Cao, X., Qin, B., Wang, Z., Zhou, Z., Wang, G., Gao, Z., Xu, J., and Liu, B. (2018) Boosting ATM activity alleviates aging and extends lifespan in a mouse model of progeria. *Elife*. 10.7554/eLife.34836
69. TenNapel, M. J., Lynch, C. F., Burns, T. L., Wallace, R., Smith, B. J., Button, A., and Domann, F. E. (2014) SIRT6 minor allele genotype is associated with >5-year decrease in lifespan in an aged cohort. *PLoS ONE*. **9**, e115616
70. Li, Y., Qin, J., Wei, X., Liang, G., Shi, L., Jiang, M., Xia, T., Liang, X., He, M., and Zhang, Z. (2016) Association of SIRT6 Gene Polymorphisms with Human Longevity. *Iran. J. Public Health*. **45**, 1420–1426
71. Hirvonen, K., Laivuori, H., Lahti, J., Strandberg, T., Eriksson, J. G., and Hackman, P. (2017) SIRT6 polymorphism rs117385980 is associated with longevity and healthy aging in Finnish men. *BMC Med. Genet.* **18**, 41
72. Min, L., Ji, Y., Bakiri, L., Qiu, Z., Cen, J., Chen, X., Chen, L., Scheuch, H., Zheng, H., Qin, L., Zatloukal, K., Hui, L., and Wagner, E. F. (2012) Liver cancer initiation is controlled by AP-1 through SIRT6-dependent inhibition of survivin. *Nat. Cell Biol.* **14**, 1203–1211
73. Marquardt, J. U., Fischer, K., Baus, K., Kashyap, A., Ma, S., Krupp, M., Linke, M., Teufel, A., Zechner, U., Strand, D., Thorgeirsson, S. S., Galle, P. R., and Strand, S. (2013) Sirtuin-6-dependent genetic and epigenetic alterations are associated with poor clinical outcome in hepatocellular carcinoma patients. *Hepatology*. **58**, 1054–1064
74. Zhang, J., Yin, X.-J., Xu, C.-J., Ning, Y.-X., Chen, M., Zhang, H., Chen, S.-F., and Yao, L.-Q. (2015) The histone deacetylase SIRT6 inhibits ovarian cancer cell proliferation via down-regulation of Notch 3 expression. *Eur Rev Med Pharmacol Sci.* **19**, 818–824

75. Zhang, Y., Nie, L., Xu, K., Fu, Y., Zhong, J., Gu, K., and Zhang, L. (2019) SIRT6, a novel direct transcriptional target of FoxO3a, mediates colon cancer therapy. *Theranostics*. **9**, 2380–2394
76. Qi, J., Cui, C., Deng, Q., Wang, L., Chen, R., Zhai, D., Xie, L., and Yu, J. (2018) Downregulated SIRT6 and upregulated NMNAT2 are associated with the presence, depth and stage of colorectal cancer. *Oncol Lett*. **16**, 5829–5837
77. Barretina, J., Caponigro, G., Stransky, N., Venkatesan, K., Margolin, A. A., Kim, S., Wilson, C. J., Lehár, J., Kryukov, G. V., Sonkin, D., Reddy, A., Liu, M., Murray, L., Berger, M. F., Monahan, J. E., Morais, P., Meltzer, J., Korejwa, A., Jané-Valbuena, J., Mapa, F. A., Thibault, J., Bric-Furlong, E., Raman, P., Shipway, A., Engels, I. H., Cheng, J., Yu, G. K., Yu, J., Aspesi, P., de Silva, M., Jagtap, K., Jones, M. D., Wang, L., Hatton, C., Palesscandolo, E., Gupta, S., Mahan, S., Sougnez, C., Onofrio, R. C., Liefeld, T., MacConaill, L., Winckler, W., Reich, M., Li, N., Mesirov, J. P., Gabriel, S. B., Getz, G., Ardlie, K., Chan, V., Myer, V. E., Weber, B. L., Porter, J., Warmuth, M., Finan, P., Harris, J. L., Meyerson, M., Golub, T. R., Morrissey, M. P., Sellers, W. R., Schlegel, R., and Garraway, L. A. (2012) The Cancer Cell Line Encyclopedia enables predictive modelling of anticancer drug sensitivity. *Nature*. **483**, 603–607
78. Kugel, S., Sebastián, C., Fitamant, J., Ross, K. N., Saha, S. K., Jain, E., Gladden, A., Arora, K. S., Kato, Y., Rivera, M. N., Ramaswamy, S., Sadreyev, R. I., Goren, A., Deshpande, V., Bardeesy, N., and Mostoslavsky, R. (2016) SIRT6 Suppresses Pancreatic Cancer through Control of Lin28b. *Cell*. **165**, 1401–1415
79. Tu, H.-C., Schwitalla, S., Qian, Z., LaPier, G. S., Yermalovich, A., Ku, Y.-C., Chen, S.-C., Viswanathan, S. R., Zhu, H., Nishihara, R., Inamura, K., Kim, S. A., Morikawa, T., Mima, K.,

- Sukawa, Y., Yang, J., Meredith, G., Fuchs, C. S., Ogino, S., and Daley, G. Q. (2015) LIN28 cooperates with WNT signaling to drive invasive intestinal and colorectal adenocarcinoma in mice and humans. *Genes Dev.* **29**, 1074–1086
80. Wheatley, S. P., and Altieri, D. C. (2019) Survivin at a glance. *J. Cell. Sci.* 10.1242/jcs.223826
81. Thirumurthi, U., Shen, J., Xia, W., LaBaff, A. M., Wei, Y., Li, C.-W., Chang, W.-C., Chen, C.-H., Lin, H.-K., Yu, D., and Hung, M.-C. (2014) MDM2-mediated degradation of SIRT6 phosphorylated by AKT1 promotes tumorigenesis and trastuzumab resistance in breast cancer. *Sci Signal.* **7**, ra71
82. Lin, Z., Yang, H., Tan, C., Li, J., Liu, Z., Quan, Q., Kong, S., Ye, J., Gao, B., and Fang, D. (2013) USP10 antagonizes c-Myc transcriptional activation through SIRT6 stabilization to suppress tumor formation. *Cell Rep.* **5**, 1639–1649
83. Cai, J., Zuo, Y., Wang, T., Cao, Y., Cai, R., Chen, F.-L., Cheng, J., and Mu, J. (2016) A crucial role of SUMOylation in modulating Sirt6 deacetylation of H3 at lysine 56 and its tumor suppressive activity. *Oncogene.* **35**, 4949–4956
84. Bhardwaj, A., and Das, S. (2016) SIRT6 deacetylates PKM2 to suppress its nuclear localization and oncogenic functions. *Proc. Natl. Acad. Sci. U.S.A.* **113**, E538-547
85. Cea, M., Cagnetta, A., Adamia, S., Acharya, C., Tai, Y.-T., Fulciniti, M., Ohguchi, H., Munshi, A., Acharya, P., Bhasin, M. K., Zhong, L., Carrasco, R., Monacelli, F., Ballestrero, A., Richardson, P., Gobbi, M., Lemoli, R. M., Munshi, N., Hideshima, T., Nencioni, A., Chauhan, D., and Anderson, K. C. (2016) Evidence for a role of the histone deacetylase SIRT6 in DNA damage response of multiple myeloma cells. *Blood.* **127**, 1138–1150

86. Lai, C.-C., Lin, P.-M., Lin, S.-F., Hsu, C.-H., Lin, H.-C., Hu, M.-L., Hsu, C.-M., and Yang, M.-Y. (2013) Altered expression of SIRT gene family in head and neck squamous cell carcinoma. *Tumour Biol.* **34**, 1847–1854
87. Wang, J. C., Kafeel, M. I., Avezbakiyev, B., Chen, C., Sun, Y., Rathnasabapathy, C., Kalavar, M., He, Z., Burton, J., and Lichter, S. (2011) Histone deacetylase in chronic lymphocytic leukemia. *Oncology.* **81**, 325–329
88. Cagnetta, A., Soncini, D., Orecchioni, S., Talarico, G., Minetto, P., Guolo, F., Retali, V., Colombo, N., Carminati, E., Clavio, M., Miglino, M., Bergamaschi, M., Nahimana, A., Duchosal, M., Todoerti, K., Neri, A., Passalacqua, M., Bruzzone, S., Nencioni, A., Bertolini, F., Gobbi, M., Lemoli, R. M., and Cea, M. (2018) Depletion of SIRT6 enzymatic activity increases acute myeloid leukemia cells' vulnerability to DNA-damaging agents. *Haematologica.* **103**, 80–90
89. Jackson, S. P. (1997) DNA-dependent protein kinase. *Int. J. Biochem. Cell Biol.* **29**, 935–938
90. Bauer, I., Grozio, A., Lasigliè, D., Basile, G., Sturla, L., Magnone, M., Sociali, G., Soncini, D., Caffa, I., Poggi, A., Zoppoli, G., Cea, M., Feldmann, G., Mostoslavsky, R., Ballestrero, A., Patrone, F., Bruzzone, S., and Nencioni, A. (2012) The NAD<sup>+</sup>-dependent histone deacetylase SIRT6 promotes cytokine production and migration in pancreatic cancer cells by regulating Ca<sup>2+</sup> responses. *J. Biol. Chem.* **287**, 40924–40937
91. Wehrhahn, J., Kraft, R., Harteneck, C., and Hauschildt, S. (2010) Transient receptor potential melastatin 2 is required for lipopolysaccharide-induced cytokine production in human monocytes. *J. Immunol.* **184**, 2386–2393

92. Lee, N., Ryu, H. G., Kwon, J.-H., Kim, D.-K., Kim, S. R., Wang, H. J., Kim, K.-T., and Choi, K. Y. (2016) SIRT6 Depletion Suppresses Tumor Growth by Promoting Cellular Senescence Induced by DNA Damage in HCC. *PLoS ONE*. **11**, e0165835
93. Ran, L.-K., Chen, Y., Zhang, Z.-Z., Tao, N.-N., Ren, J.-H., Zhou, L., Tang, H., Chen, X., Chen, K., Li, W.-Y., Huang, A.-L., and Chen, J. (2016) SIRT6 Overexpression Potentiates Apoptosis Evasion in Hepatocellular Carcinoma via BCL2-Associated X Protein-Dependent Apoptotic Pathway. *Clin. Cancer Res.* **22**, 3372–3382
94. Zhang, Z.-G., and Qin, C.-Y. (2014) Sirt6 suppresses hepatocellular carcinoma cell growth via inhibiting the extracellular signal-regulated kinase signaling pathway. *Mol Med Rep.* **9**, 882–888
95. Greiss, S., and Gartner, A. (2009) Sirtuin/Sir2 phylogeny, evolutionary considerations and structural conservation. *Mol. Cells.* **28**, 407–415
96. Zhu, A. Y., Zhou, Y., Khan, S., Deitsch, K. W., Hao, Q., and Lin, H. (2012) Plasmodium falciparum Sir2A preferentially hydrolyzes medium and long chain fatty acyl lysine. *ACS Chem. Biol.* **7**, 155–159
97. Du, J., Zhou, Y., Su, X., Yu, J. J., Khan, S., Jiang, H., Kim, J., Woo, J., Kim, J. H., Choi, B. H., He, B., Chen, W., Zhang, S., Cerione, R. A., Auwerx, J., Hao, Q., and Lin, H. (2011) Sirt5 is a NAD-dependent protein lysine demalonylase and desuccinylase. *Science*. **334**, 806–809
98. Rossmann, M. G., Moras, D., and Olsen, K. W. (1974) Chemical and biological evolution of nucleotide-binding protein. *Nature*. **250**, 194–199
99. Sanders, B. D., Jackson, B., and Marmorstein, R. (2010) Structural basis for sirtuin function: what we know and what we don't. *Biochim. Biophys. Acta*. **1804**, 1604–1616



100. Madsen, A. S., Andersen, C., Daoud, M., Anderson, K. A., Laursen, J. S., Chakladar, S., Huynh, F. K., Colaço, A. R., Backos, D. S., Fristrup, P., Hirschey, M. D., and Olsen, C. A. (2016) Investigating the Sensitivity of NAD<sup>+</sup>-dependent Sirtuin Deacylation Activities to NADH. *J. Biol. Chem.* **291**, 7128–7141
101. Jin, L., Wei, W., Jiang, Y., Peng, H., Cai, J., Mao, C., Dai, H., Choy, W., Bemis, J. E., Jirousek, M. R., Milne, J. C., Westphal, C. H., and Perni, R. B. (2009) Crystal structures of human SIRT3 displaying substrate-induced conformational changes. *J. Biol. Chem.* **284**, 24394–24405
102. Borra, M. T., Langer, M. R., Slama, J. T., and Denu, J. M. (2004) Substrate specificity and kinetic mechanism of the Sir2 family of NAD<sup>+</sup>-dependent histone/protein deacetylases. *Biochemistry*. **43**, 9877–9887
103. Klein, M. A., Liu, C., Kuznetsov, V. I., Feltenberger, J. B., Tang, W., and Denu, J. M. (2020) Mechanism of activation for the sirtuin 6 protein deacylase. *J Biol Chem.* **295**, 1385–1399
104. Finnin, M. S., Donigian, J. R., and Pavletich, N. P. (2001) Structure of the histone deacetylase SIRT2. *Nat. Struct. Biol.* **8**, 621–625
105. Schuetz, A., Min, J., Antoshenko, T., Wang, C.-L., Allali-Hassani, A., Dong, A., Loppnau, P., Vedadi, M., Bochkarev, A., Sternglanz, R., and Plotnikov, A. N. (2007) Structural basis of inhibition of the human NAD<sup>+</sup>-dependent deacetylase SIRT5 by suramin. *Structure*. **15**, 377–389
106. Ronnebaum, S. M., Wu, Y., McDonough, H., and Patterson, C. (2013) The ubiquitin ligase CHIP prevents SirT6 degradation through noncanonical ubiquitination. *Mol. Cell. Biol.* **33**, 4461–4472

107. Kalous, K. S., Wynia-Smith, S. L., Olp, M. D., and Smith, B. C. (2016) Mechanism of Sirt1 NAD<sup>+</sup>-dependent Protein Deacetylase Inhibition by Cysteine S-Nitrosation. *J. Biol. Chem.* **291**, 25398–25410
108. Sherman, J. M., Stone, E. M., Freeman-Cook, L. L., Brachmann, C. B., Boeke, J. D., and Pillus, L. (1999) The conserved core of a human SIR2 homologue functions in yeast silencing. *Mol. Biol. Cell.* **10**, 3045–3059
109. Min, J., Landry, J., Sternglanz, R., and Xu, R. M. (2001) Crystal structure of a SIR2 homologue-NAD complex. *Cell.* **105**, 269–279
110. Wood, M., Rymarchyk, S., Zheng, S., and Cen, Y. (2018) Trichostatin A inhibits deacetylation of histone H3 and p53 by SIRT6. *Arch. Biochem. Biophys.* **638**, 8–17
111. Finnin, M. S., Donigian, J. R., Cohen, A., Richon, V. M., Rifkind, R. A., Marks, P. A., Breslow, R., and Pavletich, N. P. (1999) Structures of a histone deacetylase homologue bound to the TSA and SAHA inhibitors. *Nature.* **401**, 188–193
112. You, W., and Steegborn, C. (2018) Structural Basis of Sirtuin 6 Inhibition by the Hydroxamate Trichostatin A: Implications for Protein Deacetylase Drug Development. *J. Med. Chem.* **61**, 10922–10928
113. Huang, Z., Zhao, J., Deng, W., Chen, Y., Shang, J., Song, K., Zhang, L., Wang, C., Lu, S., Yang, X., He, B., Min, J., Hu, H., Tan, M., Xu, J., Zhang, Q., Zhong, J., Sun, X., Mao, Z., Lin, H., Xiao, M., Chin, Y. E., Jiang, H., Xu, Y., Chen, G., and Zhang, J. (2018) Identification of a cellularly active SIRT6 allosteric activator. *Nat. Chem. Biol.* **14**, 1118–1126

114. You, W., Rotili, D., Li, T.-M., Kambach, C., Meleshin, M., Schutkowski, M., Chua, K. F., Mai, A., and Steegborn, C. (2017) Structural Basis of Sirtuin 6 Activation by Synthetic Small Molecules. *Angew. Chem. Int. Ed. Engl.* **56**, 1007–1011
115. Rahnasto-Rilla, M., Tyni, J., Huovinen, M., Jarho, E., Kulikowicz, T., Ravichandran, S., A Bohr, V., Ferrucci, L., Lahtela-Kakkonen, M., and Moaddel, R. (2018) Natural polyphenols as sirtuin 6 modulators. *Sci Rep.* **8**, 4163
116. Rauh, D., Fischer, F., Gertz, M., Lakshminarasimhan, M., Bergbrede, T., Aladini, F., Kambach, C., Becker, C. F. W., Zerweck, J., Schutkowski, M., and Steegborn, C. (2013) An acetylome peptide microarray reveals specificities and deacetylation substrates for all human sirtuin isoforms. *Nature Communications.* **4**, 1–10
117. Zhang, X., Khan, S., Jiang, H., Antonyak, M. A., Chen, X., Spiegelman, N. A., Shrimp, J. H., Cerione, R. A., and Lin, H. (2016) Identifying the functional contribution of the defatty-acylase activity of SIRT6. *Nat Chem Biol.* **12**, 614–620
118. Zhang, X., Spiegelman, N. A., Nelson, O. D., Jing, H., and Lin, H. (2017) SIRT6 regulates Ras-related protein R-Ras2 by lysine defatty-acylation. *eLife.* **6**, e25158
119. Miteva, Y. V., and Cristea, I. M. (2014) A proteomic perspective of Sirtuin 6 (SIRT6) phosphorylation and interactions and their dependence on its catalytic activity. *Mol. Cell Proteomics.* **13**, 168–183
120. Strom, A. R., Emelyanov, A. V., Mir, M., Fyodorov, D. V., Darzacq, X., and Karpen, G. H. (2017) Phase separation drives heterochromatin domain formation. *Nature.* **547**, 241–245

121. Guthmann, M., Burton, A., and Torres-Padilla, M.-E. (2019) Expression and phase separation potential of heterochromatin proteins during early mouse development. *EMBO Rep.* **20**, e47952
122. Tennen, R. I., and Chua, K. F. (2011) Chromatin regulation and genome maintenance by mammalian SIRT6. *Trends Biochem. Sci.* **36**, 39–46
123. Dephoure, N., Zhou, C., Villén, J., Beausoleil, S. A., Bakalarski, C. E., Elledge, S. J., and Gygi, S. P. (2008) A quantitative atlas of mitotic phosphorylation. *Proc. Natl. Acad. Sci. U.S.A.* **105**, 10762–10767
124. Olsen, J. V., Vermeulen, M., Santamaria, A., Kumar, C., Miller, M. L., Jensen, L. J., Gnad, F., Cox, J., Jensen, T. S., Nigg, E. A., Brunak, S., and Mann, M. (2010) Quantitative phosphoproteomics reveals widespread full phosphorylation site occupancy during mitosis. *Sci Signal.* **3**, ra3
125. Tanner, K. G., Landry, J., Sternglanz, R., and Denu, J. M. (2000) Silent information regulator 2 family of NAD- dependent histone/protein deacetylases generates a unique product, 1-O-acetyl-ADP-ribose. *Proc. Natl. Acad. Sci. U.S.A.* **97**, 14178–14182
126. Cen, Y., and Sauve, A. A. (2010) Transition state of ADP-ribosylation of acetyllysine catalyzed by *Archaeoglobus fulgidus* Sir2 determined by kinetic isotope effects and computational approaches. *J. Am. Chem. Soc.* **132**, 12286–12298
127. Smith, B. C., and Denu, J. M. (2007) Sir2 deacetylases exhibit nucleophilic participation of acetyl-lysine in NAD<sup>+</sup> cleavage. *J. Am. Chem. Soc.* **129**, 5802–5803
128. Smith, B. C., and Denu, J. M. (2006) Sir2 protein deacetylases: evidence for chemical intermediates and functions of a conserved histidine. *Biochemistry.* **45**, 272–282

129. Smith, B. C., and Denu, J. M. (2007) Mechanism-based inhibition of Sir2 deacetylases by thioacetyl-lysine peptide. *Biochemistry*. **46**, 14478–14486
130. Sauve, A. A., Celic, I., Avalos, J., Deng, H., Boeke, J. D., and Schramm, V. L. (2001) Chemistry of gene silencing: the mechanism of NAD<sup>+</sup>-dependent deacetylation reactions. *Biochemistry*. **40**, 15456–15463
131. Hawse, W. F., Hoff, K. G., Fatkins, D. G., Daines, A., Zubkova, O. V., Schramm, V. L., Zheng, W., and Wolberger, C. (2008) Structural insights into intermediate steps in the Sir2 deacetylation reaction. *Structure*. **16**, 1368–1377
132. Jackson, M. D., Schmidt, M. T., Oppenheimer, N. J., and Denu, J. M. (2003) Mechanism of nicotinamide inhibition and transglycosidation by Sir2 histone/protein deacetylases. *J. Biol. Chem.* **278**, 50985–50998
133. Shi, Y., Zhou, Y., Wang, S., and Zhang, Y. (2013) Sirtuin Deacetylation Mechanism and Catalytic Role of the Dynamic Cofactor Binding Loop. *J Phys Chem Lett*. **4**, 491–495
134. Frye, R. A. (1999) Characterization of five human cDNAs with homology to the yeast SIR2 gene: Sir2-like proteins (sirtuins) metabolize NAD and may have protein ADP-ribosyltransferase activity. *Biochem. Biophys. Res. Commun.* **260**, 273–279
135. Haigis, M. C., Mostoslavsky, R., Haigis, K. M., Fahie, K., Christodoulou, D. C., Murphy, A. J., Valenzuela, D. M., Yancopoulos, G. D., Karow, M., Blander, G., Wolberger, C., Prolla, T. A., Weindruch, R., Alt, F. W., and Guarente, L. (2006) SIRT4 inhibits glutamate dehydrogenase and opposes the effects of calorie restriction in pancreatic beta cells. *Cell*. **126**, 941–954

136. Kowieski, T. M., Lee, S., and Denu, J. M. (2008) Acetylation-dependent ADP-ribosylation by *Trypanosoma brucei* Sir2. *J. Biol. Chem.* **283**, 5317–5326
137. Milne, J. C., Lambert, P. D., Schenk, S., Carney, D. P., Smith, J. J., Gagne, D. J., Jin, L., Boss, O., Perni, R. B., Vu, C. B., Bemis, J. E., Xie, R., Disch, J. S., Ng, P. Y., Nunes, J. J., Lynch, A. V., Yang, H., Galonek, H., Israelian, K., Choy, W., Iffland, A., Lavu, S., Medvedik, O., Sinclair, D. A., Olefsky, J. M., Jirousek, M. R., Elliott, P. J., and Westphal, C. H. (2007) Small molecule activators of SIRT1 as therapeutics for the treatment of type 2 diabetes. *Nature.* **450**, 712–716
138. Feldman, J. L., Dittenhafer-Reed, K. E., Kudo, N., Thelen, J. N., Ito, A., Yoshida, M., and Denu, J. M. (2015) Kinetic and Structural Basis for Acyl-Group Selectivity and NAD(+) Dependence in Sirtuin-Catalyzed Deacylation. *Biochemistry.* **54**, 3037–3050
139. Howitz, K. T., Bitterman, K. J., Cohen, H. Y., Lamming, D. W., Lavu, S., Wood, J. G., Zipkin, R. E., Chung, P., Kisielewski, A., Zhang, L.-L., Scherer, B., and Sinclair, D. A. (2003) Small molecule activators of sirtuins extend *Saccharomyces cerevisiae* lifespan. *Nature.* **425**, 191–196
140. Baur, J. A., Pearson, K. J., Price, N. L., Jamieson, H. A., Lerin, C., Kalra, A., Prabhu, V. V., Allard, J. S., Lopez-Lluch, G., Lewis, K., Pistell, P. J., Poosala, S., Becker, K. G., Boss, O., Gwinn, D., Wang, M., Ramaswamy, S., Fishbein, K. W., Spencer, R. G., Lakatta, E. G., Le Couteur, D., Shaw, R. J., Navas, P., Puigserver, P., Ingram, D. K., de Cabo, R., and Sinclair, D. A. (2006) Resveratrol improves health and survival of mice on a high-calorie diet. *Nature.* **444**, 337–342
141. Hubbard, B. P., Gomes, A. P., Dai, H., Li, J., Case, A. W., Considine, T., Riera, T. V., Lee, J. E., E, S. Y., Lamming, D. W., Pentelute, B. L., Schuman, E. R., Stevens, L. A., Ling, A. J. Y., Armour, S. M., Michan, S., Zhao, H., Jiang, Y., Sweitzer, S. M., Blum, C. A., Disch, J. S., Ng, P. Y., Howitz, K. T., Rolo, A. P., Hamuro, Y., Moss, J., Perni, R. B., Ellis, J. L., Vlasuk, G. P., and

Sinclair, D. A. (2013) Evidence for a common mechanism of SIRT1 regulation by allosteric activators. *Science*. **339**, 1216–1219

142. Mercken, E. M., Mitchell, S. J., Martin-Montalvo, A., Minor, R. K., Almeida, M., Gomes, A. P., Scheibye-Knudsen, M., Palacios, H. H., Licata, J. J., Zhang, Y., Becker, K. G., Khraiwesh, H., González-Reyes, J. A., Villalba, J. M., Baur, J. A., Elliott, P., Westphal, C., Vlasuk, G. P., Ellis, J. L., Sinclair, D. A., Bernier, M., and de Cabo, R. (2014) SRT2104 extends survival of male mice on a standard diet and preserves bone and muscle mass. *Aging Cell*. **13**, 787–796

143. Mitchell, S. J., Martin-Montalvo, A., Mercken, E. M., Palacios, H. H., Ward, T. M., Abulwerdi, G., Minor, R. K., Vlasuk, G. P., Ellis, J. L., Sinclair, D. A., Dawson, J., Allison, D. B., Zhang, Y., Becker, K. G., Bernier, M., and de Cabo, R. (2014) The SIRT1 activator SRT1720 extends lifespan and improves health of mice fed a standard diet. *Cell Rep*. **6**, 836–843

144. Dai, H., Sinclair, D. A., Ellis, J. L., and Steegborn, C. (2018) Sirtuin activators and inhibitors: Promises, achievements, and challenges. *Pharmacol. Ther.* **188**, 140–154

145. Lavu, S., Boss, O., Elliott, P. J., and Lambert, P. D. (2008) Sirtuins--novel therapeutic targets to treat age-associated diseases. *Nat Rev Drug Discov*. **7**, 841–853

146. Najt, C. P., Khan, S. A., Heden, T. D., Witthuhn, B. A., Perez, M., Heier, J. L., Mead, L. E., Franklin, M. P., Karanja, K. K., Graham, M. J., Mashek, M. T., Bernlohr, D. A., Parker, L., Chow, L. S., and Mashek, D. G. (2020) Lipid Droplet-Derived Monounsaturated Fatty Acids Traffic via PLIN5 to Allosterically Activate SIRT1. *Mol. Cell*. **77**, 810-824.e8

147. Yasuda, M., Wilson, D. R., Fugmann, S. D., and Moaddel, R. (2011) Synthesis and characterization of SIRT6 protein coated magnetic beads: identification of a novel inhibitor of SIRT6 deacetylase from medicinal plant extracts. *Anal. Chem*. **83**, 7400–7407

148. Rahnasto-Rilla, M., Kokkola, T., Jarho, E., Lahtela-Kakkonen, M., and Moaddel, R. (2016) N-Acylethanolamines Bind to SIRT6. *Chembiochem.* **17**, 77–81
149. You, W., Zheng, W., Weiss, S., Chua, K. F., and Steegborn, C. (2019) Structural basis for the activation and inhibition of Sirtuin 6 by quercetin and its derivatives. *Sci Rep.* **9**, 19176
150. Kumar, S., and Pandey, A. K. (2013) Chemistry and biological activities of flavonoids: an overview. *ScientificWorldJournal.* **2013**, 162750
151. He, J., and Giusti, M. M. (2010) Anthocyanins: natural colorants with health-promoting properties. *Annu Rev Food Sci Technol.* **1**, 163–187
152. Rahnasto-Rilla, M. K., McLoughlin, P., Kulikowicz, T., Doyle, M., Bohr, V. A., Lahtela-Kakkonen, M., Ferrucci, L., Hayes, M., and Moaddel, R. (2017) The Identification of a SIRT6 Activator from Brown Algae *Fucus distichus*. *Mar Drugs.* 10.3390/md15060190
153. Schlicker, C., Boanca, G., Lakshminarasimhan, M., and Steegborn, C. (2011) Structure-based development of novel sirtuin inhibitors. *Aging (Albany NY).* **3**, 852–872
154. Smith, B. C., Hallows, W. C., and Denu, J. M. (2009) A continuous microplate assay for sirtuins and nicotinamide-producing enzymes. *Anal. Biochem.* **394**, 101–109
155. Iachettini, S., Trisciuglio, D., Rotili, D., Lucidi, A., Salvati, E., Zizza, P., Di Leo, L., Del Bufalo, D., Ciriolo, M. R., Leonetti, C., Steegborn, C., Mai, A., Rizzo, A., and Biroccio, A. (2018) Pharmacological activation of SIRT6 triggers lethal autophagy in human cancer cells. *Cell Death Dis.* **9**, 996
156. Guan, X., Upadhyay, A., Munshi, S., and Chakrabarti, R. (2018) Biophysical characterization of hit compounds for mechanism-based enzyme activation. *PLoS ONE.* **13**, e0194175



157. Krautkramer, K. A., Reiter, L., Denu, J. M., and Dowell, J. A. (2015) Quantification of SAHA-Dependent Changes in Histone Modifications Using Data-Independent Acquisition Mass Spectrometry. *J. Proteome Res.* **14**, 3252–3262
158. Damonte, P., Sociali, G., Parenti, M. D., Soncini, D., Bauer, I., Boero, S., Grozio, A., Holtey, M. von, Piacente, F., Becherini, P., Sanguineti, R., Salis, A., Damonte, G., Cea, M., Murone, M., Poggi, A., Nencioni, A., Del Rio, A., and Bruzzone, S. (2017) SIRT6 inhibitors with salicylate-like structure show immunosuppressive and chemosensitizing effects. *Bioorg. Med. Chem.* **25**, 5849–5858
159. Sociali, G., Magnone, M., Ravera, S., Damonte, P., Vigliarolo, T., Von Holtey, M., Vellone, V. G., Millo, E., Caffa, I., Cea, M., Parenti, M. D., Del Rio, A., Murone, M., Mostoslavsky, R., Grozio, A., Nencioni, A., and Bruzzone, S. (2017) Pharmacological Sirt6 inhibition improves glucose tolerance in a type 2 diabetes mouse model. *FASEB J.* **31**, 3138–3149
160. Khan, R. I., Nirzhor, S. S. R., and Akter, R. (2018) A Review of the Recent Advances Made with SIRT6 and its Implications on Aging Related Processes, Major Human Diseases, and Possible Therapeutic Targets. *Biomolecules*. 10.3390/biom8030044
161. Bitterman, K. J., Anderson, R. M., Cohen, H. Y., Latorre-Esteves, M., and Sinclair, D. A. (2002) Inhibition of silencing and accelerated aging by nicotinamide, a putative negative regulator of yeast sir2 and human SIRT1. *J. Biol. Chem.* **277**, 45099–45107
162. Avalos, J. L., Bever, K. M., and Wolberger, C. (2005) Mechanism of sirtuin inhibition by nicotinamide: altering the NAD(+) cosubstrate specificity of a Sir2 enzyme. *Mol. Cell.* **17**, 855–868

163. Zhao, K., Harshaw, R., Chai, X., and Marmorstein, R. (2004) Structural basis for nicotinamide cleavage and ADP-ribose transfer by NAD(+)-dependent Sir2 histone/protein deacetylases. *Proc. Natl. Acad. Sci. U.S.A.* **101**, 8563–8568
164. Sauve, A. A., and Schramm, V. L. (2003) Sir2 regulation by nicotinamide results from switching between base exchange and deacetylation chemistry. *Biochemistry*. **42**, 9249–9256
165. Hu, J., He, B., Bhargava, S., and Lin, H. (2013) A fluorogenic assay for screening Sirt6 modulators. *Org. Biomol. Chem.* **11**, 5213–5216
166. Anderson, R. M., Bitterman, K. J., Wood, J. G., Medvedik, O., and Sinclair, D. A. (2003) Nicotinamide and PNC1 govern lifespan extension by calorie restriction in *Saccharomyces cerevisiae*. *Nature*. **423**, 181–185
167. Fatkins, D. G., Monnot, A. D., and Zheng, W. (2006) Nepsilon-thioacetyl-lysine: a multi-facet functional probe for enzymatic protein lysine Nepsilon-deacetylation. *Bioorg. Med. Chem. Lett.* **16**, 3651–3656
168. Kokkonen, P., Rahnasto-Rilla, M., Kiviranta, P. H., Huhtiniemi, T., Laitinen, T., Poso, A., Jarho, E., and Lahtela-Kakkonen, M. (2012) Peptides and Pseudopeptides as SIRT6 Deacetylation Inhibitors. *ACS Med Chem Lett.* **3**, 969–974
169. Zang, W., Hao, Y., Wang, Z., and Zheng, W. (2015) Novel thiourea-based sirtuin inhibitory warheads. *Bioorg. Med. Chem. Lett.* **25**, 3319–3324
170. Liu, J., and Zheng, W. (2016) Cyclic peptide-based potent human SIRT6 inhibitors. *Org. Biomol. Chem.* **14**, 5928–5935

171. Heltweg, B., Gatbonton, T., Schuler, A. D., Posakony, J., Li, H., Goehle, S., Kollipara, R., Depinho, R. A., Gu, Y., Simon, J. A., and Bedalov, A. (2006) Antitumor activity of a small-molecule inhibitor of human silent information regulator 2 enzymes. *Cancer Res.* **66**, 4368–4377
172. Lain, S., Hollick, J. J., Campbell, J., Staples, O. D., Higgins, M., Aoubala, M., McCarthy, A., Appleyard, V., Murray, K. E., Baker, L., Thompson, A., Mathers, J., Holland, S. J., Stark, M. J. R., Pass, G., Woods, J., Lane, D. P., and Westwood, N. J. (2008) Discovery, in vivo activity, and mechanism of action of a small-molecule p53 activator. *Cancer Cell.* **13**, 454–463
173. Rotili, D., Tarantino, D., Carafa, V., Lara, E., Meade, S., Botta, G., Nebbioso, A., Schemies, J., Jung, M., Kazantsev, A. G., Esteller, M., Fraga, M. F., Altucci, L., and Mai, A. (2010) Identification of tri- and tetracyclic pyrimidinediones as sirtuin inhibitors. *ChemMedChem.* **5**, 674–677
174. Mai, A., Massa, S., Lavu, S., Pezzi, R., Simeoni, S., Ragno, R., Mariotti, F. R., Chiani, F., Camilloni, G., and Sinclair, D. A. (2005) Design, synthesis, and biological evaluation of sirtinol analogues as class III histone/protein deacetylase (Sirtuin) inhibitors. *J. Med. Chem.* **48**, 7789–7795
175. Parenti, M. D., Grozio, A., Bauer, I., Galeno, L., Damonte, P., Millo, E., Sociali, G., Franceschi, C., Ballestrero, A., Bruzzone, S., Del Rio, A., and Nencioni, A. (2014) Discovery of novel and selective SIRT6 inhibitors. *J. Med. Chem.* **57**, 4796–4804
176. Sociali, G., Galeno, L., Parenti, M. D., Grozio, A., Bauer, I., Passalacqua, M., Boero, S., Donadini, A., Millo, E., Bellotti, M., Sturla, L., Damonte, P., Puddu, A., Ferroni, C., Varchi, G., Franceschi, C., Ballestrero, A., Poggi, A., Bruzzone, S., Nencioni, A., and Del Rio, A. (2015)

Quinazolinone SIRT6 inhibitors sensitize cancer cells to chemotherapeutics. *Eur J Med Chem.* **102**, 530–539

177. Liu, Y., Xie, Q. R., Wang, B., Shao, J., Zhang, T., Liu, T., Huang, G., and Xia, W. (2013) Inhibition of SIRT6 in prostate cancer reduces cell viability and increases sensitivity to chemotherapeutics. *Protein Cell.* **4**, 702–710

178. Jiang, H., Cheng, S.-T., Ren, J.-H., Ren, F., Yu, H.-B., Wang, Q., Huang, A.-L., and Chen, J. (2019) SIRT6 Inhibitor, OSS\_128167 Restricts Hepatitis B Virus Transcription and Replication Through Targeting Transcription Factor Peroxisome Proliferator-Activated Receptors  $\alpha$ . *Front Pharmacol.* **10**, 1270

179. Chang, A. R., Ferrer, C. M., and Mostoslavsky, R. (2019) SIRT6, a Mammalian Deacetylase with Multitasking Abilities. *Physiological Reviews.* **100**, 145–169

180. Tasselli, L., Zheng, W., and Chua, K. F. (2017) SIRT6: Novel Mechanisms and Links to Aging and Disease. *Trends Endocrinol. Metab.* **28**, 168–185

181. Hall, J. A., Dominy, J. E., Lee, Y., and Puigserver, P. (2013) The sirtuin family's role in aging and age-associated pathologies. *J Clin Invest.* **123**, 973–979

182. Maity, S., Muhamed, J., Sarikhani, M., Kumar, S., Ahamed, F., Spurthi, K. M., Ravi, V., Jain, A., Khan, D., Arathi, B. P., Desingu, P. A., and Sundaresan, N. R. (2019) Sirtuin 6 deficiency transcriptionally up-regulates TGF- $\beta$  signaling and induces fibrosis in mice. *J. Biol. Chem.* 10.1074/jbc.RA118.007212

183. Sundaresan, N. R., Vasudevan, P., Zhong, L., Kim, G., Samant, S., Parekh, V., Pillai, V. B., Ravindra, P. V., Gupta, M., Jeevanandam, V., Cunningham, J. M., Deng, C.-X., Lombard, D. B.,

Mostoslavsky, R., and Gupta, M. P. (2012) The sirtuin SIRT6 blocks IGF-Akt signaling and development of cardiac hypertrophy by targeting c-Jun. *Nat. Med.* **18**, 1643–1650

184. Fulda, S., and Kögel, D. (2015) Cell death by autophagy: emerging molecular mechanisms and implications for cancer therapy. *Oncogene*. **34**, 5105–5113

**CHAPTER 2: Mechanism of activation for the sirtuin 6 protein deacylase\***

**Mark A. Klein<sup>1,2</sup>, Can Liu<sup>3</sup>, Vyacheslav I. Kuznetsov<sup>1,2</sup>, John B. Feltenberger<sup>4</sup>, Weiping Tang<sup>3</sup>, John M. Denu<sup>1,2, 5 Ψ</sup>**

From the <sup>1</sup>Wisconsin Institute for Discovery, University of Wisconsin-Madison; <sup>2</sup>Department of Biomolecular Chemistry, University of Wisconsin-Madison; <sup>3</sup>School of Pharmacy, University of Wisconsin-Madison; <sup>4</sup>School of Pharmacy, Medicinal Chemistry Center, University of Wisconsin-Madison; <sup>5</sup>Morgridge Institute for Research, University of Wisconsin-Madison

\*This chapter was published in the Journal of Biological Chemistry. 2020 Jan 31; 295(5): 1385-1399

## **2.1 Abstract**

The histone deacetylase sirtuin 6 (SIRT6) regulates numerous biological functions, including transcriptional repression, DNA repair, and telomere maintenance. Recombinant SIRT6 displays catalytic efficiencies 2 orders of magnitude greater for long-chain deacylation than deacetylation against peptide substrates; however, deacetylation can be enhanced by allosteric small-molecule activators. Here, we investigated the mechanisms of activated lysine deacetylation and enhanced long-chain acyl-group removal by SIRT6. Activity-based screening identified compounds that activated histone peptide deacetylation 18-48-fold. Chemical optimization based on structure–activity relationships yielded an activator with improved potency and selectivity for SIRT6. Using this novel activator, we conducted biochemical and kinetic analyses revealing that SIRT6 is activated via acceleration of a catalytic step occurring after substrate binding but before  $\text{NAD}^+$  cleavage. We identified a SIRT6 variant, R65A, that maintains basal deacetylase activity but cannot be activated and failed to enhance long-chain deacylation. Additional biochemical studies revealed that Arg-65 is critical for activation by facilitating a conformational step that initiates chemical catalysis. This work suggests that SIRT6 activation of deacetylation involves a similar mechanism to improved catalysis as that of long-chain deacylation. The identification of novel SIRT6 activators and the molecular insights into activation and catalysis presented here provide a foundational understanding for physiological SIRT6 activation and for rational design of activating molecules

## 2.2 Introduction

Sirtuins are an evolutionarily conserved family of proteins originally defined as the class III histone deacetylases (HDACs). Whereas sirtuins can deacetylate histones, it is now widely accepted that these enzymes deacetylate diverse protein substrates and regulate many processes, including metabolism and cellular stress response (1). This family of proteins share a conserved central catalytic domain and the ability to couple the cleavage of  $\text{NAD}^+$  to the removal of an acyl group from the  $\epsilon$ -amino group of lysines (2). Each family member (SIRT1–7) contains variable N-terminal and C-terminal domains and has diverse subcellular localization and function (3, 4). Sirtuins bind substrate between a structural  $\text{Zn}^{2+}$ -binding domain and a Rossmann-fold domain in an isoform-specific pocket, conferring distinct deacylase activities across family members (5, 6).

SIRT6 has garnered the attention of scientists due to its vast repertoire of physiological roles, including as a metabolic regulator (7-9), as a tumor suppressor (10-12), in mediating DNA repair (13-15), and due to its strong positive link with longevity (16, 17). SIRT6 overexpression lowers low-density lipoprotein and triglyceride levels, improves glucose tolerance, and increases the lifespan of male mice (16, 18). Additionally, overexpression in ovarian cancer cell lines inhibits proliferation (12). These studies implicate SIRT6 as a potential pharmacological target for small molecule activation and are a compelling reason to resolve the mechanism of SIRT6 activity.

Recent studies have revealed that each sirtuin uniquely accommodates varying long-chain acyl substrates (19, 20). SIRT6, for example, has an elongated hydrophobic pocket and is hundreds-fold more catalytically efficient toward long-chain (*e.g.* myristoylated) peptide substrates compared with acetylated peptide substrates (5, 20). In an apparent contradiction, *in vivo* roles of SIRT6 indicate that acetylated forms of histone H3 lysine 9 (H3K9), H3K18, and H3K56 are *bona fide* substrates through which SIRT6 elicits its ascribed physiological roles (21-



23). The discovery that long-chain free fatty acids (FFAs) could activate the deacetylation of SIRT6 provided a potential resolution to these discordant observations (19). As described by Feldman *et al.* (19), FFAs such as myristic acid stimulate the deacetylase activity and competitively inhibit the demyristoylase activity of SIRT6, consistent with the notion that the free myristic acid occupies the same binding pocket as the myristoylated peptide. Ensuing research has led to the discovery of additional small-molecule activators of SIRT6 (24-27); however, the mechanism of small molecule activation and its relationship to enhanced catalysis of long-chain deacylation is poorly understood.

In the case of SIRT1, Sinclair and colleagues (28-30) have identified natural products and synthetic molecules that act as allosteric activators. Enhanced catalytic activity involves the N-terminal region of SIRT1, where ligand binding improves acetyl-substrate binding. With encouraging evidence in animal studies (31, 32), the therapeutic potential of SIRT1 activation is being evaluated to treat age-associated diseases (33).

Herein, we describe a screen for small-molecule activators of SIRT6 deacetylation, the subsequent development of the novel activator 2-(3-chloro-4-(2,4,6-trichloro-*N*-(2,4,6-trichlorobenzoyl)benzamido)phenyl)-1,3-dioxoisindoline-5-carboxylic acid (CL5D), and use of this model compound to investigate the mechanisms of activation. During the characterization of several mutant enzymes, we discovered a SIRT6 variant (R65A) that cannot be stimulated toward deacetylation by activator compounds. The R65A variant is similarly deficient in the ability to display enhanced catalysis with myristoylated substrates, suggesting that common catalytic steps are hampered. We reveal that Arg-65 mediates a conformational change after substrate binding and that the rate of this change is enhanced by small-molecule activation of deacetylation and during demyristoylation. These results are relevant for understanding the cellular regulation of

SIRT6 activity, for providing molecular insight into human mutations that affect this conformational step, and for the therapeutic design of SIRT6 activators.

## 2.3 Results

### 2.3.1 Targeted screen for SIRT6 activators

Our previous work demonstrated free fatty acids of varying acyl chain length as activators of SIRT6 deacetylation (19). Importantly, we showed that myristic acid is a competitive inhibitor of SIRT6 demyristoylation, suggesting that free fatty acids can occupy the same hydrophobic pocket as that for the peptide-conjugated myristoyl chain. Here, we conducted a targeted screen of diverse fatty acids and lipid-like molecules (Fig. 2-1A) to probe the mechanism of activation, as well as to identify candidate small molecules that could be further developed as potent and selective SIRT6 allosteric activators.

Two compound libraries were selected for initial targeted screening comprising 64 fatty acids (BML-2803) and 190 bioactive lipids (BML-2800). Our previous *in vitro* analysis of selected FFAs revealed EC<sub>50</sub> values of SIRT6 activation ranging from 90 to 240  $\mu$ M (19). Accordingly, each compound was screened at 100  $\mu$ M for its ability to stimulate SIRT6 deacetylation against a histone H3 acetyl-lysine 9 (H3K9ac) peptide. H3K9ac substrate and H3K9 product were separated and quantified by HPLC to determine rates of reaction. Structural analysis of the positive hits identified from the two compound libraries revealed two distinct substructure clusters beyond that of previously reported FFAs: conjugated fatty acids and aromatic carboxylates. Based on this analysis, an additional 178 compounds related to the aforementioned compound classes were selected from the University of Wisconsin Small Molecule Screening Facility's libraries for subsequent screening (Fig. 2-2).

In total, 432 compounds were screened with 71 (16%) displaying over 5-fold activation and 23 (5%) displaying over 10-fold activation (Table 1). Of the 71 compounds displaying >5-fold activation in SIRT6-specific activity, 97% contain a terminal negative charge carried by a

carboxylic acid, phosphate, or sulfate, and 89% contain a linear aliphatic chain. As expected, a number of FFAs were capable of activating SIRT6, accounting for 70% of the identified hits displaying between 5- and 12-fold activation. Myristic acid displayed a 3.7-fold activation, consistent with previous reports under the same conditions (19). Ten compounds displayed greater than 15-fold activation, from which oleoyl-lysophosphatidic acid (LPA), linoleoyl-glycine (L-Gly), arotinoid acid (TTNPB), and 2-(3-chloro-4-(2,4-dichlorobenzamido)phenyl)-1,3-dioxoisindoline-5-carboxylic acid (CL-4) were selected for further characterization (Table 2-1).

**Figure 2-1: Identification of novel SIRT6 activators.**

*A*, compound libraries BML-2803 and BML-2800 and an additional set of 178 cherry-picked molecules were screened at 100  $\mu\text{M}$  for their ability to stimulate SIRT6 (1  $\mu\text{M}$ ) deacetylation of H3K9ac peptide (20  $\mu\text{M}$ ) in the presence of 0.5 mM  $\text{NAD}^+$ . SIRT6 activity was measured by HPLC quantification of H3K9ac, and deacetylated product and -fold activations relative to DMSO control were determined and compiled. *B*, -fold activation of SIRT6 (1  $\mu\text{M}$ ) determined in the presence of either 0–400  $\mu\text{M}$  CL4, 0–150  $\mu\text{M}$  TTNPB, 0–100  $\mu\text{M}$  LPA, or 0–200  $\mu\text{M}$  L-Gly. Maximum -fold activation and  $\text{EC}_{50}$  were determined by sigmoidal curve fit. *C*, steady-state kinetic analysis of SIRT6 (1  $\mu\text{M}$ ) deacetylation was conducted with 0–250  $\mu\text{M}$  H3K9ac peptide in the presence of 100  $\mu\text{M}$  CL4, 50  $\mu\text{M}$  TTNPB, 50  $\mu\text{M}$  LPA, or 50  $\mu\text{M}$  L-Gly. Constants  $K_m$ ,  $\text{H3K9ac}$  and  $k_{\text{cat}}$  were determined by fitting data to the Michaelis–Menten equation. *D*, -fold activations of SIRT1 (0.1  $\mu\text{M}$ ), SIRT2 (0.2  $\mu\text{M}$ ), SIRT3 (1  $\mu\text{M}$ ), SIRT5 (2  $\mu\text{M}$ ), and SIRT6 (1  $\mu\text{M}$ ) determined in the presence of CL4 (100  $\mu\text{M}$ ), TTNPB (50  $\mu\text{M}$ ), and LPA (50  $\mu\text{M}$ ) relative to DMSO control against 20  $\mu\text{M}$  H3K9ac peptide and 0.5 mM  $\text{NAD}^+$ . Mean values are reported with *error bars* representing S.D. of at least three replicates.

**Figure 2-1: Identification of novel SIRT6 activators.**

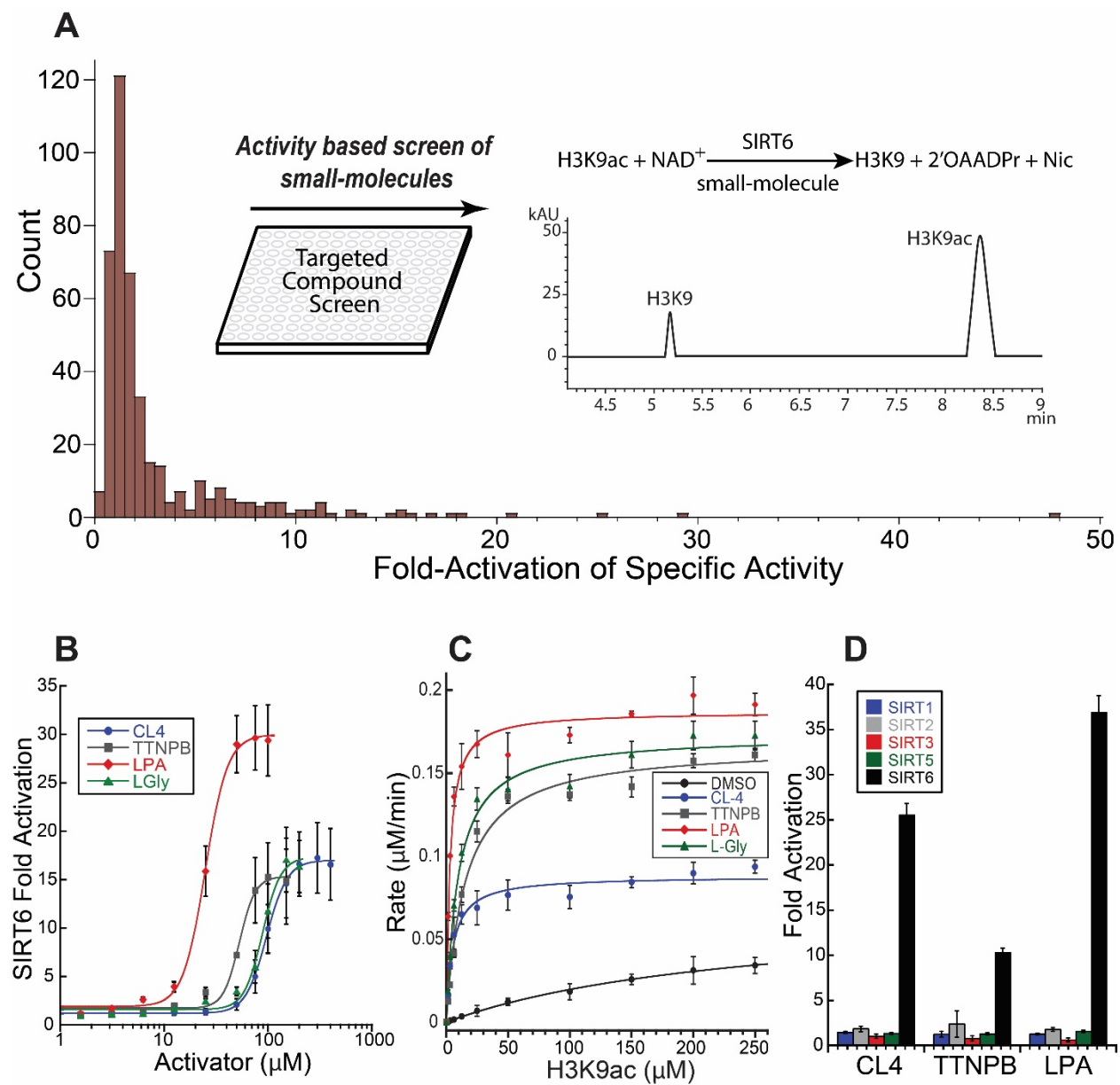


**Figure 2-2: Targeted selection of 178 additional compounds for SIRT6 activation screening.**

Prior screening of the compound libraries BML-2803 and BML-2800 yielded recurring classes of hits including N-acyl amino acids (Type 1) and aromatic carboxylates (Type 2). An additional 39 Type 1 and 85 Type 2 compounds were selected for subsequent screening. Additionally, 14 thiazolidinediones and 40 tetrazoles were selected given that they are bioisosteres of carboxylates with better cell permeability and pharmaceutical precedent (44).

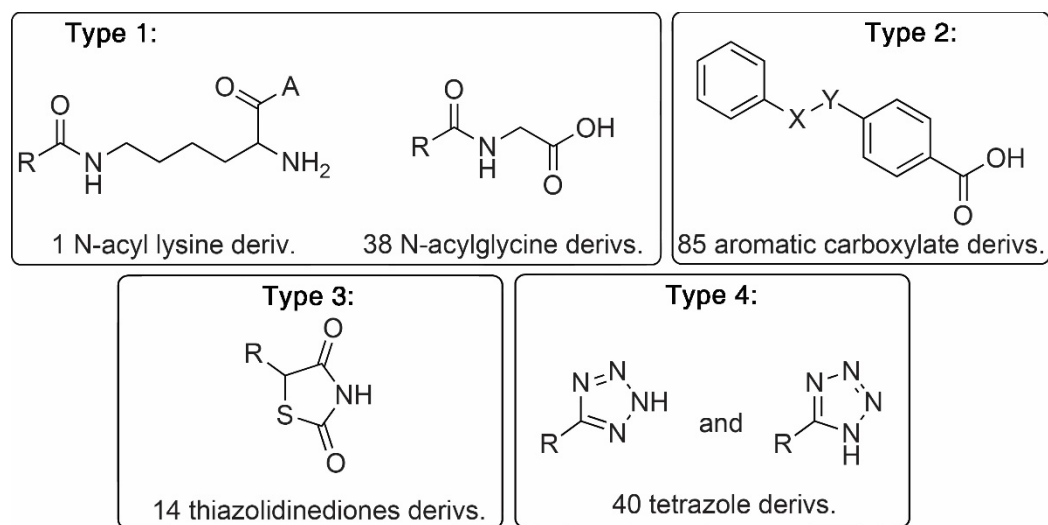


**Table 2-1: Structures of top 10 identified SIRT6 activators with corresponding -fold activations (F.A.) at 100  $\mu$ M.**

Compound ID	Structure	F.A.
Lysophosphatidic acid		48
N-Linoleoylglycine		29
2-Fluoropalmitic acid		25
TTNPB		21
CL-4		18
L-NASPA		18
Eicosatrienoic acid (20:3 n-3)		17
Mead acid (20:3 n-9)		16
Arachidonic acid (20:4 n-6)		15



### 2.3.2 Biochemical characterization of small molecule activators

Having identified a number of novel SIRT6-activating compounds with varying structural features, LPA, L-Gly, TTNPB, and CL-4 were selected for characterization. Dose-response analysis of these compounds yielded apparent  $EC_{50}$  values ranging from 25 to 97  $\mu\text{M}$  (Fig. 2-1B). High concentrations of each activator (>50–300  $\mu\text{M}$ ) led to loss of SIRT6 activation (Fig. 2-2A). Due to the amphipathic nature of these compounds, it was speculated that loss of activation at these high concentrations was due to micelle or aggregate formation. Using the fluorescent membrane probe diphenylhexatriene, micelle formation was observed for LPA and L-Gly at >50 and >300  $\mu\text{M}$ , respectively, corresponding to concentrations at which activation was lost (Fig. 2-2B). Autofluorescence of TTNPB interfered with diphenylhexatriene fluorescent quantification, and CL-4 was not observed to form micelles in this assay format. To test whether loss of activity was indeed the result of general micelle-like formation at high concentration, the deacetylase activity of SIRT1, SIRT2, and SIRT6 were tested in the presence of 400  $\mu\text{M}$  LPA and the CL4 derivative, CL5D (Fig. 2-2C). All sirtuins were inhibited under these conditions, suggesting a nonspecific effect at high concentrations of LPA and CL5D.

To determine which kinetic parameters are enhanced by small molecule SIRT6 activation, steady-state kinetic analyses were performed by measuring initial rates of reaction across varying H3K9ac peptide concentrations in the presence of each activator (Fig. 1C). Data were fitted to the Michaelis–Menten equation to solve for the intrinsic kinetic parameters of SIRT6 and revealed 1.4–2.9-fold increases for  $k_{\text{cat}}$  and 52–312-fold increases in  $k_{\text{cat}}/K_{m, \text{H3K9ac}}$  across the activators tested. The ratio of these two terms is used to derive  $K_{m, \text{H3K9ac}}$ , which is decreased 16–88-fold across activators (Table 2-2). This strong decrease in  $K_{m, \text{H3K9ac}}$  implies that activation greatly improves the capture of acetyl-substrate, which could be attributed to either improved substrate

binding ( $K_d$ , H3K9ac) or the improvement of one or more of the steps prior to the first irreversible step, release of nicotinamide (Scheme 2-1).

The ability of these selected small molecules to activate other mammalian sirtuins (SIRT1, SIRT2, SIRT3, and SIRT5) was evaluated. All sirtuins tested displayed measurable activity against the H3K9ac peptide. With the exception of weak stimulation (<2-fold) of SIRT2, none of the other sirtuins displayed increased activity in the presence of SIRT6 activators. Compounds CL-4, TTNPB, and LPA displayed greater than 19-fold, 4-fold, and 30-fold specificity for SIRT6 over SIRT2, respectively (Fig. 2-1D).

**Figure 2-3: Characterization of SIRT6 activators identified from screen.**

*A*, Fold-activation of SIRT6 (1  $\mu$ M) determined in the presence of either 0-400  $\mu$ M CL4, 0-400  $\mu$ M TTNPB, 0-400  $\mu$ M Lysophosphatidic acid (LPA), or 0-400  $\mu$ M linoleoylglycine (LGly). Full dose-response shows inhibition at high concentration of activator. *B*, Critical micelle concentration determined by DPH (5  $\mu$ M) assay (45), TTNPB autofluorescence prevented CMC determination. *C*, Deacetylase activity of SIRT1 (0.1  $\mu$ M), SIRT2 (0.2  $\mu$ M), and SIRT6 (1  $\mu$ M) determined in the presence of DMSO, 400  $\mu$ M LPA, or 400  $\mu$ M CL5D. Mean value of at least three replicates reported with error bars representing standard deviation.

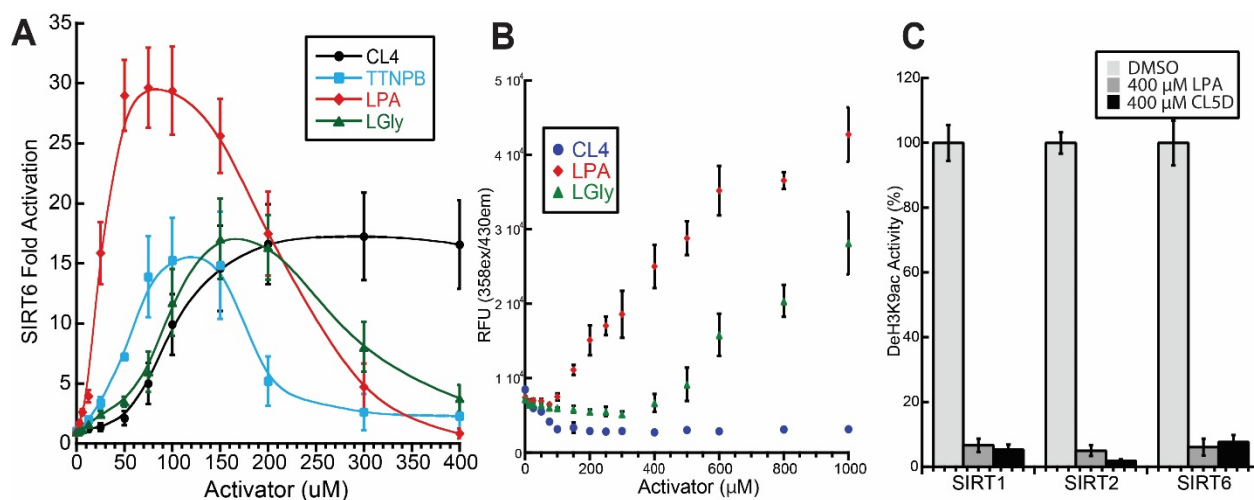
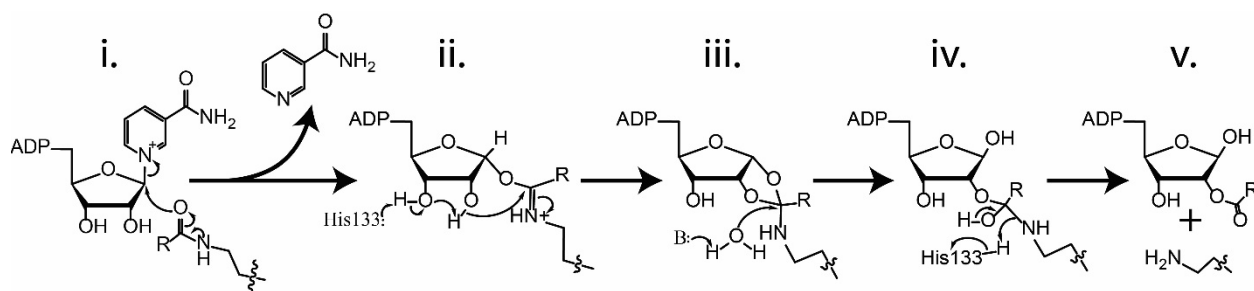


**Table 2-2:** Dose-response and Michaelis-Menten parameters of activation by novel SIRT6 activators as determined in Fig 2-1.

Dose response			Michaelis-Menten parameters			
	EC <sub>50</sub> (μM)	FA <sub>max</sub>		K <sub>m,H3K9ac</sub> (μM)	k <sub>cat</sub> (s <sup>-1</sup> ) x10 <sup>-3</sup>	k <sub>cat</sub> /K <sub>m</sub> (M <sup>-1</sup> s <sup>-1</sup> )
CL-4	97 ± 2	17 ± 0.2	DMSO	247 ± 27	1.1 ± 0.1	3.6 ± 0.5
TTNPB	53 ± 3	15 ± 0.8	CL-4	5.2 ± 0.8	1.5 ± 0.3	284 ± 37
LPA	25 ± 1	30 ± 0.5	TTNPB	15 ± 2	2.8 ± 0.1	186 ± 20
L-Gly	88 ± 4	17 ± 0.8	LPA	2.8 ± 0.3	3.2 ± 0.1	1,126 ± 125
			L-Gly	9.4 ± 1.1	2.8 ± 0.1	307 ± 32

**Scheme 2-1: Mechanism of SIRT6-catalyzed deacetylation.**

*i*, Substrate acyl-oxygen performs nucleophilic addition on the 1'-carbon of the nicotinamide ribose resulting in the C1'-*O*-alkylamidate intermediate and release of nicotinamide. *ii*, His133 acts as a general base to facilitate the intra-molecular nucleophilic attack of the nicotinamide ribose 2'-hydroxyl on the *O*-alkylamidate carbon affording the 1',2'-cyclic intermediate. *iii*, Water catalyzed hydrolysis of the 1',2'-cyclic intermediate yields the tetrahedral intermediate. *iv*, Positively charged His133 donates a proton to the imino group of the tetrahedral intermediate resulting in cleavage of the C-N bond and yielding the final products. *v*, *O*-Acyl-ADPr and deacetylated lysine products are released from SIRT6.



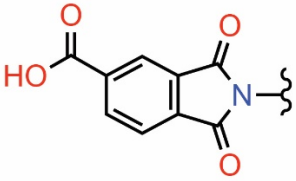
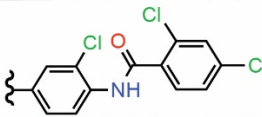
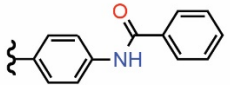
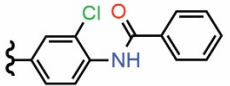
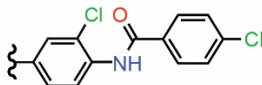
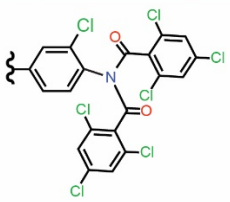
### 2.3.3 Development and analysis of CL5D as a SIRT6 activator

To improve potency and investigate the mechanism of activation, CL-4 was selected for chemical derivatization and structure–activity relation studies. CL-4 consists of a 4-carboxyphthalimide conjugated to a 2'-chloro-*N*-benzanilide. The scaffold molecule, 2-(4-benzamidophenyl)-1,3-dioxoisindoline-5-carboxylic acid (CL-5), was synthesized without chloro groups and demonstrated no activation of SIRT6 at concentrations up to 400  $\mu$ M, suggesting a critical role of halogenation (Table 2-3). The progressive addition of chloro groups to the scaffold restored the ability to activate SIRT6. Derivatization with a trichlorobenzoyl group led to di-substitution at the aniline nitrogen resulting in CL5D. All synthetic compounds utilized in this study were confirmed by  $^1\text{H}$  NMR,  $^{13}\text{C}$  NMR, and LC-MS (Fig. S7 – see published article supplementals). CL5D displayed a 7-fold increased potency over CL-4 as measured by the concentration required to stimulate a 4-fold activation in SIRT6 deacetylase activity (Table 2-3). The only compound with substantially altered activity was the methyl-ester of CL5D, which was devoid of stimulatory effects (Fig. 2-4). Taken together, these data demonstrate that electron-rich terminal aromatic groups and anionic headgroup are important for SIRT6 stimulation in this series of compounds.

To determine which kinetic parameters are affected by CL5D, a steady-state kinetic analysis of CL5D was conducted and demonstrated a dose-dependent 50-fold increase in  $k_{\text{cat}}/K_m$ ,  $\text{H3K9ac}$  values with a concurrent 2.1-fold increase in  $k_{\text{cat}}$  value (Fig. 2-5A). CL5D activation via improved  $k_{\text{cat}}/K_m$ ,  $\text{H3K9ac}$  is consistent with the previous analysis of LPA, L-Gly, TTNPB, and CL4, suggesting that either substrate binding or a step prior to nicotinamide release is enhanced during small-molecule activation. Previous studies have suggested that SIRT6 activators bind to the same hydrophobic pocket that accommodates long-acyl substrates (19). Demyristoylation assays in the

presence of increasing concentrations of CL5D demonstrate competitive inhibition with a  $K_i$  value of  $13.4 \pm 4.8 \mu\text{M}$  (Fig. 2-5B). This  $K_i$  value agrees well with the  $\text{EC}_{50}$  value ( $15.5 \pm 3.2 \mu\text{M}$ ). Competitive inhibition suggests that CL5D binds to the same hydrophobic pocket as long acyl-group substrates. We next tested whether CL5D would stimulate SIRT6 deacetylase activity against a full-length histone substrate. Histones were acid-extracted from HEK293T cells and subjected to *in vitro* SIRT6 deacetylation in the presence of either CL5D or the inactive scaffold, CL5. Cells were treated with SAHA, a histone deacetylase inhibitor, to increase the relative levels of acetylated histones prior to extraction. Immunoblot analysis demonstrated time-dependent deacetylation at H3K9 by SIRT6 that was stimulated by CL5D but not CL5, establishing CL5D as an activator of SIRT6 against whole histone substrate (Fig. 2-5C).

**Table 2-3:** Structure-activity relationship during development of CL5D. The concentration required to stimulate 4-fold activation of SIRT6 (1  $\mu$ M) against H3K9ac (20  $\mu$ M) with 0.5 mM NAD<sup>+</sup> was determined for each compound.

		4-fold activation
CL-4		35 $\mu$ M
CL-5		>400 $\mu$ M
CL-5A		>400 $\mu$ M
CL-5B		78 $\mu$ M
CL-5D		3 $\mu$ M



**Figure 2-4: Methylation of the CL5D carboxylate abolishes potency.**

CL5D-me was synthesized in which the terminal carboxylate is methylated and thus uncharged. Fold-activation of SIRT6 (1  $\mu$ M) determined against H3K9ac (20  $\mu$ M) in the presence of either various concentrations of CL5D or CL5D-me.

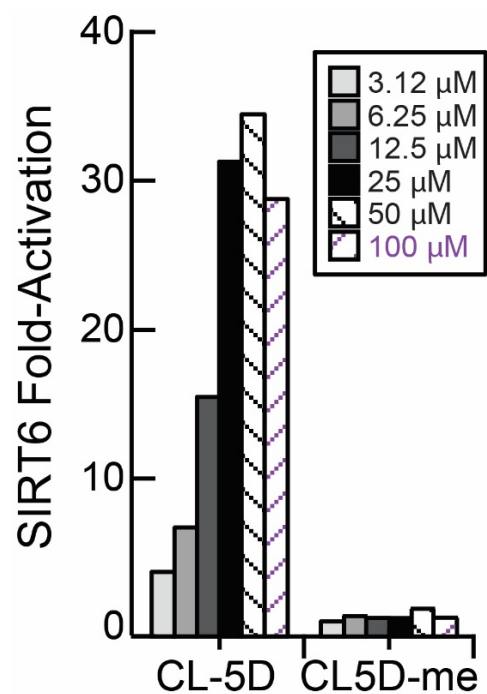
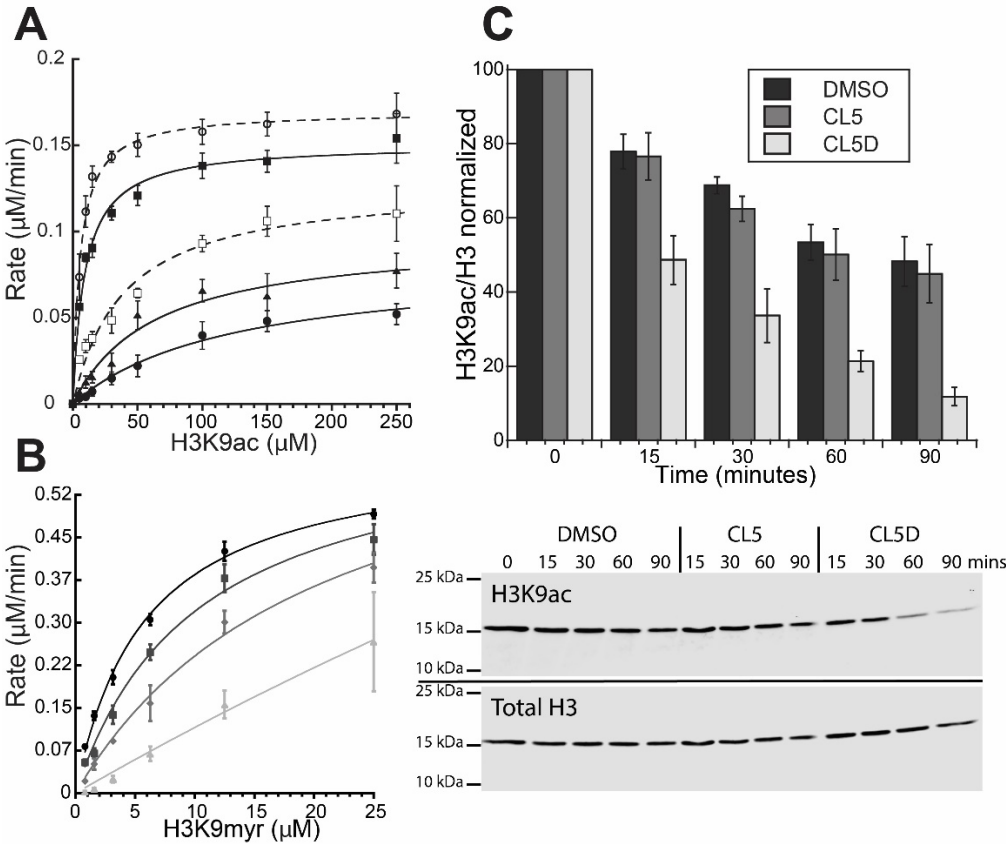


**Figure 2-5. Characterization of SIRT6 activator CL5D.**

*A*, Steady-state kinetic analysis of SIRT6 (1  $\mu$ M) deacetylation was conducted with 0-250  $\mu$ M H3K9ac peptide and 0.5 mM NAD<sup>+</sup> in the presence of DMSO (●), 5  $\mu$ M CL5D (▲), 10  $\mu$ M CL5D (□), 25  $\mu$ M CL5D (■), and 50  $\mu$ M CL5D (○). Data were fitted to Michaelis-Menten equation. *B*, SIRT6 demyristoylase activity determined in the presence of 0-25  $\mu$ M H3K9myr peptide, 0.5 mM NAD<sup>+</sup> and 5% DMSO (●), 12.5  $\mu$ M CL5D (■), 25  $\mu$ M CL5D (◆), and 50  $\mu$ M CL5D (▲). Data were fitted to a competitive model of inhibition with  $K_i = 13.4 \mu\text{M} \pm 4.8 \mu\text{M}$ . *C*, SIRT6 (1  $\mu$ M) activity measured against acid extracted mammalian histones (75  $\mu$ g/mL) with 0.5 mM NAD<sup>+</sup> and either 5% DMSO, 50  $\mu$ M CL5, or 50  $\mu$ M CL5D. H3K9ac levels were normalized to total H3 with a representative immunoblot shown. Mean values of at least three replicates are reported with *error bars* representing S.D.



#### 2.3.4 Role of CL5D in mediating SIRT6-substrate interaction

The initial hits selected for characterization as well as the developed activator, CL5D, stimulated SIRT6 deacetylation primarily through the improvement of  $k_{\text{cat}}/K_{m, \text{H3K9ac}}$ , whereas the  $k_{\text{cat}}$  was only modestly increased. The large stimulation observed in the  $k_{\text{cat}}/K_{m, \text{H3K9ac}}$  values could represent a substantial decrease in  $K_{d, \text{H3K9ac}}$  value or a rate enhancement of a catalytic step after substrate binding but before the release of nicotinamide, the first irreversible step. CL5D is subsequently utilized as a model compound for interrogating the mechanism of activation. To determine whether the  $K_{d, \text{H3K9ac}}$  value is directly affected by activators, we sought to measure the effect of CL5D on the binding constants for the acetylated peptide. Initial isothermal titration calorimetry (ITC) experiments yielded no measurable heats of binding of H3K9ac to SIRT6, whether CL5D was present or not (data not shown). The inability of this verified substrate to bind SIRT6 brought into question whether  $\text{NAD}^+$  binding may precede that of acetyl-peptide.

Previous mechanistic analysis of SIRT1, SIRT2, and SIRT3 demonstrated an ordered substrate binding in which acyl-lysine substrate binds prior to  $\text{NAD}^+$ , whereas SIRT6 was able to bind  $\text{NAD}^+$  in the absence of acetylated substrate (5). We hypothesized that SIRT6 may display a reversed ordered binding mechanism in which  $\text{NAD}^+$  binds prior to acetylated peptide substrate. To avoid the complication of enzyme turnover, we utilized ADP-ribose (ADPr) in place of  $\text{NAD}^+$ . ADPr is a competitive inhibitor of SIRT6 with respect to  $\text{NAD}^+$ , and both  $\text{NAD}^+$  and ADPr have been shown to bind to SIRT6 with similar affinities (34, 35). We then investigated the ability of  $\text{NAD}^+$  and ADPr to induce SIRT6 conformational changes. Changes in sensitivity to partial proteolysis by subtilisin were monitored in the presence of ADPr,  $\text{NAD}^+$ , or H3K9ac (Fig. 2-6A). Partial protection from proteolysis was observed under saturating conditions of either  $\text{NAD}^+$  or ADPr, when compared with no-ligand controls. The addition of 100  $\mu\text{M}$  H3K9ac provided minimal

protection from proteolysis; however, the addition of both H3K9ac and ADPr increased protection relative to ADPr alone. These results suggest that ADPr and  $\text{NAD}^+$  induce a similar conformational change in SIRT6 and, importantly, show that ADPr can be used as an  $\text{NAD}^+$ -binding surrogate that can co-occupy SIRT6 with H3K9ac to investigate substrate binding under noncatalytic conditions.

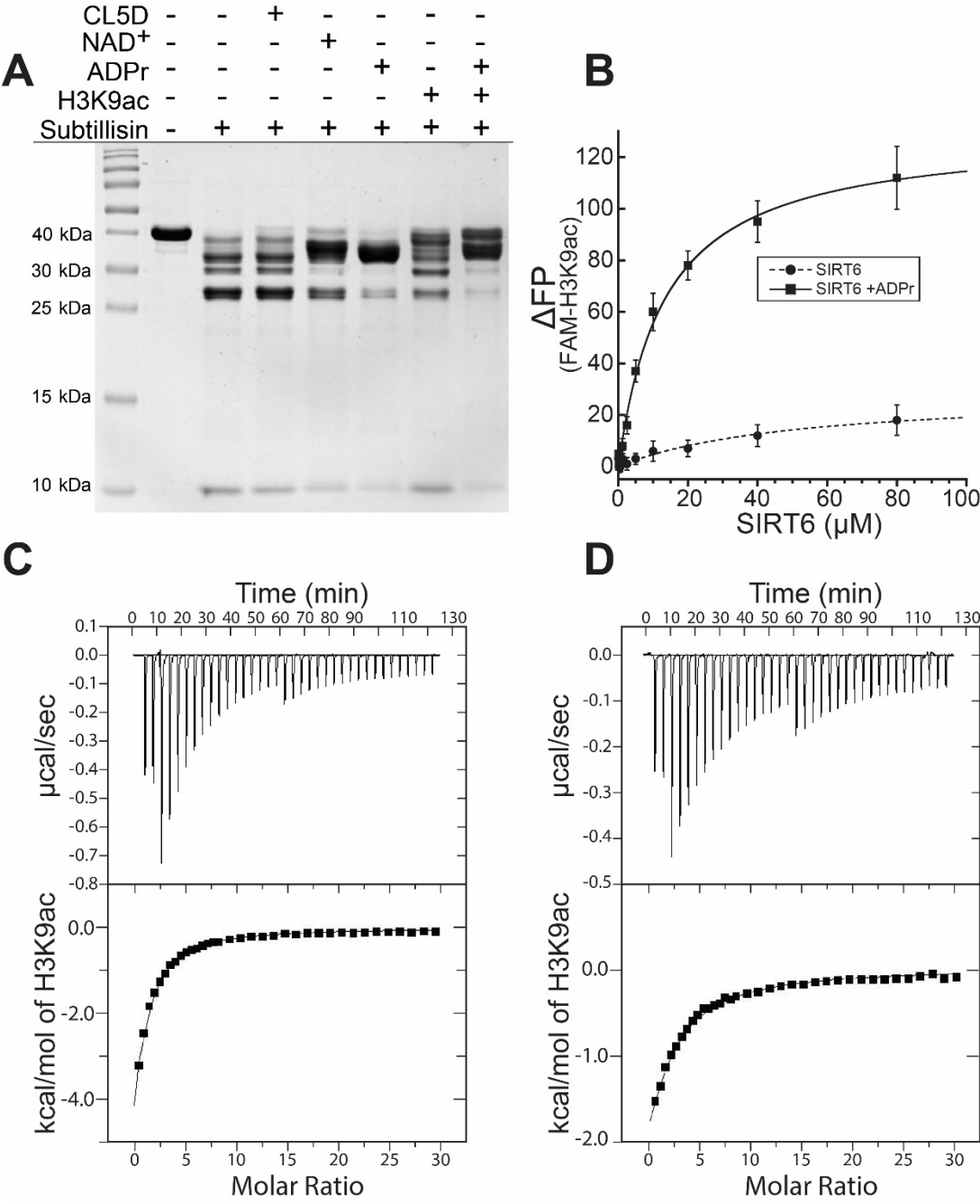
To determine whether ADPr binding must precede acetylated substrate binding, we first synthesized a fluorescein-labeled H3K9ac peptide (FAM-H3K9ac) amenable for fluorescent polarization binding assays. Binding of FAM-H3K9ac to SIRT6 was then assessed by fluorescent polarization in the presence and absence of saturating amounts of ADPr (Fig. 2-6B). These results demonstrate efficient binding of FAM-H3K9ac only in the presence of ADPr and were confirmed via ITC, where the addition of ADPr allowed for quantification of H3K9ac peptide binding with a measured  $K_{d, \text{H3K9ac}}$  of  $34.4 \pm 4.4 \mu\text{M}$  (Fig. 2-6C).

To address our initial question of whether activators enhance  $K_{d, \text{H3K9ac}}$ , ITC was used to determine the binding constant of H3K9ac in the presence of CL5D and requisite ADPr. Quantification yielded a  $K_{d, \text{H3K9ac}}$  of  $72.6 \pm 8.1 \mu\text{M}$  in the presence of CL5D (Fig. 2-6D). Together, these data demonstrate that SIRT6 displays ordered binding in which  $\text{NAD}^+$  binding precedes substrate binding and that the mechanism of SIRT6 activation does not involve improved binding affinity for acetyl-substrate. These results suggest that the greatest rate enhancement by small-molecule activation involves a catalytic step(s) after substrate binding but prior to nicotinamide dissociation.

**Figure 2-6: SIRT6 displays ordered binding and CL5D does not improve H3K9ac binding.**

*A*, partial proteolysis of SIRT6 (0.67 mg) was conducted with subtilisin (0.67  $\mu$ g) at room temperature for 25 minutes with either no additive, CL5D (50  $\mu$ M),  $\text{NAD}^+$  (300  $\mu$ M), ADPr (300  $\mu$ M), H3K9ac (100  $\mu$ M), or  $\text{NAD}^+$  and H3K9ac. *B*, Fluorescence polarization of N'-FAM-H3K9ac was measured in the presence of SIRT6 (0-80  $\mu$ M) with or without ADPr (300  $\mu$ M). Polarization in the absence of SIRT6 was subtracted from each data set with mean value reported and error bars representing standard deviation. Binding experiment ran in triplicate with mean value reported and error bars representing standard deviation. Data were fitted to a sigmoidal curve. *C* and *D*, representative ITC trace of three separate experiments obtained from 37 automatic injections (1-8  $\mu$ L) of *C*; H3K9ac (0.6 mM) and ADPr (0.5 mM) into SIRT6 (15  $\mu$ M) and ADPr (0.5 mM),  $K_{d,\text{H3K9ac}}=34.4 \pm 4.4$   $\mu$ M ( $N=0.70 \pm 0.14$ ) or *D*; H3K9ac (0.6 mM), ADPr (0.5 mM), and CL5D (50  $\mu$ M) into SIRT6 (15  $\mu$ M), ADPr (0.5 mM), and CL5D (50  $\mu$ M),  $K_{d,\text{H3K9ac}}=72.6 \pm 8.1$   $\mu$ M ( $N=0.97 \pm 0.37$ ). Mean  $K_d$  and  $n$  of three replicates reported with *error bars* representing S.D.

**Figure 2-6: SIRT6 displays ordered binding and CL5D does not improve H3K9ac binding.**



### 2.3.5 Identification of non-activatable SIRT6 R65A mutant

Activation of deacetylation by CL5D is primarily driven through improvement of the  $k_{\text{cat}}/K_m$ , H3K9ac parameter, which suggests the enhancement of a catalytic step(s) including or prior to nicotinamide release. These steps include the rate of alkylamidate formation or a potential slow conformational change of SIRT6 subsequent to substrate binding (see Fig. 2-10D). The rate of alkylamidate formation for various sirtuins has previously been determined utilizing single-turnover kinetics, in which substoichiometric amounts of substrate are saturated with enzyme (5). However, the prohibitively high concentration ( $\sim 1\text{--}2$  mM) of SIRT6 required to saturate H3K9ac peptide substrate in rapid-quench experiments precludes the use of single-turnover kinetics to interrogate the rate of alkylamidate formation during enhanced deacetylation.

In an effort to identify residues critical for the enhancement of SIRT6 catalysis, we screened several mutants (R76A, R65A, K81A, and K160A) and assessed the ability of these variants to be activated by small molecules (Fig. 2-7A). Subsequent analysis of these mutants revealed that all retained base level deacetylase activity; however, only SIRT6 R65A could not be activated by CL5D (Table 2-4). Steady-state kinetic analysis of SIRT6 R65A confirmed the inability to be stimulated by CL5D over a large range of H3K9ac peptide substrate concentrations (Fig. 2-7B).

Structural analysis revealed that Arg-65 is positioned on a kinked turn of the  $\text{NAD}^+$ -binding loop and makes extensive contacts with the adenosine ribose and pyrophosphate of ADPr (Fig. 2-7C). Previous studies have identified loss-of-function mutations of a neighboring aspartate to either tyrosine or histidine (D63Y/H). SIRT6 D63Y was selected for in naturally occurring human tumors, and D63H was identified as a driving mutation in four consecutive late fetal losses of a

consanguineous couple (11, 36). These studies and our analysis suggest that SIRT6 catalysis is particularly sensitive to mutation of the NAD<sup>+</sup>-binding loop.

Previously, SIRT6 Arg-65 was reported to be critical for deacetylation in cells, but a detailed mechanistic understanding was never provided (14). Here, *in vitro* analysis reveals that SIRT6 R65A lacks the ability to be stimulated toward deacetylation by small-molecule activators. Together, this suggests a critical role for endogenous SIRT6 activation.

SIRT6 is a more efficient long-chain deacylase than deacetylase; therefore, the inability of the R65A mutant to perform activated deacetylation led us to ask whether this mutant was also a poorer demyristoylase (5, 19, 20). Remarkably, SIRT6 R65A deacylase activity against H3K9myr peptide is greatly reduced relative to WT (Fig. 2-7D). The inability of the R65A variant to perform activated deacetylation or efficient demyristoylation suggests a common allosteric role of Arg-65 in mediating enhanced SIRT6 catalysis. Therefore, SIRT6 R65A is utilized as a tool in subsequent analyses to investigate which catalytic steps are affected during enhanced catalysis.



**Figure 2-7: Identification of the non-activatable R65A SIRT6 mutant.**

*A*, arginine and lysine residues (*magenta*) selected for mutation due to proximity to myristoyl binding pocket (*tan sticks*) and active site pocket (Protein Data Bank code 3ZG6). *B*, initial rates of SIRT6 WT and R65A (1  $\mu$ M) were measured in triplicate over a range of H3K9ac substrate (0-250  $\mu$ M) in the presence or absence of CL5D (50  $\mu$ M) and mean values fitted to Michaelis-Menten equation with *error bars* representing S.D. *C*, Arg-65 is positioned on the NAD<sup>+</sup>-binding loop and makes interactions with nicotinamide ribose and pyrophosphate of ADPr. Structure of SIRT6 (*transparent blue*) liganded with H3K9myr (*yellow*) and ADPr (*orange*). The NAD<sup>+</sup> binding loop of SIRT6 (*cyan*) contains Arg-65 (*magenta*) at the kink of a loop and making hydrogen bonds with the adenosine ribose and pyrophosphate of ADPr (Protein Data Bank code 3ZG6). *D*, SIRT6 WT and R65A (1  $\mu$ M) demyristoylase activity was measured in the presence of 20  $\mu$ M H3K9myr peptide substrate. Mean value of at least three replicates reported.

**Figure 2-7: Identification of the non-activatable R65A SIRT6 mutant.**

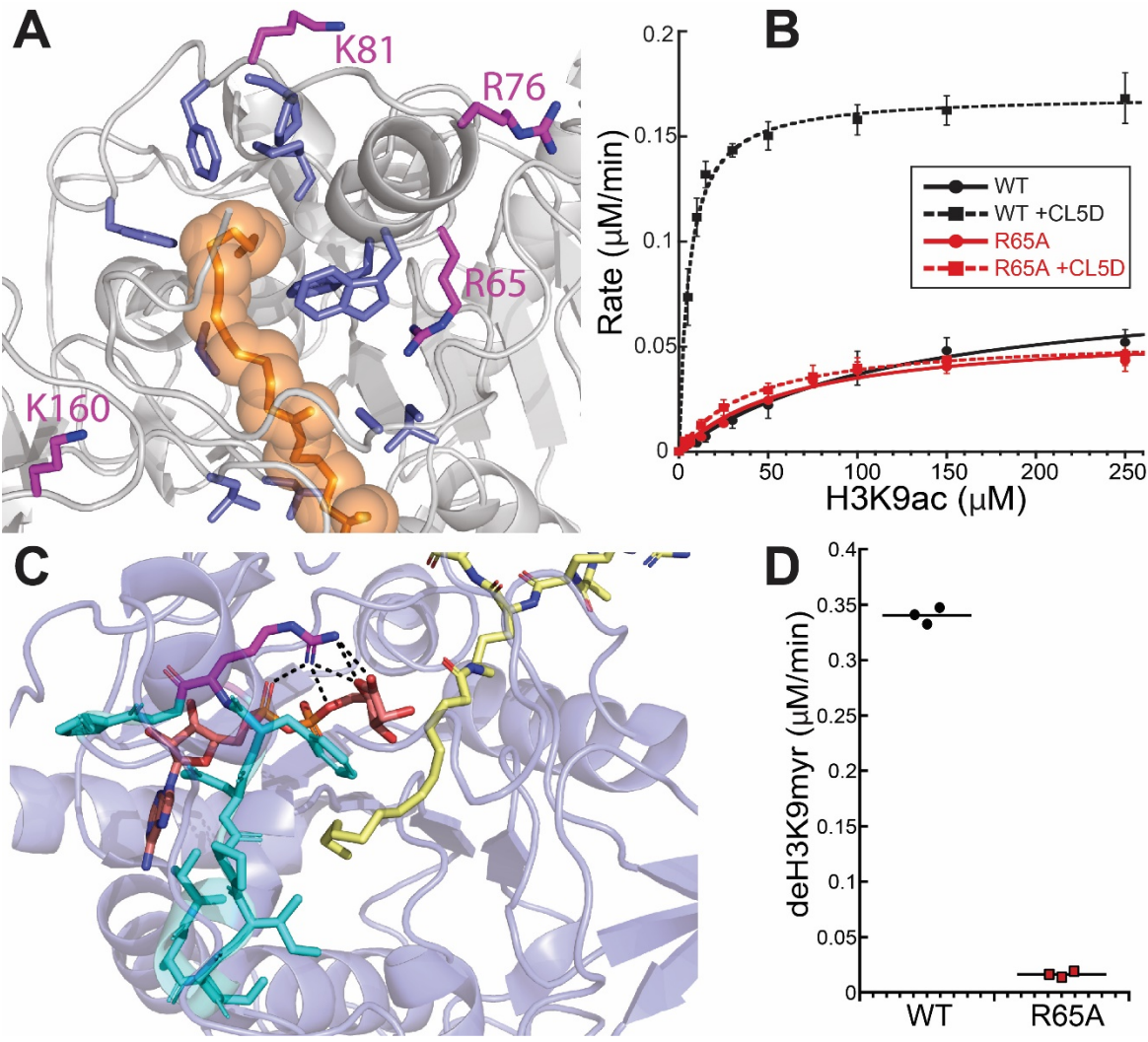


**Table 2-4.** Steady-state rates of deacetylation of SIRT6 WT, R76A, K81A, K160A, and R65A (1  $\mu$ M) against H3K9ac (40  $\mu$ M) with or without CL5D (50  $\mu$ M). Reactions were performed in triplicate for 25 minutes with mean value reported and error representing standard deviation of runs.

Mutant	Rate <sub>DMSO</sub> ( $\mu$ M/min)	Rate <sub>CL5D</sub> ( $\mu$ M/min)	Fold Activation
WT	0.013 $\pm$ 0.0008	0.164 $\pm$ 0.008	12.9
R76A	0.016 $\pm$ 0.0004	0.155 $\pm$ 0.004	9.8
K81A	0.014 $\pm$ 0.0005	0.125 $\pm$ 0.003	8.6
K160A	0.009 $\pm$ 0.0006	0.126 $\pm$ 0.006	13.5
R65A	0.010 $\pm$ 0.0004	0.014 $\pm$ 0.004	1.3

### 2.3.6 Characterization of SIRT6 R65A catalysis and binding parameters

Having demonstrated that Arg-65 facilitates enhanced SIRT6 catalysis, we performed global steady-state analysis of SIRT6 WT and R65A demyristoylation to isolate kinetic parameters associated with enhanced catalysis. Bisubstrate kinetic analyses on WT and R65A SIRT6 were performed by measuring initial turnover rates under a matrix of H3K9myr peptide and  $\text{NAD}^+$  concentrations (Fig. 2-8, *A* and *B*). Through fitting to a sequential bisubstrate reaction equation, values for  $k_{\text{cat}}$ ,  $K_{d, \text{NAD}^+}$ ,  $K_{d, \text{H3K9myr}}$ ,  $K_{m, \text{NAD}^+}$ , and  $K_{m, \text{H3K9myr}}$  were determined, and the -fold increase in each parameter observed in WT *versus* R65A SIRT6 was calculated (Table 2-5). The R65A mutant enzyme yielded a 65-fold decrease in  $k_{\text{cat}}$  and a 8.0-fold decrease in  $k_{\text{cat}}/K_{m, \text{H3K9myr}}$  that cannot be fully accounted for by the 1.2-fold decrease in  $K_{d, \text{H3K9myr}}$ . Fluorescence polarization was used to determine the effect of the R65A on the binding of a fluorescein-labeled H3K9myr peptide (Fig. 2-9). The R65A variant demonstrated an improved  $K_{d, \text{FAM-H3K9myr}}$  over WT SIRT6 ( $0.51 \pm 0.04$  and  $2.1 \pm 0.13$   $\mu\text{M}$ , respectively), which is in agreement with the  $K_{d, \text{H3K9myr}}$  values determined by bisubstrate kinetic analysis ( $3.9 \pm 1.7$  and  $5.0 \pm 2.5$   $\mu\text{M}$ , respectively). An effect on  $k_{\text{cat}}/K_{m, \text{H3K9myr}}$  not accounted for by binding of substrates is in agreement with enhanced catalysis involving a step(s) after substrate binding but prior to the release of nicotinamide. Importantly, this affected step(s) is mediated by Arg-65. The large decrease in the  $k_{\text{cat}}$  of demyristoylation for SIRT6 R65A suggests that a step including or subsequent to the formation of the 1',2'-bicyclic intermediate, which is not reflected in  $k_{\text{cat}}/K_{m, \text{H3K9myr}}$ , is impaired (Scheme 2-1). This impaired step is unique to demyristoylation, as SIRT6 R65A does not demonstrate impaired  $k_{\text{cat}}$  of deacetylation relative to WT, suggesting that the rate-limiting steps of deacetylation and demyristoylation differ in the R65A mutant. From prior work on a sirtuin homolog, HST2, product release was limiting for overall  $k_{\text{cat}}$  values (37). Accordingly, the release

of the hydrophobic *O*-myristoyl-ADPr product may become rate-limiting for SIRT6 R65A-mediated demyristoylation.

Together, these results suggest that Arg-65 mediates a catalytic step reflected in the  $k_{\text{cat}}/K_m$ ,  $\text{H3K9myr}$  of enhanced deacylation after substrate binding but prior to the release of nicotinamide (Fig. 2-10D). As such, the  $k_{\text{cat}}/K_m$ ,  $\text{H3K9myr}$  might reflect the rate of alkylamidate formation or a conformational change subsequent to substrate binding.

**Figure 2-8: Kinetic analysis of SIRT6 wild type and R65A demyristoylation.**

*A* and *B*, steady-state demyristoylation rates of H3K9myr (0.33-27  $\mu\text{M}$ ) by SIRT6 WT and R65A (1  $\mu\text{M}$ ) were determined in the presence of 1-500  $\mu\text{M}$   $\text{NAD}^+$ . These experiments were repeated on different days, with one set of representative curves with fits shown. Results from duplicate experiments are tabulated in Table 5. The data were fitted to an ordered sequential bi-substrate equation to derive  $V_{\text{max}}$ ,  $K_{\text{m, H3K9myr}}$ ,  $K_{\text{m, NAD}^+}$ ,  $K_{\text{d, H3K9myr}}$ , and  $K_{\text{d, NAD}^+}$ . *C* and *D*, pre-steady state single-turnover kinetics of SIRT6 WT and R65A (18  $\mu\text{M}$ ) were determined with 300  $\mu\text{M}$   $\text{NAD}^+$  in the presence of 5  $\mu\text{M}$  H3K9myr. Nicotinamide and demyristoylated product were monitored by HPLC and curves were fitted to a single exponential to determine first order rate constants. Mean value of three replicates plotted with *error bars* representing S.D.

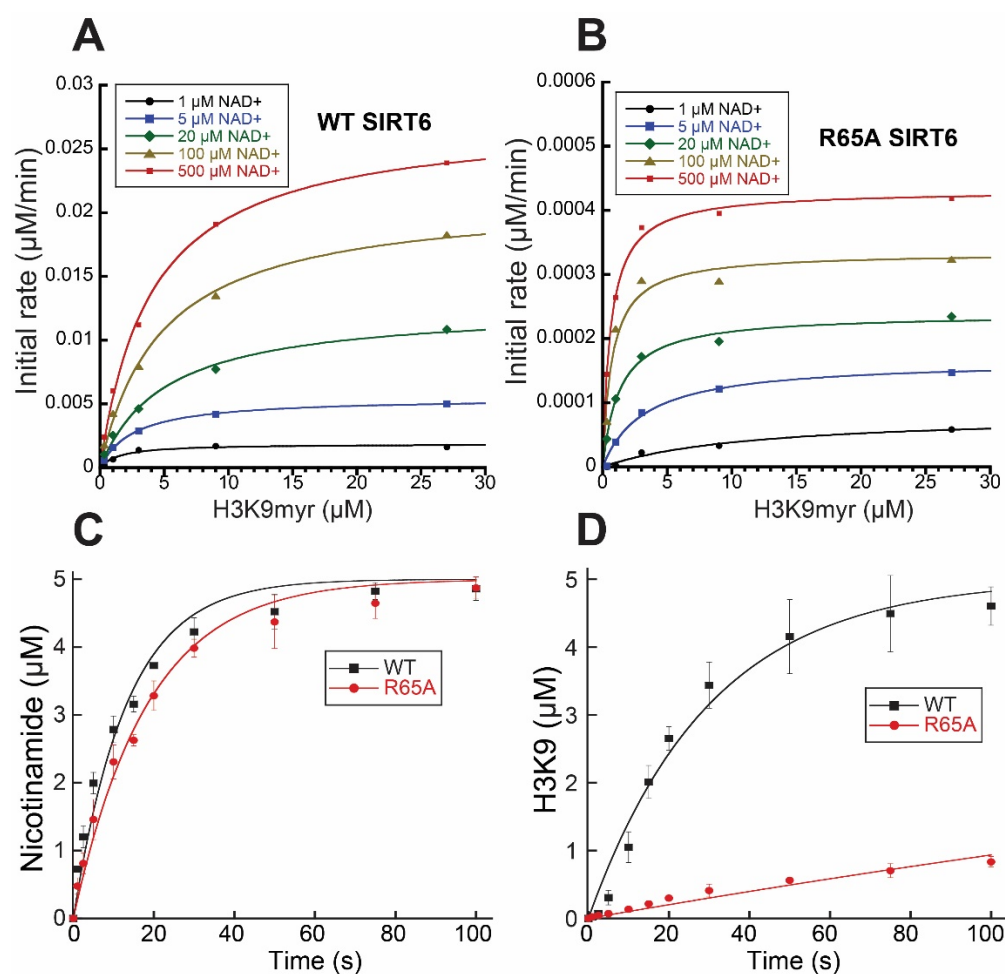
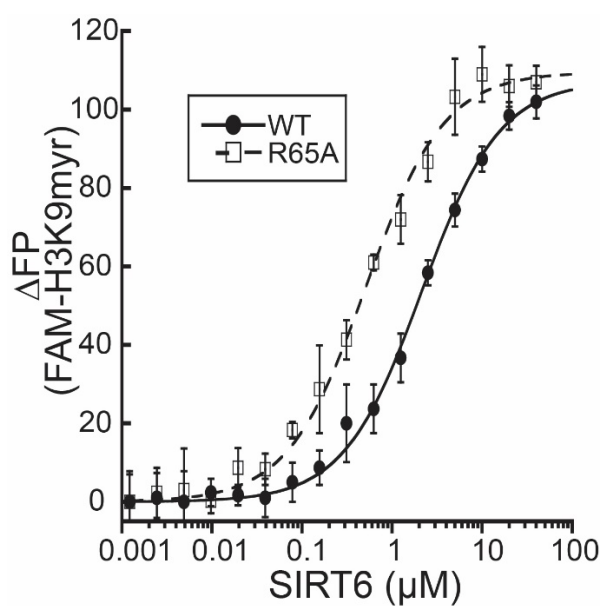


**Table 2-5:** Sequential bi-substrate reaction parameters and single-turnover rates of alkylamidate and 1'2'-bicyclic formation determined for SIRT6 WT and R65A demyristoylation from Figure 5. Sequential bi-substrate reaction conducted twice with second set shown in parentheses, errors represent error of fit. Single-turnover kinetics were performed in triplicate with errors representing standard deviation.

	R65A	WT	Avg. Fold Increase
$k_{cat}$ ( $s^{-1}$ )	$1.0 \times 10^{-4} \pm 3.9 \times 10^{-6}$ ( $9.4 \times 10^{-5} \pm 3.16 \times 10^{-6}$ )	$7.0 \times 10^{-3} \pm 3.4 \times 10^{-4}$ ( $5.9 \times 10^{-3} \pm 3.2 \times 10^{-4}$ )	65.3
$K_M$ , H3K9myr ( $\mu M$ )	$0.47 \pm 0.11$ ( $0.45 \pm 0.11$ )	$4.2 \pm 0.65$ ( $4.0 \pm 0.68$ )	8.2
$K_M$ , NAD <sup>+</sup> ( $\mu M$ )	$11 \pm 2.4$ ( $12 \pm 2.3$ )	$25 \pm 5.1$ ( $22 \pm 4.9$ )	2.1
$K_d$ , H3K9myr ( $\mu M$ )	$3.9 \pm 1.7$ ( $4.2 \pm 1.6$ )	$5.0 \pm 2.5$ ( $4.6 \pm 2.4$ )	1.2
$K_d$ , NAD <sup>+</sup> ( $\mu M$ )	$90 \pm 40$ ( $96 \pm 42$ )	$30 \pm 13$ ( $26 \pm 14$ )	0.30
$k_{cat}/K_M$ , H3K9myr ( $s^{-1} \cdot M^{-1}$ )	$220 \pm 49$ ( $177 \pm 35$ )	$1,700 \pm 197$ ( $1,470 \pm 189$ )	8.0
$k_{cat}/K_M$ , NAD <sup>+</sup> ( $s^{-1} \cdot M^{-1}$ )	$9.4 \pm 1.9$ ( $7.8 \pm 1.4$ )	$280 \pm 50$ ( $259 \pm 47$ )	31.6
Alkylimidate formation ( $s^{-1}$ )	$0.054 \pm 0.003$	$0.076 \pm 0.006$	1.4
1'2'-bicyclic formation ( $s^{-1}$ )	$0.0021 \pm 0.0001$	$0.033 \pm 0.002$	15.7

**Figure 2-9: H3K9myr binding to SIRT6 wild type and R65A.**

Fluorescence polarization of N'-FAM-H3K9myr was measured in the presence of wild-type and R65A SIRT6 (0-40  $\mu\text{M}$ ). Polarization in the absence of SIRT6 was subtracted from each data set and all data were fit to a sigmoidal dose-response curve. Binding constants ( $K_{d,\text{FAM-H3K9myr}}$ ) were determined as the concentration required for half maximal binding. Mean value of three replicates reported with *error bars* representing S.D.





### 2.3.7 Single turnover kinetic analysis of SIRT6 R65A demyristoylation

Changes in catalytic efficiency ( $k_{\text{cat}}/K_m$ ) reflect the rates of substrate binding and all subsequent steps through the first irreversible step, the release of nicotinamide. The steady-state reaction parameters of WT and R65A SIRT6 revealed differences in catalytic efficiency during enhanced SIRT6 catalysis.

To provide mechanistic details about the individual steps during enhanced catalysis, a single-turnover, rapid-quench kinetic analysis was performed to monitor the rates of alkylamidate and 1',2'-bicyclic intermediate formation. Assays were performed with limiting myristoyl-substrate, permitting only a single turnover of the enzyme. WT and R65A SIRT6 (18  $\mu\text{M}$ ) were incubated with saturating  $\text{NAD}^+$  and 5  $\mu\text{M}$  myristoyl-peptide. Following rapid acid quenching (1–100 s), nicotinamide and demyristoylated peptide were quantified by HPLC, and the rates of each were determined using a single-exponential fit (Fig. 2-8, *C* and *D*). In this analysis, the formation of the alkylamidate occurs concomitant with the formation of nicotinamide, which was detected and used to quantify this rate (Scheme 2-1, *step i*). The subsequent step, formation of the 1',2'-cyclic intermediate (Scheme 2-1, *step ii*), results in an acid-labile intermediate that decomposes following acid quench to form deacylated peptide, which was detected and used to quantify this rate (Table 2-5). The rate of alkylamidate formation between WT and R65A (0.075 and 0.054  $\text{s}^{-1}$ , respectively) was similar; however, the rate of 1',2'-cyclic formation for R65A was reduced 16-fold compared with WT (0.002 and 0.033  $\text{s}^{-1}$ , respectively). These data implicate Arg-65 in facilitating the formation of the 1',2'-cyclic intermediate.

Despite the fact that the R65A mutant has an impaired rate of 1',2'-cyclic formation (0.002  $\text{s}^{-1}$ ) (Scheme 2-1, *step ii*), this rate is still an order of magnitude greater than the steady-state  $k_{\text{cat}}$  value of demyristoylation (0.0001  $\text{s}^{-1}$ ), suggesting that a subsequent nonreversible

catalytic step or product release becomes rate-limiting during SIRT6 R65A demyristoylation. Given that  $k_{\text{cat}}$  of SIRT6 R65A demyristoylation ( $0.0001 \text{ s}^{-1}$ ) is an order of magnitude slower than the corresponding  $k_{\text{cat}}$  of deacetylation ( $0.001 \text{ s}^{-1}$ ), it is likely that product release of the bulky hydrophobic *O*-myristoyl-ADPr becomes rate-limiting for the R65A mutant.

The nonactivatable R65A mutant shows a minimal 1.4-fold decrease in the rate of alkylamidate formation (Scheme 2-1, *step i*), the only chemical step reflected in  $k_{\text{cat}}/K_{m, \text{H3K9myr}}$ . This modest involvement of Arg-65 in facilitating alkylamidate formation is insufficient to explain the decrease in  $k_{\text{cat}}/K_{m, \text{H3K9myr}}$  compared with WT SIRT6 and suggests that enhanced catalysis is nearly independent of changes to the rate of alkylamidate formation. This kinetic data can be explained by the existence of additional nonchemical steps that precede alkylamidate formation. We propose a conformational change mediated by Arg-65 that drives efficient demyristoylation of WT SIRT6. Kinetic analysis of deacetylation is required to evaluate whether activated deacetylation is also driven by the improvement of a nonchemical step.

### 2.3.8 Evidence for slow conformational change after substrate binding

Enhancement of deacetylation by CL5D improves  $k_{\text{cat}}/K_{m, \text{H3K9ac}}$  for SIRT6 by 50-fold, and this improvement is absent from the R65A variant. To further dissect the catalytic step(s) in  $k_{\text{cat}}/K_{m, \text{H3K9ac}}$  that are enhanced in the presence of activator, reaction conditions were set up to identify the existence of product “bursts” during the first catalytic turnover. High concentrations of SIRT6 (10  $\mu\text{M}$ ) in the presence of 400  $\mu\text{M}$  H3K9ac peptide were rapidly mixed with 500  $\mu\text{M}$   $\text{NAD}^+$ , and after an acid quench at different times, the products nicotinamide and deacetylated peptide were resolved and quantified by HPLC. Plotting the products formed as a function of time revealed no product bursts (Fig. 2-10A and Fig. 2-11), only a linear rate that was in agreement with steady-state  $k_{\text{cat}}$  values, and a consistent 1.8-fold rate enhancement in the presence of CL5D. The order of substrate mixing had no effect on the product curves (Fig. 2-11). The lack of a nicotinamide burst suggests that a step after binding but before the first chemical step is relatively slow. Such a rate-determining step prior to the first catalytic step is likely to be a slow conformational step, and the fact that all tested activators display a large increase in  $k_{\text{cat}}/K_{m, \text{H3K9ac}}$  suggests that activators enhance this step.

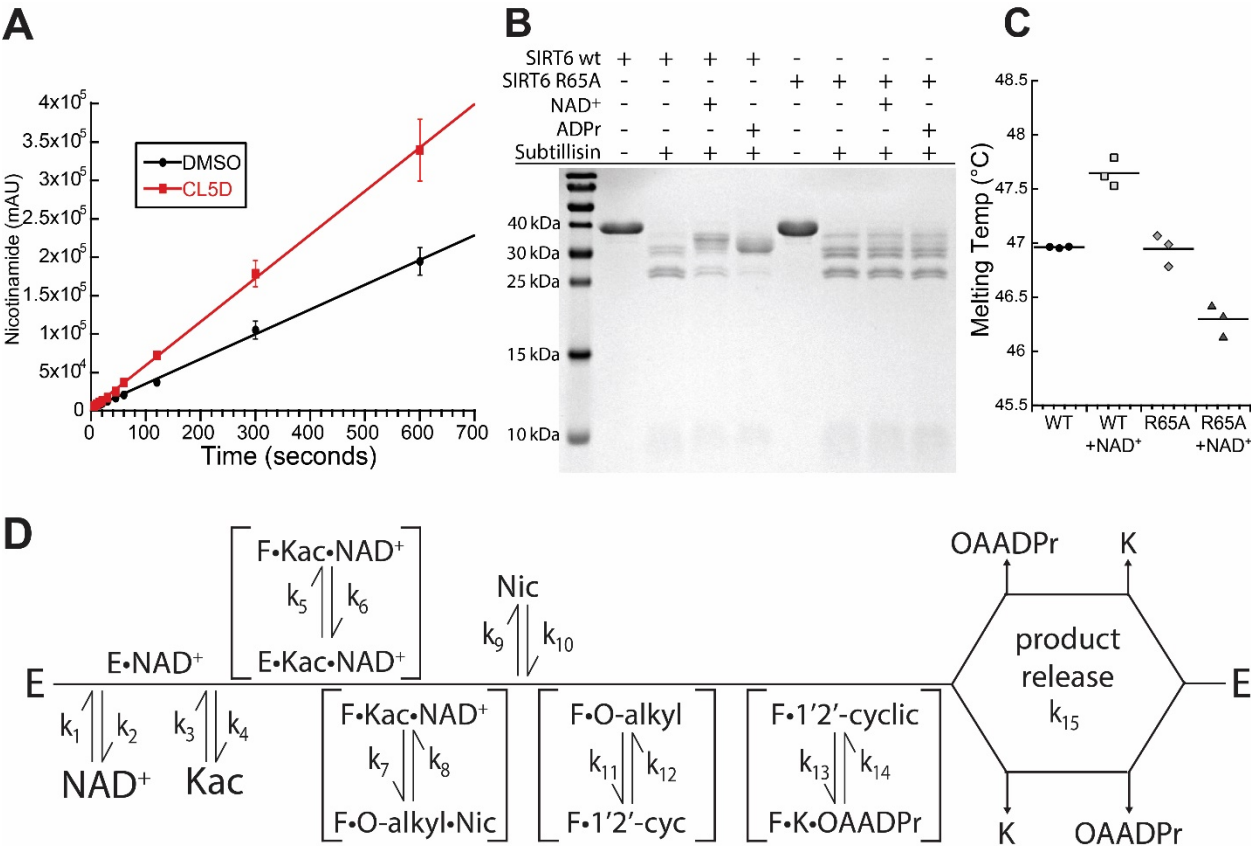
Lack of product burst suggests that the rate-limiting step of deacetylation occurs prior to the release of nicotinamide and is therefore reflected in the  $k_{\text{cat}}/K_{m, \text{H3K9ac}}$ , allowing this term to be modeled using an example equation provided by Johnson (38). This equation includes a conformational step subsequent to substrate binding followed by an irreversible step, the last rate encompassed in  $k_{\text{cat}}/K_{m, \text{H3K9ac}}$  and reflective of the rate of alkylamidate formation in our analysis. Modeling suggests that, for example, a 100-fold increase in the forward rate of conformational change coupled with a 6-fold decrease in the reverse rate would be sufficient to improve  $k_{\text{cat}}/K_{m, \text{H3K9ac}}$  from 2.2 to 554  $\text{M}^{-1} \text{s}^{-1}$ , in agreement with the empirically measured improvement by small-

molecule activation from  $3.6$  to  $511 \text{ M}^{-1} \text{ s}^{-1}$  (Fig. 2-12). Further kinetic modeling of the  $k_{\text{cat}}/K_m$ ,  $\text{H3K9ac}$  term demonstrates that improvements to the rate of alkylamidate formation sufficient to drive the observed activation would necessitate a rate  $\sim 150$ -fold faster than that of  $k_{\text{cat}}$ . Such a rate improvement would have yielded a burst in nicotinamide production, suggesting that an enhancement to a conformational rate is more likely. Together, these analyses demonstrate that small-molecule activation cannot be accounted for solely by an improvement in alkylamidate formation. Instead, activated deacetylation by small-molecule binding involves the improved equilibrium of a conformational change that is prior to the first chemical step and facilitated by Arg-65.

**Figure 2-10: R65 facilitates conformational change during enhanced catalysis.**

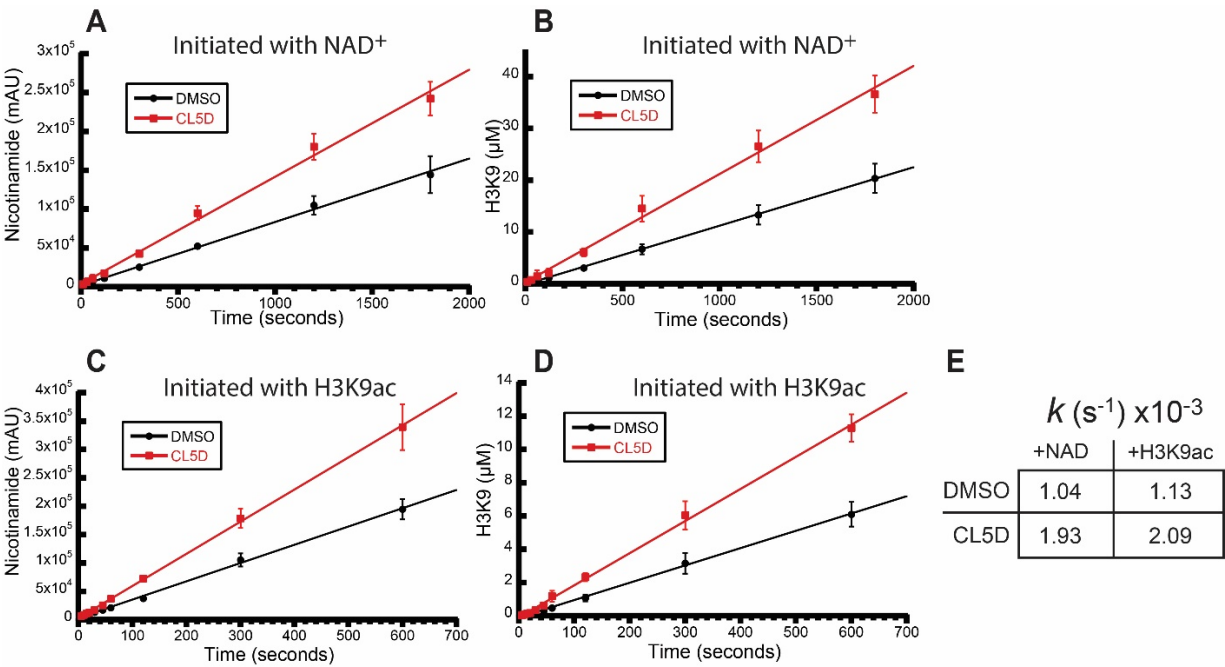
*A*, SIRT6 (10  $\mu\text{M}$ ) was pre-mixed with 400  $\mu\text{M}$  H3K9ac peptide prior to reaction initiation with 500  $\mu\text{M}$   $\text{NAD}^+$ . Reactions were allowed to proceed for 10-600 seconds prior to HPLC quantification of nicotinamide. Reactions were performed in duplicate with average value plotted and *error bars* representing S.D. These kinetics were also performed in duplicate with reversed order of substrate addition (Fig. 2-11). *B*, partial proteolysis of SIRT6 WT or R65A (0.67 mg) was conducted with subtilisin (0.67  $\mu\text{g}$ ) at room temperature for 25 minutes with either no additive,  $\text{NAD}^+$  (300  $\mu\text{M}$ ), or ADPr (300  $\mu\text{M}$ ). *C*, melting temperatures determined for SIRT6 WT and R65A (10  $\mu\text{M}$ ) with and without  $\text{NAD}^+$  (1 mM). Thermal denaturation was performed in triplicate with mean value reported. *D*, the general kinetic scheme of sirtuins has been previously proposed (5), however here we propose an updated deacylation scheme for SIRT6. First, ordered binding in which SIRT6 binds  $\text{NAD}^+$  prior to acyl-substrate. Subsequent to substrate binding we include a conformational step that is improved during enhanced catalysis in an R65-dependent manner.

**Figure 2-10: R65 facilitates conformational change during enhanced catalysis.**



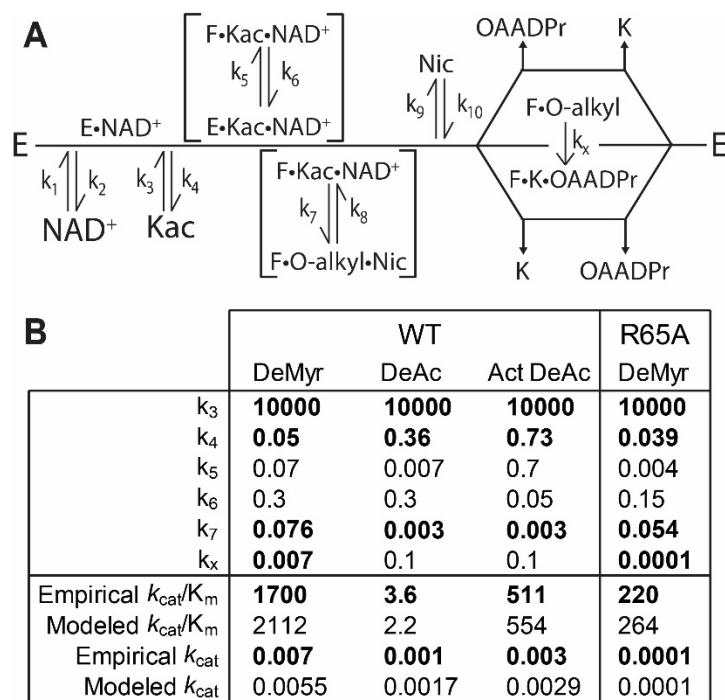
**Figure 2-11. SIRT6 burst kinetics of deacetylation suggest rate limiting step occurs prior to catalysis.**

SIRT6 (10  $\mu$ M) was pre-mixed with either 400  $\mu$ M H3K9ac peptide (A,B) or 500  $\mu$ M NAD<sup>+</sup> (C,D) prior to reaction initiation by either 500  $\mu$ M NAD<sup>+</sup> (A,B) or 400  $\mu$ M H3K9ac peptide (C,D). Reactions were ran from 10-1800 seconds prior to HPLC quantification of nicotinamide (A,C) and deacetylated H3K9(B,D). Reactions were conducted in duplicate with data representing the average value and *error bars* representing the S.D. of duplicates. (E) Catalytic rates (*k*) determined through linear fitting.



**Figure 2-12: Kinetic modeling of SIRT6 demyristoylation and activation of deacetylation.**

*A*, kinetic modeling was conducted using the kinetic scheme presented in Figure 2-10, however the irreversible steps following nicotinamide release including product release were collapsed into a single term,  $k_x$ , to simplify the analysis. *B*, the rates  $k_3$ - $k_7$  and  $k_x$  are used to calculate the modeled  $k_{cat}/K_m$  and  $k_{cat}$  values using the equations listed in the following discussion. Bolded values were determined empirically.

**Figure 2-12 Discussion: Kinetic modeling of enhanced SIRT6 catalysis**

In an effort to evaluate the effects of various SIRT6 catalytic steps on the kinetic parameters  $k_{cat}/K_m$  and  $k_{cat}$ , kinetic modeling was conducted. Modeling of  $k_{cat}/K_m$  utilized an example equation provided by Johnson et al. (38), including a conformational step ( $k_5$  and  $k_6$ ) subsequent to substrate binding ( $k_3$  and  $k_4$ ) followed by an irreversible step. In this analysis of  $k_{cat}/K_m$ , nicotinamide release



is assumed to occur significantly faster than all other steps, allowing  $k_7$  to be modeled as the first irreversible step.

$$\frac{k_{cat}}{K_{m,H3K9}} = k_3 \frac{k_5 k_7}{k_5 k_7 + k_4 (k_6 + k_7)}$$

Modeling of  $k_{cat}$  utilized a simplified kinetic scheme (Supplemental Fig. 6A) in which all irreversible steps following nicotinamide release including product release (Scheme 1) were collapsed into the single term,  $k_x$ . This allows  $k_{cat}$  to be expressed using the following equation however prevents assignment of the rate-limiting step (equation 2). For demyristoylation,  $k_x$  is assumed to be the steady-state term  $k_{cat}$  since  $k_7 > k_{cat}$  (Table 5). For deacetylation,  $k_x$  is assumed to be  $> k_7$  since no burst of nicotinamide is observed during burst kinetic analysis (Fig. 6A, Supplemental Fig.5) and here is assigned with an arbitrary and unimpactful value of  $0.1 \text{ s}^{-1}$ .

$$k_{cat} = \frac{k_5 k_7 k_x}{k_5 k_7 + k_5 k_x + k_7 k_x}$$

First, empirical  $K_{d,H3K9myr}$  and  $k_7$  values for SIRT6 wild type demyristoylation were used to estimate the rate of conformational change ( $k_5$  and  $k_6$ ) that achieve empirically determined rates of  $k_{cat}/K_{m,H3K9myr}$  (Supplemental Fig. 6B). The value of  $k_5$  was constrained to be  $\geq k_7$  due to the fact that no lag phase was observed in pre-steady-state kinetics of SIRT6 demyristoylation (Fig. 5C,D).

Next, for unactivated deacetylation it was determined that a 10 fold decrease in forward rate of conformational change ( $k_5$ ) could account for the empirically measured rate of  $k_{cat}/K_{m,H3K9ac}$ . Subsequent modeling of activated deacetylation demonstrates that a 100 fold increase in the forward rate of conformational change ( $k_5$ ) coupled with a 6 fold decrease in the reverse rate ( $k_6$ ) is sufficient to drive the empirically measured improved rate of  $k_{cat}/K_{m,H3K9ac}$ . Importantly, kinetic modeling utilizing the KinTek Explorer software (KinTek Corporation, Snow Shoe, PA)

demonstrates that these modeled rates predict a linear rate of nicotinamide formation for unactivated and activated deacetylation as observed in our burst kinetic analysis (Fig. 6A, Supplemental Fig.5).

Finally, we demonstrate that an impaired rate of conformational change for SIRT6 R65A demyristoylation is sufficient to drive the decreased  $k_{\text{cat}}/K_{\text{m,H3K9myr}}$  observed for this variant.

### 2.3.9 Involvement of R65 in SIRT6 conformation

To provide evidence that Arg-65 facilitates conformational changes of SIRT6, the sensitivity of the R65A variant to limited proteolysis was assessed in the presence of 300  $\mu\text{M}$   $\text{NAD}^+$  or ADPr. Unlike WT enzyme in the presence of cofactor, the R65A variant lacked protection from proteolysis in the presence of  $\text{NAD}^+$  or ADPr, suggesting that the R65A variant is deficient in the ability to adopt the conformational change (Fig. 2-10B). To determine whether proteolytic protection of WT SIRT6 by cofactors is associated with an increased stability of the enzyme, thermal denaturation assays were conducted, yielding melting temperature ( $T_m$ ) values of WT and R65A proteins in the presence of 1 mM  $\text{NAD}^+$ . The addition of  $\text{NAD}^+$  led to an increase of WT SIRT6  $T_m$  by 0.7  $^{\circ}\text{C}$ , whereas the  $T_m$  of SIRT6 R65A was decreased by 0.6  $^{\circ}\text{C}$  (Fig. 2-10C). The destabilization of SIRT6 R65A in the presence of  $\text{NAD}^+$  suggests that the enzyme still binds cofactor, in agreement with the bisubstrate kinetic analysis (Table 2-5).

Collectively, the detailed kinetic and biochemical analyses strongly suggest that SIRT6 activation of deacetylation by the small molecules revealed in this study occurs primarily through an enhancement of a slow conformational change after substrate binding that is mediated by Arg-65. To reflect these new results, an updated kinetic model of SIRT6 catalysis includes this conformational step (Fig. 2-10D). Efficient long-chain deacylation is also dependent on Arg-65, suggesting that long-chain acyl substrates facilitate this conformational change leading to enhanced catalysis. Furthermore, the R65A variant displays a decreased  $k_{\text{cat}}$  of demyristoylation below that of deacetylation, suggesting that Arg-65 also facilitates a conformational step required for release of the bulky *O*-myristoyl-ADPr product.

## 2.4 Discussion

In this study, we report a targeted screen for small-molecule activators of SIRT6 deacetylation and the subsequent development of a novel activator, CL5D, which was utilized to investigate the mechanism of SIRT6 activation. Mutagenic studies revealed that Arg-65 mediates activation of deacetylation by small molecules and enables efficient demyristoylation, suggesting a common mechanism of enhanced catalysis. Kinetic analysis and binding studies reveal a slow conformational step in SIRT6 catalysis that is enhanced by activators of deacetylation or directly by long-acyl substrates.

Targeted screening of 432 compounds yielded novel SIRT6 activators, including *N*-acyl fatty acid conjugates, halogenated fatty acids, and heterocycles. Structural analysis of compounds eliciting strong activation revealed that 97% contain a terminal negative charge, suggesting this is a critical feature of potent SIRT6 activators. The importance of a terminal negative charge is a novel feature identified in the current study. A few activators described by others lack this feature and are structurally unrelated (25,–27), suggesting that there may be multiple activator binding modes or alternative mechanisms of activation. Unfortunately, the mechanism of activation for these previously described compounds is unknown. Here, derivatives of the initial hit compound CL4 were synthesized and demonstrated a correlation between potency and increased electron density of the terminal benzoyl group(s). CL5D was synthesized with two terminal trichlorobenzoyl groups and was utilized in the subsequent analysis of SIRT6 activation. In agreement with the SAR analysis, methylation of the carboxylate of CL5D yielded an uncharged compound (CL5D-me), which was incapable of stimulating SIRT6 deacetylation. Initial characterization of CL5D along with four initial screen hits demonstrated that all compounds drive activated deacetylation through an improved  $k_{\text{cat}}/K_m$ , H3K9ac.

Mutagenic studies revealed that Arg-65 is critical for both activated deacetylation and efficient demyristoylation, suggesting that common catalytic steps are involved. CL5D, as with free fatty acids (19), displayed competitive inhibition of demyristoylation, suggesting that these molecules occupy the same hydrophobic pocket as the myristoyl-substrate. Arginine 65 is located on a kinked turn of the  $\text{NAD}^+$ -binding loop and makes extensive contacts with the adenosine ribose and pyrophosphate of ADPr in reported crystal structures (Fig. 4C). Previously, the mechanism of deacetylation for the SIRT6 homolog, Sir2Tm, was characterized using molecular dynamics (39). This study predicts that the conserved Arg-34 (Arg-65 in SIRT6) is critical for stabilizing catalytic intermediates and high-energy transition states. Additional studies have identified loss-of-function mutations of a neighboring aspartate to either tyrosine or histidine (D63Y/H) in pathological human samples (11, 30), indicating that the  $\text{NAD}^+$ -binding loop of SIRT6 is particularly sensitive to perturbation. Here we demonstrate that Arg-65 is dispensable for  $\text{NAD}^+$  binding. Rather, Arg-65 is critical for mediating a structural change after substrates have bound, aligning catalytic residues for chemical catalysis. Although other regions of the enzyme may be involved, the structural changes are likely isolated to the loop containing Arg-65 and the nearby hydrophobic pocket that binds the acyl chain of myristoylated substrates. For deacetylation, activator and acetylated substrate similarly stabilize this productive conformation.

In a prior report, SIRT6 R65A displayed no deacetylase activity against H3K9ac when expressed in human fibroblast cells (14). We note that the WT and R65A variant display very similar basal rates of deacetylation. This suggests that SIRT6 requires cellular activation to conduct its physiological role as a histone deacetylase. Although physiological fatty acids can activate SIRT6 *in vitro* (19), there is as yet no direct *in vivo* evidence. Interestingly, lamin A was reported as a cellular SIRT6 activator (40). Further investigations are necessary to establish

whether endogenous small molecules and/or protein-binding partners regulate deacetylation *in vivo*.

Kinetic analysis revealed that small-molecule activation of deacetylation is primarily driven through an increase of the steady-state kinetic parameter  $k_{\text{cat}}/K_{m, \text{H3K9ac}}$ , which reflects substrate binding and catalytic steps up to and including nicotinamide release. To identify the steps of enhanced activity, we utilized a variety of binding and kinetic assays (rapid reaction and steady-state) with WT and R65A enzymes. Activation was largely isolated to a previously unreported conformational step subsequent to substrate binding but prior to alkylamidate formation. The existence of this conformational step is supported by the inability of the nonactivatable R65A mutant to adopt a stabilized conformation in response to  $\text{NAD}^+$  binding. Furthermore, kinetic modeling demonstrated that enhancement of this proposed conformational rate would be sufficient to drive the changes in  $k_{\text{cat}}/K_{m, \text{H3K9ac}}$  elicited by small-molecule activation. This work additionally reveals the novel finding that SIRT6 exhibits ordered binding in which  $\text{NAD}^+$  binding precedes substrate binding.

SIRT6 is a more efficient long-chain deacylase than deacetylase; however, this disparity is absent in the R65A variant. Steady-state analysis of SIRT6 R65A demyristoylation revealed that the loss of efficiency was due to decreases in both  $k_{\text{cat}}/K_{m, \text{H3K9myr}}$  and  $k_{\text{cat}}$ . Enhancement of  $k_{\text{cat}}/K_{m, \text{H3K9myr}}$  in WT SIRT6 is confined to a conformational change similar to that of activated deacetylation and depends on Arg-65. Decreased  $k_{\text{cat}}$  for demyristoylation of the R65A variant was isolated to an impaired step following 1'2'-bicyclic intermediate formation. The turnover number for deacetylation is not impaired by R65A mutation, suggesting that product release of *O*-myristoyl-ADPr, unique to demyristoylation, is facilitated by Arg-65 and becomes rate-limiting in

the R65A variant. A conformational step involving Arg-65 that permits *O*-myristoyl-ADPr release would be consistent with the model.

In conclusion, we have determined the novel kinetic mechanism of SIRT6 catalysis and have revealed that activation of deacetylation by small molecules and enhanced catalysis against myristoyl-substrate share a similar mechanism involving a critical conformational step prior to catalysis. Here, the development of novel SIRT6 activators and the molecular insight into activation and catalysis provide important foundations for understanding physiological activation of SIRT6 and for therapeutic design of activators.

## 2.5 Experimental procedures

### 2.5.1 Expression and purification of recombinant SIRT1-3 and SIRT5-6

His-tagged SIRT1, SIRT2, SIRT3, SIRT5, and SIRT6 were expressed in BL21 DE3 *E. coli* following induction by 0.5 mM isopropyl 1-thio- $\beta$ -D-galactopyranoside at  $A_{600}$  of 1–1.2 at 25 °C and 12 h of subsequent growth prior to harvest. Cells were resuspended in 50 mM sodium phosphate, pH 7.2, 250 mM NaCl, 5 mM imidazole, 1 mM  $\beta$ -mercaptoethanol, and protease inhibitors (aprotinin (2  $\mu$ g/ml), leupeptin (2  $\mu$ g/ml), pepstatin (1  $\mu$ g/ml), and 4-benzenesulfonyl fluoride hydrochloride (0.5 mM)). Cell suspension was lysed by three passes through an EmulsiFlex-C5 (Avestin) at 10,000–15,000 p.s.i., clarified at  $50,000 \times g$  at 4 °C, and purified by nickel-affinity chromatography. SIRT6 used in ITC and quench-flow was further purified using heparin ion-exchange chromatography. Following nickel chromatography and overnight dialysis in 50 mM sodium phosphate, pH 7.2, 50 mM NaCl, 5% glycerol, and 1 mM  $\beta$ -mercaptoethanol, SIRT6 was loaded onto a pre-equilibrated HiTrap Heparin HP affinity column (GE Healthcare). SIRT6 was eluted on a linear gradient from 50 to 1000 mM NaCl in 50 mM sodium phosphate, pH 7.2, and 1 mM  $\beta$ -mercaptoethanol. Fractions containing SIRT6 were pooled, concentrated, and dialyzed into 50 mM Tris, pH 8.0 (4 °C), 150 mM NaCl, 100  $\mu$ M TCEP, and 5% (w/v) glycerol. Protein concentrations were determined by Bradford assay.

### 2.5.2 Synthesis and analysis of H3K9 peptides

Peptides corresponding to residues 4–17 of histone H3 (acetyl, Ac-KQTARKacSTGGKAPRWW-NH<sub>2</sub>; myristoylated, Ac-KQTARKmyrSTGGKAPRWW-NH<sub>2</sub>) were synthesized by standard Fmoc (*N*-(9-fluorenyl)methoxycarbonyl)-solid phase peptide synthesis. Two tryptophan residues were added to the C terminus for quantification at 280 nm. *N*<sup>ε</sup>-Acetyl-L-lysine was directly incorporated to position 9 of the acetyl peptide; however, for the myristoylated peptide,



the side chain of lysine 9 was protected with the 1-(4,4-dimethyl-2,6-dioxocyclohex-1-ylidene)-3-methylbutyl (ivDde) group. Following synthesis of both peptides, the N terminus was acetylated using acetic anhydride. The ivDde group was then removed by incubating the peptide resin with 4% hydrazine in dimethylformamide for 10 min. The liquid was extracted, and the incubation was repeated for a total of seven times. The peptide resin was then incubated with 528 mM myristic anhydride in toluene overnight. The resin was then washed with dimethylformamide followed by dichloromethane. The peptides were cleaved with a mixture of TFA, 5% thioanisole, and 2.5% ethanedithiol. The cleaved crude peptides were then precipitated in ice-cold ether and resuspended in water and lyophilized. The peptides were purified over a preparative C18 HPLC column. The chromatographic purity of the peptide was determined to be  $\geq 95\%$ , and mass spectrometric analysis on a Bruker REFLEX II: MALDI-TOF instrument confirmed the identity of the peptide. The peptides were then dissolved in water.

### 2.5.3 Small molecule SIRT6 activator screen

In collaboration with University of Wisconsin's Small Molecule Screening Facility (UWSMSF), compounds from BML-2803 and BML-2800 (Enzo Life Sciences) and 178 cherry-picked compounds from UWSMSF libraries were distributed to 384-well plates using Biomek 2000 (Beckman). Mastermix containing SIRT6, buffer, and H3K9ac peptide were distributed to wells using a Microflex peristaltic dispenser (Beckman). Plates were spun and preheated to 37 °C before the addition of  $\text{NAD}^+$  using a peristaltic dispenser. After 60 min, reactions were quenched with 2% TFA final using a peristaltic dispenser and then sealed and spun again before in-house HPLC separation and quantification of substrate and product peptides. Reaction conditions were as follows: 1  $\mu\text{M}$  SIRT6, 0.5 mM  $\text{NAD}^+$ , 20 mM H3K9ac(4–17), 20 mM potassium phosphate, pH 7.5,

10% DMSO, and either 10 or 100  $\mu\text{M}$  compound determined by 10-fold dilution of stock library concentration.

#### 2.5.4 Steady-state sirtuin deacylation assay and HPLC analysis

All sirtuin deacylation assays were carried out at 37 °C in 20 mM potassium phosphate, pH 7.5, with 0.5 mM  $\text{NAD}^+$ , 10% DMSO, and 20  $\mu\text{M}$  H3K9ac or H3K9myr peptides, unless otherwise noted, and quenched by the addition of 2% TFA final. Steady-state reactions were constrained to less than 20% substrate turnover to prevent product inhibition. A variety of times were required to monitor SIRT6 deacetylation (2–60 min) under this restraint, given the ability to strongly activate catalysis. In these cases, specific activities were determined and either reported as is or as -fold activation of specific activity. Deacylation reactions were analyzed by reversed-phase HPLC on a Kinetex C18 column (100 Å, 100  $\times$  4.6 mm, 2.6  $\mu\text{m}$ ; Phenomenex) by monitoring the formation of the deacylated product at 214 nm. Deacetylation reactions were analyzed using a gradient of 33–100% B (30% acetonitrile with 0.05% TFA) in 8 min at 1.6 ml min<sup>-1</sup>. Demyristoylation reactions were analyzed using a gradient of 3–100% B (acetonitrile with 0.05% TFA) in 10 min at 1.6 ml min<sup>-1</sup>. The product and substrate peaks were quantified, and the ratio of these allowed for quantification of product formation. Three independent experiments were performed for each condition with averages being plotted and *error bars* representing the S.D. values of these replicates.

#### 2.5.5 Synthesis of CL5D and derivatives

Step 1: A mixture of 2-chloro-4-nitroaniline (400 mg, 2.32 mmol) and 2,4,6-trichlorobenzoyl chloride (682 mg, 2.8 mmol) was made, to which N,N-Diisopropylethylamine (0.85 ml, 5.1 mmol) and dichloroethane (0.5 ml) were added. The 2,4,6-trichlorobenzoyl was substituted with either

benzoyl chloride to produce CL-5 and CL-5A or 4-chlorobenzoyl chloride to produce CL-5B. The synthesis of CL-5 further required 2-chloro-4-nitroaniline to be substituted for 4-nitroaniline. The resulting solution was stirred at 100 °C overnight. The reaction was cooled down to room temperature, diluted by methylene chloride, and quenched by sodium bicarbonate. The organic layer was separated, washed with brine, and dried over sodium sulfate. The solvent was evaporated, and the resulting residue was purified via flash chromatography (hexane/ethyl acetate, 5:1), which yielded a solid (568 mg, 69% yield).

Step 2: The resultant amide (568 mg, 0.97 mmol) and iron (840 mg, 15 mmol) were added into a solution of 10% aqueous HCl (12 ml), methanol (13 ml), and water (13 ml). The mixture was stirred at 60 °C for 3 h. After the starting material disappeared, the solution was quenched by saturated sodium carbonate and extracted with ethyl acetate. The combined organic layers were dried over sodium sulfate. The solvent was evaporated, and the resulting residue was purified by flash chromatography (hexane/ethyl acetate, 4:1), which yielded a solid (402 mg, 74% yield).

Step 3: The resultant aniline (102 mg, 0.18 mmol) and trimellitic anhydride (65.3 mg, 0.34 mmol) were added to acetic acid (10 ml). The resulting solution was stirred at 130 °C overnight. The reaction was then cooled to room temperature. The solid precipitate was filtered and washed with water and ethanol to yield the final product (CL5D yielded 70 mg, 53% yield). Each product was verified by  $^1\text{H}$  NMR,  $^{13}\text{C}$  NMR, and LC-MS.

#### 2.5.6 Histone extraction and immunoblot

HEK293T cells were cultured in Dulbecco's modified Eagle's medium supplemented with 10% fetal bovine serum. Cells were treated with 10  $\mu\text{M}$  SAHA for 24 h prior to harvest. Cells were trypsinized and pelleted prior to washing twice with ice-cold PBS. Cells were then resuspended in 800  $\mu\text{l}$  of ice-cold 10 mM HEPES, pH 7.4, 10 mM KCl, 0.05% Nonidet P-40, and histone

deacetylase and protease inhibitors (1 mM sodium butyrate, 4  $\mu$ M trichostatin A, 100  $\mu$ M phenylmethylsulfonyl fluoride, 10  $\mu$ g/ml leupeptin, and 10  $\mu$ g/ml aprotinin) for 20 min. After a  $1,000 \times g$  10-min spin at 4 °C, the pelleted nuclei were resuspended in 0.2 M HCl and incubated on ice for 20 min. Following a 10-min spin at  $21,000 \times g$  at 4 °C, the acid-extracted supernatant was neutralized with 1 M Tris-HCl, pH 8, prior to measurement of BCA protein concentration. Histone deacetylation assays were run with 75  $\mu$ g/ml extracted histones, 1  $\mu$ M SIRT6, 50  $\mu$ M CL5 or CL5D or 5% DMSO control, 0.5 mM  $\text{NAD}^+$ , in 20 mM potassium phosphate, pH 7.5. Reactions were run at 37 °C prior to quench with SDS loading dye and 5 min boil. 540 ng of nuclei acid extract following sirtuin reaction were loaded for 15% SDS-PAGE, followed by transfer to nitrocellulose. Membrane was blocked with 1% milk before being blotted with anti-H3K9ac (Active Motif 39917) 1:3,000 and imaged. Membrane was then stripped with Thermo Restore PLUS Strip for 10 min and then blocked and blotted with anti-H3 (Abcam 46765) 1:3,000 and reimaged. Prior to imaging, 800CW anti-rabbit IgG (LI-COR Biosciences catalog no. 925-32211) 1:10,000 was incubated on membrane, and imaging was conducted on Odyssey (LI-COR Biosciences). Bands were quantified using Image Studio Lite (LI-COR Biosciences).

#### 2.5.7 Partial proteolysis

SIRT6 WT or R65A (0.67 mg/ml) was mixed with either no ligand,  $\text{NAD}^+$  (300  $\mu$ M), ADPr (300  $\mu$ M), or CL5D (50  $\mu$ M) in 20 mM potassium phosphate, pH 7.5, and 0.5% DMSO. Subtilisin was added to this mixture at a final concentration of 67 ng/ml with a final reaction volume of 15  $\mu$ l. Reactions were incubated for 15 min at 22 °C and quenched by the addition of 5  $\mu$ l of 5 $\times$  SDS-PAGE loading buffer followed by immediate 5-min incubation at 95 °C. Quenched reactions (3–5  $\mu$ g of SIRT6) were subjected to electrophoresis on a 15% acrylamide gel prior to Coomassie staining.

### 2.5.8 Fluorescence polarization

Reactions (20  $\mu$ l) were assembled in black flat bottom nonbinding 384-well plates containing SIRT6 WT or R65A (0–80  $\mu$ M), 1.25% glycerol (w/v), 12.5 mM Tris, pH 8, 20 mM potassium phosphate, pH 7.5, 37.5 mM NaCl, 25  $\mu$ M TCEP, and 20 nM FAM-labeled peptide. SIRT6 was diluted to 4 $\times$  final concentration in final dialysis buffer prior to the addition to a 384-well plate to normalize for dialysis buffer contribution. Peptide was either FAM-H3K9ac (FAM-PEG4-KQTARKacSTGGKAPR-NH<sub>2</sub>) or FAM-H3K9myr (FAM-PEG4-KQTARKmyrSTGGKAPR-NH<sub>2</sub>). Reaction plate was spun at 300  $\times$  g for 2 min and incubated at room temperature for 10 min prior to reading. Three independent experiments were performed for each condition with averages being plotted and *error bars* representing the S.D. of these replicates.

### 2.5.9 Global bisubstrate kinetic analysis

Bi-substrate kinetic analysis of SIRT6 (0.25  $\mu$ M) demyristoylation was performed at concentrations of NAD<sup>+</sup> spanning 1-500  $\mu$ M and H3K9myr spanning 0.33-27  $\mu$ M all in 20 mM potassium phosphate pH 7.5 and 10% DMSO. SIRT6 was preincubated to 37 °C with varying concentrations of H3K9myr prior to catalytic initiation by addition of varying concentrations of NAD<sup>+</sup>. Reactions were carried out in 20  $\mu$ L final in a 384-well plate and quenched after 3 minutes by the addition of 20  $\mu$ L 4% TFA in acetonitrile. Demyristoylated peptide product was quantified by HPLC as described in steady-state sirtuin deacylation assay methods section. Rates of demyristoylation were determined and data were globally fitted to a sequential ordered Bi-Bi equation using KinetAsyst (IntelliKinetics, State College, PA) and a nonlinear least squares analysis in order to determine  $V_{\max}$ ,  $K_{m,H3K9myr}$ ,  $K_{m,NAD^+}$ ,  $K_{d,H3K9myr}$ ,  $K_{d,NAD^+}$ ,  $V/K_{m,H3K9myr}$ , and  $V/K_{m,NAD^+}$ .

$v$

$$= \frac{V_{max} * [NAD^+] * [H3K9myr]}{K_{d,NAD} * K_{m,H3K9myr} + K_{m,NAD} * [H3K9myr] + K_{m,H3K9myr} * [NAD^+] + [NAD^+] * [H3K9myr]}$$

#### 2.5.10 Thermal denaturation assay

Differential scanning fluorimetry was used to determine the  $T_m$  of WT and R65A SIRT6. Proteins were diluted to 10  $\mu$ M (20 mM sodium phosphate, pH 7.5) containing 3.75 $\times$  Sypro Orange (Invitrogen, delivered at 5,000 $\times$ ). Samples (35  $\mu$ l) were aliquoted into PCR strip tubes and placed in a Bio-Rad CFX96 RealTime System C1000 thermal cycler. The temperature was increased at a rate of 0.5  $^{\circ}$ C/min over a range of 10–95  $^{\circ}$ C, and fluorescence was monitored with the FRET channel. Three trials were performed for each SIRT6 variant. The measured fluorescence was normalized so that the minimum fluorescence was set to 0 and the maximum fluorescence was set to 1. The data were fit as reported previously (41) to obtain the  $T_m$ . Three independent experiments were performed for each SIRT6 variant with the mean being plotted, and *error bars* represent the S.D. of these replicates.

#### 2.5.11 Isothermal titration calorimetry

ITC was conducted using a VP-ITC microcalorimeter from MicroCal, LLC (Northampton, MA). Titrations were performed in 50 mM Tris, pH 7.5 (25  $^{\circ}$ C), 150 mM NaCl, 100  $\mu$ M TCEP, 0.5% DMSO, and 5% (w/v) glycerol. Ligands (ADPr and synthesized H3K9ac) were suspended in the dialysis buffer used to store SIRT6. H3K9ac peptide (0.6 mM) and ADPr (0.5 mM) were titrated into SIRT6 (27  $\mu$ M) and ADPr (0.5 mM). The same titration was conducted in which both the syringe and cell contained 50  $\mu$ M CL5D. For each experiment, 37 injections (1–8  $\mu$ l) were titrated into the cell (initial cell volume 1.42 ml) while being stirred at 300 rpm. Each titration was also performed in the absence of SIRT6, and the background heats of titration were subtracted from the

corresponding experimental measurements prior to fitting. Experimental data were fit to a one-site binding model using Origin scientific plotting software as described previously (29). Each titration was performed in triplicate with mean  $K_d$  value reported with *error bars* representing S.D. of the measurements. A single representative curve is shown for each titration.

#### 2.5.12 Rapid quench flow kinetics

Single-turnover kinetics to determine the rates of nicotinamide and demyristoylated peptide formation were performed using a Hi-Tech RQF-63 device (Hi-Tech Scientific, Bradford-on-Avon, UK) as described previously (42). Reactions contained SIRT6 WT or R65A (18  $\mu$ M), 300  $\mu$ M NAD<sup>+</sup>, 5  $\mu$ M H3K9myr, and 20 mM potassium phosphate, pH 7.5. Reactions were monitored from 1 to 100 s and automatically quenched with TFA to a final concentration of 1%. Nicotinamide and demyristoylated peptide were separated by reverse-phase HPLC using a gradient of 0–4% B (100% acetonitrile with 0.05% TFA) over 12.5 min, followed by 20–100% B over 30 min on a Vydac 201SP104 C18 column. Buffer A was water with 0.05% acetonitrile. Nicotinamide peaks were integrated at 260 nm and quantified based on a standard curve of nicotinamide. Demyristoylated peptide product was determined as described above for steady-state kinetics. The first-order rate constants ( $k$ ) of product formation were determined by fitting quantified product to a single-exponential equation,  $p = [S]_0 (1 - e^{-kt})$ , where  $P$  is the concentration of product formed,  $[S]_0$  is the initial concentration of H3K9myr, and  $t$  is the reaction time (43). Each progression curve was performed in triplicate with mean product formed at each time point plotted with *error bars* representing the S.D. of the measurements.

### 2.5.13 Burst kinetic analysis of SIRT6 deacetylation

SIRT6 (10  $\mu\text{M}$ ) was mixed with either H3K9ac peptide (400  $\mu\text{M}$ ) or  $\text{NAD}^+$  (500  $\mu\text{M}$ ) in 20 mM potassium phosphate, pH 7.5, and preheated to 37 °C for 3 min. Reactions were initiated through the addition of either  $\text{NAD}^+$  (500  $\mu\text{M}$  final) or H3K9ac peptide (400  $\mu\text{M}$  final) and quenched after 10–1,800 s by the addition of 3% TFA final. For each experiment, a control reaction in which H3K9ac peptide was excluded was collected at each time point and subtracted from corresponding experimental reactions to control for  $\text{NAD}^+$  degradation. Nicotinamide and deacetylated peptide product were quantified by reverse-phase HPLC as described under “Rapid quench-flow kinetics.”



## 2.6 References

1. Morris B. J. (2013) Seven sirtuins for seven deadly diseases of aging. *Free Radic. Biol. Med.* 56, 133–171 10.1016/j.freeradbiomed.2012.10.525
2. Feldman J. L., Dittenhafer-Reed K. E., and Denu J. M. (2012) Sirtuin catalysis and regulation. *J. Biol. Chem.* 287, 42419–42427 10.1074/jbc.R112.378877
3. Michishita E., Park J. Y., Burneskis J. M., Barrett J. C., and Horikawa I. (2005) Evolutionarily conserved and nonconserved cellular localizations and functions of human SIRT proteins. *Mol. Biol. Cell.* 16, 4623–4635 10.1091/mbc.e05-01-0033
4. Pan M., Yuan H., Brent M., Ding E. C., and Marmorstein R. (2012) SIRT1 contains N- and C-terminal regions that potentiate deacetylase activity. *J. Biol. Chem.* 287, 2468–2476 10.1074/jbc.M111.285031
5. Feldman J. L., Dittenhafer-Reed K. E., Kudo N., Thelen J. N., Ito A., Yoshida M., and Denu J. M. (2015) Kinetic and structural basis for acyl-group selectivity and NAD<sup>+</sup>-dependence in sirtuin-catalyzed deacylation. *Biochemistry* 54, 3037–3050 10.1021/acs.biochem.5b00150
6. Du J., Zhou Y., Su X., Yu J. J., Khan S., Jiang H., Kim J., Woo J., Kim J. H., Choi B. H., He B., Chen W., Zhang A., Cerione R. A., Auwerx J., et al. (2011) Sirt5 is a NAD-dependent protein lysine demalonylase and desuccinylase. *Science* 334, 806–809 10.1126/science.1207861
7. Kugel S., and Mostoslavsky R. (2014) Chromatin and beyond: the multitasking roles for SIRT6. *Trends Biochem. Sci.* 39, 72–81 10.1016/j.tibs.2013.12.002
8. Zhong L., D'Urso A., Toiber D., Sebastian C., Henry R. E., Vadysirisack D. D., Guimaraes A., Marinelli B., Wikstrom J. D., Nir T., Clish C. B., Vaitheesvaran B., Iliopoulos O., Kurland I., Dor

- Y., et al. (2010) The histone deacetylase Sirt6 regulates glucose homeostasis via Hif1 $\alpha$ . *Cell* 140, 280–293 10.1016/j.cell.2009.12.041
9. Tao R., Xiong X., DePinho R. A., Deng C. X., and Dong X. C. (2013) FoxO3 transcription factor and Sirt6 deacetylase regulate low density lipoprotein (LDL)-cholesterol homeostasis via control of the proprotein convertase subtilisin/kexin type 9 (Pcsk9) gene expression. *J. Biol. Chem.* 288, 29252–29259 10.1074/jbc.M113.481473
10. Sebastián C., Zwaans B. M. M., Silberman D. M., Gymrek M., Goren A, Zhong L., Ram O., Truelove J., Guimaraes A. R., Toiber D., Cosentino C., Greenson J. K., MacDonald A. I., McGlynn L., Maxwell F., et al. (2012) The histone deacetylase SIRT6 is a tumor suppressor that controls cancer metabolism. *Cell* 151, 1185–1199 10.1016/j.cell.2012.10.047
11. Kugel S., Feldman J. L., Klein M. A., Silberman D. M., Sebastián C., Mermel C., Dobersch S., Clark A. R., Getz G., Denu J. M., and Mostoslavsky R. (2015) Identification of and molecular basis for SIRT6 loss-of-function point mutations in cancer. *Cell Rep.* 13, 479–488 10.1016/j.celrep.2015.09.022
12. Zhang J., Yin X. J., Xu C. J., Ning Y. X., Chen M., Zhang H., Chen S. F., and Yao L. Q. (2015) The histone deacetylase SIRT6 inhibits ovarian cancer cell proliferation via down-regulation of Notch 3 expression. *Eur. Rev. Med. Pharmacol. Sci.* 19, 818–824
13. Mostoslavsky R., Chua K. F., Lombard D. B., Pang W. W., Fischer M. R., Gellon L., Liu P., Mostoslavsky G., Franco S., Murphy M. M., Mills K. D., Patel P., Hsu J. T., Hong A. L., Ford E., et al. (2006) Genomic instability and aging-like phenotype in the absence of mammalian SIRT6. *Cell* 124, 315–329 10.1016/j.cell.2005.11.044

14. Mao Z., Hine C., Tian X., Van Meter M., Au M., Vaidya A., Seluanov A., and Gorbunova V. (2011) SIRT6 promotes DNA repair under stress by activating PARP1. *Science* 332, 1443–1446  
10.1126/science.1202723
15. Toiber D., Erdel F., Bouazoune K., Silberman D. M., Zhong L., Mulligan P., Sebastian C., Cosentino C., Martinez-Pastor B., Giacosa S., D'Urso A., Näär A. M., Kingston R., Rippe K., and Mostoslavsky R. (2013) SIRT6 recruits SNF2H to DNA break sites, preventing genomic instability through chromatin remodeling. *Mol. Cell* 51, 454–468 10.1016/j.molcel.2013.06.018
16. Kanfi Y., Naiman S., Amir G., Peshti V., Zinman G., Nahum L., Bar-Joseph Z., and Cohen H. Y. (2012) The sirtuin SIRT6 regulates lifespan in male mice. *Nature* 483, 218–221  
10.1038/nature10815
17. Tian X., Firsanov D., Zhang Z., Cheng Y., Luo L., Tomblin G., Tan R., Simon M., Henderson S., Steffan J., Goldfarb A., Tam J., Zheng K., Cornwell A., Johnson A., et al. (2019) SIRT6 is responsible for more efficient DNA double-strand break repair in long-lived species. *Cell* 177, 622–638.e22 10.1016/j.cell.2019.03.043
18. Kanfi Y., Peshti V., Gil R., Naiman S., Nahum L., Levin E., Kronfeld-Schor N., and Cohen H. Y. (2010) SIRT6 protects against pathological damage caused by diet-induced obesity. *Aging Cell* 9, 162–173 10.1111/j.1474-9726.2009.00544.x
19. Feldman J. L., Baeza J., and Denu J. M. (2013) Activation of the protein deacetylase SIRT6 by long-chain fatty acids and widespread deacylation by mammalian sirtuins. *J. Biol. Chem.* 288, 31350–31356 10.1074/jbc.C113.511261

20. Jiang H., Khan S., Wang Y., Charron G., He B., Sebastian C., Du J., Kim R., Ge E., Mostoslavsky R., Hang H. C., Hao Q., and Lin H. (2013) SIRT6 regulates TNF- $\alpha$  secretion through hydrolysis of long-chain fatty acyl lysine. *Nature* 496, 110–113 10.1038/nature12038
21. Michishita E., McCord R. A., Berber E., Kioi M., Padilla-Nash H., Damian M., Cheung P., Kusumoto R., Kawahara T. L., Barrett J. C., Chang H. Y., Bohr V. A., Ried T., Gozani O., and Chua K. F. (2008) SIRT6 is a histone H3 lysine 9 deacetylase that modulates telomeric chromatin. *Nature* 452, 492–496 10.1038/nature06736
22. Yang B., Zwaans B. M. M., Eckersdorff M., and Lombard D. B. (2009) The sirtuin SIRT6 deacetylates H3 K56Ac *in vivo* to promote genomic stability. *Cell Cycle* 8, 2662–2663 10.4161/cc.8.16.9329
23. Tasselli L., Xi Y., Zheng W., Tennen R. I., Odrowaz Z., Simeoni F., Li W., and Chua K. F. (2016) SIRT6 deacetylates H3K18ac at pericentric chromatin to prevent mitotic errors and cellular senescence. *Nat. Struct. Mol. Biol.* 23, 434–440 10.1038/nsmb.3202
24. Rahnasto-Rilla M. K., McLoughlin P., Kulikowicz T., Doyle M., Bohr V. A., Lahtela-Kakkonen M., Ferrucci L., Hayes M., and Moaddel R. (2017) The identification of a SIRT6 activator from brown algae *Fucus distichus*. *Mar. Drugs* 15, E190 10.3390/md15060190
25. Rahnasto-Rilla M., Tyni J., Huovinen M., Jarho E., Kulikowicz T., Ravichandran S., Bohr V. A., Ferrucci L., Lahtela-Kakkonen M., and Moaddel R. (2018) Natural polyphenols as sirtuin 6 modulators. *Sci. Rep.* 8, 4163 10.1038/s41598-018-22388-5
26. Huang Z., Zhao J., Deng W., Chen Y., Shang J., Song K., Zhang L., Wang C., Lu S., Yang X., He B., Min J., Hu H., Tan M., Xu J., et al. (2018) Identification of a cellularly active SIRT6 allosteric activator. *Nat. Chem. Biol.* 14, 1118–1126 10.1038/s41589-018-0150-0

27. Iachettini S., Trisciuoglio D., Rotili D., Lucidi A., Salvati E., Zizza P., Di Leo L., Del Bufalo D., Ciriolo M. R., Leonetti C., Steegborn C., Mai A., Rizzo A., and Biroccio A. (2018) Pharmacological activation of SIRT6 triggers lethal autophagy in human cancer cells. *Cell Death Dis.* 9, 996 10.1038/s41419-018-1065-0
28. Howitz K. T., Bitterman K. J., Cohen H. Y., Lamming D. W., Lavu S., Wood J. G., Zipkin R. E., Chung P., Kisielewski A., Zhang L. L., Scherer B., and Sinclair D. A. (2003) Small molecule activators of sirtuins extend *Saccharomyces cerevisiae* lifespan. *Nature* 425, 191–196 10.1038/nature01960
29. Baur J. A., Pearson K. J., Price N. L., Jamieson H. A., Lerin C., Kalra A., Prabhu V. V., Allard J. S., Lopez-Lluch G., Lewis K., Pistell P. J., Poosala S., Becker K. G., Boss O., Gwinn D., et al. (2006) Resveratrol improves health and survival of mice on a high-calorie diet. *Nature* 444, 337–342 10.1038/nature05354
30. Hubbard B. P., Gomes A. P., Dai H., Li J., Case A. W., Considine T., Riera T. V., Lee J. E., E S. Y., Lamming D. W., Pentelute B. L., Schuman E. R., Stevens L. A., Ling A. J., Armour S. M., et al. (2013) Evidence for a common mechanism of SIRT1 regulation by allosteric activators. *Science* 339, 1216–1219 10.1126/science.1231097
31. Mercken E. M., Mitchell S. J., Martin-Montalvo A., Minor R. K., Almeida M., Gomes A. P., Scheibye-Knudsen M., Palacios H. H., Licata J. J., Zhang Y., Becker K. G., Khraiwesh H., González-Reyes J. A., Villalba J. M., Baur J. A., et al. (2014) SRT2104 extends survival of male mice on a standard diet and preserves bone and muscle mass. *Aging Cell* 13, 787–796 10.1111/accel.12220

32. Mitchell S. J., Martin-Montalvo A., Mercken E. M., Palacios H. H., Ward T. M., Abulwerdi G., Minor R. K., Vlasuk G. P., Ellis J. L., Sinclair D. A., Dawson J., Allison D. B., Zhang Y., Becker K. G., Bernier M., and de Cabo R. (2014) The SIRT1 activator SRT1720 extends lifespan and improves health of mice fed a standard diet. *Cell Rep.* 6, 836–843  
10.1016/j.celrep.2014.01.031
  
33. Dai H., Sinclair D. A., Ellis J. L., and Steegborn C. (2018) Sirtuin activators and inhibitors: promises, achievements, and challenges. *Pharmacol. Ther.* 188, 140–154  
10.1016/j.pharmthera.2018.03.004
  
34. Madsen A. S., Andersen C., Daoud M., Anderson K. A., Laursen J. S., Chakladar S., Huynh F. K., Colaço A. R., Backos D. S., Fristrup P., Hirschey M. D., and Olsen C. A. (2016) Investigating the sensitivity of NAD<sup>+</sup>-dependent sirtuin deacylation activities to NADH. *J. Biol. Chem.* 291, 7128–7141 10.1074/jbc.M115.668699
  
35. Pan P. W., Feldman J. L., Devries M. K., Dong A., Edwards A. M., and Denu J. M. (2011) Structure and biochemical functions of SIRT6. *J. Biol. Chem.* 286, 14575–14587  
10.1074/jbc.M111.218990
  
36. Ferrer C. M., Alders M., Postma A. V., Park S., Klein M. A., Cetinbas M., Pajkrt E., Glas A., van Koningsbruggen S., Christoffels V. M., Mannens M. M. A. M., Knecht L., Etchegaray J. P., Sadreyev R. I., Denu J. M., et al. (2018) An inactivating mutation in the histone deacetylase SIRT6 causes human perinatal lethality. *Genes Dev.* 32, 373–388 10.1101/gad.307330.117
  
37. Smith B. C., and Denu J. M. (2006) Sir2 protein deacetylases: evidence for chemical intermediates and functions of a conserved histidine. *Biochemistry* 45, 272–282  
10.1021/bi052014t

38. Johnson K. A. (2019) New standards for collecting and fitting steady state kinetic data. *Beilstein J. Org. Chem.* 15, 16–29 10.3762/bjoc.15.2
39. Shi Y., Zhou Y., Wang S., and Zhang Y. (2013) Sirtuin deacetylation mechanism and catalytic role of the dynamic cofactor binding loop. *J. Phys. Chem. Lett.* 4, 491–495 10.1021/jz302015s
40. Ghosh S., Liu B., Wang Y., Hao Q., and Zhou Z. (2015) Lamin A is an endogenous SIRT6 activator and promotes SIRT6-mediated DNA repair. *Cell Rep.* 13, 1396–1406 10.1016/j.celrep.2015.10.006
41. Albaugh B. N., Arnold K. M., Lee S., and Denu J. M. (2011) Autoacetylation of the histone acetyltransferase Rtt109. *J. Biol. Chem.* 286, 24694–24701 10.1074/jbc.M111.251579
42. Borra M. T., Langer M. R., Slama J. T., and Denu J. M. (2004) Substrate specificity and kinetic mechanism of the Sir2 family of NAD<sup>+</sup>-dependent histone/protein deacetylases. *Biochemistry* 43, 9877–9887 10.1021/bi049592e
43. Smith B. C., and Denu J. M. (2007) Sir2 deacetylases exhibit nucleophilic participation of acetyl-lysine in NAD<sup>+</sup> cleavage. *J. Am. Chem. Soc.* 129, 5802–5803 10.1021/ja070162w
44. Lassalas, P., Gay, B., Lasfargeas, C., James, M.J., Tran, V., et al. (2016) Structure Property Relationships of Carboxylic Acid Isosteres. *J. Med. Chem.* 59, 3183–3203. 10.1021/acs.jmedchem.5b01963
45. Yuan, C., Sidhu, R.S., Kuklev, D.V., et al. (2009) Cyclooxygenase Allosterism, Fatty Acid-mediated Cross-talk between Monomers of Cyclooxygenase Homodimers. *J. Biol. Chem.* 284, 10046–10055. 10.1074/jbc.M808634200

### **CHAPTER 3: Nucleosome binding enhances SIRT6 deacetylation\***

**Mark A. Klein<sup>1,2</sup>, José D. Moran<sup>1,2</sup>, Wallace H. Liu<sup>1,2</sup>, John M. Denu<sup>1,2,3</sup>**

From the <sup>1</sup>Wisconsin Institute for Discovery, University of Wisconsin-Madison; <sup>2</sup>Department of Biomolecular Chemistry, University of Wisconsin-Madison; <sup>3</sup>Morgridge Institute for Research, University of Wisconsin-Madison

\*This ongoing and unpublished work represents a thrilling forefront of mechanistic SIRT6 work.

I am proud to be sharing it here while honored and excited for the places José will take it.

\*\*This body of work references work authored by Wallace H. Liu titled “Multivalent Interactions Drive Nucleosome Binding and Efficient Chromatin Deacetylation 2 by SIRT6” which has been accepted however not yet published at Nature Communication. The in-text citation referencing this work appears as “(Liu. et al. 2020 *Nat. Comm.*)”



### 3.1 Introduction

Sirtuin 6 (SIRT6) is a lysine deacylase most recognized for its histone deacetylase activity and physiological contributions as a metabolic regulator (1–3), tumor suppressor (4–6) DNA repair factor (7–9), and due to its positive link with longevity (10, 11). The absence of these functions manifests on a phenotypic level in SIRT6-deficient mice, which display genomic instability, dysregulated glycolysis, increased tumorigenesis, and progeria, ultimately dying at 4 weeks of age (4, 7). Loss-of-function homozygous mutation of SIRT6 led to muscle and brain developmental defects and late fetal loss in both humans and cynomolgus monkeys (12, 13). Furthermore, naturally arising loss-of-function mutations have been identified in human cancers and were later shown to be sufficient to drive tumor formation in mice (5). The wealth of phenotypic data available for SIRT6 is a testament to its vast overarching biology and interest as a therapeutic target for activation (14–16). However, *in vitro* challenges in characterizing and understanding the catalytic activities of SIRT6 have tempered the development of pharmacological compounds.

Sirtuins couple the stoichiometric hydrolysis of  $\text{NAD}^+$  to the removal of an acyl moiety from the  $\epsilon$ -amino group of a substrate lysine (17). Investigations into the deacetylase functions of SIRT6 had lagged those of SIRT1 owing to its poor *in vitro* activity which is nearly 1,000 times lower than that of other sirtuins (18). Subsequent detailed studies demonstrated that SIRT6 is hundreds-fold more active against long-chain acyl substrates, supported by structural data revealing that these long-acyl groups are accommodated in a hydrophobic pocket extending past the active site (19, 20). However, this *in vitro* data was at odds with the wealth of biological data supporting an essential role for SIRT6 deacetylation, whereas limited data has been presented supporting the *in vivo* roles of long-chain deacylation (19, 21). More recently, a number of small molecule activators of SIRT6 deacetylation have been reported, demonstrating the ability of SIRT6

to perform efficient deacetylation (22–28). A mechanistic study we conducted of one such activator demonstrated that SIRT6 activation was mediated by arginine-65 (R65), which previously was found to be required for cellular deacetylation (8, 28). Together these data suggested that cellular activation of SIRT6 is required for physiological deacetylation of nucleosomes. Nonetheless, endogenous activators responsible for facilitating the efficient deacetylase activity of SIRT6 have yet to be identified.

Many histone deacetylases act as part of large multi-subunit complexes that serve to direct chromatin localization and stimulate deacetylase activity (29). Although SIRT6 is not known to function as part of a complex, the majority of cellular SIRT6 remains bound to chromatin (7, 30). Additionally, it was demonstrated that SIRT6 more efficiently deacetylated nucleosomes than histones, together suggesting that SIRT6 may intrinsically bind to nucleosomes (31). This observation was supported by a detailed study from our lab demonstrating that two molecules of SIRT6 bind asymmetrically per nucleosome with high affinity and that this interaction is mediated by the intrinsically disordered C-terminus of SIRT6 (Liu. et al. 2020 *Nat. Comm.*). This C-terminal mediated interaction was required for productive deacetylation in cells and was independent of acetylated lysine residues on the nucleosome, indicating that substrate independent nucleosome binding mediates efficient SIRT6 deacetylation. Although nucleosome tethering of SIRT6 proximal to its histone tail substrate provides a rationale for efficient cellular deacetylation, this study did not examine whether nucleosome binding directly stimulated SIRT6 catalysis.

Here we provide preliminary results that nucleosome binding directly enhances the deacetylase, but not long-chain demyristoylase activity of SIRT6 using peptide substrates. This enhanced deacetylase activity was further observed against homogenously acetylated nucleosome substrate. We find this enhancement to be mediated, at least in part, by R65 and appears similar to

the activation mechanism described with CL5D small molecule activation. Interestingly, the recently reported SIRT6 activator, MDL-800, when incubated with SIRT6, increased the ability of SIRT6 to deacetylate mononucleosomes under non-steady-state conditions. Together, these data suggest that nucleosome binding can stimulate SIRT6 inter-molecular deacetylation against peptide substrates. Preliminary results with activator compounds suggest that distinct mechanisms of small-molecule activation are likely and that the nature of the substrate and activator will reveal variable efficiencies of activation.

## 3.2 Results and discussion

### 3.2.1 Nucleosome binding stimulates SIRT6 deacetylation of peptide substrate

Sirtuin 6 (SIRT6) demonstrates weak deacetylase activity towards peptide substrate *in vitro* however can be stimulated by small molecule activators (20, 28). Prior work in our lab and others demonstrated that nucleosomes are a better substrate for SIRT6 than histones alone and that SIRT6 binds with low nanomolar affinity to nucleosomes (Liu. et al. 2020 *Nat Comm*, (31)). Liu et al. showed that the C-terminus of SIRT6 was required for high affinity nucleosome binding and efficient deacetylation of histone H3K9ac in cells. However, this data does not deconvolute whether efficient deacetylation in cells is due to high affinity towards substrate nucleosome or whether nucleosome binding improves SIRT6 catalytic parameters.

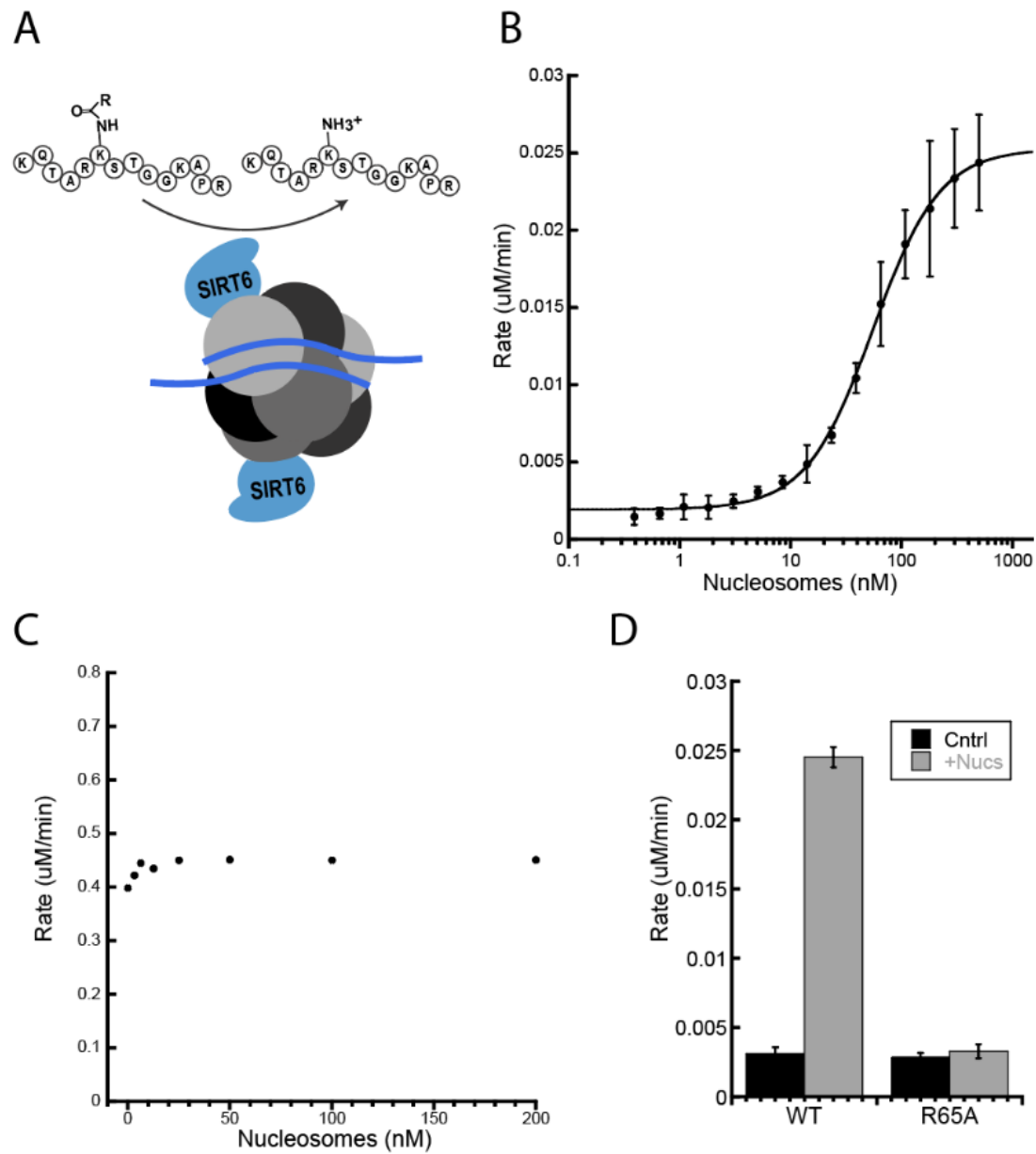
To determine whether nucleosome binding enhances deacetylation of SIRT6 independent of tethering to nucleosome substrate, recombinantly assembled unmodified nucleosomes were titrated into a reaction containing SIRT6 and H3K9ac peptide substrate (Fig. 3-1A,B). These results demonstrate a strong activation of SIRT6 by nucleosomes ( $EC_{50} = 55 \pm 2$  nM) towards acetylated peptide substrate. The  $EC_{50}$  of activation is similar to the previously determined  $K_d$  of SIRT6-nucleosome binding (13 nM), suggesting that direct nucleosome binding stimulates the intermolecular deacetylation of peptide substrate (Liu. et al. 2020 *Nat. Comm.*). SIRT6 has previously been shown to harbor efficient long-chain deacylase activity, however most small molecule activators of deacetylation either fail to activate long-chain deacylation or act as competitive inhibitors (20, 25, 27, 28). To assess whether nucleosome binding enhances long-chain deacylase function of SIRT6, nucleosomes were titrated into a reaction containing SIRT6 and myristoylated histone 3 lysine-9 (H3K9myr) peptide (Fig. 3-1C). Unlike deacetylation, the presence of nucleosomes failed to enhance the rate of demyristoylation.

Previously we showed that the small molecule activator of deacetylation, CL5D, enhanced a conformational rate preceding the first chemical step of catalysis that was mediated by arginine-65 (28). Mutation of this arginine to alanine (R65A) rendered SIRT6 nonactivatable by CL5D and reduced rates of demyristoylation to those of deacetylation. Together this suggested that activated deacetylation and the intrinsic high efficiency of demyristoylation utilized a common pathway to enhanced catalysis mediated by R65. To test whether nucleosome binding utilizes a similar mechanism of activation, we looked at the ability of nucleosomes to activate SIRT6 R65A towards the deacetylation of H3K9ac peptide substrate (Fig. 3-1D). Whereas nucleosomes activated wild-type SIRT6, the R65A mutant was unable to be activated under the conditions tested, despite retaining the ability to bind nucleosomes with high affinity (data not shown), suggesting that nucleosome binding stimulates deacetylation in a mechanism requiring R65.

Recombinant nucleosomes show an exquisitely low  $EC_{50}$  relative to other reported SIRT6 activators when using acetylated peptide substrates. Cellular SIRT6 is primarily chromatin bound and has been shown to directly bind to nucleosomes with high affinity ((7), Liu. et al. 2020 *Nat. Comm.*). Importantly, we demonstrated that the R65A mutant, which fails to perform efficient deacetylation in cells (8), cannot be activated by nucleosome binding. Together this suggests a mechanism by which chromatin association serves to endogenously activate the deacetylase activity of SIRT6. These data highlight the importance of context when evaluating the deacetylase activities of SIRT6. To this end, we continue our studies using acetylated nucleosomes as a substrate.

**Figure 3-1: Nucleosomes stimulate SIRT6 deacetylation of peptide substrate in an R65-dependent manner.** (A) In these series of experiments, unmodified recombinant nucleosomes were evaluated as an activator for SIRT6 deacylation against peptide substrate. Under these conditions SIRT6 has been reported to bind efficiently to nucleosomes with a  $K_d$  of 13 nM (Liu. et al. 2020 *Nat. Comm.*). (B) The activity of 100 nM SIRT6 was monitored against 40  $\mu$ M H3K9ac peptide in the presence of 1 mM  $\text{NAD}^+$  for 45 minutes with increasing concentrations of unmodified nucleosome. An  $\text{EC}_{50}$  of  $55 \pm 2$  nM was determined for nucleosomes with a Hill coefficient of  $1.44 \pm 0.07$ . Mean value of three replicates reported with error bars representing standard deviation. (C) The activity of 100 nM SIRT6 was monitored against 20  $\mu$ M H3K9myr peptide over 3 minutes with increasing concentrations of unmodified nucleosome,  $n=1$ . (D) WT and R65A SIRT6 (100 nM) were incubated with 40  $\mu$ M H3K9ac peptide and 200 nM unmodified nucleosomes in the presence of 1 mM  $\text{NAD}^+$  for 90 minutes. Nucleosome storage buffer was added in place of nucleosomes for control reaction. Mean value of three replicates reported with error bars representing standard deviation.

**Figure 3-1: Nucleosomes stimulate SIRT6 deacetylation of peptide substrate in an R65-dependent manner.**



### 3.2.2 Validating acetylated H3K9ac nucleosomes as a SIRT6 substrate

In order to create acetylated nucleosome substrate for the kinetic studies of SIRT6, histone H3 acetylated at lysine-9 was generated using amber codon suppression prior to incorporation in nucleosome core particles (32–34). Successful nucleosome preparation was validated by native-PAGE shift of 601 DNA used for mononucleosome assembly. Reactions containing various concentrations of SIRT6 and H3K9ac nucleosomes (nucH3K9ac) were performed and analyzed by both dot blot and western blot analysis (Fig. 3-2A,B). These data show an  $\text{NAD}^+$ , SIRT6, and time dependent deacetylation, validating nucH3K9ac as a substrate for SIRT6. Deacetylation appears to occur more quickly in identical samples analyzed by western blot, suggesting that the use of 1x SDS-PAGE loading dye may not have quenched the reaction as instantaneously as the 1% TFA used in the dot blot analysis. Owing to the instantaneous quench of TFA, molecularly defined assay conditions, and ability to quickly quantify many samples on a single membrane, dot blot analysis was used in subsequent experiments.

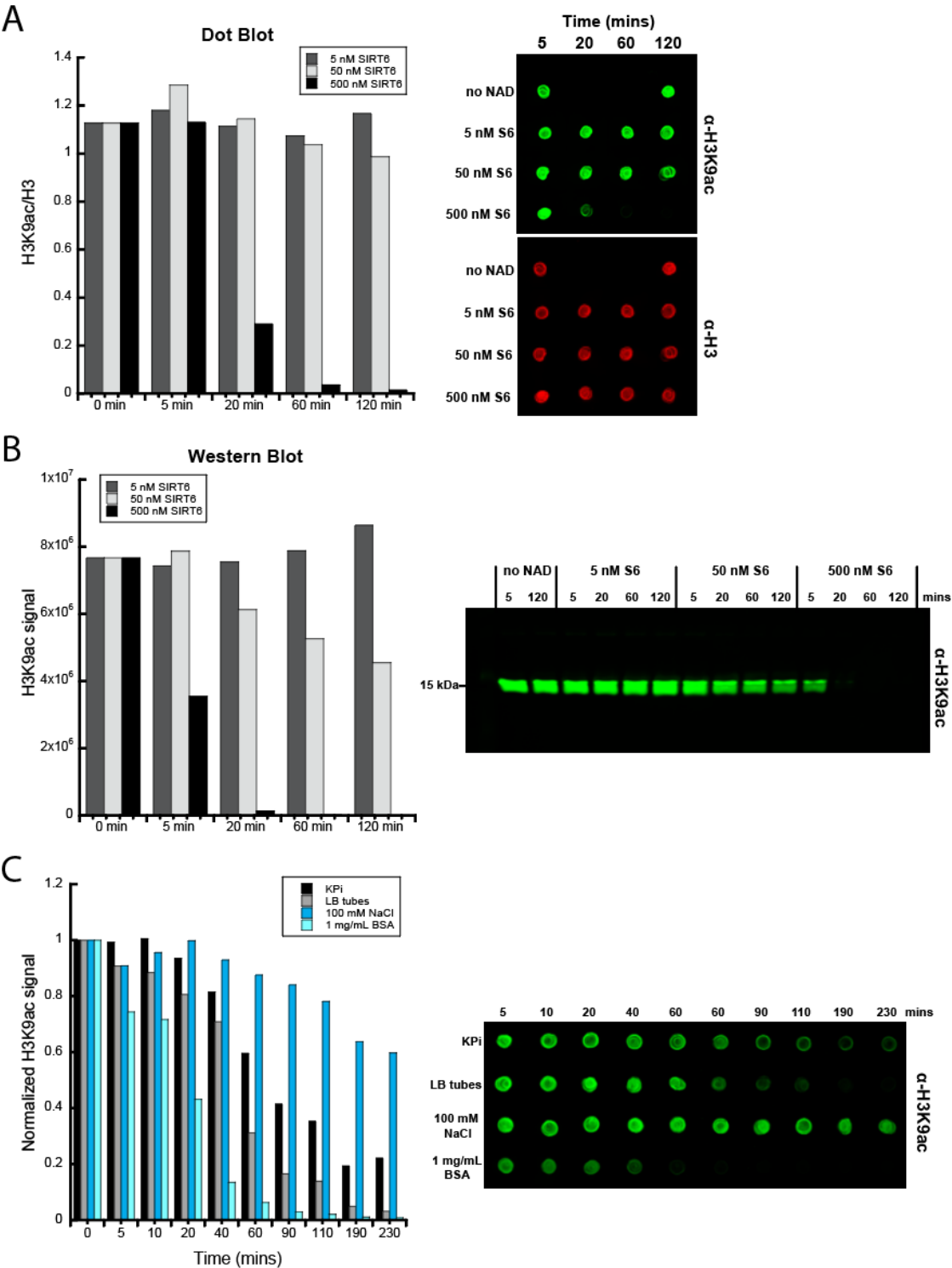
Next, we wanted to examine how various assay conditions including the use of low-binding tubes, BSA, and salt affected the deacetylase activity of SIRT6 (Fig. 3-2C). Both low-binding tubes and 1 mg/mL BSA resulted in increased rate of deacetylation against nucH3K9ac, suggesting that the low concentration of SIRT6 and/or nucH3K9ac used in these assays may be subject to non-specific adhesion to reaction tubes in the absence of crowding agent. Low-binding tubes were used subsequently for all nucleosome deacetylation reactions. The minimum concentration of BSA required to maximize the rate of deacetylation under these conditions was further optimized to 0.25 mg/mL (data not shown). Additionally, the rate of deacetylation was observed to decrease in the presence of 100 mM NaCl which could be attributed to the decreased stability of nucleosome core particles at elevated ionic strength (35, 36). Together these data validate nucH3K9ac as a



substrate for  $\text{NAD}^+$  dependent deacetylation and provide suitable reaction conditions used in the subsequent kinetic analysis of nucleosome deacetylation by SIRT6.

**Figure 3-2. Recombinant nucleosomes homogenously acetylated at histone 3 lysine 9 are an *in vitro* substrate for SIRT6.** (A,B) Various concentrations of SIRT6 incubated with 750 nM H3K9ac nucleosomes, 1 mM NAD<sup>+</sup>, and 20 mM potassium phosphate (KP<sub>i</sub>) pH 7.5 for either 5, 20, 60, or 120 minutes at 37 °C. Following incubation, reactions were quenched either by the addition of 1% TFA final and analyzed by dot blot (A) or by addition of 1x SDS-PAGE loading dye followed by 5 minute incubation at 95 °C and analysis by western blot (B). Control reactions in the absence of NAD<sup>+</sup> were only conducted for 5 and 120 minutes, n=1. (C) SIRT6 (100 nM) was incubated with 750 nM H3K9ac nucleosomes and 1 mM NAD<sup>+</sup> at 37 °C for various timepoints and quenched by addition of 1% TFA final. Reactions were conducted either in 20 mM KP<sub>i</sub> pH 7.5 in regular Eppendorf tubes, 20 mM KP<sub>i</sub> pH 7.5 in low-binding Eppendorf tubes, 20 mM KP<sub>i</sub> pH 7.5 with 100 mM NaCl in regular Eppendorf tubes, or 20 mM KP<sub>i</sub> pH 7.5 with 1 mg/mL BSA in regular Eppendorf tubes. Reactions were quantified by dot blot, n=1.

**Figure 3-2. Recombinant nucleosomes homogenously acetylated at histone 3 lysine 9 are an *in vitro* substrate for SIRT6.**



### 3.2.3 SIRT6 performs efficient deacetylation against acetylated nucleosomes

It has previously been shown that nucleosomes are a better substrate for SIRT6 than histones alone (31), however this study used nucleosomes derived from chicken erythrocytes which are heterogeneously modified. Endogenously sourced nucleosomes have been shown to be lowly acetylated (<2%) at H3K9 making them poorly suited for the determination of kinetic rates (37). Having assembled and validated homogeneously acetylated nucleosomes (nucH3K9ac) we sought to determine the kinetic constants,  $k_{\text{cat}}$  and  $K_{\text{m}}$ , of nucleosome deacetylation by SIRT6. To this end, we monitored the deacetylation of nucH3K9ac by SIRT6 beginning under steady-state conditions and continuing to complete substrate depletion (Fig. 3-3A). This non-linear progress curve was fitted to an integrated form of the Michaelis-Menten equation which utilizes the change in instantaneous velocity over the course of substrate depletion to determine kinetic rate constants (38, 39). From this fit, we determined a  $k_{\text{cat}}$  and  $K_{\text{m}}$  of  $0.012 \pm 0.004 \text{ s}^{-1}$  and  $701 \pm 354 \text{ nM}$  respectively and an overall catalytic efficiency of  $17,118 \text{ M}^{-1}\text{s}^{-1}$ . The catalytic efficiency of nucH3K9ac deacetylation is nearly 5,000 fold higher than that of peptide deacetylation alone ( $3.6 \text{ M}^{-1}\text{s}^{-1}$ ) and 10-15 fold higher than small molecule activated peptide deacetylation ( $1,126 \text{ M}^{-1}\text{s}^{-1}$ ) and peptide demyristoylation ( $1,700 \text{ M}^{-1}\text{s}^{-1}$ ) (28). We next sought to determine which step in catalysis was being enhanced against nucleosome substrate compared to peptide substrate.

To provide mechanistic details about individual steps during nucleosome deacetylation, a single-turnover, rapid-quench kinetic analysis was performed to monitor the rate of alkylamidate intermediate formation (Fig. 3-3B). This assay was performed with limiting nucleosome substrate, permitting only a single turnover of the enzyme. SIRT6 ( $2 \text{ }\mu\text{M}$ ) was incubated with saturating  $\text{NAD}^{+}$  and  $100 \text{ nM}$  nucH3K9ac. Following rapid acid-quenching (10-720 seconds), deacetylated nucleosome was quantified by dot blot analysis and data were fitted to a single-exponential curve.

The first chemical step of catalysis is the formation of the alkylamidate intermediate ( $k_{\text{alk}}$ ) which occurs concomitant with the formation of nicotinamide. The formation of this covalent intermediate was monitored by the decrease in H3K9ac detection by dot blot analysis. Fitting of data yielded a  $k_{\text{alk}}$  of  $0.0085 \pm 0.0005 \text{ s}^{-1}$ . Importantly, this rate is within error of the previously determined  $k_{\text{cat}}$  ( $0.012 \pm 0.004 \text{ s}^{-1}$ ) indicating that the formation of alkylamidate intermediate is rate-limiting for the deacetylation of nucleosomes by SIRT6. Previous studies have determined that the rate-limiting step of peptide deacylation by SIRT6 is the catalytic step subsequent to alkylamidate formation, generation of the 1'2'-bicyclic intermediate (28, 40). The shift in rate-limiting step between peptide and nucleosome substrate indicates that nucleosome binding enhances a catalytic step following alkylamidate formation, likely the formation of the 1',2'-bicyclic intermediate. Furthermore, the similarity of the rates  $k_{\text{alk}}$  and steady-state  $k_{\text{cat}}$  suggests that product release occurs quickly relative to catalysis, although it remains to be determined whether product release entails dissociation of SIRT6 from nucleosome or simply release of tail peptide from active site pocket.

The staggering ~5,000-fold difference in catalytic efficiency between peptide and nucleosome deacetylation provides rationale as to how an enzyme renowned for its poor *in vitro* deacetylase activity performs wide reaching and critical cellular roles as a deacetylase. It is not known whether other nuclear sirtuins can be activated by nucleosome binding, however the ability to intrinsically associate with chromatin is unique to SIRT6 compared to SIRT1 and it is likely that this route to activation is intimately linked to nucleosome binding (7). Single-turnover kinetic analysis revealed that the rate-limiting step of intra-nucleosome catalysis is the formation of alkylamidate intermediate, contrary to that of peptide deacetylation in which the rate-limiting step is the subsequent formation of 1'2'-bicyclic intermediate. Together this indicates that nucleosome

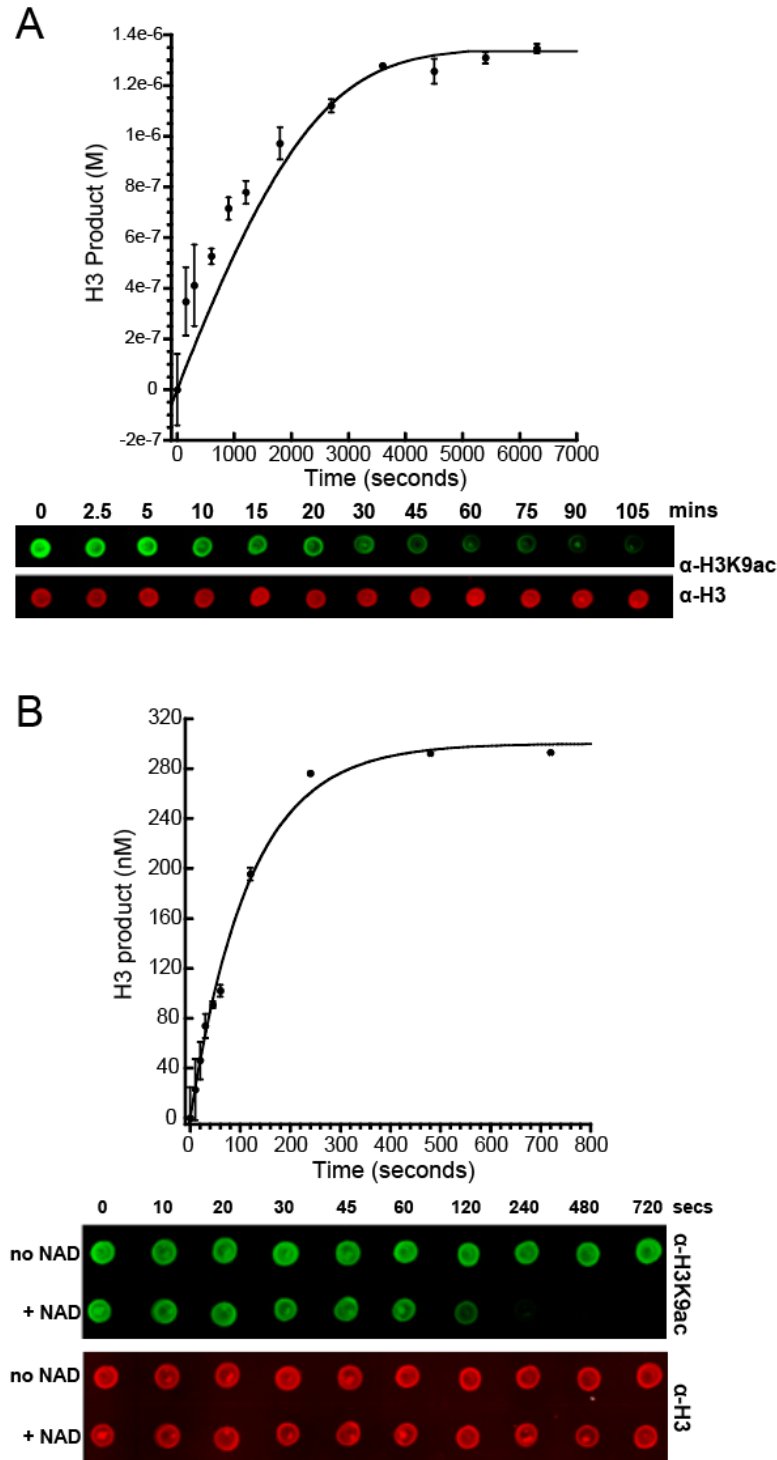
binding stimulates a catalytic step following alkylamidate formation. Furthermore, the similar rates of  $k_{\text{alk}}$  and  $k_{\text{cat}}$  indicate that product release is not rate-limiting. At this point, we note that these are preliminary results and speculative conclusions. Additional experiments are needed.

**Figure 3-3. SIRT6 performs efficient deacetylation of nucleosomes.** (A) SIRT6 (75 nM) was incubated with 750 nM H3K9ac nucleosomes and 1 mM NAD<sup>+</sup> in 20 mM potassium phosphate pH 7.5 and 0.25 mg/mL BSA for varying periods of time. Following dot blot quantification, data were fitted to the integrated form of the Michaelis-Menten equation (38).

$$t = p/k_{\text{cat}}E_0 + (K_m/k_{\text{cat}}E_0) \ln(p_{\infty}/(p_{\infty} - p))$$

From this fit, the  $k_{\text{cat}}$  and  $K_m$  were determined to be  $0.012 \pm 0.004 \text{ s}^{-1}$  and  $701 \pm 354 \text{ nM}$  respectively. Mean value of three replicates reported with error bars representing standard deviation. (B) Single-turnover kinetics were performed for the deacetylation of H3K9ac nucleosomes by SIRT6. SIRT6 (2  $\mu\text{M}$ ) was incubated with 150 nM H3K9ac nucleosomes and 1 mM NAD<sup>+</sup> in 20 mM potassium phosphate pH 7.5 and 0.25 mg/mL BSA at 37 °C for given periods of time prior to quench with 1% TFA final. Reaction progress quantified by dot blot before being fitted to a single exponential curve. From this fit, it was determined that rate of alkylamidate intermediate formation was  $0.0085 \pm 0.0005 \text{ s}^{-1}$ . Mean value of three replicates reported with error bars representing standard deviation.

Figure 3-3. SIRT6 performs efficient deacetylation of nucleosomes.





### 3.2.4. *Small molecules can stimulate deacetylation of nucleosomes*

SIRT6 has garnered attention as a potential therapeutic target for activation due to its positive links with longevity and as its role as a tumor suppressor (14–16). Huang et al. reported the use of MDL-800 in models of liver fibrosis and non-small cell lung cancer (27, 41, 42). We have examined CL5D (28) for the ability to enter cells (MEFs) and stimulate the global deacetylation of H3K9ac, however we detected no significant change in global levels of H3K9ac (Fig. 3-4). At this point, it is unclear if other factors such as cell permeability, metabolic degradation of CL5D, or non-permissive culture conditions contribute. It is intriguing to speculate that CL5D and MDL-800 affect different steps in the catalytic cycle, that the nature of the substrate matters, and that whether the reaction is intra- or inter-molecular deacetylation will also determine the efficacy of the observed activation.

To address this hypothesis, we first tested whether R65 was critical for efficient deacetylation of nucleosomes by comparing the rates of nucH3K9ac deacetylation by wild-type and R65A SIRT6 (Fig. 3-5A). Consistent with its inability to be stimulated by small molecules and nucleosomes towards peptide substrates, SIRT6 R65A failed to efficiently deacetylate nucH3K9ac. We evaluated the ability of 50  $\mu$ M CL5D and MDL-800 to activate SIRT6 deacetylation of nucH3K9ac under non-steady-state conditions (Fig. 3-5B). CL5D had no significant effect on SIRT6 deacetylation of nucH3K9ac under the conditions tested, suggesting that the activation mechanism of CL5D and nucleosome binding are similar. Interestingly, MDL-800 activated SIRT6 towards deacetylation of nucH3K9ac. Together, these preliminary results suggests that MDL-800 utilizes a distinct mechanism of activation to that of nucleosome binding. To test whether MDL-800 utilizes an R65-independent mechanism of activation, the deacetylation of H3K9ac peptide substrate by wild-type and R65A SIRT6 was determined in the presence of 50

$\mu$ M CL5D and MDL-800 (Fig. 3-5C). We found that MDL-800 activated SIRT6 R65A, albeit to a lesser extent than wild-type SIRT6. Together these data indicate that MDL-800 utilizes a partially R65-independent mechanism of activation which likely contributes to its ability to stimulate deacetylation against nucleosome substrate. Subsequent studies are required to determine the specific contributions of CL5D and MDL-800 to the  $k_{\text{cat}}$  and  $k_{\text{cat}}/K_m$  parameters of SIRT6 mediated nucleosome deacetylation. The data presented here do not preclude the possibility that MDL-800 specifically activates  $k_{\text{cat}}$  whereas CL5D may in fact still activate the  $k_{\text{cat}}/K_m$  but not lead to an observed increase in activity similar to that of MDL-800 due to the high concentration of nucleosomes used in these experiments.

**Figure 3-4. Treatment of MEFs with CL5D.** Wild-type and SIRT6-knockout MEFs were treated 1 mM SAHA for 4 hours prior to treatment with 50  $\mu$ M CL5D, CL5D-me (methyl-ester), CL5 (inactive scaffold control), or 0.5% DMSO for 8 hours. Cells were harvested prior to histone isolation and western blot analysis of H3K9ac and total H3. The mean value of triplicates of the ratio of H3K9ac to H3 was reported with error bars representing standard deviation.

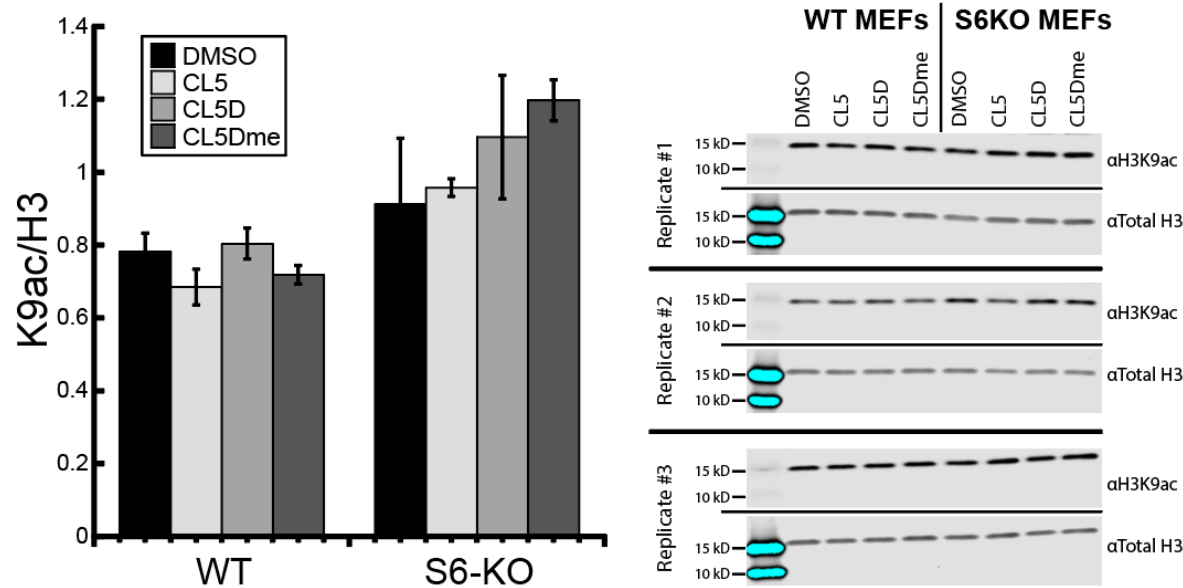
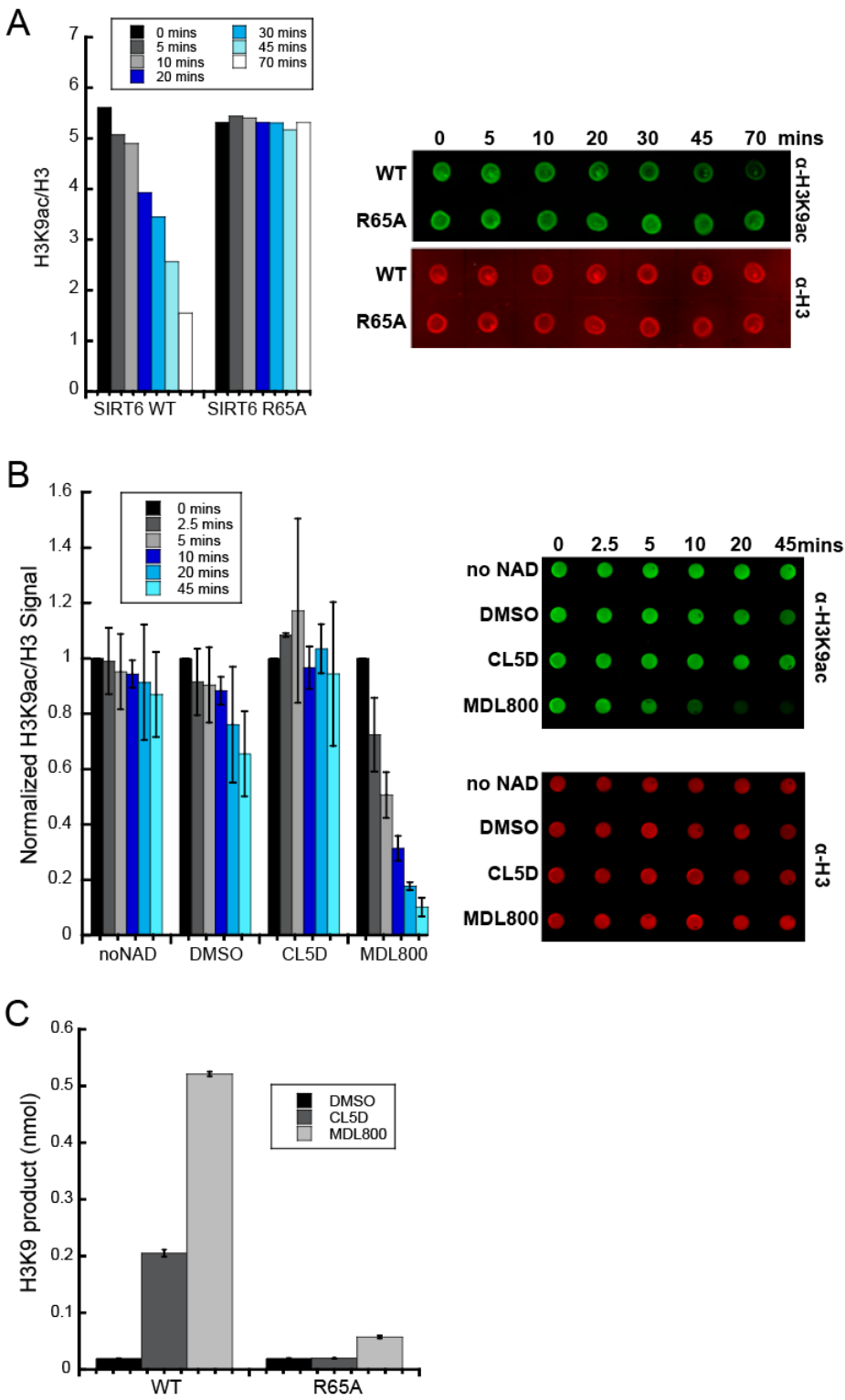


**Figure 3-5. MDL-800 stimulates SIRT6 deacetylation of nucleosomes in a mechanism partially independent of R65.** (A) SIRT6 WT or R65A (75 nM) were incubated with 750 nM H3K9ac nucleosomes and 1 mM NAD<sup>+</sup> in 20 mM potassium phosphate pH 7.5 and 0.25 mg/mL BSA at 37 °C. At varying timepoints reactions were quenched in 1% TFA final and analyzed by dot blot, n=1. (B) SIRT6 (100nM) was incubated with 500 nM H3K9ac nucleosomes under the conditions outlined above. Reactions contained 50 µM of either CL5D, MDL-800, with control reaction containing 2.5% DMSO. At varying timepoints reactions were quenched in 1% TFA final and analyzed by dot blot. Mean value of three replicates reported with error bars representing standard deviation. (C) SIRT6 WT or R65A (1 µM) were incubated with 40 µM H3K9ac peptide, 1 mM NAD<sup>+</sup>, and either 50 µM of CL5D or MDL-800 or 5% DMSO as a control. Reactions were carried out in 20 mM potassium phosphate pH 7.5 at 37 °C for 45 minutes before being quenched in 1% TFA final and quantified by HPLC. Mean value of three replicates reported with error bars representing standard deviation.

**Figure 3-5. MDL-800 stimulates SIRT6 deacetylation of nucleosomes in a mechanism partially independent of R65.**



### 3.3 Conclusion

SIRT6 demonstrates efficient demyristoylation against peptide substrate *in vitro* however is a poor peptide deacetylase, which is at odds with its primary reported biological functions as a critical regulator of histone deacetylation. Here we report that nucleosomes are efficiently deacetylated at a  $k_{\text{cat}}/K_m$  value that is orders of magnitude higher than with acetylated peptides as substrates. Interestingly, binding of SIRT6 to nucleosomes can stimulate a trans-deacetylation reaction against peptides that is comparable to rates of demyristoylation and small-molecule activated deacetylation. While nucleosome binding enhances the deacetylase, demyristoylase activity of SIRT6 is not significantly affected. In particular, the  $k_{\text{cat}}/K_m$  of SIRT6 against acetylated nucleosomes is nearly 5,000-fold higher than against peptide substrate.

Single-turnover kinetic analysis additionally revealed that alkylamidate formation becomes rate-limiting during nucleosome deacetylation, indicating enhancement of the subsequent formation of the 1'2'-bicyclic intermediate, which was previously thought to be rate-limiting in peptide substrate studies (40). The enhancement of rates following alkylamidate formation resulted in a  $k_{\text{cat}}$  approximately 10-fold higher than that of peptide deacetylation ( $0.012 \text{ s}^{-1}$  vs.  $0.0013 \text{ s}^{-1}$ ) (28). Together this analysis reveals that efficient nucleosome deacetylation by SIRT6 relies both on improved  $k_{\text{cat}}/K_m$ , owing to R65-mediated activated catalysis, and rate enhancement of catalytic steps following alkylamidate formation. Studies by Liu et al. have demonstrated efficient and intrinsic nucleosome binding by SIRT6 independent of acetylated histone substrate. The result of this binding event likely tethers SIRT6 to nucleosomes proximal to tail substrate, which would be predicted to further contribute to the improved  $k_{\text{cat}}/K_m$  of nucleosome deacetylation, likely in an intra-nucleosomal reaction..

Similar to CL5D, activation by nucleosome binding is dependent on R65, suggesting a similar mechanism of activation as discussed in Chapter 2. Subsequent studies of nucleosome deacetylation in the presence of CL5D, including single-turnover and steady-state Michaelis-Menten experiments, are required to determine whether some activation could be achieved through an improved  $k_{\text{cat}}/K_m$ , which may not have been observed under the conditions employed here. Importantly, it was previously reported that SIRT6 R65A lacked efficient deacetylase activity in cells (8). This observation in the context of the data presented here indicates that efficient nucleosomal deacetylation requires R65. Here we show preliminary *in vitro* evidence that MDL-800, which has been reported to display cellular activity (27, 41, 42), is capable of further enhancing SIRT6 towards nucleosomes in a mechanism partially independent of R65. The mechanism of activation of MDL-800 towards SIRT6-nucleosome deacetylation and whether it proceeds via improved  $k_{\text{cat}}$  or  $k_{\text{cat}}/K_m$  remains outstanding to date. We anticipate subsequent kinetic analyses will reveal distinct mechanisms of activation between CL5D and MDL-800 and determine their respective dependence on Arg-65. The data presented here provide proof of concept that SIRT6 is a viable therapeutic target and that several strategies could be employed to enhance SIRT6 functions in cells. Though our discussions have focused on nucleosome deacetylation and activators that enhance H3K9ac, additional investigations will be needed to evaluate the effects of current and future deacetylation activators against long-chain acylated substrates, other histone sites (e.g. H3K56) and non-histone proteins, as well as the reported ADP-ribosylation activity of SIRT6.

### ***3.4 Experimental procedures***

#### ***3.4.1 Expression and purification of SIRT6***

His-tagged full-length SIRT6 constructs in a pQE80 vector were overexpressed in BL21 DE3 *E. coli* following induction by 0.5 mM IPTG at OD<sub>600</sub> of 1-1.2 at 25 °C and 12 hours of subsequent growth prior to harvest. Cells were resuspended in 50 mM sodium phosphate, pH 7.2, 250 mM NaCl, 5 mM imidazole, 1 mM  $\beta$ -mercaptoethanol, and protease inhibitors (aprotinin 2  $\mu$ g/mL, leupeptin 2  $\mu$ g/mL, pepstatin 1  $\mu$ g/mL, and AEBSF 0.5 mM). Cell suspension was lysed by sonication in the presence of DNase and chicken egg lysozyme, clarified at 50,000 x g at 4°C, and purified by nickel affinity chromatography as previously reported (18). Fractions containing SIRT6 were pooled, concentrated, and dialyzed into 50 mM Tris, pH 8.0, 150 mM NaCl, 100  $\mu$ M TCEP, and 5% (w/v) glycerol.

#### ***3.4.2 Expression and purification of 147 bp DNA***

12 L of Stellar cells transformed with pUC19 vectoring carrying Widom 601 147bp DNA were harvested and stored at -80 °C. Cells were resuspended in 200 mL 25 mM Tris pH 8, 50 mM Glucose, 1 mM EDTA, 10  $\mu$ g/mL RNase A. Chemical lysis was achieved by the addition of 200 mL 0.2 M NaOH and 1% SDS and left to sit for 3 minutes. Solution neutralized by the addition of 200 mL 4 M potassium acetate and 2 N acetic acid before centrifugation at 15,000 x g for 30 minutes. NaCl and isopropanol added to supernatant to a final concentration of 0.5 M and 50% respectively and allowed to rest for 2 hours at -20 °C. Crashed DNA harvested at 15,000 x g for 30 minutes and washed once with cold 70% ethanol before being allowed to air dry. Pellets resuspended in 50 mL 10 mM Tris pH 8 and 50 mM EDTA. 25 mL 2.16 M NaCl and



24% PEG 8k added before a 60 minute incubation on ice to precipitate vector DNA, which was collected by centrifugation at 4,000 x g for 30 minutes. After one rinse with cold 70% ethanol, pellet was air dried before resuspension in 2 mL 10 mM Tris pH 8 with 0.1 mM EDTA. 601 fragment digested from vector by addition of 200  $\mu$ L EcoRV overnight at 37 °C. CIA extraction used to remove nuclease following digestion followed by precipitation and isolation of DNA in 0.5 M NaCl and 50% isopropanol at -20 °C for 2 hours. Precipitated DNA collected by centrifugation at 20,000 x g for 30 minutes. Pellet was air dried before being resuspended in 10 mL 10 mM Tris pH 8 with 1 mM EDTA. 1.92 mL 4 M NaCl and 3.46 mL 40% PEG 6k added and incubated on ice for 60 minutes to specifically precipitate pUC19 backbone while 601 fragments remain soluble. Supernatant brought to 70% ethanol and incubated overnight at -20 °C before fragments collected by centrifugation at 40,000 x g for 20 minutes. After being allowed to air dry, 601 fragments were resuspended in water.

### 3.4.3 Expression and purification of canonical histones

Untagged canonical *Xenopus laevis* histone constructs in pET expression plasmid were used to transform BL21 (DE3) pLysS competent cells. IPTG at 0.5 mM was used to induce cells at an OD<sub>600</sub> of 0.6 which were grown for an additional 3 hours at 37 °C. Cells harvested by centrifugation and stored at -80 °C. Cell pellet thawed and resuspended in wash buffer (50 mM Tris pH 7.5, 100 mM NaCl, 1 mM benzamidine, and 1 mM  $\beta$ -mercaptoethanol) before being flash frozen and thawed two additional times. Cells lysed on ice by sonication and spun at 25,000 x g at 4 °C for 20 minutes and supernatant discarded. The following step was performed 4 times; fully resuspend pellet in wash buffer + 1% Triton X-100 before spinning at 25,000 x g at 4 °C for 10 minutes and discarding supernatant. The previous step was performed one additional time

in the absence of Triton producing extracted inclusion body which was frozen at -80 °C overnight. Inclusion body thawed and resuspended in 1 mL DMSO and allowed to incubate at room temperature for 30 minutes. 8 mL of 6 M guanidinium HCl, 20 mM Tris pH 7.5, and 5 mM DTT added to pellet, mixed well, and allowed to incubate for 1 hour at room temperature with stirring. Histone extract spun at 25,000 x g for 20 minutes at 4 °C before being dialyzed into SAU buffer (7 M urea, 20 mM sodium acetate pH 5.2, 1 mM EDTA, and 1 mM DTT) with 200 mM NaCl. A Q HP column was placed in line and preceding a SP HP column, and both were preequilibrated with SAU + 200 mM NaCl. Dialyzed histone extract was loaded over both columns after which the Q HP column was removed. The SP HP column was then washed with 5 CVs of SAU + 200 mM NaCl. Histones were eluted on a linear gradient of SAU buffer from 200 to 800 mM NaCl over 10 CVs. Fractions containing pure histone were pooled, dialyzed into water with 1 mM  $\beta$ -mercaptoethanol, and lyophilized (34, 43).

#### 3.4.4 Expression and purification of Histone H3K9ac

Histone H3 (*Xenopus laevis*) was expressed using amber codon suppression to homogenously incorporate acetyl-lysine at position 9 (32, 44). To assist purification of the poorly expressing construct, a his-tag and TEV cleavage site were added to the N-terminus of histone H3 (coding sequence below) and inserted into a pCDF duet vector along with tRNA to facilitate acetyl-lysine incorporation.

```
atgggcagcagccatcaccatcatcaccacagccaggatccggaaaacctgtacttccagggccgtaccaagcagaccgcccgttagtcc
accggagggaaggctccccgaagcagctggccaccaaggcagccaggaagtccgctcctgctaccggcggagtcaagaaacctcac
cggtaccggcccggcacagtcgctctccgcgagatccgccgctaccagaaatccaccgagctgctcatccgcaaactgcctttccagcgc
```

ctgggtccgggagatcgctcaggacttcaagaccgacctgcgcttccagagctcgccggttatggctctgcaggaggccagcgaggcttat  
ctgggtcgctctctttgaggacaccaacctgtgcgccatccacgccaagagggtcaccatcatgccaaggacatccagctggcccgcaga  
atccgaggcgagagggttaa

BL21 (DE3)  $\Delta$ CoB cells were transformed with both the previously mentioned pCDF vector and pBK-AckRS-3. One liter growths were grown to  $OD_{600} = 1.1-1.3$  at 37 °C before the addition of 20 mM nicotinamide and 10 mM acetyl-lysine. Protein expression was induced 20 minutes later by the addition of 0.5 mM IPTG and growth was continued at 37 °C for an additional 12 hours before cells were harvested. This extended post-induction growth time was critical for the robust expression of histone H3K9ac. Histone was purified using a modified method of the previously reported rapid histone purification (43). Briefly, 6 L of cells were resuspended in 40 mL nickel unfolding (NU) buffer (50 mM potassium phosphate pH 7.5, 6 M urea, 5 mM  $\beta$ -mercaptoethanol, 10 mM lysine, 10 mM imidazole, 250 mM NaCl). Cells were resuspended by dounce homogenization and lysed by extensive sonication (35% amplitude, 20 seconds on, 60 seconds off, for a total of 10 minutes of sonication). Lysate clarified by centrifugation at 70,000 x g for 35 minutes at 4 °C. A Q SP column was placed in line and preceding a HisTrap HP column and preequilibrated with NU buffer. Clarified lysate loaded over both columns before Q HP column removed. Remaining HisTrap column washed with 6 CVs of NU buffer. The following segmented gradient elution protocol using NU as buffer A and NU with 250 mM imidazole used as buffer B was used to elute pure histones; 0-10% B over 1 CV, 10% B for 8 CV, 10-100% B over 15 CV, 100% B for 6 CV. Fractions containing pure histone were pooled, dialyzed into water with 1 mM  $\beta$ -mercaptoethanol, and lyophilized. Following lyophilization, histone H3K9ac was resuspended in TEV cleavage buffer (50 mM Tris pH 8, 0.5

mM EDTA, 1 mM DTT) to between 1-5 mg/mL. His-tagged TEV protease (10 mg/mL) was added at a ratio of 5  $\mu$ L per mL of dissolved histone and allowed to incubate overnight at 4 °C. The next morning, imidazole was added to a final concentration of 10 mM. HisPur Ni-NTA resin slurry added to TEV digested histone reaction at a ratio of 2 mL per 20 mL digest solution and rocked for 2 hours at 4 °C. Flowthrough containing cleaved histone H3K9ac collected and dialyzed into water with 1 mM  $\beta$ -mercaptoethanol before being lyophilized.

#### 3.4.5 Assembly of nucleosome core particles

Histone H2A, H2B, H3 (or H3K9ac), and H4 were individually dissolved to 2 mg/mL in unfolding buffer (7 M guanidinium HCl, 20 mM Tris pH 7.5, 10 mM DTT) and mixed gently for 1 hour at room temperature. Dissolved histone was spun at 25,000 x g for 10 minutes and protein concentration of supernatant determined. Histones were mixed in equimolar ratios and adjusted to a final total concentration of 1 mg/mL with unfolding buffer. Histone mixture fully dialyzed in refolding buffer (2 M NaCl, 10 mM Tris pH 7.5, 1 mM EDTA, 5 mM  $\beta$ -mercaptoethanol) at 4 °C. Precipitated protein removed by centrifugation before remaining mixture concentrated to <1.5 mL. A HiLoad 16/60 Superdex 200 column was preequilibrated with refolding buffer prior to injection of clarified and concentrated histone mixture. Peaks containing octamer were pooled and stored at 4 °C. To assemble nucleosome core particle, histone octamer and Widom 147 bp DNA were mixed in a 1:1.1 ratio in 2 M NaCl and adjusted to a final DNA concentration of 6  $\mu$ M. Mixture dialyzed against 400 mL RB high (2 M NaCl, 10 mM Tris pH 7.5, 1 mM EDTA, 1 mM DTT) for one hour at 4 °C. To this dialysate, an additional 1.6 L of RB low (250 mM NaCl, 10 mM Tris pH 7.5, 1 mM EDTA, 1 mM DTT) was added over the course of 24 hours using a peristaltic pump. Following this gradient dialysis, the sample was dialyzed for an additional 3

hours against fresh RB low buffer. Finally, this sample was heat positioned at 37 °C for 1 hour before being ran on native gel to monitor for a single band of supershifted DNA indicating the assembly of nucleosome core particles (NCP). NCPs were stored at 4 °C prior to experimental use.

#### 3.4.6 Nucleosome deacetylation assays

Nucleosome deacetylation assays were carried out at 37 °C with 500 nM nucleosomes and 100 nM SIRT6 in 20 mM potassium phosphate pH 7.5, 0.25 mg/mL ultrapure BSA, and 1 mM NAD<sup>+</sup> unless otherwise noted. Low-binding tubes were used to reduce non-specific adhesion of proteins to tube walls. For timecourse reactions in which multiple samples were pulled from a single tube, the total reaction volume was twice as large as the total sample being pulled to reduce reaction concentration due to evaporative loss. Small-molecule activators (CL5D, UBCS039, MDL-800) were used at 50 µM and a final DMSO concentration of 2.5%. Reactions were preheated to 37 °C for 3-5 minutes before being initiated by the addition of NAD<sup>+</sup>. Following desired incubation time, 2 µL reaction was removed and quenched with equal volume of 2% TFA (1% final) in PCR tubes. Quenched reactions were briefly spun and kept on ice prior to analysis and quantification by dot blot analysis.

#### 3.4.7 Dot blot analysis of H3K9ac

Dot blots were conducted two varying ways utilizing either direct manual spotting of sample onto membrane or using the Bio-Dot apparatus. Both methods demonstrated equivalent quantification of signal and therefore a preference was given to manual spotting owing to the

ease and speed of use. For manual spotting, 3  $\mu$ L of quenched sample was directly applied to a dry piece of nitrocellulose membrane and allowed to air dry for 20 minutes. For Bio-Dot applications, nitrocellulose was first wetted in PBS before being assembled in the apparatus. The quenched sample was diluted with 100  $\mu$ L 1% TFA and loaded through the apparatus according to the manufacturer's protocol. The membrane was then removed from the apparatus and allowed to air dry for 45 minutes. Dried membranes were then blocked in PBS with 5% milk for 1 hour at room temperature while rocking before being drained from membrane. Primary antibodies for H3 (Abcam #24834) and H3K9ac (Active Motif #39038) were added in a 1:3,000 ratio with PBST with 5% milk and incubated either at room temperature for 1 hour or overnight at 4 °C with rocking. Primary antibody was removed and after 2 quick rinses with PBS, membranes were washed two additional times for 5 minutes with PBST. Fluorescent secondary antibodies (LiCor #925-32211 and #925-68070) were added in a 1:10,000 ratio in PBST with 5% milk and rocked at room temperature for 1 hour. Membranes were quickly rinsed twice with PBS before two additional 5 minute rinses in PBST. After 2 additional quick rinses in PBS, membranes were imaged on an Odyssey 9120 imager. The signal ratio of H3K9ac to H3 was determined and normalized to a maximum of 1 (NormRatio). The value of 1-NormRatio was multiplied by the concentration of H3K9ac used in the assay to determine the concentration of product formed.

#### 3.4.8 SIRT6 activity assays against peptide substrate

Sirtuin peptide deacylation assays were carried out at 37 °C in 20 mM potassium phosphate pH 7.5 with 0.5 mM NAD<sup>+</sup>, 10% DMSO, and 20  $\mu$ M H3K9ac or H3K9myr peptides, unless otherwise noted in legend, and quenched by the addition of 2% TFA final. Steady-state reactions

were constrained to less than 20% substrate turnover to prevent product inhibition. A variety of times were required to monitor SIRT6 deacetylation (2-60 minutes) under this restraint given the ability to strongly activate catalysis. In these cases, specific activities were determined and either reported as is or as fold-activation of specific activity. Deacylation reactions were analyzed by reversed phase high-performance liquid chromatography on a Kinetex C18 column (100 Å, 100 × 4.6 mm, 2.6 µm, Phenomenex) by monitoring the formation of the deacylated product at 214 nm. Deacetylation reactions were analyzed using a gradient of 33-100% B (30% acetonitrile with 0.05% TFA) in 8 min at 1.6 mL\*min<sup>-1</sup>. Demyristoylation reactions were analyzed using a gradient of 3-100% B (acetonitrile with 0.05% TFA) in 10 min at 1.6 mL\*min<sup>-1</sup>. The product and substrate peaks were quantified and ratio of these allowed for quantification of product formation. Three independent experiments were performed for each condition with averages being plotted and error bars representing the standard deviation of these replicates.

#### 3.4.9 Culture and small-molecule treatment of mouse embryonic fibroblasts

Wild-type and SIRT6-knockout MEFs seeded into 100 mm plates and passaged twice before splitting into experimental plates. Cells were grown in DMEM supplemented with 10% FBS. 1x10<sup>6</sup> cells of WT-MEFs (p11) and SIRT6-KO-MEFs (p10) were plated in 60 mm dishes containing 3 mL of media. Media was aspirated off 24 hours later, cells washed with PBS, and replaced with 3 mL DMEM supplemented with 10% FBS and 1 mM SAHA (0.005% DMSO). 4 hours later, 250 µL of 650 µM CL5, CL5D, or CL5D-me (6.5% DMSO, 93.5% DMEM) added to a final concentration of 50 µM at 0.5% DMSO. 8 hours later, media was aspirated off, washed with PBS, and harvested by trypsin.

#### 3.4.10 Histone Isolation from mouse embryonic fibroblasts

Cell pellets were resuspended in 800  $\mu$ l of ice-cold Buffer A (10 mM Tris-HCl pH 7.4, 10 mM NaCl, and 3 mM  $MgCl_2$ ) supplemented with 10  $\mu$ g/ml leupeptin, 10  $\mu$ g/ml aprotinin, 100  $\mu$ M phenylmethylsulfonyl fluoride, 10 mM nicotinamide, 1 mM sodium-butyrate, and 4  $\mu$ M trichostatin A, followed by 80 strokes of light pestle homogenization in a 1 ml Wheaton dounce homogenizer. Cell homogenate was then transferred to a 1.5 ml microcentrifuge Eppendorf tube and centrifuged at 800 x g for 10 minutes at 4°C to pellet nuclei. Pelleted nuclei were resuspended in 500  $\mu$ L of 0.4 N sulfuric acid and rotated at 4°C for 4 hours before being centrifuged at 3,400 x g for 5 minutes at 4°C. The supernatant was transferred to a new tube and 125  $\mu$ L 100% trichloroacetic acid was added and incubated overnight on ice. Samples were centrifuged at 3,400 x g for 5 minutes at 4°C. The pellet was washed gently with 1 mL ice-cold acetone with 0.1% hydrochloric acid before centrifuged at 3,400 x g for 2 minutes at 4°C. The pellet was washed for a second time with ice-cold acetone and spun again to discard the supernatant. The tube was left open and allowed to dry for 20 minutes before the histones were resuspended in 35  $\mu$ L water and stored at -20°C. A Bradford assay using BSA as a standard was used to determine the protein concentration of each sample.

#### 3.4.11 Immunoblot of H3K9ac and total H3 from histone isolate

Histone samples were thawed and 4  $\mu$ g of each sample was subject to SDS-PAGE on 4-15% acrylamide gels at 160 V for 30 minutes. Transfer to nitrocellulose was conducted at 40 V for 60 minutes. Nitrocellulose was blocked in PBS + 1% milk for 1 hour. Primary antibodies for total histone H3 (Cell Signaling #3638) and H3K9ac (Active Motif #39917) were diluted 1:3,000 in PBST + 5% milk and rocked on nitrocellulose at room temperature for 1 hour. Membrane



washed 4 x 5 minutes with PBST. Secondary antibodies including IRDye 680RD anti-mouse (LiCor #926-68070) and IRDye 800CW anti-rabbit (LiCor #925-32211) were diluted 1:10,000 in PBST + 5% milk and rocked on membrane at room temperature for 1 hour. Membrane was washed 4 x 5 minutes with PBST and 2 x 1 minute with PBS before imaging on Odyssey 9120 (LiCor). Bands were quantified using ImageStudio Lite (LiCor).

### 3.5 References

1. Kugel, S., and Mostoslavsky, R. (2014) Chromatin and beyond: the multitasking roles for SIRT6. *Trends Biochem. Sci.* **39**, 72–81
2. Zhong, L., D’Urso, A., Toiber, D., Sebastian, C., Henry, R. E., Vadysirisack, D. D., Guimaraes, A., Marinelli, B., Wikstrom, J. D., Nir, T., Clish, C. B., Vaitheesvaran, B., Iliopoulos, O., Kurland, I., Dor, Y., Weissleder, R., Shiriha, O. S., Ellisen, L. W., Espinosa, J. M., and Mostoslavsky, R. (2010) The histone deacetylase Sirt6 regulates glucose homeostasis via Hif1alpha. *Cell*. **140**, 280–293
3. Tao, R., Xiong, X., DePinho, R. A., Deng, C.-X., and Dong, X. C. (2013) FoxO3 transcription factor and Sirt6 deacetylase regulate low density lipoprotein (LDL)-cholesterol homeostasis via control of the proprotein convertase subtilisin/kexin type 9 (Pcsk9) gene expression. *J. Biol. Chem.* **288**, 29252–29259
4. Sebastián, C., Zwaans, B. M. M., Silberman, D. M., Gymrek, M., Goren, A., Zhong, L., Ram, O., Truelove, J., Guimaraes, A. R., Toiber, D., Cosentino, C., Greenson, J. K., MacDonald, A. I., McGlynn, L., Maxwell, F., Edwards, J., Giacosa, S., Guccione, E., Weissleder, R., Bernstein, B. E., Regev, A., Shiels, P. G., Lombard, D. B., and Mostoslavsky, R. (2012) The histone deacetylase SIRT6 is a tumor suppressor that controls cancer metabolism. *Cell*. **151**, 1185–1199
5. Kugel, S., Feldman, J. L., Klein, M. A., Silberman, D. M., Sebastián, C., Mermel, C., Dobersch, S., Clark, A. R., Getz, G., Denu, J. M., and Mostoslavsky, R. (2015) Identification of and Molecular Basis for SIRT6 Loss-of-Function Point Mutations in Cancer. *Cell Rep.* **13**, 479–488

6. Zhang, J., Yin, X.-J., Xu, C.-J., Ning, Y.-X., Chen, M., Zhang, H., Chen, S.-F., and Yao, L.-Q. (2015) The histone deacetylase SIRT6 inhibits ovarian cancer cell proliferation via down-regulation of Notch 3 expression. *Eur Rev Med Pharmacol Sci.* **19**, 818–824
7. Mostoslavsky, R., Chua, K. F., Lombard, D. B., Pang, W. W., Fischer, M. R., Gellon, L., Liu, P., Mostoslavsky, G., Franco, S., Murphy, M. M., Mills, K. D., Patel, P., Hsu, J. T., Hong, A. L., Ford, E., Cheng, H.-L., Kennedy, C., Nunez, N., Bronson, R., Frendewey, D., Auerbach, W., Valenzuela, D., Karow, M., Hottiger, M. O., Hursting, S., Barrett, J. C., Guarente, L., Mulligan, R., Demple, B., Yancopoulos, G. D., and Alt, F. W. (2006) Genomic instability and aging-like phenotype in the absence of mammalian SIRT6. *Cell.* **124**, 315–329
8. Mao, Z., Hine, C., Tian, X., Van Meter, M., Au, M., Vaidya, A., Seluanov, A., and Gorbunova, V. (2011) SIRT6 promotes DNA repair under stress by activating PARP1. *Science.* **332**, 1443–1446
9. Toiber, D., Erdel, F., Bouazoune, K., Silberman, D. M., Zhong, L., Mulligan, P., Sebastian, C., Cosentino, C., Martinez-Pastor, B., Giacosa, S., D’Urso, A., Näär, A. M., Kingston, R., Rippe, K., and Mostoslavsky, R. (2013) SIRT6 recruits SNF2H to DNA break sites, preventing genomic instability through chromatin remodeling. *Mol. Cell.* **51**, 454–468
10. Kanfi, Y., Naiman, S., Amir, G., Peshti, V., Zinman, G., Nahum, L., Bar-Joseph, Z., and Cohen, H. Y. (2012) The sirtuin SIRT6 regulates lifespan in male mice. *Nature.* **483**, 218–221
11. Tian, X., Firsanov, D., Zhang, Z., Cheng, Y., Luo, L., Tomblin, G., Tan, R., Simon, M., Henderson, S., Steffan, J., Goldfarb, A., Tam, J., Zheng, K., Cornwell, A., Johnson, A., Yang, J.-N., Mao, Z., Manta, B., Dang, W., Zhang, Z., Vijg, J., Wolfe, A., Moody, K., Kennedy, B. K., Bohmann, D., Gladyshev, V. N., Seluanov, A., and Gorbunova, V. (2019) SIRT6 Is Responsible

for More Efficient DNA Double-Strand Break Repair in Long-Lived Species. *Cell*. **177**, 622-638.e22

12. Ferrer, C. M., Alders, M., Postma, A. V., Park, S., Klein, M. A., Cetinbas, M., Pajkrt, E., Glas, A., van Koningsbruggen, S., Christoffels, V. M., Mannens, M. M. A. M., Knecht, L., Etchegaray, J.-P., Sadreyev, R. I., Denu, J. M., Mostoslavsky, G., van Maarle, M. C., and Mostoslavsky, R. (2018) An inactivating mutation in the histone deacetylase SIRT6 causes human perinatal lethality. *Genes Dev.* **32**, 373–388

13. Zhang, W., Wan, H., Feng, G., Qu, J., Wang, J., Jing, Y., Ren, R., Liu, Z., Zhang, L., Chen, Z., Wang, S., Zhao, Y., Wang, Z., Yuan, Y., Zhou, Q., Li, W., Liu, G.-H., and Hu, B. (2018) SIRT6 deficiency results in developmental retardation in cynomolgus monkeys. *Nature*. **560**, 661–665

14. Klein, M. A., and Denu, J. M. (2020) Biological and catalytic functions of sirtuin 6 as targets for small-molecule modulators. *J. Biol. Chem.* **295**, 11021–11041

15. Chang, A. R., Ferrer, C. M., and Mostoslavsky, R. (2019) SIRT6, a Mammalian Deacylase with Multitasking Abilities. *Physiological Reviews*. **100**, 145–169

16. Khan, R. I., Nirzhor, S. S. R., and Akter, R. (2018) A Review of the Recent Advances Made with SIRT6 and its Implications on Aging Related Processes, Major Human Diseases, and Possible Therapeutic Targets. *Biomolecules*. 10.3390/biom8030044

17. Tanner, K. G., Landry, J., Sternglanz, R., and Denu, J. M. (2000) Silent information regulator 2 family of NAD- dependent histone/protein deacetylases generates a unique product, 1-O-acetyl-ADP-ribose. *Proc. Natl. Acad. Sci. U.S.A.* **97**, 14178–14182

18. Pan, P. W., Feldman, J. L., Devries, M. K., Dong, A., Edwards, A. M., and Denu, J. M. (2011) Structure and biochemical functions of SIRT6. *J. Biol. Chem.* **286**, 14575–14587
19. Jiang, H., Khan, S., Wang, Y., Charron, G., He, B., Sebastian, C., Du, J., Kim, R., Ge, E., Mostoslavsky, R., Hang, H. C., Hao, Q., and Lin, H. (2013) SIRT6 regulates TNF- $\alpha$  secretion through hydrolysis of long-chain fatty acyl lysine. *Nature*. **496**, 110–113
20. Feldman, J. L., Baeza, J., and Denu, J. M. (2013) Activation of the protein deacetylase SIRT6 by long-chain fatty acids and widespread deacylation by mammalian sirtuins. *J. Biol. Chem.* **288**, 31350–31356
21. Zhang, X., Khan, S., Jiang, H., Antonyak, M. A., Chen, X., Spiegelman, N. A., Shrimp, J. H., Cerione, R. A., and Lin, H. (2016) Identifying the functional contribution of the defatty-acylase activity of SIRT6. *Nat Chem Biol.* **12**, 614–620
22. Rahnasto-Rilla, M., Kokkola, T., Jarho, E., Lahtela-Kakkonen, M., and Moaddel, R. (2016) N-Acylethanolamines Bind to SIRT6. *Chembiochem.* **17**, 77–81
23. Rahnasto-Rilla, M., Tyni, J., Huovinen, M., Jarho, E., Kulikowicz, T., Ravichandran, S., A Bohr, V., Ferrucci, L., Lahtela-Kakkonen, M., and Moaddel, R. (2018) Natural polyphenols as sirtuin 6 modulators. *Sci Rep.* **8**, 4163
24. Rahnasto-Rilla, M. K., McLoughlin, P., Kulikowicz, T., Doyle, M., Bohr, V. A., Lahtela-Kakkonen, M., Ferrucci, L., Hayes, M., and Moaddel, R. (2017) The Identification of a SIRT6 Activator from Brown Algae *Fucus distichus*. *Mar Drugs*. 10.3390/md15060190

25. You, W., Rotili, D., Li, T.-M., Kambach, C., Meleshin, M., Schutkowski, M., Chua, K. F., Mai, A., and Steegborn, C. (2017) Structural Basis of Sirtuin 6 Activation by Synthetic Small Molecules. *Angew. Chem. Int. Ed. Engl.* **56**, 1007–1011
26. Iachettini, S., Trisciuglio, D., Rotili, D., Lucidi, A., Salvati, E., Zizza, P., Di Leo, L., Del Bufalo, D., Ciriolo, M. R., Leonetti, C., Steegborn, C., Mai, A., Rizzo, A., and Biroccio, A. (2018) Pharmacological activation of SIRT6 triggers lethal autophagy in human cancer cells. *Cell Death Dis.* **9**, 996
27. Huang, Z., Zhao, J., Deng, W., Chen, Y., Shang, J., Song, K., Zhang, L., Wang, C., Lu, S., Yang, X., He, B., Min, J., Hu, H., Tan, M., Xu, J., Zhang, Q., Zhong, J., Sun, X., Mao, Z., Lin, H., Xiao, M., Chin, Y. E., Jiang, H., Xu, Y., Chen, G., and Zhang, J. (2018) Identification of a cellularly active SIRT6 allosteric activator. *Nat. Chem. Biol.* **14**, 1118–1126
28. Klein, M. A., Liu, C., Kuznetsov, V. I., Feltenberger, J. B., Tang, W., and Denu, J. M. (2020) Mechanism of activation for the sirtuin 6 protein deacetylase. *J Biol Chem.* **295**, 1385–1399
29. Grozinger, C. M., and Schreiber, S. L. (2002) Deacetylase enzymes: biological functions and the use of small-molecule inhibitors. *Chem. Biol.* **9**, 3–16
30. Tennen, R. I., Berber, E., and Chua, K. F. (2010) Functional dissection of SIRT6: identification of domains that regulate histone deacetylase activity and chromatin localization. *Mech. Ageing Dev.* **131**, 185–192
31. Gil, R., Barth, S., Kanfi, Y., and Cohen, H. Y. (2013) SIRT6 exhibits nucleosome-dependent deacetylase activity. *Nucleic Acids Res.* **41**, 8537–8545

32. Neumann, H., Hancock, S. M., Buning, R., Routh, A., Chapman, L., Somers, J., Owen-Hughes, T., van Noort, J., Rhodes, D., and Chin, J. W. (2009) A Method for Genetically Installing Site-Specific Acetylation in Recombinant Histones Defines the Effects of H3 K56 Acetylation. *Molecular Cell*. **36**, 153–163
33. Neumann, H. (2012) Rewiring translation – Genetic code expansion and its applications. *FEBS Letters*. **586**, 2057–2064
34. Luger, K., Rechsteiner, T. J., and Richmond, T. J. (1999) Preparation of nucleosome core particle from recombinant histones. *Meth. Enzymol.* **304**, 3–19
35. Ruiz-Carrillo, A., Jorcano, J. L., Eder, G., and Lurz, R. (1979) In vitro core particle and nucleosome assembly at physiological ionic strength. *Proc Natl Acad Sci U S A*. **76**, 3284–3288
36. Cotton, R. W., and Hamkalo, B. A. (1981) Nucleosome dissociation at physiological ionic strengths. *Nucleic Acids Res.* **9**, 445–457
37. Krautkramer, K. A., Reiter, L., Denu, J. M., and Dowell, J. A. (2015) Quantification of SAHA-Dependent Changes in Histone Modifications Using Data-Independent Acquisition Mass Spectrometry. *J. Proteome Res.* **14**, 3252–3262
38. Berndsen, C. E., and Denu, J. M. (2005) Assays for mechanistic investigations of protein/histone acetyltransferases. *Methods*. **36**, 321–331
39. Orsi, B. A., and Tipton, K. F. (1979) [8] Kinetic analysis of progress curves. in *Methods in Enzymology*, pp. 159–183, Elsevier, **63**, 159–183

40. Feldman, J. L., Dittenhafer-Reed, K. E., Kudo, N., Thelen, J. N., Ito, A., Yoshida, M., and Denu, J. M. (2015) Kinetic and Structural Basis for Acyl-Group Selectivity and NAD(+) Dependence in Sirtuin-Catalyzed Deacylation. *Biochemistry*. **54**, 3037–3050
41. Zhang, J., Li, Y., Liu, Q., Huang, Y., Li, R., Wu, T., Zhang, Z., Zhou, J., Huang, H., Tang, Q., Huang, C., Zhao, Y., Zhang, G., Jiang, W., Mo, L., Zhang, J., Xie, W., and He, J. (2020) Sirt6 alleviated liver fibrosis by deacetylating conserved lysine 54 on Smad2 in hepatic stellate cells. *Hepatology*. 10.1002/hep.31418
42. Shang, J.-L., Ning, S.-B., Chen, Y.-Y., Chen, T.-X., and Zhang, J. (2020) MDL-800, an allosteric activator of SIRT6, suppresses proliferation and enhances EGFR-TKIs therapy in non-small cell lung cancer. *Acta Pharmacol. Sin.* 10.1038/s41401-020-0442-2
43. Klinker, H., Haas, C., Harrer, N., Becker, P. B., and Mueller-Planitz, F. (2014) Rapid Purification of Recombinant Histones. *PLOS ONE*. **9**, e104029
44. Neumann, H., Peak-Chew, S. Y., and Chin, J. W. (2008) Genetically encoding N(epsilon)-acetyllysine in recombinant proteins. *Nat. Chem. Biol.* **4**, 232–234



## **CHAPTER 4: Development of a NanoBiT assay for monitoring binding kinetics of a SIRT6-nucleosome complex**

**Mark A. Klein<sup>1,2</sup>, José D. Moran<sup>1,2</sup>, Wallace H. Liu<sup>1,2</sup>, John M. Denu<sup>1,2,3</sup>**

From the <sup>1</sup>Wisconsin Institute for Discovery, University of Wisconsin-Madison; <sup>2</sup>Department of Biomolecular Chemistry, University of Wisconsin-Madison; <sup>3</sup>Morgridge Institute for Research, University of Wisconsin-Madison

\*This ongoing and unpublished work represents the development of a novel and hopefully widely applicable strategy for the biochemical analysis of nucleosome binding kinetics. I am proud to be sharing it here while honored and excited for the places José will take it.

\*\*This body of work references work conducted by Wallace H. Liu titled “Multivalent Interactions Drive Nucleosome Binding and Efficient Chromatin Deacetylation 2 by SIRT6” which has been accepted however not yet published at Nature Communication. The in-text citation referencing this work appears as “(Liu. et al. 2020 *Nat. Comm.*)”

## 4.1 Introduction

Sirtuin 6 (SIRT6) is a histone deacetylase (HDAC) with cellular functions as a metabolic regulator (1–3), tumor suppressor (4–6), and DNA repair factor (7–9). Knockout or loss-of-function mutations can result in genomic instability, increased tumorigenesis, brain and muscle developmental defects, or progeria (4, 7, 10, 11). SIRT6 has been shown to display poor *in vitro* deacetylase activity against peptide substrate (12, 13), however this activity can be enhanced by small molecule activators (14–16). Although no endogenous small-molecule activators have been identified, we recently reported that nucleosome binding facilitates a ~5,000-fold increase in the catalytic efficiency of SIRT6 deacetylation (Chapter 3). Furthermore, nuclear SIRT6 is primarily bound to chromatin (7), which we described is mediated by an intrinsic ability of SIRT6 to tightly bind nucleosomes (Liu. et al. 2020 *Nat Comm*), providing a rationale for the robust deacetylase activity of cellular SIRT6.

Many HDACs are members of multi-subunit complexes that have distinct and separate nucleosome binding proteins (17, 18). The intrinsic nucleosome-binding capacity of SIRT6 affords it the unique ability for its catalysis to be directly regulated by chromatin occupation. Whereas many HDACs rely on reader domains to direct chromatin localization, less is known about the factors driving SIRT6 localization. Various studies have shown that SIRT6 colocalizes with the transcription factors HIF-1 $\alpha$  (2, 19), c-Myc (20, 21), and NF- $\kappa$ B (22) to deacetylate promoter proximal chromatin. It remains an outstanding how these transcription factors direct the loci-specific binding of SIRT6 given the low relative quantity of non-chromatin bound SIRT6 (7) and the intrinsic high affinity binding of SIRT6 to nucleosomes in the absence of additional factors (Liu. et al. 2020 *Nat Comm*). Given these constraints it is also curious that the global chromatin localization of SIRT6 is highly dynamic during TNF- $\alpha$  stress response (23) and cell-cycle

progression (24). Current strategies to monitor *in vitro* binding of SIRT6 to nucleosomes utilize electromobility shift and fluorescence resonance energy transfer assays whereas *in vivo* strategies utilize immunoprecipitation assays. In both cases these end-point approaches fail to capture the real-time kinetics underlying the dynamic nucleosome binding of SIRT6.

Here we sought to develop a novel assay that would allow for us to monitor the dynamic binding of SIRT6 to nucleosomes. With this in mind we identified a series of criteria that would facilitate a suitable assay: (i) a solution based assay; (ii) the ability to monitor the real-time interaction of SIRT6 with nucleosomes within a single sample over an extended duration; (iii) a large dynamic range allowing the detection of sub-nanomolar concentrations of SIRT6 and nucleosomes given their high affinity binding; and (iv) the ability of the assay to be extended for use in cell culture. To this end we leveraged the recently developed NanoLuc split luciferase system (NanoBiT) (25). This protein-fragment complementation system utilizes the small and bright NanoLuc luciferase which has been split into two subunits (SmBiT and LgBiT) which can be individually fused to interacting proteins. On their own, SmBiT and LgBiT display poor affinity ( $K_d = 190 \mu\text{M}$ ) however, when proximally tethered by interacting proteins (i.e. SIRT6 and nucleosomes), will reconstitute luciferase activity. We demonstrate the ability to employ NanoBiT to determine equilibrium and dissociative binding kinetics of SIRT6 to nucleosomes. This assay was used to demonstrate that ADPr cofactor binding stimulated higher affinity binding of SIRT6 to acetylated nucleosomes suggesting that histone tail substrate binding is distinct from intrinsic nucleosome binding and is dependent on the presence of acetyl-lysine and cofactor. Furthermore, we show that the deacetylase activity of SIRT6 facilitates its dissociation from nucleosomes.

## **4.2 Results and discussion**

### *4.2.1 Cellular optimization of NanoBiT reconstitution by SIRT6 and histones*

We sought to develop a split-luciferase protein-fragment complementation assay based on the recently developed NanoBiT system (25) to assess the binding kinetics of SIRT6 on nucleosomes. We envisioned a system in which SmBiT (1.3 kDa) tagged histones were incorporated into nucleosome core particles and LgBiT (18kDa) tagged SIRT6 would bind these nucleosomes to reconstitute luciferase activity (Fig. 4-1). We chose to fuse the smaller and less invasive SmBiT tag onto histones as this would be expected to have less of an effect on its ability to be incorporated into nucleosomes. Histones H3.3 and H2B were selected as candidate histones for fusion with SmBiT. Histone H3.3 is found in dynamically regulated genes and at pericentric and telomeric regions of DNA, regions of known regulation by SIRT6, and furthermore upon acetylation is the direct substrate for SIRT6 (26, 27). Histone H2B was selected owing to the precedent of H2B fusion proteins being readily incorporated into cellular chromatin (28, 29).

The ability for luciferase activity to be reconstituted following SIRT6-nucleosome binding relies on a permissive structural orientation of SmBiT and LgBiT (30, 31). To this end we evaluated 8 pairs of fusion proteins including N' and C'-terminally SmBiT-tagged H3.3 and H2B with either N' or C'-terminally LgBiT-tagged SIRT6 (Fig. 4-2A). To facilitate successful future use of this system in cellular systems, selection of paired fusion proteins was conducted in HEK293T cells. Each pair of SmBiT/LgBiT fusion proteins were transiently transfected in HEK293T cells (Fig. 4-2B). Following an 18 hour transfection, luciferase activity was measured by a simple mix-and-read analysis through the use of a cell-permeable luciferase substrate (Fig. 4-2C). This analysis revealed the brightest pair of fusion proteins were N'-terminally SmBiT-tagged H2B (SmBiT-H2B) with C'-terminally LgBiT-tagged SIRT6 (SIRT6-LgBiT). SIRT6-LgBiT was

cotransfected with HaloTag-SmBiT to evaluate potential non-specific binding mediated by weak NanoBiT subunit interaction. This demonstrated luciferase activity 22-fold lower than SIRT6-LgBiT co-transfected with SmBiT-H2B, suggesting that luciferase reconstitution was mediated via SIRT6-nucleosome interactions. Transfection by SIRT6-LgBiT alone yielded luciferase activity 230-fold lower than when cotransfected with SmBiT-H2B indicating negligible background luciferase activity of LgBiT.

In order to validate that C'-terminal tagging of SIRT6 does not disrupt its catalytic activity, SIRT6-LgBiT was recombinantly expressed and purified for *in vitro* analysis. The rate of H3K9ac peptide deacetylation by SIRT6 wild-type and SIRT6-LgBiT was evaluated either without activator or in the presence of recombinant nucleosomes (100 nM) or the small molecule activator CL5D (50  $\mu$ M) (Fig. 4-2D). These results demonstrate that SIRT6-LgBiT retains base levels of peptide deacetylation and the ability to be stimulated by both small molecule activators and nucleosomes. Having determined a suitable pair of NanoBiT fusion proteins that can be applied to future cell-based studies, we next sought to apply this system for the *in vitro* study of SIRT6-nucleosome binding.

**Figure 4-1. NanoBiT split luciferase assay to monitor nucleosome binding by SIRT6.** This envisioned assay utilizes the tagging of split luciferase subunits (SmBiT and LgBiT) to each SIRT6 and a histone, which is incorporated into nucleosomes. Each subunit on its own displays negligible luciferase activity and have weak affinity for each other ( $\sim 190 \mu\text{M}$ ). Binding of SIRT6 to nucleosomes results in proximal tethering and binding of SmBiT and LgBiT, reconstituting luciferase activity in the presence of furimazine substrate.

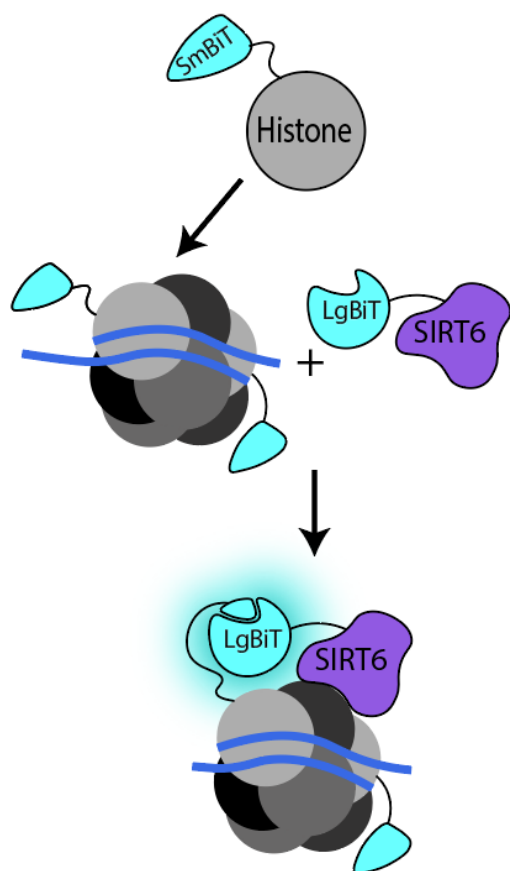
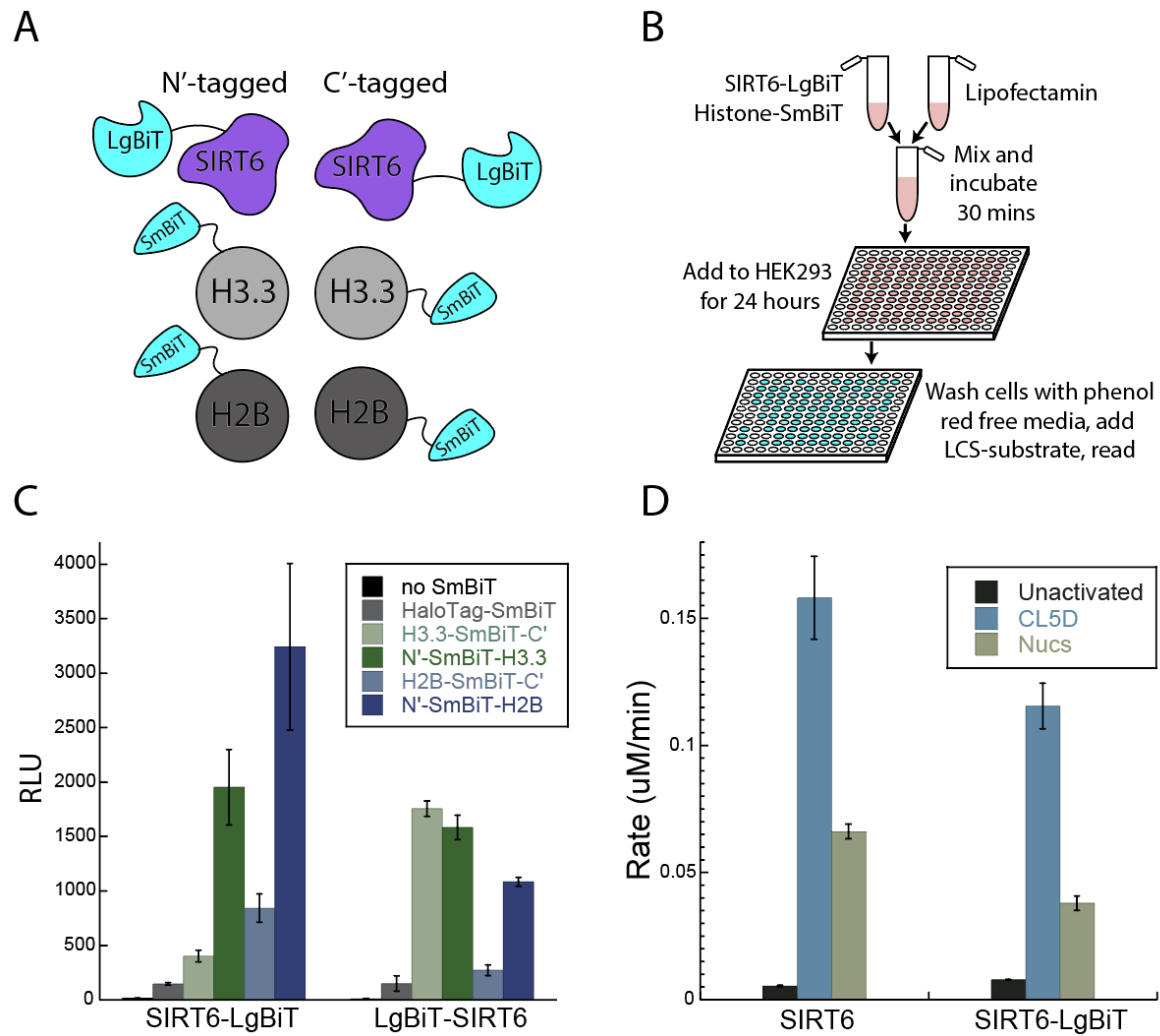


**Figure 4-2. Determination of ideal SmBiT and LgBiT orientation for productive luciferase activity.** In order for luciferase activity to be observed following nucleosome binding by SIRT6, the structural positioning of SmBiT and LgBiT must facilitate proper luciferase reconstitution. To determine the ideal positioning of these tags, various combinations of N' and C'-terminally tagged SIRT6, H2B, and H3.3 were transiently transfected in HEK293T cells. (A) Workflow for lipofectamine-mediated transient transfection of HEK293T cells and luciferase detection of SIRT6-nucleosome interaction. (B) In total, 8 pairs of N' and C'-terminally tagged SIRT6, H2B, and H3.3 were evaluated for optimal luciferase output. (C) Each combination of SIRT6 and histone were transiently expressed in HEK293T cells before quantification of luciferase activity. HaloTag-SmBiT was used as a control for non-specific interaction between SmBiT and LgBiT. Additionally, each SIRT6 construct was transfected in the absence of a SmBiT-histone to control for background luciferase activity of LgBiT. Mean value of three replicates reported with error bars representing standard deviation. (D) C'-terminally tagged SIRT6 (SIRT6-LgBiT) was selected for subsequent use and therefore evaluated *in vitro* to validate that it retains deacetylase activity and the ability to be activated. SIRT6 and SIRT6-LgBiT were incubated with 40  $\mu$ M H3K9ac peptide substrate in the presence of 50  $\mu$ M CL5D or 100 nM unmodified nucleosomes. Mean value of three replicates reported with error bars representing standard deviation.

**Figure 4-2. Determination of ideal SmBiT and LgBiT orientation for productive luciferase activity.**





#### 4.2.2 ADPr stimulates tighter binding of SIRT6 to H3K9ac nucleosomes

We first sought to use this NanoBiT system to determine the equilibrium dissociation constant ( $K_d$ ) of SIRT6-nucleosome complex by titrating SIRT6-LgBiT into a fixed concentration of SmBiT-nucleosomes and monitoring the saturation of binding by luciferase activity. Recombinantly assembled nucleosomes incorporating SmBiT-H2B (SmBiT-nuc) were assembled. Histones expressed in *E. coli* are typically insoluble, forming inclusion bodies which can be isolated to facilitate purification (32, 33). Addition of the N'-terminal SmBiT tag to histone H2B resulted in a majority of the histone remaining soluble. To assist the purification of SmBiT-H2B and additional N'-terminal his-tag was added prior to a TEV cleavage site for subsequent removal. This his-tagged SmBiT-H2B was purified utilizing a novel nickel column approach (method section) adapted from a previously published rapid histone purification strategy (34). Bulk TEV cleavage of purified SmBiT-H2B resulted in complete protein precipitation. We found that his-tag removal by TEV cleavage was only tolerated following octamer assembly. Cleaved his-tag and TEV protease were subsequently removed by size-exclusion chromatography. This strategy was also successfully applied to assembly of SmBiT-nucleosomes containing histone H3 homogenously acetylated at K9ac (SmBiT-nuc-H3K9ac) through amber codon suppression.

To begin assessing assay conditions for equilibrium binding studies, we first evaluated the binding of SIRT6-LgBiT to various fixed concentrations of SmBiT-nucs (0.1, 1, and 10 nM) (Fig. 4-3A). Following addition of luciferase substrate, light generation continued to increase over 6 minutes prior to equilibrium being reached, at which point the luciferase signal was read. Binding curves were successfully generated with an increase of maximum luciferase signal being directly proportional to the amount of fixed SmBiT-nuc. The sensitivity of this assay allowed us to proceed with the lowest tested concentration of SmBiT-nucs (100 pM) which both facilitates the accurate

quantification of high affinity binding interactions and displays a more stable signal over time owing to the slower consumption of luciferase substrate. Additionally, background luciferase activity from SmBiT-nucs and SIRT6-LgBiT alone were small compared to experimental signals. SmBiT and LgBiT subunits can self-assemble into active luciferase with a  $K_d$  of 190  $\mu$ M (25). To validate that the observed binding was mediated by nucleosome-SIRT6 binding, the LgBiT subunit was recombinantly expressed, purified, and titrated against SmBiT-nucs (Fig. 4-3B). An interaction mediated by LgBiT alone was observed beginning between 1.7-5  $\mu$ M. However, SIRT6-LgBiT had already saturated SmBiT-nuc binding at similar concentrations, indicating that non-specific interactions between SmBiT and LgBiT do not contribute to the binding curves generated through SIRT6-nucleosome interactions.

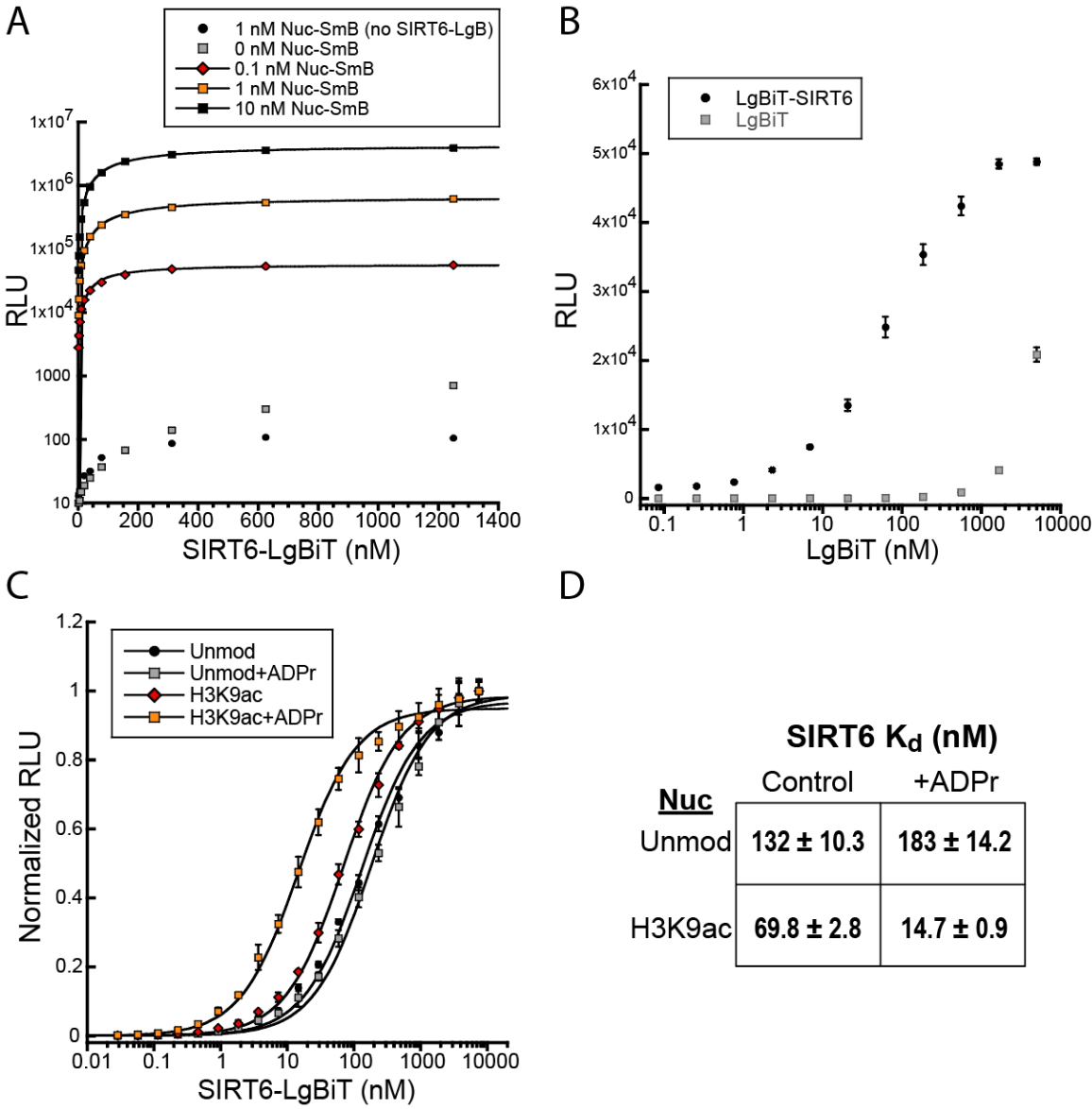
Having validated this NanoBiT assay for use *in vitro* we sought to determine the equilibrium binding constant ( $K_d$ ) for SIRT6 against nucleosomes. SIRT6-LgBiT was titrated against either unmodified or H3K9ac SmBiT-nucs and data were fitted to a single site binding curve. (Fig 4-3C,D). SIRT6 bound approximately twofold tighter to nucleosomes acetylated at histone H3K9 (69.8 nM compared to 132 nM), suggesting that SIRT6 can make additional contacts with the histone tail substrate. Previous studies utilizing electromobility shift assays have reported a  $K_d$  for SIRT6-nucleosome binding of 13 nM (Liu. et al. 2020 *Nat Comm*). It is unclear precisely why our observed binding affinity is ~10-fold weaker, however one possibility is the use of BSA (0.25 mg/mL) under these conditions. This crowding agent was found to facilitate efficient *in vitro* deacetylation of nucleosomes by SIRT6 (Chapter 3) and was therefore chosen as an additive here. It is possible that BSA prevents non-productive binding of SIRT6 to nucleosomes, however further investigation is required.

Previously we have shown that  $\text{NAD}^+$  binding by SIRT6 precedes acetylated peptide substrate in an ordered binding mechanism (15). Furthermore, ADPr can be used as a non-catalytic surrogate to stimulate the binding of peptide substrate by SIRT6. Here, we looked at whether ADPr would stimulate nucleosome binding by SIRT6 (Fig. 4-3C,D). Consistent with *in vitro* peptide binding studies, the inclusion of ADPr resulted in ~5-fold tighter binding of SIRT6 to SmBiT-nuc-H3K9ac but had negligible effects towards unmodified SmBiT-nucs. This suggests that SIRT6 makes distinct contacts with acetyl-histone H3 tail in an ADPr-dependent manner separate from those intrinsic to nucleosome binding. The ADPr-induced multivalent binding of SIRT6 to nucleosomes suggests that in the absence of  $\text{NAD}^+$ /ADPr cofactor or acetyl-lysine histone tail substrate, the histone tail is not likely bound by SIRT6 and could be accessible to other chromatin modifying factors.

**Figure 4-3. ADPr increases affinity of H3K9ac dependent nucleosome binding by SIRT6. (A)**

The ability of SIRT6-LgBiT to bind SmBiT-nucleosomes was evaluated *in vitro*. SIRT6-LgBiT was titrated against various fixed concentrations of SmBiT-nucleosomes prior to luciferase detection. To control for background luciferase activity of individual subunits, SIRT6-LgBiT was titrated in the absence of nucleosomes and the signal generated from 1 nM SmBiT-nucleosome in the absence of SIRT6-LgBiT was determined,  $n=1$ . (B) We evaluated whether the interaction between SIRT6-LgBiT and SmBiT-nucleosome was specific or whether it was driven by SmBiT/LgBiT interaction. Both LgBiT-SIRT6 and LgBiT alone were titrated against 100 pM SmBiT-nucleosome prior to luciferase detection. Mean value of three replicates reported with error bars representing standard deviation. (C) SIRT6-LgBiT was titrated against 100 pM of both unmodified and H3K9ac SmBiT-nucleosome with and without 0.5 mM ADPr. Data were fitted to an equation for one site binding and  $K_d$  values reported in (D). Mean value of three replicates reported with error bars representing standard deviation.

**Figure 4-3. ADPr increases affinity of H3K9ac dependent nucleosome binding by SIRT6.**



### 4.2.3 SIRT6 catalysis facilitates dissociation from nucleosomes

SIRT6 catalysis is enhanced upon nucleosome binding, which itself is regulated by cofactor binding. Our understanding of this multifarious SIRT6-nucleosome interaction is limited by the sole prior use of equilibrium binding assays. Here we aimed to employ the NanoBiT system for the real-time analysis of SIRT6-nucleosome interaction. We envisioned equilibrating SIRT6-LgBiT with SmBiT-nucs (10 minutes) prior to the addition of luciferase substrate. Following the development of a stable luciferase signal (6 minutes), an excess of unlabeled nucleosomes would be added to soak up unbound SIRT6 (Fig. 4-4A). In this way, a decrease in luciferase signal would correspond to the dissociation of SIRT6-LgBiT from SmBiT-nucs.

This analysis was performed against unmod-SmBiT-nucs and H3K9ac-SmBiT-nucs with and without  $\text{NAD}^+$  and ADPr (Fig. 4-4B,C). Data were fitted to an equation for dissociation to determine  $k_{\text{off}}$  and residence time ( $1/k_{\text{off}}$ ) (Fig. 4-4D). In the absence of  $\text{NAD}^+$ /ADPr, SIRT6 displayed a modestly longer residence time against H3K9ac-SmBiT-nucs compared to unmodified-SmBiT-nucs, 77 minutes and 50 minutes respectively. This residence time is long compared to a variety of chromatin factors including nuclear hormone receptors, transcription factors, and remodeling enzyme which have demonstrated residence time on the order of seconds as determined by FRAP and single-molecule imaging (35–38). The addition of ADPr resulted in increased residence time of SIRT6 on both unmodified and H3K9ac nucleosomes. This contrasts our previous finding that ADPr specifically increased the  $K_d$  of SIRT6 towards H3K9ac-nucs. The equilibrium binding constant  $K_d$  is a function of both  $k_{\text{on}}$  and  $k_{\text{off}}$ , indicating that ADPr binding may increase the  $K_d$  of SIRT6 for H3K9ac-nucs through an increase in  $k_{\text{on}}$  rather than a decrease of  $k_{\text{off}}$ . Interestingly,  $\text{NAD}^+$  greatly reduced enhanced the rate of  $k_{\text{off}}$  specifically for SIRT6 against

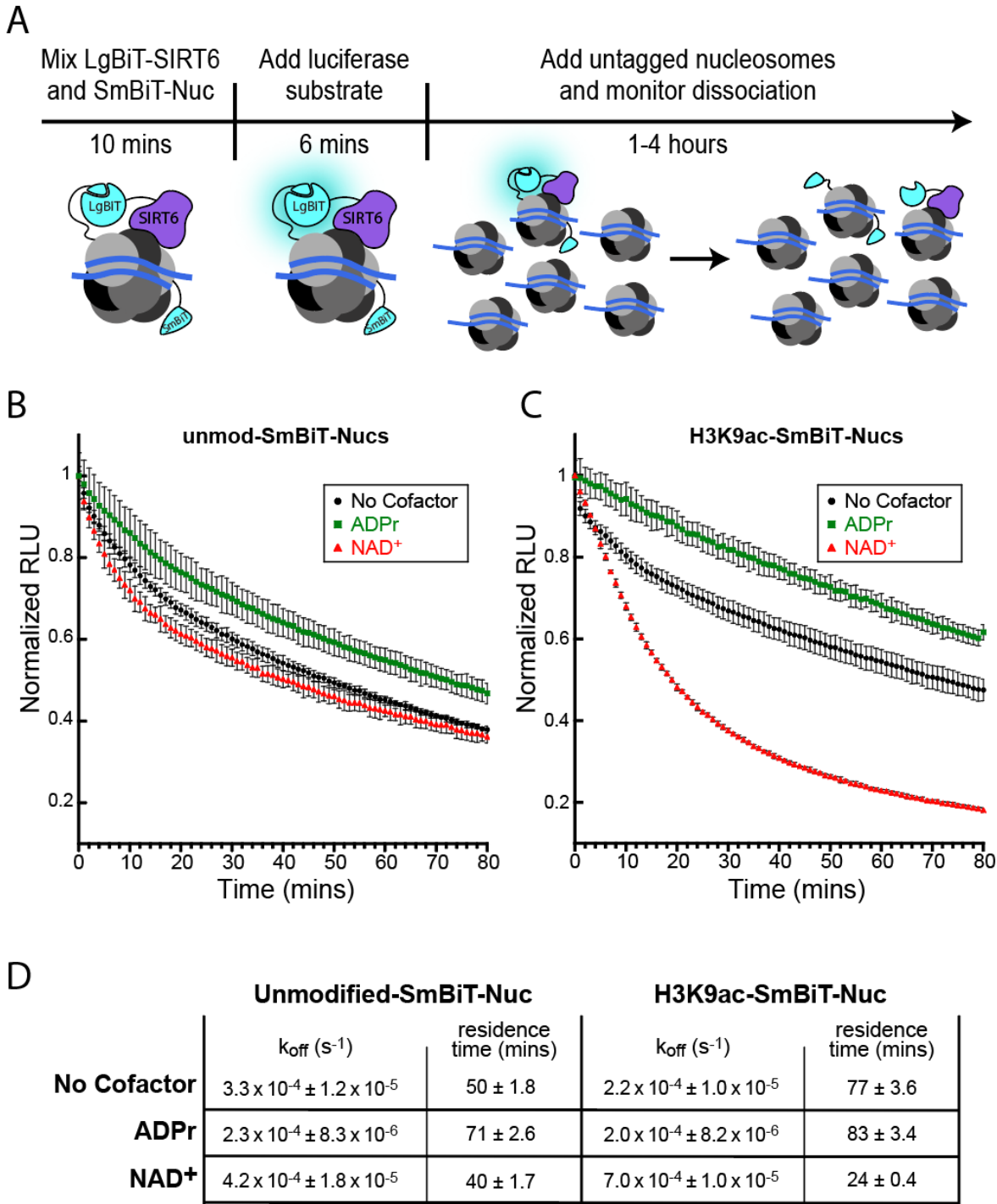
H3K9ac-nucs (Fig. 4-4C,D), suggesting that catalysis facilitates SIRT6 dissociation from nucleosomes.

The dissociation of SIRT6-LgBiT (50 nM) from H3K9ac-SmBiT-nucs (100 pM) in the presence of  $\text{NAD}^+$  was evaluated under subsaturating kinetic conditions given constraints of the assay. To determine whether  $k_{\text{off}}$  was synchronized with catalysis we used the kinetic parameters for H3K9ac-nucleosome deacetylation by SIRT6 ( $K_m = 701 \text{ nM}$ ,  $k_{\text{cat}} = 0.012 \text{ s}^{-1}$ ), as previously determined in Chapter 3, to estimate the reaction velocity under these dissociation conditions. This analysis yielded an estimated rate of deacetylation of  $7.9 \times 10^{-4} \text{ s}^{-1}$  which parallels the empirically determined off rate ( $k_{\text{off}} = 7.0 \times 10^{-4} \text{ s}^{-1}$ ) and suggests that catalysis is directly linked to nucleosome dissociation. Together these data highlight the dynamic binding of SIRT6 to nucleosomes which is regulated by cofactor binding and catalysis. Furthermore, the development of this NanoBiT protein-fragment complementation assay to monitor binding kinetics *in vitro* could be applied to various chromatin readers and likely extended to use in living cells.

**Figure 4-4. Catalysis facilitates nucleosome dissociation by SIRT6.** (A) Workflow for the real-time analysis of SIRT6 dissociation from nucleosomes. SIRT6-LgBiT is preequilibrated with SmBiT-nucleosomes prior to the addition of excess unlabeled nucleosomes. The dissociation of LgBiT-SIRT6 is represented by a decrease of luciferase activity. (B,C) The dissociation of SIRT6-LgBiT (50 nM) from unmodified (B) or H3K9ac (C) SmBiT-nucleosomes (100 pM) was monitored following the addition of untagged nucleosomes (100 nM) with or without ADPr (0.4 mM) or NAD<sup>+</sup> (0.4 mM). The decay of luciferase activity was monitored, and data were fitted to an equation of dissociation to determine  $k_{\text{off}}$  and residence time as reported in (D). Mean value of three replicates reported with error bars representing standard deviation.



Figure 4-4. Catalysis facilitates nucleosome dissociation by SIRT6.



### 4.3 Conclusion

SIRT6 exhibits an intrinsic ability to tightly bind nucleosomes which in turn directly activates its deacetylase activity (Liu. et al. 2020 *Nat Comm*, Chapter 3). Despite this exquisitely high affinity interaction and the majority of nuclear SIRT6 being chromatin bound (7), SIRT6 retains the ability to regulate loci of chromatin dynamically, temporally, and specifically (19–24). This contradiction highlights the importance of being able to experimentally monitor the binding kinetics of SIRT6 to nucleosomes beyond that of equilibrium studies. Here we report the early stage development of a split luciferase protein complementation assay utilizing the NanoBiT system (25) for monitoring the real-time interaction of SIRT6 with nucleosomes. We demonstrate the ability to perform rapid solution-based studies for the determination of equilibrium binding constants ( $K_d$ ) as well as dissociation studies to determine off rates ( $k_{off}$ ) and residence times of chromatin readers. Optimization of SmBiT and LgBiT tag orientation was performed in HEK293T cells to facilitate future cell-based work anticipated to evaluate chromatin occupation of SIRT6 throughout cell-cycle progression and in response to DNA-damage (see future aims section). We expect this system will be readily applied to other chromatin readers for both mechanistic *in vitro* biochemical binding studies and live cell monitoring of chromatin binding.

Previously it had been shown that SIRT6 binding to nucleosomes was mediated by the C-terminal domain and N-terminal helix of SIRT6, regions distant from the active site of SIRT6. Applying this NanoBiT system to the study of SIRT6 we further demonstrate that ADPr, a non-catalytic  $NAD^+$  surrogate, improves the equilibrium binding constant ( $K_d$ ) of SIRT6 specifically to nucleosomes acetylated at histone H3K9. Consistent with our previous mechanistic studies demonstrating an ordered binding mechanism in which  $NAD^+$ /ADPr cofactor binding precedes H3K9ac peptide substrate binding (15), this suggests that cofactor binding stimulates histone tail

substrate capture at the SIRT6 active site resulting in a multivalent interaction with improved binding affinity. This further suggests that in the absence of cellular  $\text{NAD}^+$ , SIRT6 will not strongly engage with the histone H3 tail, allowing it to be accessible to other chromatin factors.

This NanoBiT system was subsequently used to assess the rate of dissociation of SIRT6 from nucleosomes. We found that SIRT6 displays a long residence time (~50 minutes) making it unique from a host of other chromatin factors which have residence times on the order of 5-20 seconds (35–38). This interaction was modestly stabilized further in the presence of ADPr, as anticipated from our previous equilibrium binding studies. Interestingly, the addition of  $\text{NAD}^+$  resulted in an increased rate of dissociation of SIRT6 specifically from nucleosomes acetylated at histone H3K9. Importantly, the rate of  $k_{\text{off}}$  ( $7.0 \times 10^{-4} \text{ s}^{-1}$ ) was equivalent to the estimated reaction velocity ( $7.9 \times 10^{-4} \text{ s}^{-1}$ ) under the conditions used for dissociation studies. This suggests that catalysis ultimately results in dissociation and provides a cellular rationale for the dissociation of a high affinity chromatin factor. This work demonstrates the feasibility of monitoring the dynamic binding of SIRT6 with nucleosomes and establishes a complex relationship between SIRT6 and nucleosomes in which binding activates SIRT6 deacetylation which in turn results in its dissociation.

## ***4.4 Experimental procedures***

### ***4.4.1 Cloning of NanoBiT constructs for cellular transfection***

The mammalian coding sequence for SIRT6 was inserted to N-terminally and C-terminally LgBiT-tagged pBiT vectors acquired from Promega (cat#N2014). Similarly, the mammalian coding sequences for histones H2B and H3.3 were inserted to N-terminally and C-terminally SmBiT-tagged pBiT vectors. All constructs were made using Gibson assembly following vector digestion by EcoRI and SacI. Following assembly and sequence validation, transfection-ready plasmid was purified from 250 mL cultures of Rosetta cells using PureYield Plasmid Maxiprep System (Promega #A2392).

### ***4.4.2 Transient transfection of NanoBiT constructs and luciferase detection***

HEK293T cells cultures in DMEM (HEPES, high glucose, glutamine) were plated as a density of 25,000 cells per well in white opaque 96-well culture plates at a final volume of 100  $\mu$ L and left to adhere for 24 hours. Wells around perimeter of plate were not used and instead filled with 150  $\mu$ L of sterile water to serve as a heat sink to maintain temperature of inner experimental wells. Transfection mixtures containing each vector and lipofectamine 2000 were made in OptiMEM, incubated for 30 minutes, and 20  $\mu$ L was added per well such that 50 ng each of SmBiT and LgBiT tagged vectors were added per condition. Cells incubated for an additional 18 hours. Media aspirated from wells and rinsed with 100  $\mu$ L OptiMEM (no phenol red) reduced serum media before being replaced with an additional 100  $\mu$ L OptiMEM (no phenol red) reduced serum media and placed back in incubator for 15 minutes. 25  $\mu$ L prepared Nano-Glo LCS luciferase substrate (Promega cat#N2011) added per well before being quickly placed into 37 °C BioTek Synergy plate reader. Plates were set to shake on low for 15 seconds followed by a 20 second delay

prior to read. Luciferase signal was integrated for 1 second at a sensitivity of 100 and a 1 mm optic offset. Three experimental wells were used per BiT combination with the average luciferase signal reported and the error representing the standard deviation.

#### 4.4.3 Cloning and expression of recombinant wild-type and SIRT6-LgBiT

His-tagged wild-type SIRT6 containing a C-terminal LgBiT tag according to the sequence below was cloned in to a pQE80 expression plasmid using Gibson assembly.

atgagaggatcgcacatcaccatcacatgtcgggtgaattacgcggcggggctgtcgccgtacgcggacaagggcaagtgcggcct  
 cccggagatcttcgacccccggaggagctggagcgggaaggtgtgggaactggcgaggctggcttggcagtttccaatgtggtgttcca  
 cacgggtgccggcatcagcactgcctctggcatccccacttcaggggtccccacggagtctggaccatggaggagcagaggtctcccc  
 ccaagttcgacaccacntttgagagcgcgcggccacgcagaccacatggcgctggtgcagctggagcgcgtgggcctcctccgcttc  
 ctggtcagccagaacgtggacgggtccatgtgcgtcaggttccccagggacaaactggcagagctccacgggaacatgtttgtgga  
 gaatgtgccaagtgaagacgcagtagctccgagacacagtcgtgggcacatgggcctgaaggccacgggccggctctgcaccgtgg  
 ctaaggcaagggggctgcgagcctgcaggggagagctgaggacacacatcctagactgggaggactccctgcccagccgggacctgg  
 cactcgccgatgaggccagcaggaacgccgacctgtccatcacgtgggtacatcgctgcagatccggcccagcgggaacctgccgt  
 ggctaccaagcggccgggagggcgcctggtcatcgtcaacctgcagcccaccaagcacgaccgcatgctgacctccgcatcatggct  
 acgttgacgaggtcatgacccggctcatgaagcacctggggctggagatccccgcctgggacggccccctgtgtgtggagagggcgt  
 gccaccctgccccgcccaccccccaagctggagcccaaggaggaatctccaccggatcaacggctctatccccgcccggcccc  
 aagcaggagccctgcgcccagcacaacggctcagagcccgccagcccaaacgggagcggcccaccagccctgccccacagacc  
 cccaaaagggtgaaggccaaggcgtccccagcaagcatctcgagcgggtggcgaggagcggaggtggagggtcgtcaggtgtcttc  
 aactcgaagatttcgttgggactgggaacagacagccgcctacaacctggaccaagtcctgaacaggaggtgtgtccagtttctgc  
 agaatctcgccgtgtccgtaactccgatcaaaggattgtccggagcgggtgaaaatgcctgaagatcgacatccatgtcatcatccgtat  
 gaaggtctgagcggcgaccaaattggcccagatcgaagaggtgttaaggtggtgtaccctgtggatgatcatcactttaaggtgatcctgcc

ctatggcacactggtaatcgacgggggttacgccgaacatgctgaactatttcggacggccgtatgaaggcatcgccgtgttcgacggcaaa  
 aagatcactgtaacagggaccctgtggaacggcaacaaaattatcgacgagcgcctgatcacccccgacggctccatgctgtccgagtaa  
 ccatcaacagctaa

This construct as well as a his-tagged wild-type SIRT6 construct were overexpressed in BL21 DE3 *E. coli* following induction by 0.5 mM IPTG at OD<sub>600</sub> of 1-1.2 at 25 °C and 12 hours of subsequent growth prior to harvest. Cells were resuspended in 50 mM sodium phosphate, pH 7.2, 250 mM NaCl, 5 mM imidazole, 1 mM  $\beta$ -mercaptoethanol, and protease inhibitors (aprotinin 2  $\mu$ g/mL, leupeptin 2  $\mu$ g/mL, pepstatin 1  $\mu$ g/mL, and AEBSF 0.5 mM). Cell suspension was lysed by sonication in the presence of DNase and chicken egg lysozyme, clarified at 50,000 x g at 4°C, and purified by nickel affinity chromatography as previously reported (12). Fractions containing SIRT6 were pooled, concentrated, and dialyzed into 50 mM Tris, pH 8.0, 150 mM NaCl, 100  $\mu$ M TCEP, and 5% (w/v) glycerol.

#### 4.4.4 Cloning and expression of recombinant SmBiT-H2B

*E. coli* optimized histone H2B (*Homo sapiens*) containing an N-terminal SmBiT tag was cloned into a pQE80 expression vector. Addition of the SmBiT tag resulted in a more soluble histone H2B making inclusion body purification inefficient. To assist purification of this histone, a his-tag and TEV cleavage site were added to the N-terminus of histone H2B (coding sequence below).

atgggacatcaccaccaccacatgggggcagtgagaacttgacttccagggtgtgactggctaccgcttattgaggagatcttaggtct  
 tctggtggaggaggagcgggtgggggaggctcttctggaggagctcctgaccccgccaaatctgcaccggctccaaaaaggggtcga  
 agaaagcagtgacgaaggttcaaaaaaggacgggaaaaaacgtaaacgctcccgtaaagaaagctacagcgatatgtgtataaggtgt

tgaacaagtcacatccagatactggtatctcatctaaggcgatgggcattatgaacagttttgtaacgacattttgagcgattgcgggggaa  
gctagccgcctggcgactataataaacgtagtacaatcacttcacgtgaaatccaaactgctgttcgtttattactgccaggagagtttagcca  
aacacgccgtaagtgaaggaaccaaggcggttaccaagtacacctcttcaaataccgcgcaatttatcgctactaaaccagggggcagcg  
aggatcgtagcctcccccttctcaattatctgcaattccacctttttgttggtgctgcgcgcaggaattgctgggcaagtgaatag

BL21 (DE3) pLysS cells were transformed with the previously described vector. One liter growths were grown to  $OD_{600} = 1.0$  at 37 °C before the addition of 0.5 mM IPTG and growth was continued at 37 °C for an additional 6 hours before cells were harvested. Histone was purified using a modified method of the previously reported rapid histone purification (34). Briefly, 6 L of cells were resuspended in 40 mL nickel unfolding (NU) buffer (50 mM potassium phosphate pH 7.5, 6 M urea, 5 mM  $\beta$ -mercaptoethanol, 10 mM lysine, 10 mM imidazole, 250 mM NaCl). Cells were resuspended by dounce homogenization and lysed by extensive sonication (35% amplitude, 20 seconds on, 60 seconds off, for a total of 10 minutes of sonication). Lysate clarified by centrifugation at 70,000 x g for 35 minutes at 4 °C. A Q SP column was placed in line and preceding a HisTrap HP column and preequilibrated with NU buffer. Clarified lysate loaded over both columns before Q HP column removed. Remaining HisTrap column washed with 6 CVs of NU buffer. The following segmented gradient elution protocol using NU as buffer A and NU with 250 mM imidazole used as buffer B was used to elute pure histones; 0-10% B over 1 CV, 10% B for 8 CV, 10-100% B over 15 CV, 100% B for 6 CV. Fractions containing pure histone were pooled, dialyzed into water with 1 mM  $\beta$ -mercaptoethanol, and lyophilized. Attempts to remove the his-tag by TEV cleavage prior to final lyophilization resulted in >90% protein loss to precipitation. As such, this tag was removed following octamer assembly as described in a following method section.

#### 4.4.5 Expression and purification of canonical histones

Untagged canonical *Xenopus laevis* histone constructs in pET expression plasmid were used to transform BL21 (DE3) pLysS competent cells. IPTG at 0.5 mM was used to induce cells at an OD<sub>600</sub> of 0.6 which were grown for an additional 3 hours at 37 °C. Cells harvested by centrifugation and stored at -80 °C. Cell pellet thawed and resuspended in wash buffer (50 mM Tris pH 7.5, 100 mM NaCl, 1 mM benzamidine, and 1 mM β-mercaptoethanol) before being flash frozen and thawed two additional times. Cells lysed on ice by sonication and spun at 25,000 x g at 4 °C for 20 minutes and supernatant discarded. The following step was performed 4 times; fully resuspend pellet in wash buffer + 1% Triton X-100 before spinning at 25,000 x g at 4 °C for 10 minutes and discarding supernatant. The previous step was performed one additional time in the absence of Triton producing extracted inclusion body which was frozen at -80 °C overnight. Inclusion body thawed and resuspended in 1 mL DMSO and allowed to incubate at room temperature for 30 minutes. 8 mL of 6 M guanidinium HCl, 20 mM Tris pH 7.5, and 5 mM DTT added to pellet, mixed well, and allowed to incubate for 1 hour at room temperature with stirring. Histone extract spun at 25,000 x g for 20 minutes at 4 °C before being dialyzed into SAU buffer (7 M urea, 20 mM sodium acetate pH 5.2, 1 mM EDTA, and 1 mM DTT) with 200 mM NaCl. A Q HP column was placed in line and preceding a SP HP column, and both were preequilibrated with SAU + 200 mM NaCl. Dialyzed histone extract was loaded over both columns after which the Q HP column was removed. The SP HP column was then washed with 5 CVs of SAU + 200 mM NaCl. Histones were eluted on a linear gradient of SAU buffer from 200 to 800 mM NaCl over 10 CVs. Fractions containing pure histone were pooled, dialyzed into water with 1 mM β-mercaptoethanol, and lyophilized (39, 40).



#### 4.4.6 Expression and purification of 147 bp DNA

12 L of Stellar cells transformed with pUC19 vectoring carrying Widom 601 147bp DNA were harvested and stored at -80 °C. Cells were resuspended in 200 mL 25 mM Tris pH 8, 50 mM Glucose, 1 mM EDTA, 10 µg/mL RNase A. Chemical lysis was achieved by the addition of 200 mL 0.2 M NaOH and 1% SDS and left to sit for 3 minutes. Solution neutralized by the addition of 200 mL 4 M potassium acetate and 2 N acetic acid before centrifugation at 15,000 x g for 30 minutes. NaCl and isopropanol added to supernatant to a final concentration of 0.5 M and 50% respectively and allowed to rest for 2 hours at -20 °C. Crashed DNA harvested at 15,000 x g for 30 minutes and washed once with cold 70% ethanol before being allowed to air dry. Pellets resuspended in 50 mL 10 mM Tris pH 8 with 50 mM EDTA. 25 mL 2.16 M NaCl and 24% PEG 8k added before a 60 minute incubation on ice to precipitate vector DNA, which was collected by centrifugation at 4,000 x g for 30 minutes. After one rinse with cold 70% ethanol, pellet was air dried before resuspension in 2 mL 10 mM Tris pH 8 with 0.1 mM EDTA. 601 fragment digested from vector by addition of 200 µL EcoRV overnight at 37 °C. CIA extraction used to remove nuclease following digestion followed by precipitation and isolation of DNA in 0.5 M NaCl and 50% isopropanol at -20 °C for 2 hours. Precipitated DNA collected by centrifugation at 20,000 x g for 30 minutes. Pellet was air dried before being resuspended in 10 mL 10 mM Tris pH 8 with 1 mM EDTA. 1.92 mL 4 M NaCl and 3.46 mL 40% PEG 6k added and incubated on ice for 60 minutes to specifically precipitate pUC19 backbone while 601 fragments remain soluble. Supernatant brought to 70% ethanol and incubated overnight at -20 °C before fragments collected by centrifugation at 40,000 x g for 20 minutes. After being allowed to air dry, 601 fragments were resuspended in water.

#### 4.4.7 Assembly of nucleosome core particles

Histone H2A, H2B (or SmBiT-H2B), H3 (or H3K9ac), and H4 were individually dissolved to 2 mg/mL in unfolding buffer (7 M guanidinium HCl, 20 mM Tris pH 7.5, 10 mM DTT) and mixed gently for 1 hour at room temperature. Dissolved histone was spun at 25,000 x g for 10 minutes and protein concentration of supernatant determined. Histones were mixed in equimolar ratios and adjusted to a final total concentration of 1 mg/mL with unfolding buffer. Histone mixture fully dialyzed in to refolding buffer (2 M NaCl, 10 mM Tris pH 7.5, 1 mM EDTA, 5 mM  $\beta$ -mercaptoethanol) at 4 °C. Precipitated protein removed by centrifugation before remaining mixture concentrated to <1.5 mL. Octamers containing SmBiT-H2B were incubated with 1:25 molar ratio of TEV protease overnight at 4 °C while rocking. A HiLoad 16/60 Superdex 200 column was preequilibrated with refolding buffer prior to injection of clarified and concentrated histone mixture. Peaks containing octamer were pooled and stored at 4 °C. To assemble nucleosome core particle, histone octamer and Widom 147 bp DNA were mixed in a 1:1.1 ratio in 2 M NaCl and adjusted to a final DNA concentration of 6  $\mu$ M. Mixture dialyzed against 400 mL RB high (2 M NaCl, 10 mM Tris pH 7.5, 1 mM EDTA, 1 mM DTT) for one hour at 4 °C. To this dialysate, an additional 1.6 L of RB low (250 mM NaCl, 10 mM Tris pH 7.5, 1 mM EDTA, 1 mM DTT) was added over the course of 24 hours using a peristaltic pump. Following this gradient dialysis, the sample was dialyzed for an additional 3 hours against fresh RB low buffer. Finally, this sample was heat positioned at 37 °C for 1 hour before being ran on native gel to monitor for a single band of supershifted DNA indicating the assembly of nucleosome core particles (NCP). NCPs were stored at 4 °C prior to experimental use.

#### 4.4.8 SIRT6 activity assays against peptide substrate

SIRT6 (1  $\mu$ M) peptide deacylation assays were carried out at 37 °C in 20 mM potassium phosphate pH 7.5 with 1 mM NAD<sup>+</sup>, 5% DMSO, and 40  $\mu$ M H3K9ac and quenched by the addition of 2% TFA final following 45 minutes. Deacylation reactions were analyzed by reversed phase high-performance liquid chromatography on a Kinetex C18 column (100 Å, 100  $\times$  4.6 mm, 2.6  $\mu$ m, Phenomenex) by monitoring the formation of the deacylated product at 214 nm. Deacetylation reactions were analyzed using a gradient of 33-100% B (30% acetonitrile with 0.05% TFA) in 8 min at 1.6 mL min<sup>-1</sup>. Demyristoylation reactions were analyzed using a gradient of 3-100% B (acetonitrile with 0.05% TFA) in 10 min at 1.6 mL min<sup>-1</sup>. The product and substrate peaks were quantified and ratio of these allowed for quantification of product formation. Three independent experiments were performed for each condition with averages being plotted and error bars representing the standard deviation of these replicates.

#### 4.4.9 NanoBiT assay for the detection of binding equilibriums

Mixtures (16  $\mu$ L) of SmBiT-H2B-Nucleosomes (100 pM unless otherwise noted in legend) and various concentrations of SIRT6-LgBiT were made in 20 mM potassium phosphate pH 7.5 and 0.25 mg/mL ultrapure BSA in non-binding white 384-well plates. Every other row and column of plate were used to facilitate use of multichannel pipette and to reduce bleedover of luciferase signal. Plates were sealed and spun at 400 x g for 1 minute prior to 10 a minute incubation at room temperature. Following this incubation, 4  $\mu$ L NanoGlo substrate (Promega cat#N1110), intermediately diluted in 20 mM potassium phosphate pH 7.5, was added at a final 100-fold dilution from stock. The plate was sealed and incubated at room temperature for 6 minutes prior to read. Plates were inserted in to BioTek Syngery plate reader, shook on medium for 15 seconds

prior to a 15 second delay, and read (1 mm probe offset, sensitivity 100-120, 0.5 second integration). Data were either reported as raw relative luciferase units or normalized to highest signal in binding series. Dissociation constants ( $K_d$ ) were determined by fitting data to an equation for one site binding,  $y = (B_{\max} * x) / (K_d + x)$ ,  $B_{\max}$  being the luciferase signal at maximum binding.

#### 4.4.10 Dissociation kinetic analysis by NanoBiT

Mixtures (16  $\mu$ L) of SmBiT-H2B-Nucleosomes-unmodified or SmBiT-H2B-Nucleosomes-H3K9ac (100 pM) with SIRT6-LgBiT (50 nM) were made in 20 mM potassium phosphate pH 7.5 and 0.25 mg/mL ultrapure BSA in non-binding white 384-well plates. Every other row and column of plate were used to facilitate use of multichannel pipette and to reduce bleedover of luciferase signal. Plates were sealed and spun at 400 x g for 1 minute prior to 10 a minute incubation at room temperature. Following this incubation, 4  $\mu$ L NanoGlo substrate (Promega cat#N1110), intermediately diluted in 20 mM potassium phosphate pH 7.5, was added at a final 100-fold dilution from stock. The plate was sealed and incubated at room temperature for 6 minutes. An additional 3  $\mu$ L addition containing unlabeled/unmodified nucleosomes were added and mixed well bringing the final concentration of unlabeled/unmodified nucleosomes to 100 nM. When  $\text{NAD}^+$  or ADPr were added to reactions they were incorporated into this 3  $\mu$ L addition such that their final concentrations were each 400  $\mu$ M. Plates were inserted in to BioTek Syngery plate reader and read (1 mm probe offset, sensitivity 100-120, 0.5 second integration) each minute over the course of 4 hours. Luciferase was normalized to signal at 0 minutes (point at which unlabeled nucleosomes were added) and fitted to the following equation of dissociation to determine the rate of dissociation ( $k_{\text{off}}$ );  $y = B_{\text{ns}} + (1 - B_{\text{ns}})^{(-k_{\text{off}} * x)}$ , where  $B_{\text{ns}}$  is the luciferase signal at time infinity. Experiments were ran in triplicate which each series being normalized to its own

luciferase signal at 0 minutes before mean values calculated and plotted, error bars represent standard deviation.

## 4.5 References

1. Kugel, S., and Mostoslavsky, R. (2014) Chromatin and beyond: the multitasking roles for SIRT6. *Trends Biochem. Sci.* **39**, 72–81
2. Zhong, L., D’Urso, A., Toiber, D., Sebastian, C., Henry, R. E., Vadysirisack, D. D., Guimaraes, A., Marinelli, B., Wikstrom, J. D., Nir, T., Clish, C. B., Vaitheesvaran, B., Iliopoulos, O., Kurland, I., Dor, Y., Weissleder, R., Shiriha, O. S., Ellisen, L. W., Espinosa, J. M., and Mostoslavsky, R. (2010) The histone deacetylase Sirt6 regulates glucose homeostasis via Hif1 $\alpha$ . *Cell*. **140**, 280–293
3. Tao, R., Xiong, X., DePinho, R. A., Deng, C.-X., and Dong, X. C. (2013) FoxO3 transcription factor and Sirt6 deacetylase regulate low density lipoprotein (LDL)-cholesterol homeostasis via control of the proprotein convertase subtilisin/kexin type 9 (Pcsk9) gene expression. *J. Biol. Chem.* **288**, 29252–29259
4. Sebastián, C., Zwaans, B. M. M., Silberman, D. M., Gymrek, M., Goren, A., Zhong, L., Ram, O., Truelove, J., Guimaraes, A. R., Toiber, D., Cosentino, C., Greenson, J. K., MacDonald, A. I., McGlynn, L., Maxwell, F., Edwards, J., Giacosa, S., Guccione, E., Weissleder, R., Bernstein, B. E., Regev, A., Shiels, P. G., Lombard, D. B., and Mostoslavsky, R. (2012) The histone deacetylase SIRT6 is a tumor suppressor that controls cancer metabolism. *Cell*. **151**, 1185–1199
5. Kugel, S., Feldman, J. L., Klein, M. A., Silberman, D. M., Sebastián, C., Mermel, C., Dobersch, S., Clark, A. R., Getz, G., Denu, J. M., and Mostoslavsky, R. (2015) Identification of and Molecular Basis for SIRT6 Loss-of-Function Point Mutations in Cancer. *Cell Rep.* **13**, 479–488

6. Zhang, J., Yin, X.-J., Xu, C.-J., Ning, Y.-X., Chen, M., Zhang, H., Chen, S.-F., and Yao, L.-Q. (2015) The histone deacetylase SIRT6 inhibits ovarian cancer cell proliferation via down-regulation of Notch 3 expression. *Eur Rev Med Pharmacol Sci.* **19**, 818–824
7. Mostoslavsky, R., Chua, K. F., Lombard, D. B., Pang, W. W., Fischer, M. R., Gellon, L., Liu, P., Mostoslavsky, G., Franco, S., Murphy, M. M., Mills, K. D., Patel, P., Hsu, J. T., Hong, A. L., Ford, E., Cheng, H.-L., Kennedy, C., Nunez, N., Bronson, R., Frendewey, D., Auerbach, W., Valenzuela, D., Karow, M., Hottiger, M. O., Hursting, S., Barrett, J. C., Guarente, L., Mulligan, R., Demple, B., Yancopoulos, G. D., and Alt, F. W. (2006) Genomic instability and aging-like phenotype in the absence of mammalian SIRT6. *Cell.* **124**, 315–329
8. Mao, Z., Hine, C., Tian, X., Van Meter, M., Au, M., Vaidya, A., Seluanov, A., and Gorbunova, V. (2011) SIRT6 promotes DNA repair under stress by activating PARP1. *Science.* **332**, 1443–1446
9. Toiber, D., Erdel, F., Bouazoune, K., Silberman, D. M., Zhong, L., Mulligan, P., Sebastian, C., Cosentino, C., Martinez-Pastor, B., Giacosa, S., D’Urso, A., Näär, A. M., Kingston, R., Rippe, K., and Mostoslavsky, R. (2013) SIRT6 recruits SNF2H to DNA break sites, preventing genomic instability through chromatin remodeling. *Mol. Cell.* **51**, 454–468
10. Ferrer, C. M., Alders, M., Postma, A. V., Park, S., Klein, M. A., Cetinbas, M., Pajkrt, E., Glas, A., van Koningsbruggen, S., Christoffels, V. M., Mannens, M. M. A. M., Knecht, L., Etchegaray, J.-P., Sadreyev, R. I., Denu, J. M., Mostoslavsky, G., van Maarle, M. C., and Mostoslavsky, R. (2018) An inactivating mutation in the histone deacetylase SIRT6 causes human perinatal lethality. *Genes Dev.* **32**, 373–388

11. Zhang, W., Wan, H., Feng, G., Qu, J., Wang, J., Jing, Y., Ren, R., Liu, Z., Zhang, L., Chen, Z., Wang, S., Zhao, Y., Wang, Z., Yuan, Y., Zhou, Q., Li, W., Liu, G.-H., and Hu, B. (2018) SIRT6 deficiency results in developmental retardation in cynomolgus monkeys. *Nature*. **560**, 661–665
12. Pan, P. W., Feldman, J. L., Devries, M. K., Dong, A., Edwards, A. M., and Denu, J. M. (2011) Structure and biochemical functions of SIRT6. *J. Biol. Chem.* **286**, 14575–14587
13. Feldman, J. L., Dittenhafer-Reed, K. E., Kudo, N., Thelen, J. N., Ito, A., Yoshida, M., and Denu, J. M. (2015) Kinetic and Structural Basis for Acyl-Group Selectivity and NAD(+) Dependence in Sirtuin-Catalyzed Deacylation. *Biochemistry*. **54**, 3037–3050
14. Klein, M. A., and Denu, J. M. (2020) Biological and catalytic functions of sirtuin 6 as targets for small-molecule modulators. *J. Biol. Chem.* **295**, 11021–11041
15. Klein, M. A., Liu, C., Kuznetsov, V. I., Feltenberger, J. B., Tang, W., and Denu, J. M. (2020) Mechanism of activation for the sirtuin 6 protein deacylase. *J Biol Chem*. **295**, 1385–1399
16. Huang, Z., Zhao, J., Deng, W., Chen, Y., Shang, J., Song, K., Zhang, L., Wang, C., Lu, S., Yang, X., He, B., Min, J., Hu, H., Tan, M., Xu, J., Zhang, Q., Zhong, J., Sun, X., Mao, Z., Lin, H., Xiao, M., Chin, Y. E., Jiang, H., Xu, Y., Chen, G., and Zhang, J. (2018) Identification of a cellularly active SIRT6 allosteric activator. *Nat. Chem. Biol.* **14**, 1118–1126
17. Grozinger, C. M., and Schreiber, S. L. (2002) Deacetylase enzymes: biological functions and the use of small-molecule inhibitors. *Chem. Biol.* **9**, 3–16
18. Seto, E., and Yoshida, M. (2014) Erasers of histone acetylation: the histone deacetylase enzymes. *Cold Spring Harb Perspect Biol.* **6**, a018713



19. Gertman, O., Omer, D., Hendler, A., Stein, D., Onn, L., Khukhin, Y., Portillo, M., Zarivach, R., Cohen, H. Y., Toiber, D., and Aharoni, A. (2018) Directed evolution of SIRT6 for improved deacylation and glucose homeostasis maintenance. *Sci Rep.* **8**, 3538
20. Cai, J., Zuo, Y., Wang, T., Cao, Y., Cai, R., Chen, F.-L., Cheng, J., and Mu, J. (2016) A crucial role of SUMOylation in modulating Sirt6 deacetylation of H3 at lysine 56 and its tumor suppressive activity. *Oncogene.* **35**, 4949–4956
21. Lin, Z., Yang, H., Tan, C., Li, J., Liu, Z., Quan, Q., Kong, S., Ye, J., Gao, B., and Fang, D. (2013) USP10 antagonizes c-Myc transcriptional activation through SIRT6 stabilization to suppress tumor formation. *Cell Rep.* **5**, 1639–1649
22. Zhang, N., Li, Z., Mu, W., Li, L., Liang, Y., Lu, M., Wang, Z., Qiu, Y., and Wang, Z. (2016) Calorie restriction-induced SIRT6 activation delays aging by suppressing NF- $\kappa$ B signaling. *Cell Cycle.* **15**, 1009–1018
23. Kawahara, T. L. A., Rapicavoli, N. A., Wu, A. R., Qu, K., Quake, S. R., and Chang, H. Y. (2011) Dynamic Chromatin Localization of Sirt6 Shapes Stress- and Aging-Related Transcriptional Networks. *PLoS Genet.* 10.1371/journal.pgen.1002153
24. Ardestani, P. M., and Liang, F. (2012) Sub-cellular localization, expression and functions of Sirt6 during the cell cycle in HeLa cells. *Nucleus.* **3**, 442–451
25. Dixon, A. S., Schwinn, M. K., Hall, M. P., Zimmerman, K., Otto, P., Lubben, T. H., Butler, B. L., Binkowski, B. F., Machleidt, T., Kirkland, T. A., Wood, M. G., Eggers, C. T., Encell, L. P., and Wood, K. V. (2016) NanoLuc Complementation Reporter Optimized for Accurate Measurement of Protein Interactions in Cells. *ACS Chem. Biol.* **11**, 400–408

26. Henikoff, S., and Smith, M. M. (2015) Histone variants and epigenetics. *Cold Spring Harbor Perspectives in Biology*. **7**, a019364
27. Filipescu, D., Szenker, E., and Almouzni, G. (2013) Developmental roles of histone H3 variants and their chaperones. *Trends in genetics: TIG*. **29**, 630–640
28. Kanda, T., Sullivan, K. F., and Wahl, G. M. (1998) Histone–GFP fusion protein enables sensitive analysis of chromosome dynamics in living mammalian cells. *Current Biology*. **8**, 377–385
29. Hadjantonakis, A.-K., and Papaioannou, V. E. (2004) Dynamic in vivo imaging and cell tracking using a histone fluorescent protein fusion in mice. *BMC Biotechnology*. **4**, 33
30. Lang, Y., Li, Z., and Li, H. (2019) Analysis of Protein-Protein Interactions by Split Luciferase Complementation Assay. *Current Protocols in Toxicology*. **82**, e90
31. Moustaqil, M., Bhumkar, A., Gonzalez, L., Raoul, L., Hunter, D. J. B., Carrive, P., Sierceki, E., and Gambin, Y. (2017) A Split-Luciferase Reporter Recognizing GFP and mCherry Tags to Facilitate Studies of Protein–Protein Interactions. *Int J Mol Sci*. 10.3390/ijms18122681
32. Luger, K., Rechsteiner, T., and Richmond, T. (1999) Expression and Purification of Recombinant Histones and Nucleosome Reconstitution. *Methods in molecular biology (Clifton, N.J.)*. **119**, 1–16
33. Lee, Y.-T., Gibbons, G., Lee, S. Y., Nikolovska-Coleska, Z., and Dou, Y. (2015) One-pot refolding of core histones from bacterial inclusion bodies allows rapid reconstitution of histone octamer. *Protein Expression and Purification*. **110**, 89–94

34. Klinker, H., Haas, C., Harrer, N., Becker, P. B., and Mueller-Planitz, F. (2014) Rapid Purification of Recombinant Histones. *PLOS ONE*. **9**, e104029
35. Deal, R. B., and Henikoff, S. (2010) Capturing the dynamic epigenome. *Genome Biol.* **11**, 218
36. Phair, R. D., Scaffidi, P., Elbi, C., Vecerová, J., Dey, A., Ozato, K., Brown, D. T., Hager, G., Bustin, M., and Misteli, T. (2004) Global Nature of Dynamic Protein-Chromatin Interactions In Vivo: Three-Dimensional Genome Scanning and Dynamic Interaction Networks of Chromatin Proteins. *Mol Cell Biol.* **24**, 6393–6402
37. Chen, J., Zhang, Z., Li, L., Chen, B.-C., Revyakin, A., Hajj, B., Legant, W., Dahan, M., Lionnet, T., Betzig, E., Tjian, R., and Liu, Z. (2014) Single-molecule dynamics of enhanceosome assembly in embryonic stem cells. *Cell*. **156**, 1274–1285
38. Mazza, D., Abernathy, A., Golob, N., Morisaki, T., and McNally, J. G. (2012) A benchmark for chromatin binding measurements in live cells. *Nucleic Acids Res.* **40**, e119
39. Luger, K., Rechsteiner, T. J., and Richmond, T. J. (1999) Preparation of nucleosome core particle from recombinant histones. *Meth. Enzymol.* **304**, 3–19
40. Ruiz-Carrillo, A., Jorcano, J. L., Eder, G., and Lurz, R. (1979) In vitro core particle and nucleosome assembly at physiological ionic strength. *Proc Natl Acad Sci U S A.* **76**, 3284–3288

## **CHAPTER 5: Conclusions and Future Directions**

### 5.1 Overall conclusions from research

SIRT6 is a chromatin associated histone deacetylase with widespread roles in maintaining cellular homeostasis and sits at the intersection between metabolism, gene regulation, and genomic stability (1–4). Through its regulation of metabolic genes, maintenance of telomeres, and roles in DNA repair, SIRT6 plays an important role in organismal health span and the prevention of tumorigenesis (5–12). Given these biological roles, SIRT6 has emerged as an attractive therapeutic target for pharmacological activation to treat various age-related diseases. Despite the robust and well accepted cellular roles of SIRT6, *in vitro* analysis demonstrated that its catalytic efficiency was ~1,000-fold lower than that of other sirtuins (13–15). Prior to the start of my thesis work, our lab demonstrated for the first time that the deacetylase activity of SIRT6 could be activated *in vitro* by small molecules including free fatty acids (13). The goal at the outset of my Ph.D. research was to develop potent small molecule activators of SIRT6 and describe the catalytic mechanism by which they activate deacetylation. In addition to this, I identified that nucleosome binding strongly activates SIRT6 catalysis and likely serves as an endogenous means to stimulate global chromatin deacetylation.

To begin our search for novel and potent SIRT6 activators, I conducted a targeted screen against a variety of lipids, bioactive-lipids, and additional cherry-picked compounds from the University of Wisconsin Small Molecule Screening facility. From this screen I identified the novel activator, CL4, which had no previously reported biological activities. In collaboration with Dr. Weiping Tang, we made a series of derivatives culminating in the novel activator CL5D which showed a 7-fold increase in potency ( $EC_{50} = 15.5 \mu M$ ) compared to CL4. The improved potency was attributed to unanticipated chemistry resulting in the di-substitution of a terminal

trichlorobenzoyl group. At the time of evaluation, CL5D represented the most potent SIRT6 activator to date.

I performed a detailed kinetic analysis of activated SIRT6 deacetylation to isolate catalytic steps enhanced by CL5D. Throughout the study I discovered that SIRT6 exhibits ordered binding in which  $\text{NAD}^+$  binding precedes that of H3K9ac peptide substrate, which is reversed from that of other studied sirtuins including SIRT1-3 (16, 17). Additionally, I discovered that the R65A variant of SIRT6 maintained base level deacetylase activity however could not be activated by CL5D. Utilizing this non-activatable mutant in conjunction with various kinetic analyses, thermal shift assays, and partial proteolysis, I described a slow R65-mediated conformational step that is improved in the presence of CL5D to facilitate enhanced catalysis. This previously unreported step precedes the first chemical step of catalysis and is reflected in an improved catalytic efficiency ( $k_{\text{cat}}/K_{\text{m}}$ ) of deacetylation. I also found that this R65-mediated step facilitates demyristoylation by SIRT6, suggesting that both activation of deacetylation and efficient demyristoylation utilize a common pathway to enhanced catalysis.

SIRT6 R65A had been separately shown to lack global cellular deacetylase activity against chromatin, suggesting that SIRT6 requires endogenous activation to perform its function as a histone deacetylase (9). Additionally, SIRT6 is found primarily bound to chromatin in cells and our own studies had revealed that SIRT6 exhibits an exquisitely tight intrinsic ability to bind nucleosomes ((8), Liu. et al. 2020 *Nat. Comm.*). This led us to hypothesize that nucleosome binding may enhance the deacetylase activity of SIRT6. In addressing this question, I found that nucleosome binding indeed activated SIRT6 deacetylation against peptide substrate with an  $\text{EC}_{50}$  of 55 nM. Importantly, this activation was R65-dependent and in a mechanism similar to CL5D. To better understand SIRT6 catalysis against nucleosomes, I assembled nucleosomes

homogenously acetylated at histone H3K9 for use as substrate. Kinetic analysis of SIRT6 deacetylation against whole nucleosomes yielded a catalytic efficiency of  $17,118 \text{ M}^{-1}\text{s}^{-1}$ , nearly 5,000-fold higher than against peptide substrate. SIRT6 catalysis against nucleosome substrate could be further enhanced by the cellularly active small molecule MDL-800 (18–20), but not CL5D, under the conditions tested. I further demonstrated that MDL-800 displays partially R65-independent activation of SIRT6. These findings identify nucleosome binding as an endogenous activator of SIRT6 which utilize the R65-mediated pathway of activation and demonstrate that a distinct class of R65-independent small molecule activators are capable of further activating SIRT6 deacetylation against nucleosomes.

SIRT6 is almost exclusively bound to chromatin with very little remaining soluble in the nucleus (8), a trait which is explained through the tight intrinsic binding of SIRT6 to nucleosomes (Liu. et al. 2020 *Nat. Comm.*). Nonetheless, SIRT6 retains the ability to dynamically regulate chromatin through interactions with transcription factors (5, 21–24) and in response to TNF- $\alpha$  stress response and cell-cycle progression (25, 26). In order to study the binding kinetics of SIRT6 to nucleosomes beyond traditional EMSA and FRET equilibrium measurements, I developed a split-luciferase assay based on the NanoBiT system (27). This assay allowed for the rapid and simple determination of equilibrium binding constants ( $K_d$ ) and rates of dissociation ( $k_{\text{off}}$  and residence time) of the SIRT6-nucleosome complex. Consistent with my data supporting the ordered binding of  $\text{NAD}^+$ /ADPr prior to H3K9ac peptide, I found that ADPr improved binding of SIRT6 to nucleosome only when the nucleosome was acetylated at histone H3K9. This suggests that intrinsic nucleosome binding is independent of acetylation and that SIRT6 only engages acetylated histone tail peptide in the presence of cofactor. Dissociation kinetic analysis revealed that SIRT6 displays a residence time of 50 minutes on nucleosomes, significantly longer than other

chromatin factors that display residence times on the order of 5-20 seconds (28–30). Interestingly the off rate of SIRT6 was accelerated in the presence of  $\text{NAD}^+$  only against nucleosomes acetylated at histone H3K9ac. Kinetic analysis revealed that the off rate paralleled the rate of catalysis, indicating that SIRT6 catalysis results in nucleosome dissociation.



## 5.2 Future directions

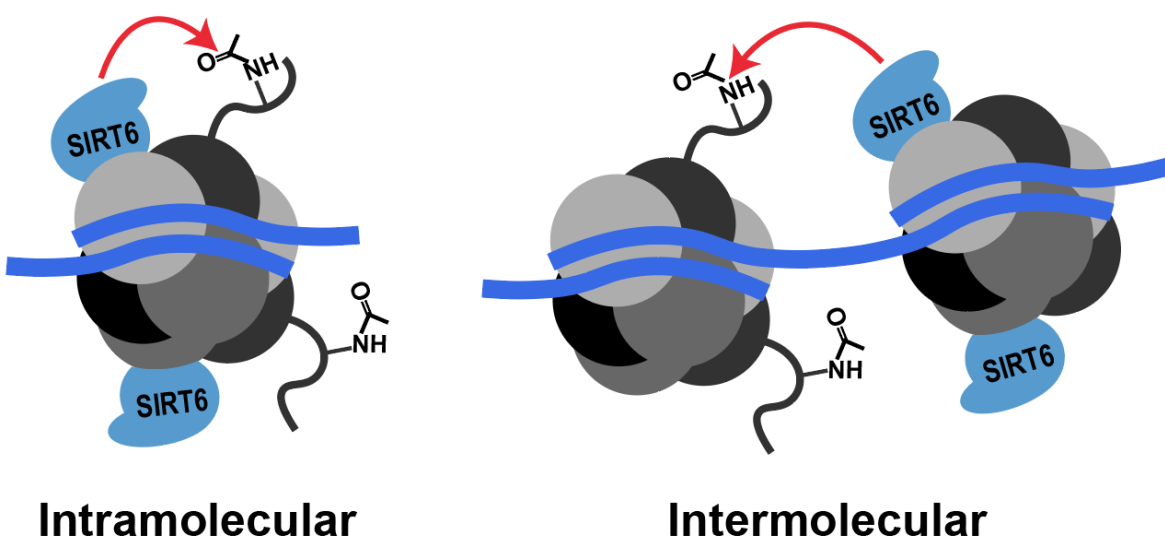
### 5.2.1. Evaluation of potential SIRT6 intermolecular deacetylation of nucleosomes

We have demonstrated that nucleosome binding activates SIRT6 deacetylation towards nucleosome substrate. It is unclear, however, whether nucleosome bound SIRT6 facilitates intramolecular deacetylation against its resident nucleosome or whether it performs intermolecular deacetylation against neighboring nucleosomes (Fig. 5-1). One could imagine that intermolecular deacetylation of nucleosomes by SIRT6 would aid in maintaining heterochromatin if a single SIRT6-nucleosome complex could access and deacetylate surrounding nucleosomes. On the other hand, this could potentially reduce the ability for SIRT6 activity to be directed in a loci-specific manner. We have shown that SIRT6 can be activated through binding to unmodified nucleosomes towards H3K9ac peptide substrate, suggesting that nucleosome bound SIRT6 can act against non-tethered histone tail peptides. This may not necessarily be possible in the context of higher order nucleosomes, and kinetic studies to directly monitor inter/intra-nucleosomal deacetylation are challenging. We have shown that the catalytic efficiency of nucleosome bound SIRT6 is  $\sim 17,000 \text{ M}^{-1}\text{s}^{-1}$ , which is approximately 14-fold higher than SIRT6 activated by small-molecule activators towards peptide substrate ( $\sim 1,200 \text{ M}^{-1}\text{s}^{-1}$ ). This difference in catalytic efficiency is smaller than would be anticipated in a model of strictly intramolecular deacetylation in which SIRT6 is tethered proximal to its substrate. Along these lines, the  $K_m$  for nucleosome deacetylation is  $\sim 700 \text{ nM}$ , significantly higher than the  $K_d$  of nucleosome interaction which has been predicted to be in the range of 13-130 nM. In fact, the  $K_m$  for nucleosomal deacetylation is more similar to the  $K_m$  for peptide substrate when SIRT6 is activated by small molecules ( $2.8 \text{ }\mu\text{M}$ ). Together these kinetic data suggest that a SIRT6:nucleosome complex may serve to intermolecularly deacetylate neighboring nucleosomes. Although it is also possible that SIRT6

binds to a nucleosome in an orientation which restricts access of the SIRT6 catalytic site to histone tail, resulting in lower than anticipated  $K_m$  term for nucleosome deacetylation.

This is kinetically challenging to definitely assess without either binding-null mutants of nucleosomes or SIRT6, or the chemical cross-labeling of a SIRT6:nucleosome complex, which both have significant drawbacks. An alternative approach could be used employing the use of our recently developed NanoBiT system. We have shown that SIRT6 catalysis leads to dissociation from nucleosomes. In this manner we could monitor the dissociation of SIRT6 from unmodified SmBiT-nucleosomes following the addition of unlabeled H3K9ac-nucleosomes. Dissociation in the presence of H3K9ac-nucleosomes but not unmodified-nucleosomes would suggest that SIRT6:SmBiT-nucleosome complex is accessing intermolecular substrate. However, a lack of dissociation could not rule out intermolecular deacetylation entirely as it is possible that only intramolecular deacetylation stimulates the conformational changes required for dissociation.

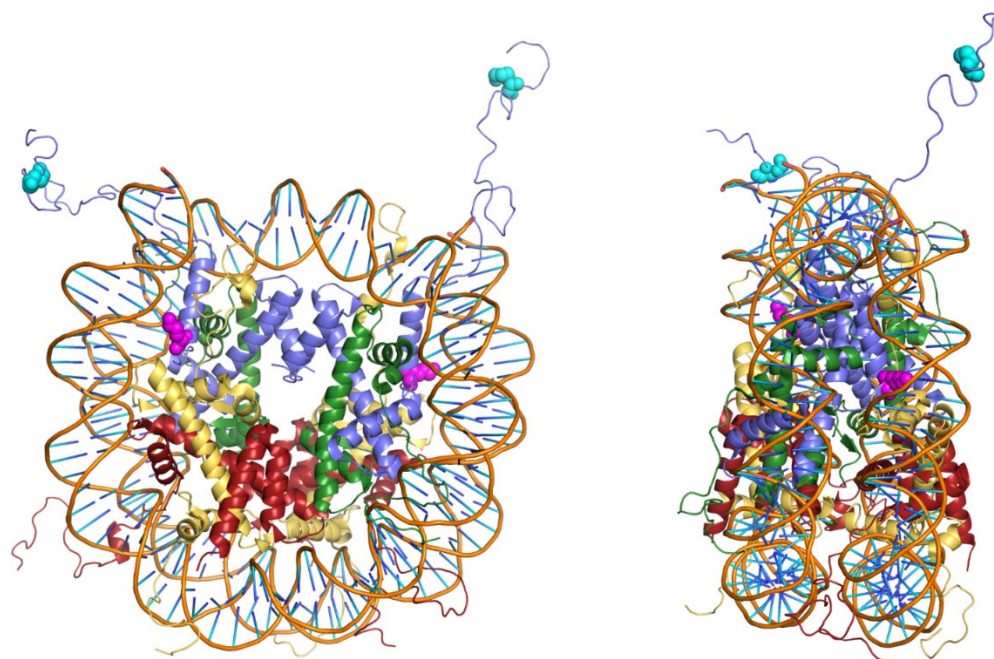
**Figure 5-1. Model for SIRT6 inter/intramolecular deacetylation of nucleosomes.** It remains an outstanding question whether SIRT6 performs deacetylation directly against its resident nucleosome (intramolecular) or whether a SIRT6:nucleosome complex catalyzes deacetylation against neighboring nucleosomes (intermolecular). In a model of intermolecular deacetylation, the SIRT6:nucleosome complex may catalyze deacetylation against an adjacent nucleosome, as pictured here, or another proximal non-contiguous nucleosome.



### 5.2.2. Characterization of SIRT6 deacetylation of nucleosome H3K56ac

Most of the work presented here focuses on SIRT6-mediated deacetylation of either H3K9ac peptide substrate or nucleosomes acetylated at H3K9. This substrate was the first validated substrate for SIRT6 and still represents the most widely understood regulatory means of SIRT6 activity (31). As SIRT6 garnered the attention of scientists, the repertoire of identified SIRT6 substrates has expanded greatly to include additional histone lysines and non-histone proteins. Interestingly these modifications include histone H3K56ac (32), which as opposed to H3K9ac, is buried in the globular domain of the nucleosome (Fig. 5-2). Given the more tightly restricted access to H3K56ac it is curious how this would affect catalysis by SIRT6. Additionally I hypothesize that whereas SIRT6 may be able to perform intermolecular deacetylation of H3K9ac, SIRT6 may be restricted to the intramolecular deacetylation of H3K56ac in which SIRT6 has to directly bind nucleosomes to access H3K56ac. Acetylation of H3K56 has been shown to increase DNA breathing and the remodeling of mononucleosomes (33, 34). Given our labs recent findings that the intrinsically disordered C-terminus of SIRT6 mediates nucleosome interactions through contacts with DNA (Liu. et al. 2020 *Nat. Comm.*) it would also be of interest to study how H3K56ac affects binding of SIRT6. I further hypothesize that SIRT6 would bind nucleosomes acetylated at H3K56 more tightly and in a C-terminal-dependent fashion. The majority of these studies could be performed following the production of homogenously acetylated H3K56 nucleosomes, which is currently ongoing.

**Figure 5-2: Molecular location of H3K9 and H3K56.** The whole structure of a mononucleosome is shown. Teal spheres highlight the location of H3K9 and magenta spheres represent H3K56. Whereas H3K9 is solvent exposed and flexible, H3K56 is buried in the globular domain of nucleosomes. The way in which the structural restriction of H3K56 affects the catalytic ability of SIRT6 has not been assessed.



### 5.2.3. Cellular application of NanoBiT system to assess SIRT6-chromatin association throughout cell-cycle progression and during DNA damage repair

SIRT6 dynamically regulates chromatin acetylation status both globally and specifically at promoter-proximal regions, however, how SIRT6 is regulated to perform these functions is relatively unknown. I have developed a NanoBiT system which allowed for the *in vitro* kinetic analysis of nucleosome binding. This split-luciferase system can be genetically encoded and used to monitor chromatin occupation by SIRT6 in live-cells owing to the cell-permeability of luciferase substrate. Phosphoproteomic efforts have revealed multiple sites of SIRT6 phosphorylation including S10, T294, S303, S330, and S338 (35). Although the function of the majority of these modifications remains unknown, phosphorylation of SIRT6 S10 by JNK facilitates its mobilization to sites of DNA-damage (36). Furthermore, all of the identified phosphorylation sites occur on the N or C-terminal regions of SIRT6, which have been demonstrated to facilitate subcellular localization and direct interactions with nucleosomes ((37), Liu. et al. 2020 *Nat. Comm.*), suggesting their modification may serve as regulatory elements for dynamic chromatin localization of SIRT6. SIRT6 has previously been shown to dynamically regulate chromatin in response to DNA-repair and throughout cell-cycle progression, a process which is highly regulated by protein phosphorylation (38). By applying our NanoBiT system in models of cell-cycle progression and DNA damage response utilizing SIRT6-LgBiT constructs which have specific serine/threonine mutations at known phosphorylation site, we can identify the functional contribution of these sites to the dynamic regulation of chromatin by SIRT6.

### ***5.3 Impact statement***

SIRT6 has emerged as a critical regulator of cellular homeostasis through its regulation of metabolic genes and maintenance of genomic stability. Many groups have endeavored to therapeutically target SIRT6 by small molecule activators to combat a host of age-related diseases. My work describes at microscopic detail a mechanism by which SIRT6 can be activated towards deacetylation by such small molecule activators. I have also described nucleosome binding as a prevalent endogenous event in cells which is sufficient to potently activate SIRT6 deacetylation through the same pathway presented for small molecule activators. Nonetheless, optimism persists for the targeting of SIRT6. I demonstrate that a distinct class of small molecules can further stimulate nucleosome deacetylation in a yet unresolved mechanism of activation. I provide a novel assay for live-cell monitoring of SIRT6-nucleosome interaction. This assay will assist in future SIRT6 studies which will likely determine the means in which SIRT6 chromatin occupancy is regulated to facilitate the widespread roles of SIRT6 in human health and disease.

## 5.4 References

1. Kugel, S., and Mostoslavsky, R. (2014) Chromatin and beyond: the multitasking roles for SIRT6. *Trends Biochem. Sci.* **39**, 72–81
2. Chang, A. R., Ferrer, C. M., and Mostoslavsky, R. (2019) SIRT6, a Mammalian Deacylase with Multitasking Abilities. *Physiological Reviews.* **100**, 145–169
3. Klein, M. A., and Denu, J. M. (2020) Biological and catalytic functions of sirtuin 6 as targets for small-molecule modulators. *J. Biol. Chem.* **295**, 11021–11041
4. Khan, R. I., Nirzhor, S. S. R., and Akter, R. (2018) A Review of the Recent Advances Made with SIRT6 and its Implications on Aging Related Processes, Major Human Diseases, and Possible Therapeutic Targets. *Biomolecules.* 10.3390/biom8030044
5. Sebastián, C., Zwaans, B. M. M., Silberman, D. M., Gymrek, M., Goren, A., Zhong, L., Ram, O., Truelove, J., Guimaraes, A. R., Toiber, D., Cosentino, C., Greenson, J. K., MacDonald, A. I., McGlynn, L., Maxwell, F., Edwards, J., Giacosa, S., Guccione, E., Weissleder, R., Bernstein, B. E., Regev, A., Shiels, P. G., Lombard, D. B., and Mostoslavsky, R. (2012) The histone deacetylase SIRT6 is a tumor suppressor that controls cancer metabolism. *Cell.* **151**, 1185–1199
6. Kugel, S., Feldman, J. L., Klein, M. A., Silberman, D. M., Sebastián, C., Mermel, C., Dobersch, S., Clark, A. R., Getz, G., Denu, J. M., and Mostoslavsky, R. (2015) Identification of and Molecular Basis for SIRT6 Loss-of-Function Point Mutations in Cancer. *Cell Rep.* **13**, 479–488
7. Zhang, J., Yin, X.-J., Xu, C.-J., Ning, Y.-X., Chen, M., Zhang, H., Chen, S.-F., and Yao, L.-Q. (2015) The histone deacetylase SIRT6 inhibits ovarian cancer cell proliferation via down-regulation of Notch 3 expression. *Eur Rev Med Pharmacol Sci.* **19**, 818–824



8. Mostoslavsky, R., Chua, K. F., Lombard, D. B., Pang, W. W., Fischer, M. R., Gellon, L., Liu, P., Mostoslavsky, G., Franco, S., Murphy, M. M., Mills, K. D., Patel, P., Hsu, J. T., Hong, A. L., Ford, E., Cheng, H.-L., Kennedy, C., Nunez, N., Bronson, R., Frendewey, D., Auerbach, W., Valenzuela, D., Karow, M., Hottiger, M. O., Hursting, S., Barrett, J. C., Guarente, L., Mulligan, R., Demple, B., Yancopoulos, G. D., and Alt, F. W. (2006) Genomic instability and aging-like phenotype in the absence of mammalian SIRT6. *Cell*. **124**, 315–329
9. Mao, Z., Hine, C., Tian, X., Van Meter, M., Au, M., Vaidya, A., Seluanov, A., and Gorbunova, V. (2011) SIRT6 promotes DNA repair under stress by activating PARP1. *Science*. **332**, 1443–1446
10. Toiber, D., Erdel, F., Bouazoune, K., Silberman, D. M., Zhong, L., Mulligan, P., Sebastian, C., Cosentino, C., Martinez-Pastor, B., Giacosa, S., D’Urso, A., Näär, A. M., Kingston, R., Rippe, K., and Mostoslavsky, R. (2013) SIRT6 recruits SNF2H to DNA break sites, preventing genomic instability through chromatin remodeling. *Mol. Cell*. **51**, 454–468
11. Ferrer, C. M., Alders, M., Postma, A. V., Park, S., Klein, M. A., Cetinbas, M., Pajkrt, E., Glas, A., van Koningsbruggen, S., Christoffels, V. M., Mannens, M. M. A. M., Knecht, L., Etchegaray, J.-P., Sadreyev, R. I., Denu, J. M., Mostoslavsky, G., van Maarle, M. C., and Mostoslavsky, R. (2018) An inactivating mutation in the histone deacetylase SIRT6 causes human perinatal lethality. *Genes Dev*. **32**, 373–388
12. Zhang, W., Wan, H., Feng, G., Qu, J., Wang, J., Jing, Y., Ren, R., Liu, Z., Zhang, L., Chen, Z., Wang, S., Zhao, Y., Wang, Z., Yuan, Y., Zhou, Q., Li, W., Liu, G.-H., and Hu, B. (2018) SIRT6 deficiency results in developmental retardation in cynomolgus monkeys. *Nature*. **560**, 661–665

13. Feldman, J. L., Baeza, J., and Denu, J. M. (2013) Activation of the protein deacetylase SIRT6 by long-chain fatty acids and widespread deacylation by mammalian sirtuins. *J. Biol. Chem.* **288**, 31350–31356
14. Feldman, J. L., Dittenhafer-Reed, K. E., Kudo, N., Thelen, J. N., Ito, A., Yoshida, M., and Denu, J. M. (2015) Kinetic and Structural Basis for Acyl-Group Selectivity and NAD(+) Dependence in Sirtuin-Catalyzed Deacylation. *Biochemistry*. **54**, 3037–3050
15. Klein, M. A., Liu, C., Kuznetsov, V. I., Feltenberger, J. B., Tang, W., and Denu, J. M. (2019) Mechanism of activation for the sirtuin 6 protein deacetylase. *J. Biol. Chem.* 10.1074/jbc.RA119.011285
16. Jin, L., Wei, W., Jiang, Y., Peng, H., Cai, J., Mao, C., Dai, H., Choy, W., Bemis, J. E., Jirousek, M. R., Milne, J. C., Westphal, C. H., and Perni, R. B. (2009) Crystal structures of human SIRT3 displaying substrate-induced conformational changes. *J. Biol. Chem.* **284**, 24394–24405
17. Borra, M. T., Langer, M. R., Slama, J. T., and Denu, J. M. (2004) Substrate specificity and kinetic mechanism of the Sir2 family of NAD<sup>+</sup>-dependent histone/protein deacetylases. *Biochemistry*. **43**, 9877–9887
18. Huang, Z., Zhao, J., Deng, W., Chen, Y., Shang, J., Song, K., Zhang, L., Wang, C., Lu, S., Yang, X., He, B., Min, J., Hu, H., Tan, M., Xu, J., Zhang, Q., Zhong, J., Sun, X., Mao, Z., Lin, H., Xiao, M., Chin, Y. E., Jiang, H., Xu, Y., Chen, G., and Zhang, J. (2018) Identification of a cellularly active SIRT6 allosteric activator. *Nat. Chem. Biol.* **14**, 1118–1126
19. Zhang, J., Li, Y., Liu, Q., Huang, Y., Li, R., Wu, T., Zhang, Z., Zhou, J., Huang, H., Tang, Q., Huang, C., Zhao, Y., Zhang, G., Jiang, W., Mo, L., Zhang, J., Xie, W., and He, J. (2020) Sirt6

alleviated liver fibrosis by deacetylating conserved lysine 54 on Smad2 in hepatic stellate cells.

*Hepatology*. 10.1002/hep.31418

20. Shang, J.-L., Ning, S.-B., Chen, Y.-Y., Chen, T.-X., and Zhang, J. (2020) MDL-800, an allosteric activator of SIRT6, suppresses proliferation and enhances EGFR-TKIs therapy in non-small cell lung cancer. *Acta Pharmacol. Sin.* 10.1038/s41401-020-0442-2

21. Gertman, O., Omer, D., Hendler, A., Stein, D., Onn, L., Khukhin, Y., Portillo, M., Zarivach, R., Cohen, H. Y., Toiber, D., and Aharoni, A. (2018) Directed evolution of SIRT6 for improved deacylation and glucose homeostasis maintenance. *Sci Rep.* **8**, 3538

22. Cai, J., Zuo, Y., Wang, T., Cao, Y., Cai, R., Chen, F.-L., Cheng, J., and Mu, J. (2016) A crucial role of SUMOylation in modulating Sirt6 deacetylation of H3 at lysine 56 and its tumor suppressive activity. *Oncogene*. **35**, 4949–4956

23. Lin, Z., Yang, H., Tan, C., Li, J., Liu, Z., Quan, Q., Kong, S., Ye, J., Gao, B., and Fang, D. (2013) USP10 antagonizes c-Myc transcriptional activation through SIRT6 stabilization to suppress tumor formation. *Cell Rep.* **5**, 1639–1649

24. Zhang, N., Li, Z., Mu, W., Li, L., Liang, Y., Lu, M., Wang, Z., Qiu, Y., and Wang, Z. (2016) Calorie restriction-induced SIRT6 activation delays aging by suppressing NF- $\kappa$ B signaling. *Cell Cycle*. **15**, 1009–1018

25. Kawahara, T. L. A., Rapicavoli, N. A., Wu, A. R., Qu, K., Quake, S. R., and Chang, H. Y. (2011) Dynamic Chromatin Localization of Sirt6 Shapes Stress- and Aging-Related Transcriptional Networks. *PLoS Genet.* 10.1371/journal.pgen.1002153

26. Ardestani, P. M., and Liang, F. (2012) Sub-cellular localization, expression and functions of Sirt6 during the cell cycle in HeLa cells. *Nucleus*. **3**, 442–451
27. Dixon, A. S., Schwinn, M. K., Hall, M. P., Zimmerman, K., Otto, P., Lubben, T. H., Butler, B. L., Binkowski, B. F., Machleidt, T., Kirkland, T. A., Wood, M. G., Eggers, C. T., Encell, L. P., and Wood, K. V. (2016) NanoLuc Complementation Reporter Optimized for Accurate Measurement of Protein Interactions in Cells. *ACS Chem. Biol.* **11**, 400–408
28. Deal, R. B., and Henikoff, S. (2010) Capturing the dynamic epigenome. *Genome Biol.* **11**, 218
29. Phair, R. D., Scaffidi, P., Elbi, C., Vecerová, J., Dey, A., Ozato, K., Brown, D. T., Hager, G., Bustin, M., and Misteli, T. (2004) Global Nature of Dynamic Protein-Chromatin Interactions In Vivo: Three-Dimensional Genome Scanning and Dynamic Interaction Networks of Chromatin Proteins. *Mol Cell Biol.* **24**, 6393–6402
30. Chen, J., Zhang, Z., Li, L., Chen, B.-C., Revyakin, A., Hajj, B., Legant, W., Dahan, M., Lionnet, T., Betzig, E., Tjian, R., and Liu, Z. (2014) Single-molecule dynamics of enhanceosome assembly in embryonic stem cells. *Cell*. **156**, 1274–1285
31. Michishita, E., McCord, R. A., Berber, E., Kioi, M., Padilla-Nash, H., Damian, M., Cheung, P., Kusumoto, R., Kawahara, T. L. A., Barrett, J. C., Chang, H. Y., Bohr, V. A., Ried, T., Gozani, O., and Chua, K. F. (2008) SIRT6 is a histone H3 lysine 9 deacetylase that modulates telomeric chromatin. *Nature*. **452**, 492–496
32. Michishita, E., McCord, R. A., Boxer, L. D., Barber, M. F., Hong, T., Gozani, O., and Chua, K. F. (2009) Cell cycle-dependent deacetylation of telomeric histone H3 lysine K56 by human SIRT6. *Cell Cycle*. **8**, 2664–2666

33. Neumann, H., Hancock, S. M., Buning, R., Routh, A., Chapman, L., Somers, J., Owen-Hughes, T., van Noort, J., Rhodes, D., and Chin, J. W. (2009) A Method for Genetically Installing Site-Specific Acetylation in Recombinant Histones Defines the Effects of H3 K56 Acetylation. *Molecular Cell*. **36**, 153–163
34. Lee, J., and Lee, T.-H. (2019) How protein binding sensitizes the nucleosome to histone H3K56 acetylation. *ACS Chem Biol*. **14**, 506–515
35. Miteva, Y. V., and Cristea, I. M. (2014) A proteomic perspective of Sirtuin 6 (SIRT6) phosphorylation and interactions and their dependence on its catalytic activity. *Mol. Cell Proteomics*. **13**, 168–183
36. Van Meter, M., Simon, M., Tomblin, G., May, A., Morello, T. D., Hubbard, B. P., Bredbenner, K., Park, R., Sinclair, D. A., Bohr, V. A., Gorbunova, V., and Seluanov, A. (2016) JNK Phosphorylates SIRT6 to Stimulate DNA Double-Strand Break Repair in Response to Oxidative Stress by Recruiting PARP1 to DNA Breaks. *Cell Rep*. **16**, 2641–2650
37. Tennen, R. I., Berber, E., and Chua, K. F. (2010) Functional dissection of SIRT6: identification of domains that regulate histone deacetylase activity and chromatin localization. *Mech. Ageing Dev*. **131**, 185–192
38. Olsen, J. V., Vermeulen, M., Santamaria, A., Kumar, C., Miller, M. L., Jensen, L. J., Gnad, F., Cox, J., Jensen, T. S., Nigg, E. A., Brunak, S., and Mann, M. (2010) Quantitative phosphoproteomics reveals widespread full phosphorylation site occupancy during mitosis. *Sci Signal*. **3**, ra3